A Bounding Surface Viscoplasticity Model for Time dependent Behaviour of Saturated and Unsaturated Soils including Tertiary Creep

Author:
Mac, Thi Ngoc

Publication Date:
2020

DOI:
https://doi.org/10.26190/unsworks/22043

A BOUNDING SURFACE VISCOPLASTICITY MODEL FOR TIME DEPENDENT BEHAVIOUR OF SATURATED AND UNSATURATED SOILS INCLUDING TERTIARY CREEP

Thi Ngoc Mac

BSc, MSc, ME

A thesis in fulfillment of the requirements for the degree of

DOCTOR OF PHILOSOPHY

SCHOOL OF CIVIL AND ENVIRONMENTAL ENGINEERING

FACULTY OF ENGINEERING

THE UNIVERSITY OF NEW SOUTH WALES

SYDNEY, AUSTRALIA

May 2020

Thesis/Dissertation Sheet

Surname/Family Name	:	**MAC**
Given Name/s	:	**THI NGOC**
Abbreviation for degree as give in the University calendar	:	**PhD**
Faculty	:	**Engineering**
School	:	**Civil and Environmental Engineering**
Thesis Title	:	**A Bounding Surface Viscoplasticity Model for Time dependent Behaviour of Saturated and Unsaturated Soils including Tertiary Creep**

Abstract 350 words maximum: (PLEASE TYPE)

A bounding surface viscoplasticity constitutive model is developed for describing the time-dependent stress-strain behaviour of fully saturated and unsaturated soils. The proposed model is formulated within the context of bounding surface plasticity using the consistency viscoplastic framework and the critical state theory. The model provides a continuous transition from rate-independent plasticity to rate-dependent viscoplasticity. The hardening parameter representing the size of the bounding surface is defined as a function of the viscoplastic volumetric strain and the viscoplastic strain rate. For unsaturated soils, the effect of suction is included as another parameter controlling the size of the bounding surface. The suction hardening effect is described using the coupled influence approach where suction has a multiplicative effect to the viscoplastic volumetric hardening. A non-associated flow rule is defined to generalize application of the model to a wide range of soils. The capability of the model to capture drained and undrained tertiary creep is particularly emphasized. The model requires minimal material parameters determined using standard laboratory testing equipment.

A fully coupled flow-deformation model is then presented for describing time-dependent behaviour of variably saturated soils. The proposed model is formulated based on the theory of multiphase mixtures using the effective stress approach. The governing equations for the flow model are derived using the equilibrium equations and the conservation equations of mass and momentum. The constitutive relations of the solid skeleton are described using the bounding surface viscoplasticity model in order to capture the time-dependent behaviour of geomaterials.

The essential elements of the model are validated by comparing the numerical results with the experimental data from the literature. The application of the model to predict the time-dependent behaviour of fully saturated and unsaturated soils is demonstrated for creep tests, constant strain rate tests and unloading-reloading relaxation tests subject to different geometric, loading, and drainage boundary conditions. Special attention is paid to the capability of the proposed model in capturing the tertiary creep and creep rupture. It is demonstrated that the model is able to capture drained creep rupture in over-consolidated clays which is the primary mode of failure in marginally stable over-consolidated soil slopes.

ORIGINALITY STATEMENT

‘I hereby declare that this submission is my own work and to the best of my knowledge it contains no materials previously published or written by another person, or substantial proportions of material which have been accepted for the award of any other degree or diploma at UNSW or any other educational institution, except where due acknowledgement is made in the thesis. Any contribution made to the research by others, with whom I have worked at UNSW or elsewhere, is explicitly acknowledged in the thesis. I also declare that the intellectual content of this thesis is the product of my own work, except to the extent that assistance from others in the project's design and conception or in style, presentation and linguistic expression is acknowledged.’

Signed ……………………………………………..............

Date ……………………………………………..............

COPYRIGHT STATEMENT

Signed ……………………………………………..........................

Date ……………………………………………..............................

AUTHENTICITY STATEMENT

‘I certify that the Library deposit digital copy is a direct equivalent of the final officially approved version of my thesis.’

Signed ……………………………………………..........................

Date ……………………………………………..............................

INCLUSION OF PUBLICATIONS STATEMENT

UNSW is supportive of candidates publishing their research results during their candidature as detailed in the UNSW Thesis Examination Procedure.

Publications can be used in their thesis in lieu of a Chapter if:

- The student contributed greater than 50% of the content in the publication and is the "primary author", ie. the student was responsible primarily for the planning, execution and preparation of the work for publication
- The student has approval to include the publication in their thesis in lieu of a Chapter from their supervisor and Postgraduate Coordinator.
- The publication is not subject to any obligations or contractual agreements with a third party that would constrain its inclusion in the thesis

Please indicate whether this thesis contains published material or not.

☐ *This thesis contains no publications, either published or submitted for publication*

☒ *Some of the work described in this thesis has been published and it has been documented in the relevant Chapters with acknowledgement*

☐ *This thesis has publications (either published or submitted for publication) incorporated into it in lieu of a chapter and the details are presented below*

CANDIDATE'S DECLARATION

I declare that:

- I have complied with the Thesis Examination Procedure
- where I have used a publication in lieu of a Chapter, the listed publication(s) below meet(s) the requirements to be included in the thesis.

Name	**Signature**	**Date (dd/mm/yy)**

ABSTRACT

A bounding surface viscoplasticity constitutive model is developed for describing the time-dependent stress-strain behaviour of fully saturated and unsaturated soils. The proposed model is formulated within the context of bounding surface plasticity using the consistency viscoplastic framework and the critical state theory. The model provides a continuous transition from rate-independent plasticity to rate-dependent viscoplasticity. The hardening parameter representing the size of the bounding surface is defined as a function of the viscoplastic volumetric strain and the viscoplastic strain rate. For unsaturated soils, the effect of suction is included as another parameter controlling the size of the bounding surface. The suction hardening effect is described using the coupled influence approach where suction has a multiplicative effect to the viscoplastic volumetric hardening. A non-associated flow rule is defined to generalize application of the model to a wide range of soils. The capability of the model to capture drained and undrained tertiary creep is particularly emphasized. The model requires minimal material parameters determined using standard laboratory testing equipment.

A fully coupled flow-deformation model is then presented for describing time-dependent behaviour of variably saturated soils. The proposed model is formulated based on the theory of multiphase mixtures using the effective stress approach. The governing equations for the flow model are derived using the equilibrium equations and the conservation equations of mass and momentum. The constitutive relations of the solid skeleton are described using the bounding surface viscoplasticity model in order to capture the time-dependent behaviour of geomaterials.

The essential elements of the model are validated by comparing the numerical results with the experimental data from the literature. The application of the model to predict the time-dependent behaviour of fully saturated and unsaturated soils is demonstrated for creep tests, constant strain rate tests and unloading-reloading relaxation tests subject to different geometric, loading, and drainage boundary conditions. Special attention is paid to the capability of the proposed model in capturing the tertiary creep and creep rupture. It is demonstrated that the model is able to capture drained creep rupture in over-consolidated clays which is the primary mode of failure in marginally stable over-consolidated soil slopes.

AKNOWLEDGEMENTS

I would like to express my respect and deep sense of gratitude to my supervisor, Professor Nasser Khalili, for his guidance, continuous supports and encouragement throughout this research.

I wish to send sincere thanks and appreciation to my co-supervisor, Dr. Babak Shahbodagh, for his excellent guidance, inspiring discussions, enthusiasm and invaluable suggestions. I have been incredibly fortunate to have a supervisor who is invested on both myself and my work, encouraging me to think critically, and being available for assistance every step of the way.

I would like to thank many members of staff in the School of Civil and Environmental Engineering for the academic, administrative and technical support during the course. Many thanks to all my colleagues and friends at UNSW Sydney who have been of great help to me throughout the completion of this thesis.

I am extremely grateful to my parents for their moral supports and encouragement. I am very lucky to have my brother share my wonderful childhood and take care the family when I am overseas. Thank you my family and all of my friends for encouraging me to take on this PhD and for all the help and inspiration you provided throughout of the process.

Finally, financial assistance in the form of TFS scholarship from The University of New South Wales (UNSW Sydney) is gratefully acknowledged.

TABLE OF CONTENTS

LIST OF FIGURES

LIST OF TABLES

LIST OF SYMBOLS

Latin Letters

a_{11}, a_{22}	Apparent compressibility of the water and air phases
a_{12}, a_{21}	Coupling terms relating the pore water and pore air volumetric deformations due to change in matric suction
c_a	Compressibility coefficient of air phase
c_w	Compressibility coefficient of water phase
c_m	Compressibility coefficient of the soil matrix with respect to change in matric suction
c'_m	Compressibility coefficient of the water phase with respect to change in matric suction
c_s	Compressibility of solid grains
c_β	Viscoplastic parameter controlling the evolution of the strain rate hardening
C_c	Compression index
$C_{\alpha e}$	Coefficient of secondary compression with respect to e
$C_{\alpha\varepsilon}$	Coefficient of secondary compression with respect to ε
d	Plastic dilatancy
e_i, e_0	Initial void ratio
f_d	Dynamic loading surface
f_s	Static yield surface function

$F(\boldsymbol{\sigma}, \phi)$	Static yield function
f	Yield function at the loading surface
F	Yield function at the bounding surface
g	Viscoplastic potential function
G	Shear modulus
h	Viscoplastic strain hardening modulus
h_b	Viscoplastic strain hardening modulus at the bounding surface
h_f	Viscoplastic strain hardening modulus at the loading surface
J_2 , J_3	The second and the third invariants of the deviator stress vector
K	Bulk modulus
k_{ra}	Relative permeability of air
k_{rw}	Relative permeability of water
M	Total mass of soil element
M_α	Mass of phase α , $(\alpha = a, w, s)$
M_{cs}	Slope of the critical state line on the $(p' \sim q)$ plane
n_α	Volumetric fraction of phase α , $(\alpha = a, w, s)$
N	Intercept of the isotropic compression line at p' = 1kPa
p_0	A dummy variable controlling the size of the viscoplastic potential
p'_0	Initial mean effective stress
p'	Mean effective stress
p_{net}	Mean net stress
p_a	Pore air pressure
P_a	Absolute gas pressure
p_{atm}	Atmospheric pressure
p'_c	Preconsolidation stress

q	Deviatoric stress
q_0	Deviator stress at the beginning of stress relaxation
s	Matric suction
s_e	Air entry/Air expulsion suction at the transition point between saturated and unsaturated states
s_{ae}	Air entry suction
s_{ex}	Air expulsion suction
S_r	Degree of saturation
S_{res}	Residual degree of saturation
s_{res}	Matric suction corresponding to the residual water content
t	Time
t_i	Reference time
$\tilde{t}$	Loading direction multiplier
V	Total volume of the soil element
V_α	Volume of phase α , $(\alpha = a, w, s)$

Greek Letters

α	Creep coefficient
β	Finite difference interpolation parameter
χ	The effective stress parameter
$\delta\lambda$	Viscoplastic multiplier
ε_q	Deviatoric strain
ε_v	Volumetric strain
ε_z	Vertical strain

$\dot{\varepsilon}$	Axial strain rate
$\dot{\varepsilon}_{\upsilon}$	Delayed volumetric strain rate
$\dot{\varepsilon}_z$	Vertical strain rate
γ	Viscoplastic parameter
θ	Lode angle
$\hat{\gamma}(s)$	Addictive suction hardening function
η	Stress ratio
λ	Slope of the critical state line on the ($\upsilon \sim \ln p'$) plane
κ	Slope of elastic swelling and recompression line on ($\upsilon \sim \ln p'$) plane.
ν	Poisson's ratio
ξ	Viscoplastic strain rate hardening modulus
μ_a	Dynamic viscosity of air
μ_w	Dynamic viscosity of water
σ'_z	Vertical effective stress
$\sigma'_{z,0}$	Initial vertical effective in situ stress
$\sigma'_{z,pc}$	Vertical preconsolidation stress
υ	Specific volume
ϕ	Overstress function
χ	Hardening parameter
Δe	Change in void ratio
Γ	Specific volume intercept of the critical state line at a reference stress of p' = 1kPa

Matrices and Vectors

$\mathbf{D}^{\mathrm{e}}$	Elastic stiffness matrix
$\mathbf{D}^{\mathrm{ep}}$	Elasto-plastic stiffness matrix
$\mathbf{D}^{\mathrm{evp}}$	Elasto-Viscoplastic stiffness matrix
$\mathbf{g}$	Gravitational acceleration vector
$[\mathrm{H}_a]$	Flow matrix corresponding to the permeability of the air phase
$[\mathrm{H}_w]$	Flow matrix corresponding to the permeability of the water phase
$[\mathrm{K}]$	Element stiffness matrix
$[\mathrm{C}]$	Coupling matrix
$[\mathrm{M}]$	Mass matrix
$\{\mathrm{P}\}$	Vector of nodal forces
$\{\mathrm{p}_a\}$	Vector of nodal pore air pressure
$\{\mathrm{p}_w\}$	Vector of nodal pore water pressure
$\{\mathrm{Q}_a\}$	Vector of nodal fluxes of air flow
$\{\mathrm{Q}_w\}$	Vector of nodal fluxes of water flow
$\{\mathrm{u}\}$	Vector of nodal displacements
$\mathbf{k}$	Intrinsic permeability tensor
$\mathbf{m}$	Gradient of the viscoplastic potential
$\mathbf{n}$	Gradient to the yield surface
$\mathbf{v}$	Velocity vector
$\boldsymbol{\delta}$	Identity vector
$\delta\boldsymbol{\varepsilon}^{\mathrm{e}}$	Elastic strain increment tensor
$\delta\boldsymbol{\varepsilon}^{\mathrm{vp}}$	Viscoplastic strain increment tensor
$\boldsymbol{\varepsilon}^{\mathrm{vp}}$	Viscoplastic strains tensor

$\dot{\boldsymbol{\varepsilon}}_{\mathrm{ij}}$	Total strain rate tensor
$\dot{\boldsymbol{\varepsilon}}_{\mathrm{ij}}^{\mathrm{e}}$	Elastic strain rate tensor
$\dot{\boldsymbol{\varepsilon}}^{\mathrm{vp}}$	Viscoplastic strain rate tensor
$\delta\boldsymbol{\sigma}$	Stress increment tensor
$\boldsymbol{\sigma}'_{\mathrm{ij}}$	Effective stress tensor
$\boldsymbol{\sigma}_{\mathrm{net}}$	Net stress tensor

CHAPTER 1

INTRODUCTION

1.1. Background

The prediction of time-dependent behaviour of geomaterials, such as creep, stress relaxation, and strain-rate dependency is of great interest in geotechnical engineering practice. The time-dependent behaviour has been recognized in a wide range of geomaterials including clays (Bjerrum, 1967; Leroueil *et al.*, 1985; Leroueil, 2006; Le *et al.*, 2015; Pineda *et al.*, 2016; Kelly *et al.*, 2017); sands (Di Benedetto *et al.*, 2002; Lade *et al.*, 2009; Yamamuro *et al.*, 2012); rocks (Hayano *et al.*, 2001; Fabre and Pellet, 2006; Huang *et al.*, 2015); and rockfill (Sherard and Cooke, 1987; Oldecop and Alonso, 2007). Creep and strain rate dependency is of particular concern in the analyses of long-term settlement of infrastructure founded on soft ground (Bjerrum, 1967; Watabe *et al.*, 2012); stability of natural and excavated soil slopes (Tavenas and Leroueil, 1981; Fell *et al.*, 2018); deformation and failure analysis of earth-structures subject to cyclic and dynamic loading (Park and Hashash, 2008; Shahbodagh, 2011; Sadeghi *et al.*, 2015); construction of tunnels in squeezing ground (Ghaboussi and Gioda, 1977; Debernardi and Barla, 2009); design of geological nuclear waste disposal facilities (Dixon *et al.*, 1985; Miura *et al.*, 2003) and dynamic penetration and anchor installation problems (Carter *et al.*, 2010; Nazem *et al.*, 2012; Sabetamal *et al.*, 2016) to name a few.

Many researchers including Bjerrum (1967), Mesri and Godlewski (1977), Leroueil *et al.* (1985), Yin (1999), Leroueil (2006) and Yin *et al.* (2011) have conducted extensive laboratory tests, mainly one-dimensional and triaxial tests, to investigate the time-dependent behaviour of soils. Following early works of Suklje (1957), Leroueil *et al.* (1985) experimentally demonstrated in experiments that the time-dependent behaviour of clays subjected to one-dimensional compression can be described by a unique stress–strain–strain-rate relationship. This, known as isotach approach, has extensively been validated for various clayey soils (e.g. Imai and Tang, 1992; Nash *et al.*, 1992; Kim and Leroueil, 2001; Marques *et al.*, 2004; Laloui *et al.*, 2008; Yang *et al.*, 2016 and Yang and Carter, 2017). The isotach approach unifies various time-dependent phenomena, i.e. creep, stress relaxation, and strain rate dependence, and is a core hypothesis in many viscoplastic constitutive models. It, however, has limitations on describing the observed time-dependent behaviour of clays at high strain rates (Leroueil *et al.*, 1985), which is crucial in dynamic analyses, or at large strains and when close to the critical state (Leroueil *et al.*, 1985; Oka *et al.*, 2003), which is important in large deformation and failure analysis of geo-structures. In addition, the time-dependent development of microstructure, i.e. bonding between soil particles, observed in some soils under low strain rates, cannot be explained by isotach approach (Augustesen *et al.*, 2004; Leroueil, 2006).

In parallel with the experimental investigations, several approaches have been developed for capturing the time-dependent behaviour of soils, including empirical models (Bjerrum, 1967; Yin, 1999), rheological models (Murayama and Shibata, 1961), and rate-dependent elasto-viscoplastic constitutive models (see Liingaard *et al.*, 2004). The elasto-viscoplastic models are the most comprehensive and numerous. They are typically developed mainly based on either the overstress elasto-plasticity theory (Perzyna, 1963, 1966) or the nonstationary flow surface theory (Naghdi and Murch, 1963; Olszak and Perzyna, 1970). Amongst the notable contributions include the overstress-type models of Zienkiewicz and Cormeau (1974), Adachi and Oka (1982), Dafalias (1982), Katona (1984), Kaliakin and Dafalias (1990a, 1990b), Kutter and Sathialingam (1992), Yin and Graham (1989, 1994, 1999), Oka *et al.* (1995), Modaressi and Laloui (1997) and Kimoto *et al.* (2013), and the nonstationary flow surface models of Sekiguchi (1984), Matsui and Abe (1985) and Qiao *et al.* (2016).

1.2. Deficiencies of Previous Works

The overstress theory was widely applied to elasto-viscoplastic models describing the time-dependent behaviour of geomaterials. Many elasto-viscoplastic models based on the concept of overstress theory (Perzyna, 1963, 1966) and the critical state framework have been found in the literature such as the works of Adachi and Okano (1974), Adachi and Oka (1982), Katona (1984), Oka *et al.* (1988), Desai and Zhang (1987), Kaliakin and Dafalias (1990a, 1990b), Kutter and Sathialingam (1992), Matsui and Abe (1988), Hashiguchi and Okayasu (2000) , Rocchi *et al.* (2003), and Yin and Graham (1989, 1994, 1999), Yin *et al.* (2002), etc. However, the main difficulty in the overstress-type models surrounds the arbitrariness of the overstress function. In addition, they do not satisfy the consistency condition and cannot be reduced to the rate independent elasto-plastic formulation for the limiting case of the fluidity parameter approaching infinity (Simo *et al.*, 1988). The overstress models are also limited in describing the tertiary creep (Oka *et al.*, 1994), i.e. creep at an accelerating strain rate leading to creep failure, unless by introducing a stress-state-dependent viscoplastic parameter, damage effect, or de-structure due to straining (Adachi *et al.*, 1987; Al-Shamrani and Sture, 1998; Yin *et al.*, 2011; Jiang *et al.*, 2017). This deficiency has been rectified in nonstationary-type models which are able to predict undrained tertiary creep in normally-consolidated clays (e.g. Sekiguchi, 1984). There were very few overstress type models which can describe the tertiary creep process and creep rupture. For example, Adachi *et al.* (1987) extended the model proposed by Adachi and Oka (1982) to describe the acceleration creep process and undrained creep rupture. However, there is currently no model of creep that can rigorously capture drained creep rupture in over-consolidated clays. This is of particular relevance to natural and excavated slopes in which creep failures are most common.

1.3. Scope and Objectives

The main objective of this research is to develop a unified viscoplastic constitutive model to capture the time-dependent mechanical behaviour of geomaterials with particular reference to drained and undrained tertiary creep. The proposed model is based on the bounding surface plasticity (Khalili *et al.*, 2005; Russell and Khalili, 2006) and the concept of viscoplastic consistency framework (Wang *et al.*, 1997; Carosio *et al.*, 2000). Within this context, the model is able to capture the accumulation of viscoplastic strains upon loading and unloading as well as drained creep rupture in over-consolidated clays. Hardening and softening characteristics of the material are captured through the effects of viscoplastic volumetric strain and viscoplastic volumetric strain rate on the evolution of the bounding surface. The hardening parameter representing the size of the bounding surface is defined as a function of viscoplastic volumetric strain and viscoplastic strain rate. For unsaturated soils, the effect of suction is included as another parameter controlling the size of bounding surface. The suction hardening effect is described using the coupled influence approach where suction has a multiplicative effect to the viscoplastic volumetric hardening. Unlike the overstress models, the proposed model meets the consistency condition and allows a smooth transition from rate-independent plasticity to rate-dependent viscoplasticity. A non-associated flow rule is defined to generalise application of the model to a wide range of soils. The model requires minimal material parameters determined using standard laboratory testing equipment. The model is validated through comparison of the simulation results with experimental data from the literature highlighting capabilities of the model.

The proposed viscoplastic constitutive model includes the following essential elements: i) the bounding surface describing the limit states of stress; ii) the loading surface, on which the current stress state lies; iii) the viscoplastic potential describing the mode and component magnitudes of viscoplastic deformation; iv) hardening rules, controlling the size and the location of the bounding surface and loading surfaces and defined as functions of viscoplastic volumetric strain and viscoplastic strain rate; and v) suction hardening for unsaturated soils, which is described using the coupled influence approach.

The governing equations for the flow model are derived using the conservation equation of mass and momentum within the context of theory of multiphase mixtures, while the deformation equations are obtained satisfying the conditions of equilibrium, compatibility and consistency. The coupling between the flow and deformation models is established using the concept of effective stress and through the compatibility requirement of the volumetric deformations of the three phases. To describe the viscoplastic behaviour of the soil matrix, the bounding surface viscoplasticity constitutive model is adopted. The bounding surface viscoplasticity model is formulated incrementally within the critical state framework using the effective stress approach.

Numerical solution to the governing equations is obtained using the finite element method. The governing equations are discretised spatially using the standard Galerkin method while the finite difference technique is employed for the discretisation of the time domain. The viscoplastic constitutive equations are integrated using the explicit integration algorithms. Performance of the model to capture the time-dependent behaviours is investigated by comparing numerical predictions with experimental results for a range of creep tests, constant strain rate tests and unloading-reloading relaxation tests on fully saturated and unsaturated soils subject to different geometric, loading, and drainage boundary conditions. Special attention is paid to the capability of the proposed model in capturing the tertiary creep and creep rupture under drained and undrained conditions. No experimental analysis is conducted in this study; however, the model is validated through comparison of the simulation results with experimental data from the literature to highlight the capabilities of the model.

The following contributions have been made in this study: i) development of a new bounding surface viscoplasticity constitutive model for time-dependent behaviour of saturated and unsaturated geomaterials including tertiary creep and creep rupture; ii) derivation of numerical solutions for the viscoplastic multiplier and stress-strain relationships; iii) development of a numerical model for fully coupled flow-deformation analysis of three phase variably saturated viscoplastic soils; iv) implementation of the proposed model into a numerical code; v) validation of the constitutive model and the numerical code using the experimental data from the literature for creep tests, constant strain rate tests and unloading, reloading relaxation tests; vi) solving several boundary value problems to demonstrate the application of the model.

1.4. Structure of the Thesis

The thesis consists of the following six chapters:

Chapter 1 introduces the importance of the topic, scope of this research and the structure of the thesis.

Chapter 2 reviews the time-dependent behaviour of geomaterials; the constitutive modelling of time-dependent behaviour of both saturated and unsaturated geomaterials. Special attention is also paid to the tertiary creep and creep rupture.

Chapter 3 presents a bounding surface viscoplasticity constitutive model for describing the time-dependent stress-strain behaviour of both fully saturated and unsaturated soils. The proposed model is formulated within the bounding surface plasticity framework using the consistency theory and the concept of the critical state.

Chapter 4 presents the governing equations of multiphase porous media and their finite element approximations. The proposed hydro-mechanical model is formulated based on the theory of multiphase mixtures using the effective stress approach and the bounding surface viscoplastic constitutive model.

Chapter 5 presents validations and applications of the proposed bounding surface viscoplasticity model to predict the time-dependent behaviour of fully saturated and unsaturated soils using the results of creep tests, constant strain rate tests and unloading reloading relaxation tests. The capability of the proposed model in capturing the tertiary creep and creep rupture is particularly emphasized.

Chapter 6 summarizes the major outcomes of this research and outlines the recommendations for further research.

CHAPTER 2

LITERATURE REVIEW

2.1. Introduction

This chapter presents a review of the most important time-dependent phenomena observed in relation to the mechanical behaviour of soils and the existing constitutive models developed to capture such phenomena. Section 2.2 describes the time-dependent behaviour of geomaterials including creep, stress relaxation and rate dependency. A number of empirical, rheological and stress–strain–strain-rate models are discussed in Section 2.3. In Section 2.4, a number of constitutive models for unsaturated soils are presented, including the viscoplasticity models simulating the time-dependent behaviour of partially saturated soils. Special attention is paid to tertiary creep and creep rupture phenomenon in Section 2.5.

2.2. Time-Dependent Behaviour of Soils

2.2.1. Creep

Creep is the development of strains over time at constant effective stress. Figure 2.1 shows a creep test performed at a low stress level with a strain path from point 1 to point 2 (1→2). Consider a soil sheared to the stress-strain state at point 1. At this point, a creep process is started with the constant stress (Figure 2.1b). Over time, the strain state moves to point 2, i.e. the strain is gradually increasing (Figure 2.1c).

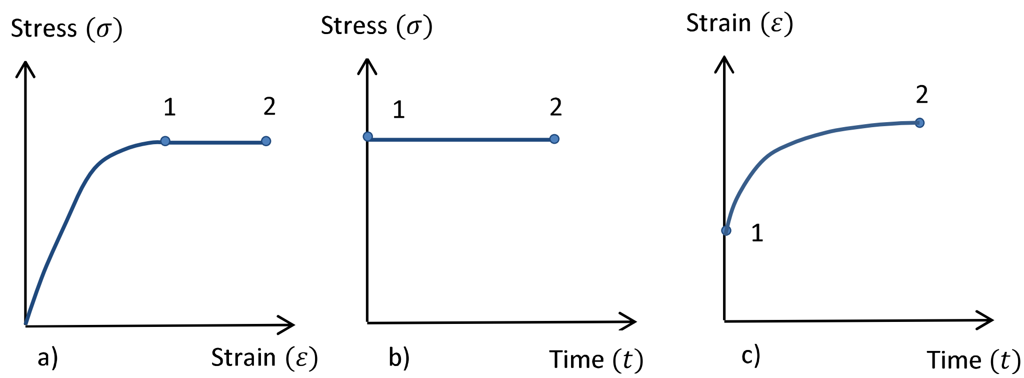

Figure 2.1 – Creep test performed at a low stress level: (a) Stress-Strain relationship; (b) Stress history; (c) Strain history

Stages of Creep Process

Creep test results can be plotted either in a strain-time diagram or logarithm of strain rate-logarithm of time diagram as shown in Figure 2.2. The creep response can be divided into three parts: 1 - Primary creep or transient creep, i.e. the creep during which the strain rate decreases with time; 2 - Secondary creep or stationary creep, i.e. the creep with nearly a constant rate; and 3 - Tertiary creep or acceleration creep, i.e. the creep which the strain rate increases with time. The tertiary creep eventually leads to failure of the soil, i.e. creep rupture. This will be discussed in more details in Section 2.5.

In triaxial creep tests, it is necessary to distinguish drained tests from undrained tests. In drained creep tests, the effective stresses, i.e. the mean effective stress p' and the deviatoric stress q, are kept constant. In undrained creep tests, p' decreases due to increase in pore pressure, while the deviatoric stress q remains constant. Hence, the drained creep represents a pure creep process (Augustesen *et al.*, 2004).

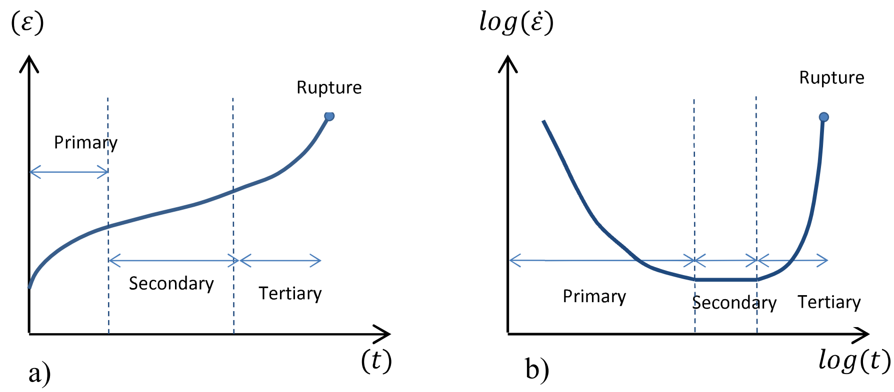

Figure 2.2 – Creep stages for a creep test performed by a triaxial apparatus: (a) Strain versus Time; (b) log Strain rate versus log Time

Interaction between Consolidation and Creep

The rate of secondary compression, i.e. creep, is controlled by the viscous resistance of the soil structure, whereas, the rate of primary consolidation is controlled by hydrodynamic lag, that is how fast the water can escape from the soil. Ladd *et al.* (1977) reported two well-known approaches in estimating secondary compression, i.e. hypotheses A and B. Hypothesis A, adopted by Mesri and Choi (1985a, 1985b), assumes that during pore pressure dissipation, there is no time-dependent creep in soil. Therefore, the secondary compression (creep) occurs only after primary consolidation. Hypothesis B, adopted by Suklje (1957), Wahls (1962), Bjerrum (1967), Leroueil *et al.* (1985) and Yin (1999), assumes that creep occurs during the whole consolidation process, i.e. the time-dependent strains also appear during the primary consolidation. Figure 2.3 demonstrates the strain development over time for both hypotheses A and B. Based on the experimental study proposed by Aboshi (1973), the real soil behaviour is located somewhere between these two extreme hypotheses.

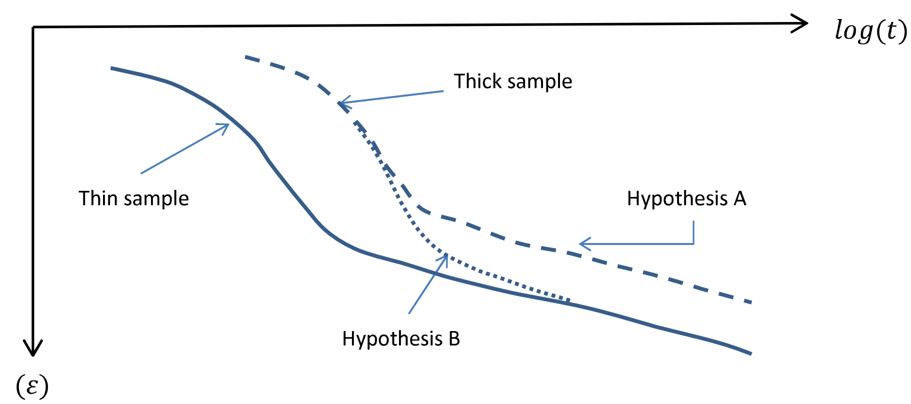

Figure 2.3 – Predicted Strain-Time curves for hypotheses A and B (after Augustesen *et al.*, 2004)

There exists some experimental evidence suggesting that creep occurs during primary consolidation (Leroueil *et al.*, 1985; Imai and Tang, 1992; Yin, 1999). The pore pressure may either dissipate, with accompanying volume change if drainage is allowed, or change slowly during creep or stress relaxation, if drainage is prevented. Creep deformation depends on the effective stress path followed and any changes in stress with time. Time-dependent volumetric response is governed both by the rate of volumetric creep and by the rate of consolidation. Because the effective stress path is controlled by the rate of loading and drainage conditions, the separation of consolidation and creep deformation can be quite difficult in the early stage of time-dependent deformation. In some cases, a fully coupled analysis of soil-pore fluid interaction with an appropriate time-dependent constitutive model is necessary to reconcile the time-dependent deformations observed in the field and laboratory (Mitchell and James Kenneth, 2005).

Effect of Stress Levels to Creep

The creep is observed at all levels of deviatoric stress. An increase in deviatoric stress level results in an increase in the rate of creep. At low levels of deviatoric stress, creep deformations are generally insignificant and cease after a certain period of time. At moderate levels of deviatoric stress, creep continues for long periods of time, with the general observation of decreasing strain rate with time. Above a certain level of deviatoric stress approaching the strength of the material, the creep initially occurs at a decreasing strain rate, then after a period of time the strain rate increases and becomes very large resulting in the failure of soil, i.e. creep rupture (Figure 2.4).

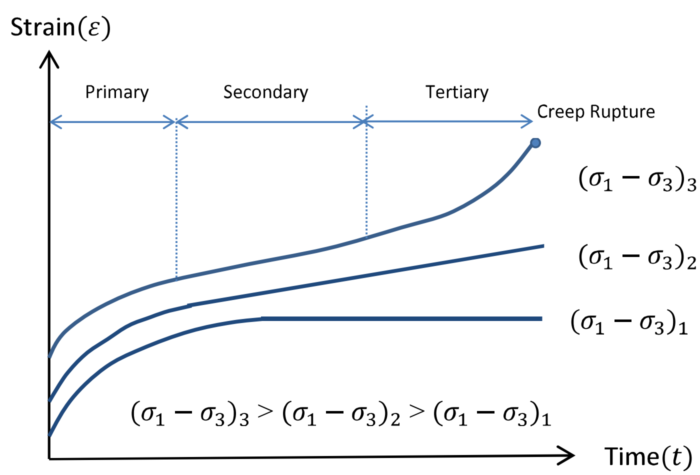

Figure 2.4 – Typical creep behaviour of soils under a constant stress

Volume Change and Pore Pressure

Pore pressure may increase, decrease or remain constant during creep, depending on the volume change tendencies of the soil structure and whether or not drainage occurs during the deformation process. Saturated soft sensitive clays under undrained conditions are most susceptible to strength loss during creep due to the reduction in effective stress caused by increase in pore water pressure with time. Many researchers have conducted extensive undrained creep tests on cohesive soils such as Osaka clay (Murayama and Shibata, 1958), San Francisco Bay mud (Arulanandan *et al.*, 1971), and Mascoushe clay from Quebec (Leroueil and Marques, 1996). Figure 2.5 shows the typical results of undrained creep tests conducted by Murayama (1958).

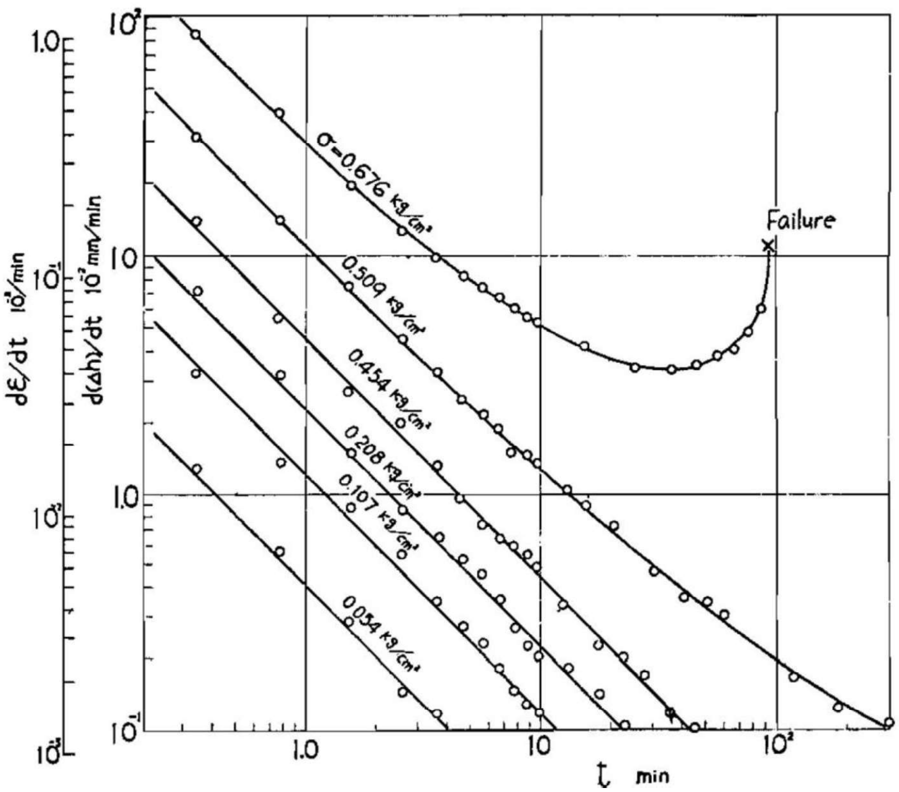

Figure 2.5 – Strain rate versus Time relationships during undrained creep of Osaka alluvial clay (after Murayama and Shibata, 1958)

Shear Creep and Volumetric Creep

Due to the known coupling effects between shearing and volumetric viscoplastic deformations in soils, an increase in either mean pressure or deviator stress can generate both types of deformations. Creep behaviour is also no exception. Time-dependent shear deformation under constant effective stress is usually referred to as deviatoric creep or shear creep, while time-dependent volume change under constant stress referred to as volumetric creep. Secondary compression is a special case of volumetric creep.

2.2.2. Stress Relaxation

Stress relaxation is a time-dependent decrease in stress at constant strain. Figure 2.6 shows a stress relaxation test with a stress path from point 1 to point 2 (1→2). At Point 1, the stress relaxation process is initiated by keeping the total strain constant over time. As time goes by, the stress-strain state moves toward Point 2. During this process, the stress is gradually decreasing, which is called stress relaxation (Figure 2.6c).

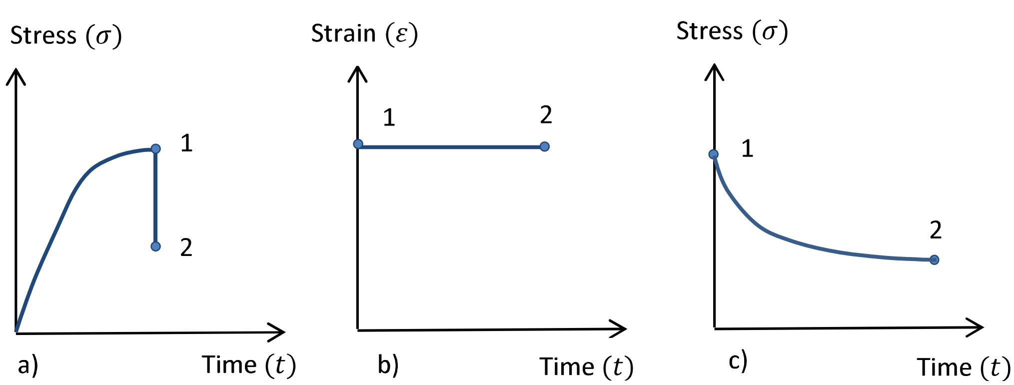

Figure 2.6 – Stress relaxation test: (a) Stress-Strain relationship; (b) Strain history; (c) Stress history

Lacerda and Houston (1973) studied stress relaxation in several clays (San Francisco Bay Mud, kaolinite, Monterey sand and Ignacio Valley Clay) under triaxial conditions. They found that the ratio between the deviator stress , q, at time t and the deviator stress at the beginning of stress relaxation , q_0, is linear with the logarithm of time after an initial time period (Figure 2.7).

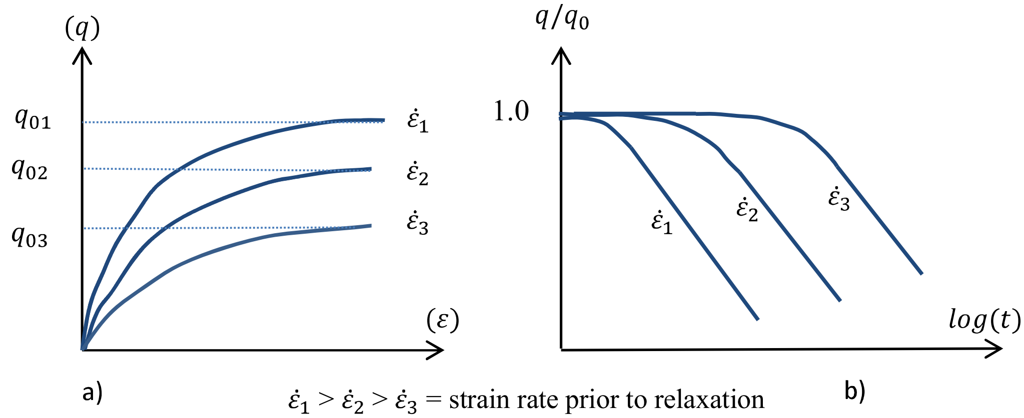

Figure 2.7 – Stress relaxation: (a) Stress-Strain diagram for three different relaxation tests; (b) Stress decay versus log Time for the stress relaxation tests.

Several undrained triaxial relaxation tests on soft overconsolidated clay were performed by Silvestri *et al.* (1988). They observed that the deviator stress reached the final relaxation level after a period of time of less than one day. They suggested that the curve joining these relaxed stress states would represent a ‘‘static effective stress state’’ curve, which is similar to the term ‘‘static yield surface’’ in the Perzyna's overstress theory (Perzyna, 1963, 1966). They also observed nearly no increase in pore-pressure during undrained relaxation. This was also observed by Sheahan *et al.* (1994) and Zhu *et al.* (1999) who conducted similar undrained relaxation tests on different soils. Lacerda and Houston (1973) also observed that the variation of excess pore water pressure during the undrained stress relaxation tests was practically zero. Similar observations were reported by Murayama and Shibata (1961). Figure 2.7 schematically shows the influence of strain rate on the results of stress relaxation tests. It is seen that the strain rate prior to the relaxation affects the time at which stress relaxation begins. It can be observed that the lower the strain rate, the more time delay prior to the initiation of deviator stress decay (Lacerda and Houston, 1973).

For sands, there have been limited investigations on stress relaxation. Matsushita (1999) observed a considerable amount of stress relaxation in triaxial tests on Hostun and Toyoura sands. Mitchell and James Kenneth (2005) reported that the relaxation behaviour of clays and sands are generally similar.

2.2.3. Strain Rate Dependency

The rate dependency was investigated extensively in the past few decades. It has been shown that the strain rate has great influence on the stress-strain behaviour of clays. There are two different strain rate dependency testing methods: constant and variable rates of strain tests.

2.2.3.1. Constant Rate of Strain (*CRS*) *Tests*

In a constant rate of strain test, the total strain rate is kept constant throughout the experiment. The stress is then measured and stress-strain relation is plotted. Figure 2.8 schematically shows a constant rate of strain test results with a strain rate $\dot{\varepsilon}$ ($\dot{\varepsilon}_1 < \dot{\varepsilon}_2 < \dot{\varepsilon}_3$). There is a general observation that the faster the loading rate, the higher the effective stress for a certain strain. In other words, the larger the strain rate, the stiffer the soil.

Leroueil *et al.* (1985) conducted a series of constant strain rate tests, in one-dimensional and triaxial conditions, on Batiscan clay to investigate the time-dependent behaviour of soils. Figure 2.9 shows the results of the CRS oedometer tests on the clay. As observed in the figure, there is a unique relationship between the vertical effective stress, strain and strain rate ($\sigma'_z - \varepsilon_z - \dot{\varepsilon}_z$).

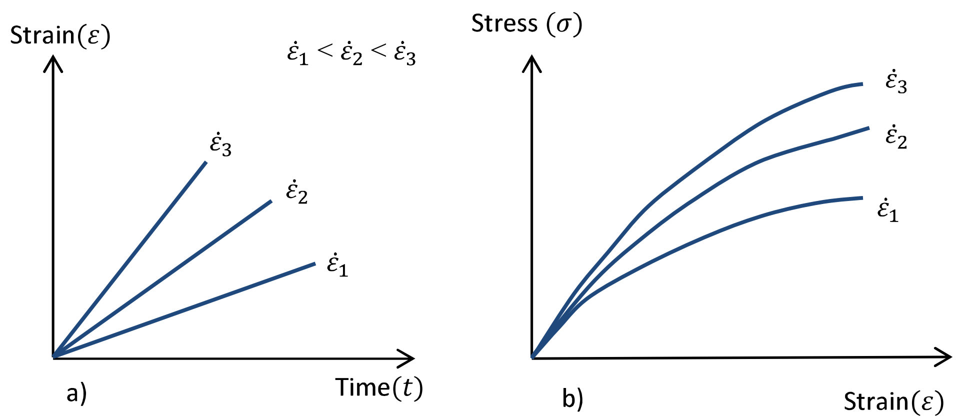

Figure 2.8 – Constant rate of strain (CRS) tests: (a) Strain history, and (b) Stress-Strain response

Figure 2.10 shows the effect of strain rate on the stress-strain behaviour of overconsolidated Leda (Saint-Jean-Vianney) clay. The undrained CRS tests were conducted by Vaid *et al.* (1979). It can be observed that the greater the strain rate, the greater the peak deviatoric strength.

Figure 2.11 schematically shows the influence of strain rate on peak strength and the size of the yield surface. As seen in Figure 2.11(a), a stress-strain curve can be assumed for the case with a constant strain rate approximately zero and with the peak strength q_0. The corresponding yield surface, in Figure 2.11(b), is denoted as 'static yield surface'. This 'static yield surface' is one of the major elements in the constitutive models developed based on Perzyna's overstress theory, which are reviewed in details in the next section.

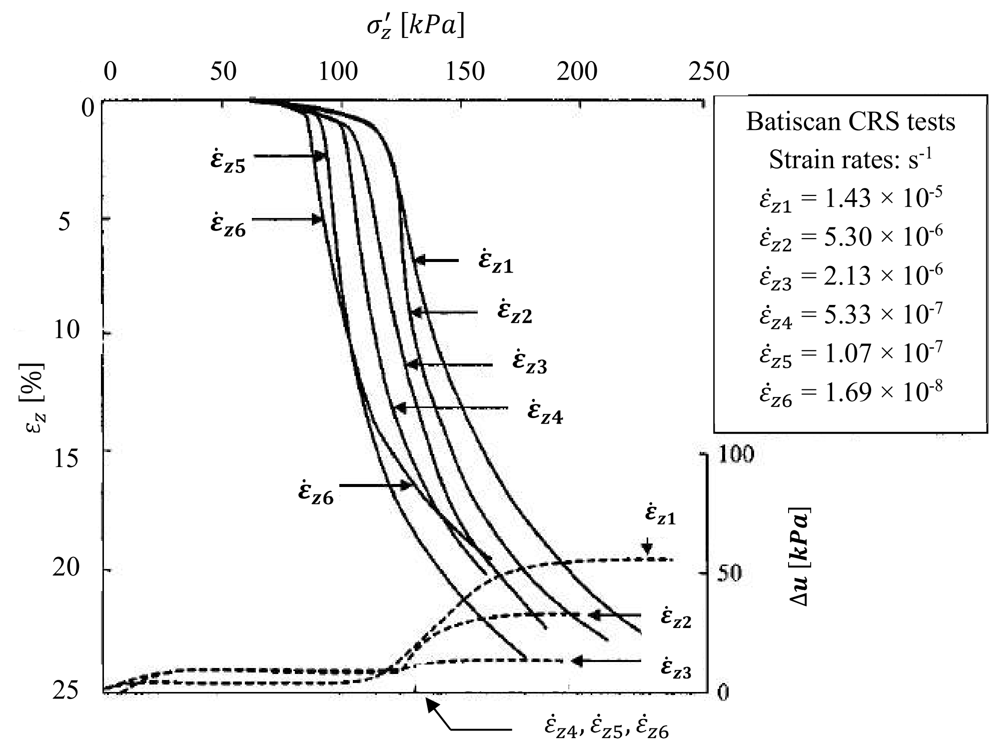

Figure 2.9 – The results of the constant rate of strain tests on Batiscan clay (after Leroueil *et al.*, 1985)

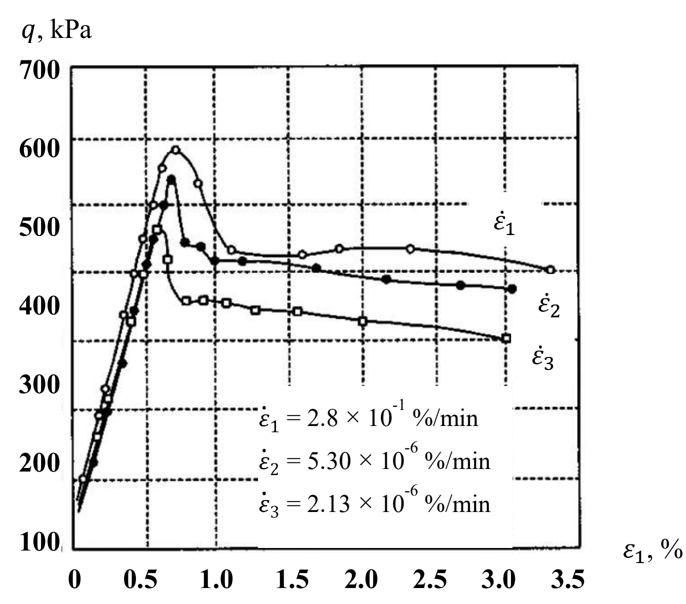

Figure 2.10 – Stress-Strain behaviour of Saint-Jean-Vianny Clay in undrained constant rate of strain tests (after Vaid *et al.*, 1979)

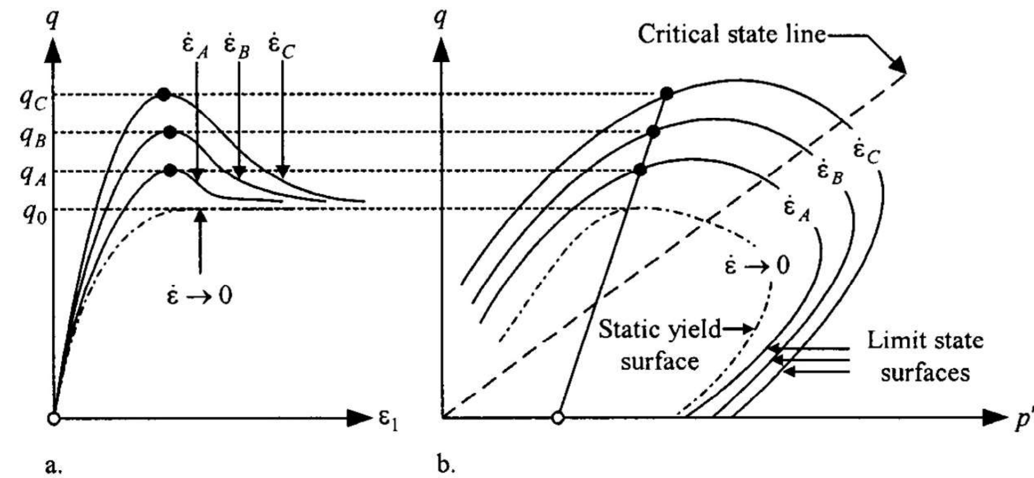

Figure 2.11 – (a) Drained Stress-Strain curves for different constant rate of strain tests (q_A, q_B, q_C are peak strengths), (b) Strain rate effect on yield surface (after Augustesen *et al.*, 2004)

2.2.3.2. Change of Rate of Strain

The existence of a unique relationship between the vertical effective stress, strain and strain rate can be confirmed by special CRS tests in which the strain rates are changed at various strain. Two such tests were performed by Leroueil *et al.* (1985) on Batiscan clay. The results show that the effect of change in strain rate is continuous and the soil stays on the same stress-strain curve until the strain rate is changed again (Figure 2.12).

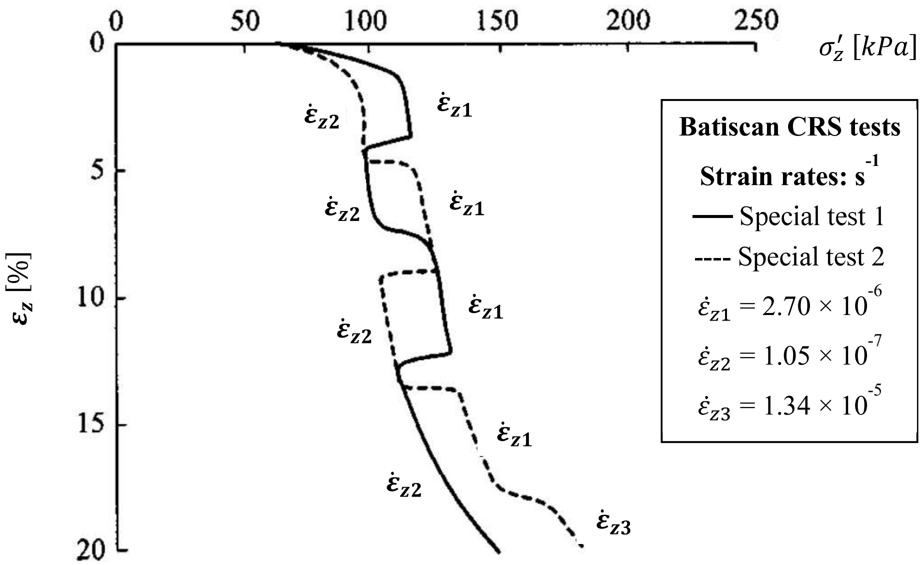

Figure 2.12 – Special constant rate of strain oedometer tests conducted by Leroueil *et al.* (1985) on Batiscan clay.

2.3. Modelling of Time-Dependent Behaviour of Soils

To simulate the time-dependent behaviour of geomaterials, various mathematical models have been developed over the past few decades. There are three main approaches developed to describe time-dependent behaviour of soils: the empirical models, the rheological models and the constitutive elasto-viscoplastic models.

2.3.1. Empirical Models

The phenomenological approach utilises the results of laboratory testing to develop empirical equations that describe the time-dependent behaviour of soil. They are widely applied in engineering practice because of their simplicity. The empirical models are categorised as primary and secondary empirical relations (Liingaard *et al.*, 2004).

2.3.1.1. *Primary Empirical Models*

The primary empirical models are obtained by directly fitting the observed test data with simple mathematical functions. They reflect actual observed soil behaviour and are often restricted to specific phenomena. Most of the empirical models are based on the semilogarithmic law of creep in which the secondary compression observed in oedometer tests is plotted against the logarithm of time. The coefficient of secondary compression is generally used to describe the magnitude of the creep strains.

One of the simplest models is based on the concept of constant coefficient of secondary compression $C_{\alpha e}$ or $C_{\alpha\varepsilon}$, defined by Raymond and Wahls (1976), Mesri and Godlewski (1977) and Terzaghi and Karl (1996) as:

$$C_{\alpha e} = \frac{\Delta e}{\Delta logt} \qquad \text{or} \qquad C_{\alpha\varepsilon} = \frac{C_{\alpha e}}{1+e_i} \tag{2.1}$$

where e_i is the initial void ratio, Δe is the change in void ratio and $C_{\alpha e}$ and $C_{\alpha\varepsilon}$ are the coefficients of secondary compression with respect to e and ε.

Ladd *et al.* (1977) introduced the modified secondary compression strain index $C_{\alpha\varepsilon}$ to estimate the secondary settlement:

$$C_{\alpha\varepsilon} = \frac{C_\alpha}{1+e_0} \qquad \text{and} \qquad s_s = C_{\alpha\varepsilon} H_0 \log\frac{t}{t_p} \tag{2.2}$$

In the simplest form, the coefficient of secondary compression is assumed constant for one specific soil. If this is evaluated in terms of vertical creep strains, the increase in secondary compression for a given soil can be written as

$$\varepsilon_z = C_{\alpha\varepsilon}\log\left(1+\frac{t}{t_i}\right) \tag{2.3}$$

in which ε_z is the vertical strain, t is time and t_i is the reference time. One of the major difficulties with this approach is the necessity for defining a start point for the creep deformation, i.e. determining the reference time t_i.

Walker and Raymond (1968) reported that the secondary compression rates in laboratory tests on sensitive Leda clay are linearly dependent on the compression index C_c over the entire effective stress range, with an average value of C_α/C_c of about 0.025. The compression index is defined as

$$C_{ce} = \frac{\Delta e}{\Delta log(\sigma'_z)} \quad \text{or} \quad C_{c\varepsilon} = \frac{C_{ce}}{1+e_i} \tag{2.4}$$

where e_i is initial void ratio; σ'_z is vertical effective stress; and C_{ce} and $C_{c\varepsilon}$ are compression indices with respect to e and ε, respectively.

Mesri and Godlewski (1977) found that C_α is dependent on the applied effective stress σ'_z and is related to the preconsolidation pressure. Both C_c and C_α increase as the effective stress approaches the preconsolidation pressure, then reach a maximum at or just beyond the preconsolidation, and then remain reasonably constant. Throughout these effective stress changes, the ratio C_α/C_c remains approximately constant.

However, C_α does not remain constant with time. The concept where the creep parameter varies with time has been presented by Yin (1999). He presented a new creep function that is capable of describing the nonlinear creep behaviour as a function of time, all within the framework of the logarithmic law:

$$\varepsilon_z = \frac{\psi}{\nu} ln\left(\frac{t + t_0}{t_0}\right) \tag{2.5}$$

where ψ/ν is identified as

$$\frac{\psi}{\nu} = \frac{\psi'_0}{1 + \left(\frac{\psi'_0}{\varepsilon_\infty}\right) ln\left(\frac{t + t_0}{t_0}\right)} \tag{2.6}$$

in which $\nu = 1 + e$ is the specific volume. If the ratio $^{\psi}/_{\nu}$ is a constant, Equation (2.6) simplifies to the traditional logarithmic law.

Singh and Mitchell (1968) proposed a simple three-parameter phenomenological equation based on the analysis of drained and undrained triaxial creep tests on various clays. The model is capable of describing either fading or nonfading creep. Lacerda and Houston (1973) applied the three-parameter model of Singh and Mitchell (1968) to describe the relationship between stress relaxation and creep parameters. However, this type of models is limited to prediction under one-dimensional conditions and is only valid for the first time loading.

Prevost (1976) developed a phenomenological approach to describe saturated clays under undrained triaxial conditions. The model is capable of describing nonlinear stress relaxation relations in $(q\sim\log(t))$ space. The model then was applied by Silvestri (1988) for interpreting the results of undrained stress relaxations tests on a soft sensitive clay. However, again this model is also restricted to one-dimensional conditions.

The main feature of the logarithmic law models is their simplicity. However, they oversimplify the volumetric confined creep of soil because of the assumption of constant coefficient of secondary compression. When time tends toward infinity, the strains tend toward infinity as well. Consequently, the logarithmic law may overestimate the long-term creep settlements. Another limitation is that it is strictly valid only for conditions that are identical to those of tests from which they have been derived, i.e. one-dimensional conditions (Liingaard *et al.*, 2004).

2.3.1.2. Secondary Semi-empirical Models

The secondary semi-empirical models are the class of models obtained by combining one or more primary models. The models can be defined as stress–strain–time or stress–strain–strain-rate models. Using this approach, both creep and stress relaxation phenomena can be captured with one particular model.

One of the first multiaxial stress-strain-time constitutive models was proposed by Kavazanjian and Mitchell (1977). They presented a model for general stress-strain-time behaviour of fine-grained soils. The volumetric and deviatoric models are assumed to have instantaneous and delayed components of the strain. The volumetric part is based on the logarithmic law for secondary compression with the assumption that $C_{\alpha\varepsilon}$ is approximately constant under normally consolidated conditions. The delayed volumetric component can be written as

$$\dot{\varepsilon}_{v} = \frac{C_{\alpha\varepsilon}}{\ln(10)}\frac{1}{t} \quad (2.7)$$

where $\dot{\varepsilon}_v$ is the delayed volumetric strain rate and $C_{\alpha\varepsilon}$ is the coefficient of secondary consolidation.

Tavenas *et al.* (1978) also divided creep deformations into volumetric and deviatoric components. Based on the results of creep tests on lightly overconsolidated clay, they concluded that the development of both volumetric and shear strains with time can be represented as

$$\dot{\varepsilon}_v = Bf(\sigma'_{ij})\left(\frac{t_i}{t}\right)^m \tag{2.8}$$

and

$$\dot{\varepsilon}_q = Ag(\sigma'_{ij})\left(\frac{t_i}{t}\right)^m \tag{2.9}$$

where $f(\sigma'_{ij})$ and $g(\sigma'_{ij})$ are the functions of the current state of effective stress σ'_{ij}; A and B are soil properties that reflect composition, structure and stress history and m is the parameter that controls the rate at which the strain rate decreases with time. Based on the shapes of the contour lines for equal strain rates at t = 100mins, Tavenas *et al.* (1978) suggested that the stress functions $f(\sigma'_{ij})$ and $g(\sigma'_{ij})$ should be expressed in terms of the limit state surface, i.e. yield surface. This has been further studied by several researchers including Feda (1992), Lade and Liu (1998) and Tatsuoka (2000).

The effect of time on the compressibility of clay in terms of secondary compression was first studied by Buisman (1936). Later, Taylor (1942) reported that there is a family of stress-strain curves for one-dimensional compression of clay. Bjerrum (1967) presented a secondary empirical model for settlement analysis of normally and lightly overconsolidated clay. He confirmed the observations by Taylor (1942) that there is not a single stress-strain curve for one-dimensional compression of clay, but a family of curves, called 'time lines'. Each curve corresponds to a different duration of the applied load in a standard oedometer test (Figure 2.13). Bjerrum (1967) proposed that the delayed compression can be described by parallel lines in an $(e - log\sigma'_z)$ diagram representing a series of equilibrium relationships after different time periods of sustained loading.

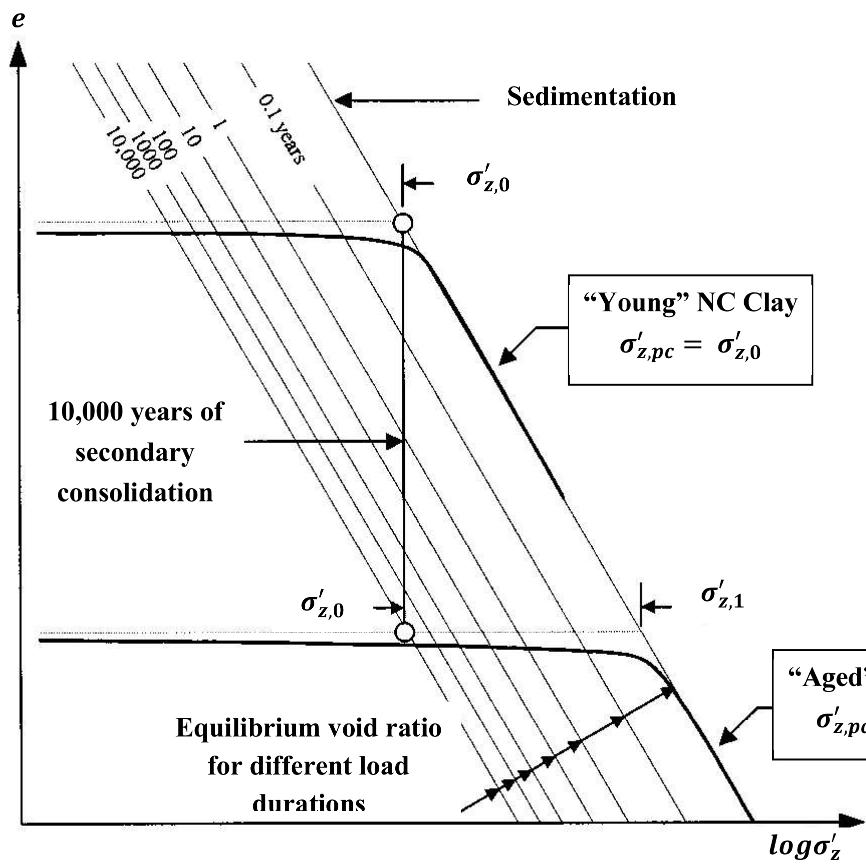

Figure 2.13 – Geological history and compressibility of young and aged normally consolidated clay (after Bjerrum and Aitchison, 1973)

The Bjerrum's model was formulated in terms of logarithmic functions as:

$$e = e_0 - e^e - e^{ep} - e^c \tag{2.10}$$

and

$$e = e_0 - C_{re}\log\left(\frac{\sigma'_{z,pc}}{\sigma'_{z,0}}\right) - C_{ce}\log\left(\frac{\sigma'_z}{\sigma'_{z,pc}}\right) - C_{\alpha e}\log\left(\frac{t_i + t}{t_i}\right) \tag{2.11}$$

where e is the void ratio, e_0 is the initial void ratio, $\sigma'_{z,pc}$ is the vertical preconsolidation stress, $\sigma'_{z,0}$ is the initial vertical effective in situ stress, σ'_z is the current vertical effective stress, t_i is the reference time and t is the elapsed time. The superscript e, ep and c denote elastic, elastic-plastic and creep, respectively.

Garlanger (1972) developed the characteristics of Bjerrum's concept in terms of the well-known recompression, compression and secondary compression indices. The elasto-viscoplastic models proposed by Yin and Graham (1989, 1994, 1999) and Yin *et al.* (2002) were developed based on Bjerrum's concept of delayed compression and Cam clay/modified Cam clay models.

The Bjerrum's model is based on the assumption that the change in void ratio is composed of three components: elastic change (e), the time-independent elastic-plastic (ep) reaction of the soil skeleton to effective stress changes, and the time-dependent change at constant effective stress (c). However, as pointed out by Zienkiewicz and Cormeau (1974), separate handling of time-dependent deformations from plastic deformations is questionable because only the combined effects may be measurable. Bjerrum's model is also based on the logarithmic law, whose limitations were discussed before.

2.3.2. Rheological Models

The terminology 'rheological models' is often used when describing linear viscoelastic behaviour of materials. The rheological models are typically developed for metals, steel and fluids. However, they are to some extent used in the study of time effects in geomaterials. In this subsection, three well-known models for geomaterials are presented: the Maxwell model, the Kelvin-Voigt model and the Bingham model.

In this type of models, the elastic, plastic and viscous properties of material are represented by elementary models of spring, slider and dashpot, respectively (Figure 2.14). The constitutive relations of soil are obtained by combining the elementary models together. Two simple viscoelastic spring and dashpot models are the Maxwell model and Kelvin-Voigt model, which can describe viscous and elastic behaviours of the material. The Maxwell model consists of a spring and a dashpot in series. The Kelvin-Voigt model is comprised of a spring and a dashpot in parallel. Another well-known viscoplastic model is Bingham model which consists of a parallel unit composed of a dashpot, a plastic slider and a linear spring connected in series.

Using the Maxwell model, stress decays exponentially with time at constant deformation, i.e. stress relaxation. However, the model does not predict creep accurately. Using the Maxwell model, the strain increases linearly with time under constant stress condition, while the creep behaviour of materials shows the decrease of strain rate with time. On the other hand, the Kelvin–Voigt model depicts creep reasonably well, but with regards to stress relaxation, the model is much less accurate. These two models are used to predict the viscoelastic response of the materials. To model the plastic behaviour of the materials, special attention is paid to Bingham model.

The Bingham model consists of two components, i.e. time-independent and time-dependent components, which are combined in series. The time-independent part consists of the spring with spring constant E, denoted the elastic element. The time-dependent part consists of the dashpot with coefficient of viscosity η and the plastic slider with a threshold stress σ_y combined in parallel, denoted the viscoplastic element (Figure 2.15). Figure 2.16 schematically shows the creep, stress relaxation and strain-rate response modelled by Bingham model.

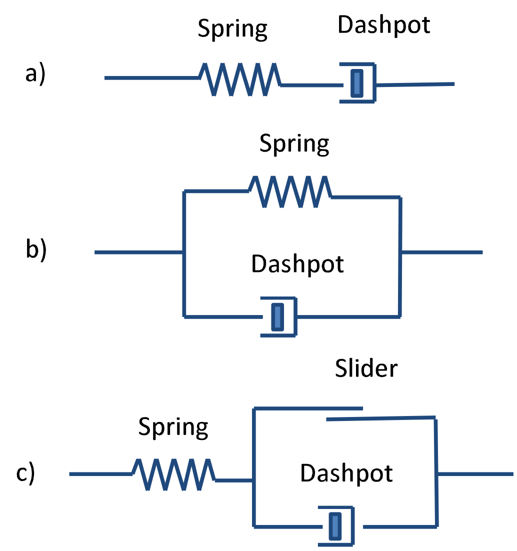

Figure 2.14 – Rheological Models: (a) Maxwell model; (b) Kelvin-Voigt model and (c) Bingham model

These mathematical models provide some insight into creep and relaxation characteristics of viscoelastic response, but they may not represent quantitative behaviour of any real geomaterials. The spring, the dashpot and the slider are assumed to describe linear constitutive relations. However, soils show highly nonlinear elastic and plastic behaviour. Singh and Mitchell (1968) reported the limitations of the rheological models, i.e. 1 – too many parameters are required to characterise the strain rate behaviour; 2 – approximations on the governing equations are necessary in order to model the time-dependent behaviour.

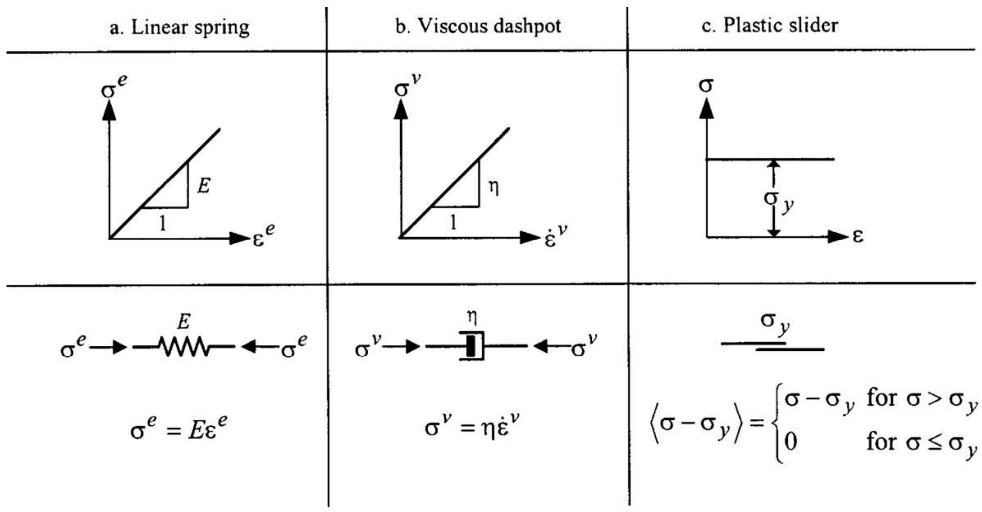

Figure 2.15 – Schematic representation of elementary material models: (a) Hookean spring; (b) Newtonian dashpot; and (c) Saint Vernant's slider (after Liingaard *et al.*, 2004)

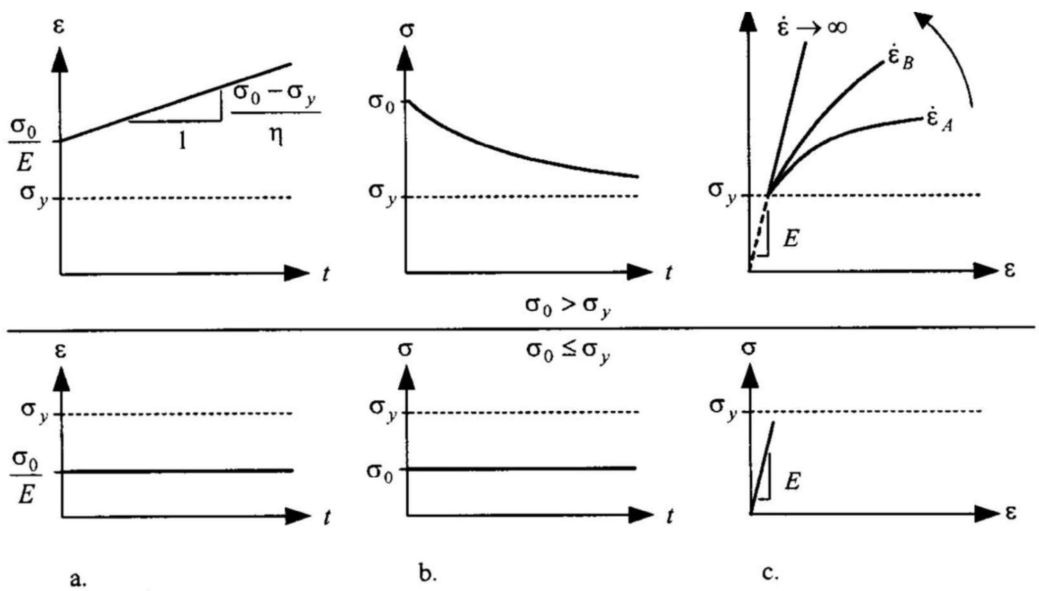

Figure 2.16 – Response of a Bingham model: (a) Response for creep; (b) Response for relaxation; and (c) Response for constant rate of strain (after Liingaard *et al.*, 2004)

2.3.3. Stress–Strain–Strain-rate Models

Since the 1970s, along with rapid development of soil constitutive models, elasto-viscoplastic (EVP) models have been developed to cover the deficiency of the traditional constitutive models in capturing the rate-dependent behaviour. The EVP models are mainly developed based on the theory of plasticity and the critical state theory. In these models, potential surfaces are defined for modelling the inelastic deformations of materials. One of the advantages of EVP models is that they can be readily implemented into numerical methods like Finite Element Method, as the framework is consistent with that of conventional plasticity.

A number of elasto-viscoplastic (EVP) models have been proposed to capture time-dependent behaviour of soils. They were developed mainly based on either the overstress theory (Perzyna, 1963, 1966) or the nonstationary flow surface theory (Naghdi and Murch, 1963; Olszak and Perzyna, 1970).

2.3.3.1. Overstress Models

The overstress approach (Perzyna, 1963, 1966) can be regarded as a generalisation of the model of Hohenemser and Prager (1932). The key assumption in this model is that viscous effects are neglected in the elastic region, i.e., no viscous strains occur within the static yield surface. In other words, the elastic strains are time independent whereas the inelastic strains are time-dependent. The overstress theory differs from the general plasticity theory because the consistency rule is not satisfied in the derivation of the final stress-strain relationships.

Two forms of the overstress function have been widely used: the exponential overstress function and the power overstress function. Adachi and Okano (1974), Adachi and Oka (1982) and Fodil *et al.* (1997) used the exponential overstress function in their models, while the models proposed by Hinchberger and Rowe (2005) and Yin *et al.* (2010) are based on the power overstress function. The overstress models can capture the strain rate influence on the soil strength and preconsolidation pressure.

Following the Perzyna's work, the overstress theory was widely applied to elasto-viscoplastic models describing the time-dependent behaviour of geomaterials. The model developed by Adachi and Okano (1974) and Adachi and Oka (1982) is capable of describing time-dependent behaviour of fully saturated normally consolidated clay. Later, Katona (1984) proposed a viscoplastic cap model for soils and rocks, and Oka *et al.* (1988) proposed a model to describe the behaviour of overconsolidated clay. Desai and Zhang (1987) introduced a viscoplastic model to describe the time-dependent behaviour of sand and rock salt. Kaliakin and Dafalias (1990a, 1990b) and Kutter and Sathialingam (1992) proposed viscoplasticity bounding surface models for cohesive soils. Other notable contributions include the overstress-type models of Matsui and Abe (1988), Hashiguchi and Okayasu (2000), Rocchi *et al.* (2003), and Yin and Graham (1989, 1994, 1999) and Yin *et al.* (2002).

The main difficulty in the overstress-type models surrounds the arbitrariness of the overstress function. In addition, they do not satisfy the consistency condition and cannot be reduced to the rate independent elasto-plastic formulation for the limiting case of the fluidity parameter approaching infinity (Simo *et al.*, 1988). The overstress models are also limited in describing the tertiary creep (Oka *et al.*, 1994), i.e. creep at an accelerating strain rate leading to creep failure, unless be introducing a stress-state-dependent viscoplastic parameter, damage effect, or de-structure due to straining (Adachi *et al.*, 1987; Al-Shamrani and Sture, 1998; Yin *et al.*, 2011; Jiang *et al.*, 2017). This deficiency has been rectified in nonstationary-type models which are able to predict undrained tertiary creep in normally-consolidated clays (e.g. Sekiguchi, 1984). There was very few overstress type models can describe the tertiary creep process and creep rupture. For example, Adachi *et al.* (1987) modified the model proposed by Adachi and Oka (1982) so that it can describe the acceleration creep process and undrained creep rupture without changing the overstress based constitutive model. However, there is currently no model of creep that can rigorously capture drained creep rupture in over-consolidated clays. This is of particular relevance to natural and excavated slopes in which creep failures are most common. The drained creep-induced instability in such slopes generally occurs at stress levels less than the peak strength and develops as a result of a reduction of shear strength with time (Tavenas *et al.*, 1978; Lefebvre, 1981; Hunter and Khalili, 2000).

2.3.3.2. Nonstationary Flow Surface Models

The nonstationary flow surface (NSFS) theory is based on the basic concept of inviscid theory of elastoplasticity. The major difference between the NSFS theory and the conventional plasticity theory is the definition of the yield condition. In the classical plasticity theory, the yield surface is a function of effective stress state and plastic strains. Hence, the yield function does not change with time when the plastic strains are held constant, i.e. the yield surface in the conventional plasticity theory can be denoted as "stationary".

$$f\left(\sigma'_{ij}, \varepsilon_{ij}^{p}\right) = 0 \tag{2.12}$$

where σ'_{ij} is the effective stress and ε_{ij}^{p} is the plastic strains.

In NSFS theory, the yield condition is time dependent. The flow surface then is defined as "nonstationary"

$$f\left(\sigma'_{ij}, \varepsilon_{ij}^{vp}, \beta\right) = 0 \tag{2.13}$$

where ε_{ij}^{vp} is the viscoplastic strain and β is a time-dependent function.

The NSFS theory was first introduced by Naghdi and Murch (1963) and extended later by Olszak and Perzyna (1966) and Olszak (1970). The NSFS models proposed by Sekiguchi (1977), Sekiguchi (1984), Matsui and Abe (1985, 1986, 1988) and Matsui *et al.* (1989) are capable to describe creep behaviour of normally consolidated clay under undrained conditions. The model proposed by Dragon and Mroz (1979) can capture the creep behaviour of rocklike materials, while the model developed by Nova (1982) is mainly for normally consolidated clay. More recently, the models proposed by Qiao *et al.* (2016) and Kavvadas and Kalos (2019) based on NSFS theory are capable to capture the time-dependent behaviour of geomaterials. Qiao *et al.* (2016) developed a viscoplastic model based on both the NSFS theory and the unique stress–strain–strain-rate concept. The unique stress–strain–strain-rate concept was also used by Laloui *et al.* (2008) and De Gennaro and Pereira (2013) in their models to reproduce the viscoplastic behaviour of soils.

According to Heeres *et al.* (2002), the NSFS theory achieve a higher convergence rate compared to overstress based models. However, as pointed out by Liingaard *et al.*

(2004), the NSFS type models are unable to describe the relaxation process or the creep process when it is initiated form a stress state inside the yield surface.

Unique Stress–Strain–Strain-rate Relationships Concept

The concept of the existence of a unique relationship between the current state of stress and strain for a given constant strain rate was proposed by Suklje (1957). Following early works of Šuklje (1957), Leroueil *et al.* (1985) demonstrated in experiments that the time-dependent behaviour of clays subjected to one-dimensional compression can be described by a unique stress–strain–strain-rate relationship. Leroueil *et al.* (1985) experimentally investigated the time-dependent behaviour of various types of clays by conducting multiple stage loading tests, constant rate of strain tests, controlled hydraulic gradient tests and long-term creep tests. This concept was also confirmed by Kabbaj *et al.* (1988), Edil *et al.* (1994), Hanson *et al.* (2001), Lo and Morin (1972) and Leroueil and Marques (1996).

This concept assumes that there is a unique relationship between the effective stress, the strain and the strain rate. This unique relationship can be simply described by two equations

$$\sigma'_v = \sigma'_q g(\varepsilon_v) \tag{2.14}$$

and

$$\sigma'_y = f(\dot{\varepsilon}_{vol}) \tag{2.15}$$

where σ'_v is the effective vertical stress, ε_v is the vertical strain and $\dot{\varepsilon}_{vol}$ is the volumetric strain rate. It is noted that normally consolidated lines obtained at different strain rates have the same slope in the (e~logσ'_v) plane, i.e. the compression index is strain rate independent. The stress–strain–strain-rate relationship is depicted in Figure 2.17.

The compression lines at different volumetric strain rates are parallel, and they become a unique line when they are normalized to their corresponding apparent preconsolidation pressures. The apparent preconsolidation pressure increases with the volumetric strain rate and a unique relationship can be used to describe this dependency.

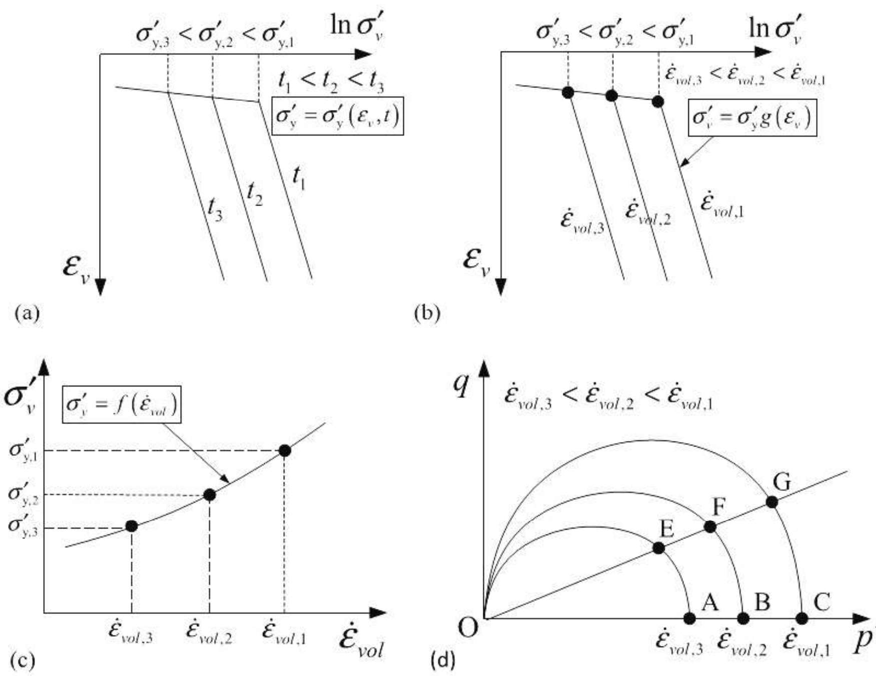

Figure 2.17 – Schematic illustration of (a) stress–strain–time behaviour in the oedometer test; (b) & (c) stress–strain–strain-rate behaviour in oedometer test; and (d) strain rate effect in the general stress space (after Qiao *et al.*, 2016)

2.4. Constitutive Modelling of Unsaturated Soils

The stress-strain behaviour of unsaturated soil is complex due to simultaneous flow of air and water and their complex interaction with the solid skeleton. The early theoretical and experimental investigations of unsaturated soils were reported by Bishop

(1959) and Bishop and Blight (1963) on the applicability of the effective stress equation to describe the volume change and shear strength characteristics of unsaturated soils. However, Jennings and Burland (1962) questioned the validity of the effective stress in unsaturated soils arguing that it cannot explain the collapse phenomenon upon wetting. The controversy stimulated the significant increase in research of unsaturated soils both in experimental works and constitutive modelling. Although the development of constitutive models for the behaviour of unsaturated soils has been behind that of saturated soils, the behaviour of unsaturated soils has been the subject of great interest in the last few decades.

Fredlund and Morgenstern (1977) suggested that the constitutive behaviour of unsaturated soils can be described using two independent stress variables, i.e. net stress and matric suction, rather than a single effective stress. Several constitutive models have been developed based on the two stress state variables approach. Notable models using extensions of Cam-Clay-type models in a critical state framework, are proposed by Alonso *et al.* (1990), Wheeler and Sivakumar (1995) and Cui and Delage (1996). These models can capture many of the behavioural characteristics of unsaturated soils, including the dependence of the size of yield surface on suction and volumetric collapse upon wetting, and simulate the stress-strain behaviour of some laboratory test results. However, they fail to reproduce some other important characteristic features of unsaturated soils such as the elastic response followed by the plastic response observed in normally consolidated clays subjected to increasing values of suction. They are also unable to capture the behaviour of unsaturated soils at suction values below the air entry suction. Another major difficulty with the two-stress state approach is that it requires determination of two sets of material parameters, one for each of the stress state variables, which in fact may not be independent, and lead to intractable stress-strain relationships.

Later, Loret and Khalili (2000) and Loret and Khalili (2002) proposed a comprehensive framework for a three phase porous medium formulated based on the effective stress principle for constitutive modelling of unsaturated soil. In the model, suction was incorporated into the effective stress using the relationship established by Khalili and Khabbaz (1998). The model can reproduce the experiments proposed by Alonso *et al.* (1990), Wheeler and Sivakumar (1995) and overcame all the above problems, including volumetric collapse upon wetting. Other remarkable constitutive models developed based on the effective stress concept are the works of Bolzon *et al.* (1996), Jommi (2000), Kogho *et al.* (2001), Sheng *et al.* (2003), Gallipoli *et al.* (2003), Laloui *et al.* (2003), Tamagnini (2004) and Russell and Khalili (2006).

All the mentioned constitutive models for unsaturated soils were developed within the framework of rate-independent plasticity. However, few contributions have tackled the problems associated with the time-dependent behaviour of unsaturated geomaterials. For examples, Oka *et al.* (2006) proposed an elasto-viscoplastic model for unsaturated soils considering the effect of suction based on an overstress-type of viscoplasticity with soil structure degradation. De Gennaro and Pereira (2013) presented a viscoplastic constitutive model to capture the coupled effect of strain rate and suction for chalk by using the isotach approach in the framework of elastoplasticity. Since the time-dependent behaviour of unsaturated soil plays an important role in many geotechnical problems such as natural slopes, man-made soil structures, it is essential to develop a comprehensive model to capture the time-dependent behaviour of unsaturated soils.

2.5. Tertiary Creep and Creep Rupture

Definition

Tertiary creep is the last phase among the three phases of creep process, where the strain rate accelerates until creep rupture occurs. In general, soils exhibit viscous behaviour. Figure 2.18 shows a typical creep curve with three phases of creep in strain-time plot. Rupture represents the terminal point on a creep curve. It is reasonable to consider that the rupture point must be related to the preceding portions or characteristics of the creep curve (Campanella and Vaid, 1974).

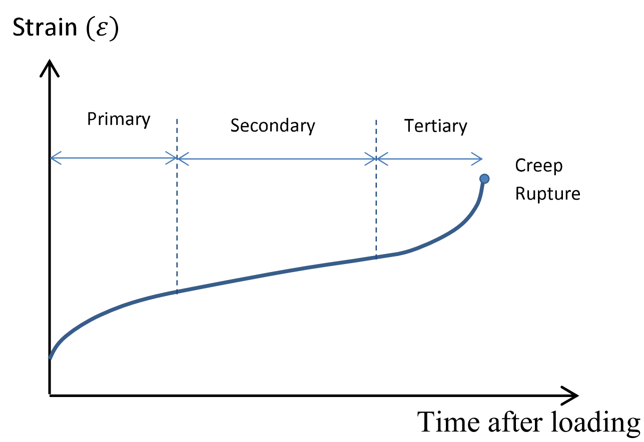

Figure 2.18 – Stages of creep under large deviator stress leading to creep rupture

The creep process is generally defined into three stages: primary creep, secondary creep and tertiary creep. However, Ter-Stepanian (1975) divided creep curve into only two phases: mobilization (the strain rate decreases with time) and rupture (the strain rate increases with time). Varnes (1982) also reported two phases of creep process as decelerating creep (primary creep) and accelerating (tertiary creep).

Sekiguchi (1984) showed that in primary creep, the deviatoric strain rate decreases, whereas in the tertiary creep, the deviatoric strain rate develops with accelerating rate and ultimately leads to failure. In between the primary and tertiary creep phases, there exists a stage at which the deviatoric strain rate takes a minimum, i.e. $\dot{\varepsilon} = \dot{\varepsilon}_{min}$ and $\ddot{\varepsilon} = 0$. This stage is called the secondary phase, which is shrunk to a single point on the creep curve as shown in Figures 2.19 and 2.20.

Kuhn and Mitchell (1993) also indicated that soils rarely evidence an extended period of secondary creep, and the strain rate either continuously decreases or increases until creep rupture takes place.

Reasons for Strength Loss during Creep

As pointed out by Mitchell (1993) , the loss of strength as a result of creep may be explained in terms of the following principles: 1) If a significant portion of the strength of a soil is due to cementation, and creep deformations cause failure of cemented bonds, then the strength will be lost. 2) In the absence of chemical or mineralogical changes, the strength depends on effective stresses. If creep causes changes in effective stress, then strength changes will also occur. 3) In almost all soils, shearing results in changes in pore pressure during undrained deformation and changes in water content during drained deformation.

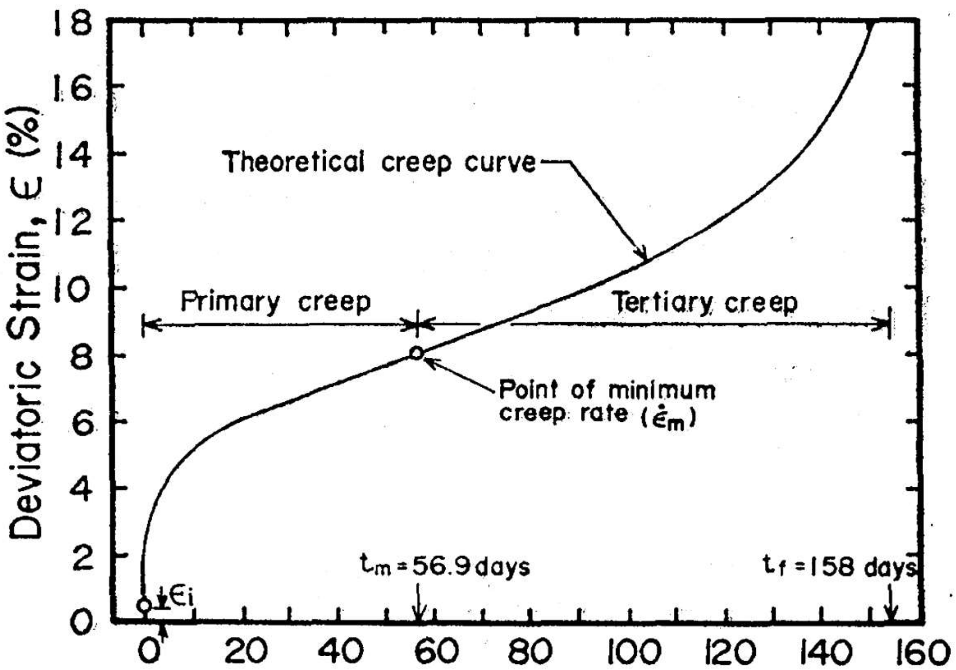

Figure 2.19 – A theoretical creep curve showing the creep phases (after Sekiguchi, 1984)

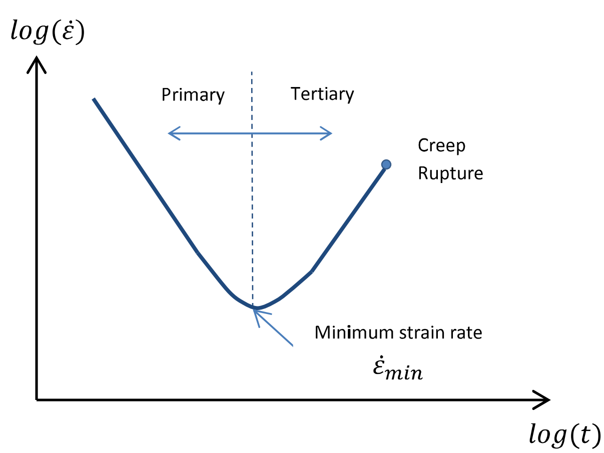

Figure 2.20 – The onset of tertiary creep at minimum strain rate in the $(log(\dot{\varepsilon}) - logt)$ plane

Strength at Failure

Failure can occur at deviatoric stress levels less than the peak strength on creep testing. Casagrande and Wilson (1951) conducted a series of creep shear strength tests on some types of brittle undisturbed clays and clay shales and concluded that those soils ultimately fail under a sustained load much less than the strength indicated by a normal laboratory compression test.

Bishop and Lovenbury (1969) conducted several creep tests on London clay and demonstrated that time effects were of limited magnitude for heavily over-consolidated clays. Tavenas *et al.* (1978) reported creep failure at stresses less than peak strength on overconsolidated samples of undisturbed sensitive clays.

Lefebvre (1981) also indicated that the peak strength in creep tests is reduced significantly with time especially for tests with very low reconsolidation pressures. They stated that there exists a stability threshold, in which shear stresses above the threshold will eventually result in failure while for shear stresses below the threshold the soil will remain stable.

Creep rupture can occur in soft normally consolidated clays under undrained condition as well as heavily overconsolidated clays under both drained and undrained conditions. Figure 2.21 illustrated the stress paths where the pre- and post-creep strengths fall on the same failure envelope. The strength loss in saturated heavily overconsolidated clays tested under undrained conditions was reported by Casagrande and Wilson (1951), Goldstein and Ter-Stepanian (1957) and Vialov and Skibitsky (1957).

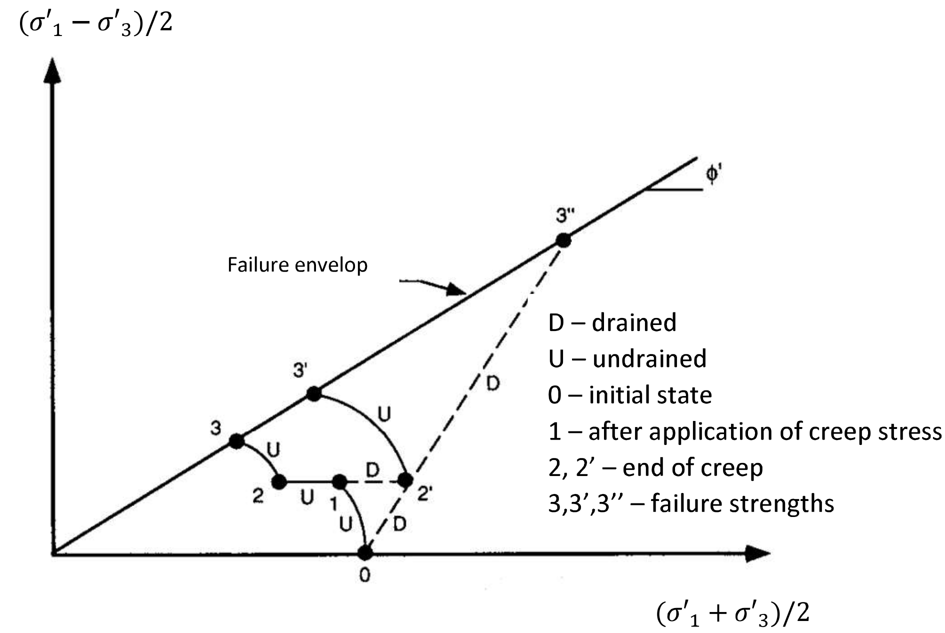

Figure 2.21 – Effect of undrained creep on the strength of normally consolidated clay (after Mitchell and James Kenneth, 2005)

Heavily overconsolidated clays under drained conditions are also susceptible to creep rupture due to softening associated with the increase in water content by dilation and swelling. For examples, creep rupture was observed in drained creep tests on Umeda clay (Murayama and Shibata, 1958), London clay (Bishop and Lovenbury, 1969), Haney clay by Snead (1970) and Campanella and Vaid (1974), Saint Alban clay (Tavenas *et al.*, 1978) and Nicolet clay (Lefebvre, 1981). Figure 2.22 show a typical creep rupture in drained creep tests on Saint Alban clay under various stress conditions (Tavenas *et al.*, 1978).

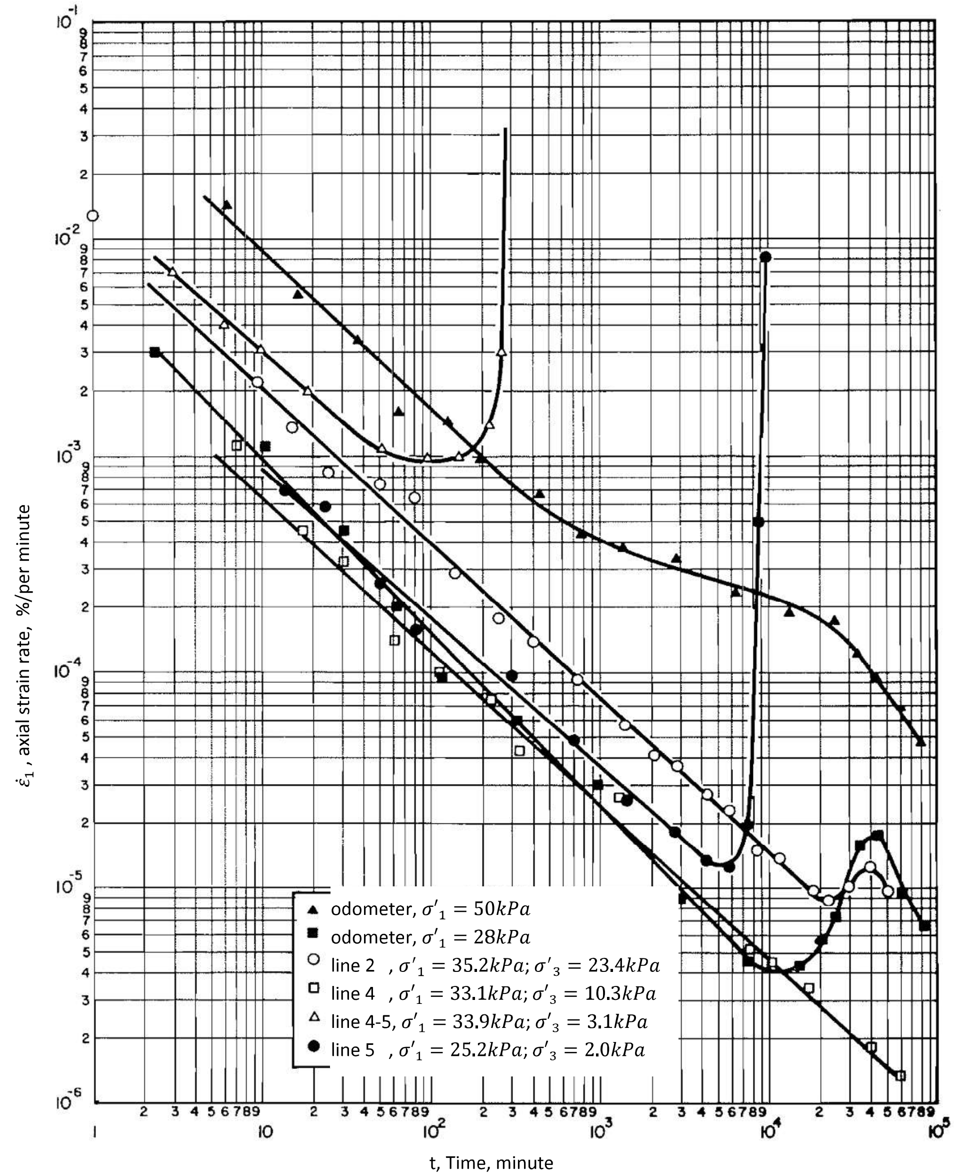

Figure 2.22 – Axial strain rate–Time relationship for drained creep tests on Saint Alban clay under various stress conditions (after Tavenas *et al.*, 1978)

Reduction of Mean Effective Stress during Undrained Creep

For the undrained creep tests, there is a variation of mean effective stress while the total stress state is maintained constant with time after application. The measured stress paths of undrained creep tests in San Francisco Bay Mud are shown in Figures 2.23 and 2.24 (Arulanandan *et al.*, 1971). As shown, the effective stress points shift towards the failure line. At higher stress levels, the specimens eventually underwent creep rupture. However, soil strength in terms of effective stress does not change during the creep period. The pre- and post-creep strengths fall on the same failure envelope. Sekiguchi (1984) also reported the shift towards the critical state line of the effective stress paths for creep tests on Umeda clay.

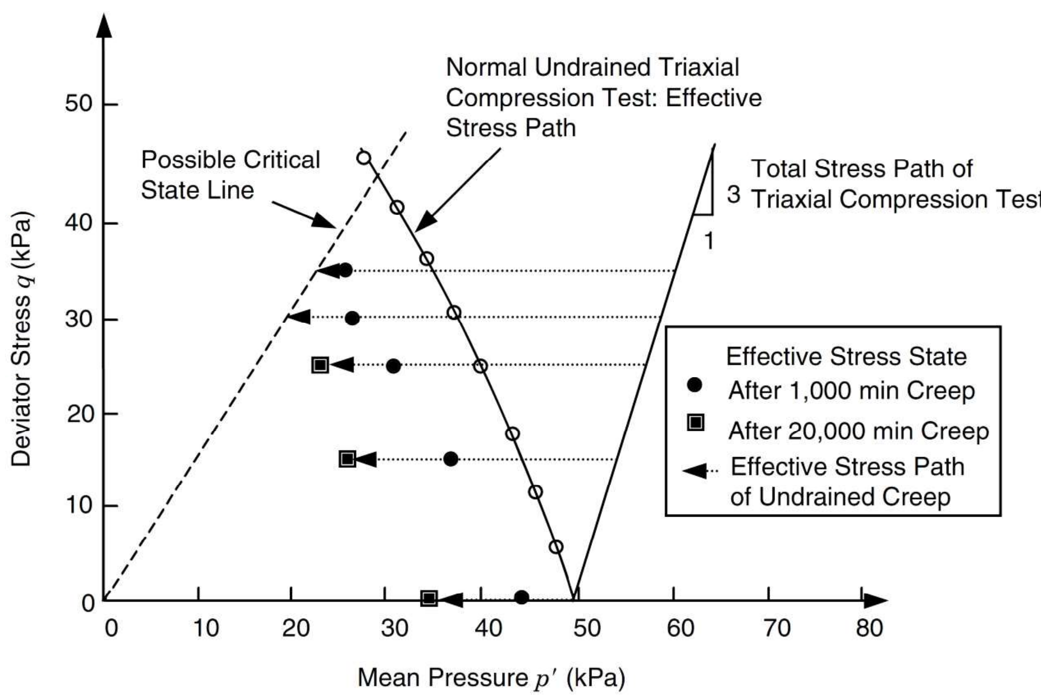

Figure 2.23 – Measured stress paths of undrained creep tests on San Francisco Bay Mud: Deviator stress versus Mean effective stress with initial confining pressure of 49kPa (after Arulanandan *et al.*, 1971)

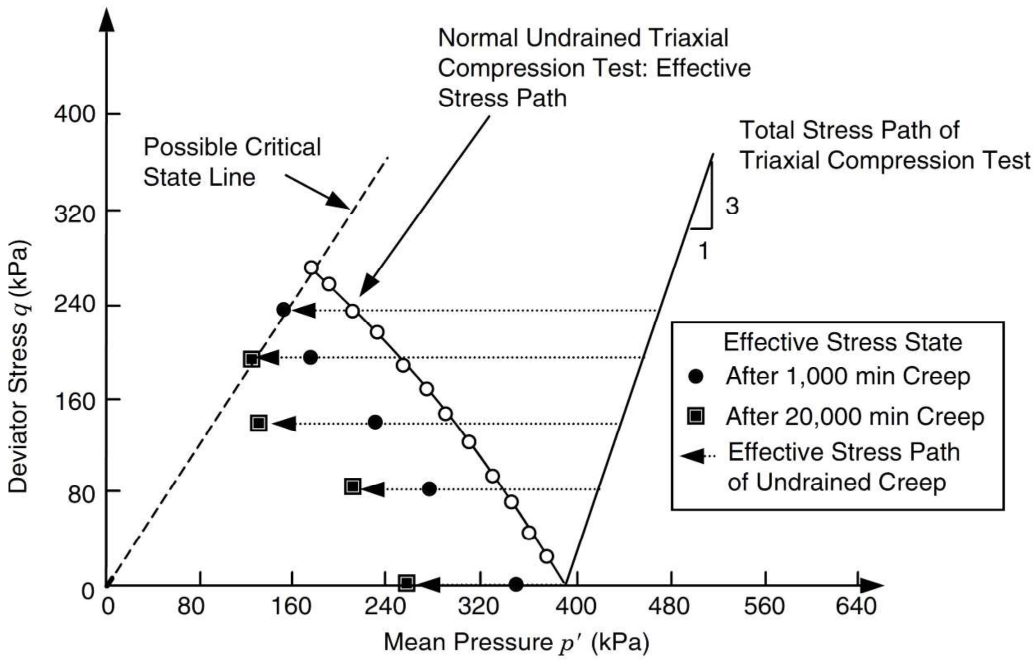

Figure 2.24 – Measured stress paths of undrained creep tests on San Francisco Bay Mud: Deviator stress versus Mean effective stress with initial confining pressure of 392kPa (after Arulanandan *et al.*, 1971)

Rupture Life

Total rupture life t_f is defined as the total elapsed time from the initiation of creep until final rupture. Campanella and Vaid (1974) reported linear relationships between log rupture life and log minimum creep rate (Figure 2.25). These linear relationships were also observed in soils with isotropic consolidation history by Saito and Uezawa (1961), Singh and Mitchell (1969), Snead (1970) and Varnes (1982).

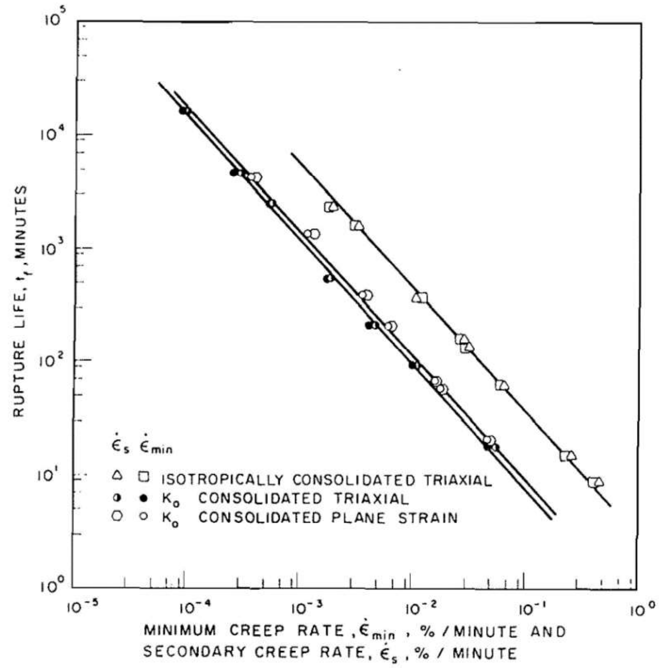

Figure 2.25 – Relationships between rupture life and minimum creep rate for normally consolidated undisturbed Haney clay (after Campanella and Vaid, 1974)

Sekiguchi (1984) proposed a function between the rupture life t_f and the dimensionless creep stress (q/p_0) for a given clay with a given set of reference state variables as shown in Figure 2.26. At one extreme, t_f becomes zero at a creep test with $q = M.p_0$ and an instantaneous rupture will occur upon application of that level of stress. At the other extreme, t_f becomes infinite as the creep stress level tends zero and there exists no lower limit of creep strength.

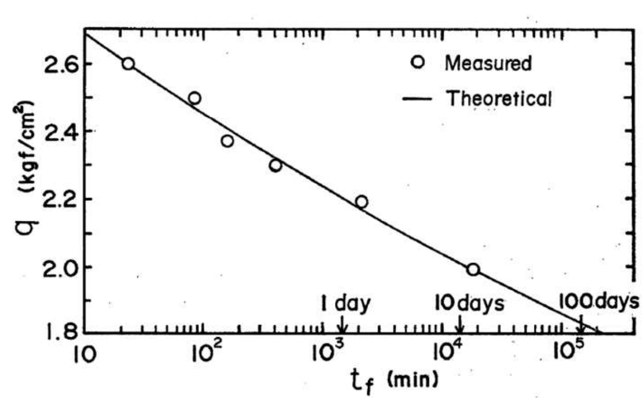

Figure 2.26 – Relationship between creep stress and rupture life (after Sekiguchi, 1984)

2.6. Conclusions

A comprehensive literature review of time-dependent behaviour of geomaterials and constitutive models developed to capture such behaviour were presented in this chapter. The time-dependent behaviour observed in soils, i.e. creep, stress relaxation and strain rate dependency, was described in details. Different classes of constitutive models developed to capture the time-dependent behaviour of soils, including empirical, rheological, and general stress-strain-strain rate models were reviewed in this chapter. A number of constitutive models developed for describing the elasto-viscoplastic behaviour of variable saturated soils were reviewed and their deficiencies were discussed. The tertiary creep and creep rupture phenomena were also discussed in this chapter.

CHAPTER 3

BOUNDING SURFACE VISCOPLASTICITY MODEL FOR TIME-DEPENDENT BEHAVIOUR OF SOILS

3.1. Introduction

The time-dependent behaviour of soils has been investigated extensively from the early stage of research in the field of soil mechanics; however, understanding various observed time- and rate-dependent phenomena such as creep, stress relaxation, and rate dependency has still not been fully explained. This is mainly due to the complexities associated with the behaviour of these materials, including the highly nonlinear time- and rate-dependent behaviour of soil matrix and complex interaction of fluid flow and deformation fields. In fact, studying the time-dependent behaviour of geomaterials and development of constitutive models for this type of materials have been a major area of research in modern geomechanics. Several approaches have been developed to capture the time-dependent behaviour of soils, including empirical models, rheological models, and elasto-viscoplastic constitutive models. However, many of the current constitutive models proposed for the time-dependent behaviour of geomaterials are not able to describe all aspects of the soil response. In particular, the majority of the models are unable to capture the tertiary creep phenomenon in soils.

In this chapter, a unique bounding surface viscoplastic constitutive model is developed to capture the time-dependent behaviour of saturated and unsaturated soils. The next two sections of this chapter, Sections 3.2 and 3.3, summarise the main features of the conventional plasticity models, the methods used for the derivation of the stress-strain relationship for an elasto-(visco)plastic constitutive model, and the approaches widely used for the development of viscoplastic constitutive models. Section 3.4 describes all ingredients of the proposed bounding surface viscoplasticity model for both saturated and unsaturated soils. The last section of this chapter, Section 3.5 demonstrates the capability of the model in simulating both drained and undrained creep rupture.

3.2. Conventional Plasticity Model

One of the major advances in the extension of metal plasticity to soil plasticity was introduced by Drucker and Prager (1952) who extended the Coulomb criterion for three-dimensional soil mechanics problems. Several plasticity models have been developed for modelling of soil behaviour. Notable models include deformation plasticity, incremental plasticity, isotropic hardening plasticity, kinematic hardening plasticity and mixed hardening plasticity (Chen and Wai-Fah, 1985). Before describing the new proposed model for time-dependent behaviour of geomaterials, the conventional plasticity models are briefly discussed in this section.

The elasto-plastic constitutive models can be divided into perfectly plastic and strain hardening models (Chen and Wai-Fah, 1985). In the theory of plasticity for strain or work-hardening materials, the development of an incremental stress-strain relation is based on the following three fundamental assumptions:

1 – The existence of initial and subsequent yield surfaces;

2 – The formulation of an appropriate hardening (softening) rule that describes the evolution of the subsequent yield surfaces; and

3 – A plastic flow rule which provides the direction of the increment of plastic strain.

During the plastic flow, the total incremental strain $\delta\boldsymbol{\varepsilon}$ can be decomposed into elastic $\delta\boldsymbol{\varepsilon}^{\mathrm{e}}$and plastic $\delta\boldsymbol{\varepsilon}^{\mathrm{p}}$ components by a simple superposition:

$$\delta\boldsymbol{\varepsilon} = \delta\boldsymbol{\varepsilon}^{\mathrm{e}} + \delta\boldsymbol{\varepsilon}^{\mathrm{p}} \tag{3.1}$$

The elastic strain increment $\delta\boldsymbol{\varepsilon}^{\mathrm{e}}$ occurs in line with any change in the effective stress as

$$\delta\boldsymbol{\sigma}' = \mathbf{D}^{\mathrm{e}}\delta\boldsymbol{\varepsilon}^{\mathrm{e}} \tag{3.2}$$

where $\mathbf{D}^{\mathrm{e}}$ is the elastic stiffness matrix.

3.2.1. Notation and Sign Convention

In the models presented, the compact matrix-vector notation is used throughout. Tensors and vectors are denoted by bold face letters. Increment is denoted by δ and rate, i.e. derivative with respect to time, is identified by the superimposed dot '·'. The model is formulated using the effective stress concept in the triaxial ($q{-}p'$) plane, where $p' = (\sigma_1' + 2\sigma_3')/3$ is the mean normal effective stress, $q = \sigma_1' - \sigma_3'$ is the deviator stress, and σ_1' and σ_3' are the axial and radial effective stresses, respectively. The corresponding work conjugate strains are volumetric strain $\varepsilon_p = \varepsilon_1 + 2\varepsilon_3$ and deviatoric strain $\varepsilon_q = 2/3(\varepsilon_1 - \varepsilon_3)$, where ε_1 and ε_3 are the axial and radial strains, respectively. In the formulation, compression is considered positive and tension is negative. The pairs of stresses and strains are abbreviated in the vector form as $\boldsymbol{\sigma}' = \{p', q\}^T$ and $\boldsymbol{\varepsilon} = \{\varepsilon_p, \varepsilon_q\}^T$.

3.2.2. Elastic-perfectly Plastic Models

For an elastic-perfectly plastic material, no hardening occurs, and all the subsequent yield surfaces coincide with the initial surface and remain fixed in the stress space. In the stress space, there is a boundary of the elastic region which can only be reached elastically. This surface is known as the yield surface, described by a yield function

$$f(\boldsymbol{\sigma}') = 0 \tag{3.3}$$

A changing stress state within the yield surface, accompanied by purely elastic or recoverable deformations

$$\begin{bmatrix} \delta\varepsilon_p^e \\ \delta\varepsilon_q^e \end{bmatrix} = \begin{bmatrix} \frac{1}{K} & 0 \\ 0 & \frac{1}{3G} \end{bmatrix} \begin{bmatrix} \delta p' \\ \delta q \end{bmatrix} \tag{3.4}$$

where K is the bulk modulus and G is the shear modulus, defined as

$$K = \frac{\upsilon p'}{\kappa}; \qquad G = K\frac{3(1-2\nu)}{2(1+\nu)} \tag{3.5}$$

υ is the specific volume ($\upsilon = 1 + e$), ν is the Poisson's ratio, p' is the mean effective stress and κ is the slope of unloading-reloading line in the ($\upsilon \sim lnp'$) plane.

The plastic strain increment $\delta\boldsymbol{\varepsilon}^{\mathrm{p}}$ occurs when the stress state lies on and remains on the yield surface during the load increment and is known as consistency condition

$$f(\boldsymbol{\sigma}') = 0; \quad \delta f = \frac{\partial f^T}{\partial \boldsymbol{\sigma}'}\delta\boldsymbol{\sigma}' = 0 \tag{3.6}$$

whereas $\partial f^T/\delta\boldsymbol{\sigma}'$ is the partial derivative of f with respect to $\boldsymbol{\sigma}'$.

According to the flow rule, the irrecoverable plastic strain increment is given by

$$\delta\boldsymbol{\varepsilon}^{\mathrm{p}} = \delta\lambda\frac{\partial g}{\partial \boldsymbol{\sigma}'} \tag{3.7}$$

where $g(\boldsymbol{\sigma}')$ is a plastic potential function, $\delta\lambda$ is a scalar plastic multiplier, which is determined as

$$\delta\lambda = \frac{\frac{\partial f^T}{\partial \boldsymbol{\sigma}'}\mathbf{D}^{\mathrm{e}}\delta\boldsymbol{\varepsilon}}{\frac{\partial f^T}{\partial \boldsymbol{\sigma}'}\mathbf{D}^{\mathrm{e}}\frac{\partial g}{\partial \boldsymbol{\sigma}}} \tag{3.8}$$

Hence, an expression for the elastic-plastic stiffness matrix giving $\delta\boldsymbol{\sigma}$ as a function of $\delta\boldsymbol{\varepsilon}$ is generated as

$$\delta\boldsymbol{\sigma} = \left[\mathbf{D}^{\mathrm{e}} - \frac{\mathbf{D}^{\mathrm{e}}\frac{\partial g}{\partial \boldsymbol{\sigma}'}\frac{\partial f}{\partial \boldsymbol{\sigma}'}^{T}\mathbf{D}^{\mathrm{e}}}{\frac{\partial f}{\partial \boldsymbol{\sigma}'}^{T}\mathbf{D}^{\mathrm{e}}\frac{\partial g}{\partial \boldsymbol{\sigma}'}}\right]\delta\boldsymbol{\varepsilon} = \mathbf{D}^{\mathrm{ep}}\delta\boldsymbol{\varepsilon} \tag{3.9}$$

One of the most well-known elastic-perfectly plastic models is the Mohr-Coulomb model. Like the other perfectly plasticity models, the ingredients of the Mohr-Coulomb model also include the elastic properties, the yield function and a plastic potential function (Figure 3.1).

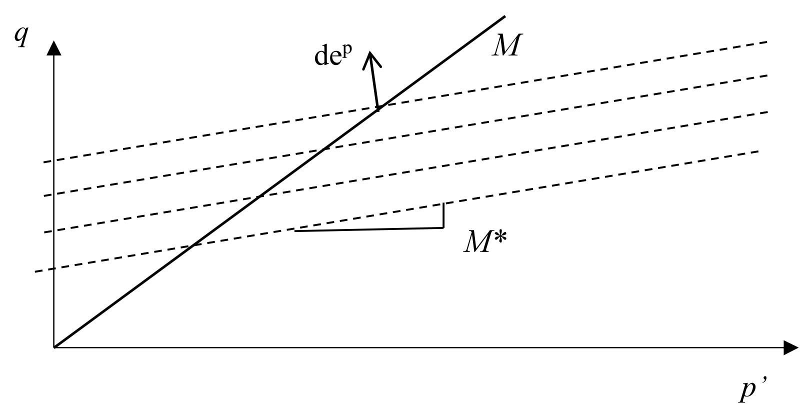

Figure 3.1 – Yield locus and plastic potential for Mohr Coulomb model

The elastic properties are defined as usual using an isotropic elastic model as in Equation (3.4).

The yield function is defined as

$$f(\boldsymbol{\sigma}') = f(p', q) = q - Mp' \tag{3.10}$$

where M is the soil property related to the friction angle ϕ of the soil in triaxial compression

$$M = \frac{6\sin\phi}{3 - \sin\phi} \tag{3.11}$$

The plastic potential function is defined as

$$g(\boldsymbol{\sigma}') = g(p', q) = q - M^* p' + k = 0 \tag{3.12}$$

where k is an arbitrary variable to allow the plastic potential function to be defined at the current state of stress, $M^* = -\delta\varepsilon_p^p / \delta\varepsilon_q^p$ is the ratio between the volumetric and deviatoric plastic strains, which can be defined as a function of dilation angle

$$M^* = \frac{6sin\psi}{3 - sin\psi} \tag{3.13}$$

Elastic-perfectly plastic models are widely used because of their simplicity. They only require minimal material parameters for elastic and failure properties, such as a limiting angle of shearing resistance for a friction model or a limiting shear stress for a cohesive model or an angle of dilation (Wood, 2004). However, the model can only describe the final failure condition together with either the initial stiffness or some average stiffness corresponding to an intermediate stress state between the beginning and the end of the test. This will not give an accurate description of the real behaviour of soil.

The perfect plasticity provides very limited possibilities for matching with observed soil behaviour. Therefore, it is necessary to develop a model which can describe the pre-failure nonlinearities.

3.2.3. Elastic-hardening Plastic Models

The elastic-hardening plastic models are the extensions of the elastic-perfectly plastic models developed for more comprehensive modelling of soil behaviour. While the elastic-perfectly plastic models are capable in reproducing the inelasticity of soil behaviour, the hardening plasticity models can describe pre-failure nonlinearity of geomaterials. The main feature of the hardening plasticity models added to the main ingredients of the elastic-perfectly plastic models is the hardening rule. Hence, there are four ingredients in the elastic-hardening plastic models: elastic properties, yield criterion, flow rule and hardening rule.

The elastic properties are similar to those described in the elastic perfectly plastic models and Equations (3.4) and (3.5), while there is an evolution in the yield criterion for the hardening plasticity models.

Yield criterion

The boundary between elastic and plastic regions or the yield function for the hardening plasticity model now includes one more parameter, apart from the stress stage as in the perfectly models, i.e. the hardening parameter χ. The stress state will remain on the yield surface when the plastic strains are being generated. Therefore, the consistency condition is defined as

$$f(\boldsymbol{\sigma}', \chi) = 0; \quad \delta f = \frac{\partial f^T}{\partial \boldsymbol{\sigma}'} \delta \boldsymbol{\sigma}' + \frac{\partial f}{\partial \chi} \delta \chi = 0 \tag{3.14}$$

Flow rule

Like the perfectly plasticity models, the plastic potential is controlled by the current stresses at yield with a scalar plastic multiplier, and is defined as in Equation (3.7).

Hardening rule

The hardening rule links the change in the size of the yield surface with the magnitude of the plastic strain, and hence provides a link between χ and λ.

For the hardening plasticity models, the hardening parameter is supposed some general function of the plastic strains, i.e. $\chi(\boldsymbol{\varepsilon}^{\mathrm{p}})$. Then, the combination of the consistency condition and the flow rule gives

$$\frac{\partial f^T}{\partial \boldsymbol{\sigma}'} \delta \boldsymbol{\sigma}' + \delta \lambda \frac{\partial f}{\partial \chi} \frac{\partial \chi}{\partial \boldsymbol{\varepsilon}^{\mathrm{p}}}^T \frac{\partial g}{\partial \boldsymbol{\sigma}'} = 0 \tag{3.15}$$

Consequently, the stiffness relationship between the stress increment and the strain increment can be written as

$$\delta \boldsymbol{\sigma} = \left[\mathbf{D}^{\mathrm{e}} - \frac{\mathbf{D}^{\mathrm{e}} \dfrac{\partial g}{\partial \boldsymbol{\sigma}'} \dfrac{\partial f}{\partial \boldsymbol{\sigma}'}^T \mathbf{D}^{\mathrm{e}}}{\dfrac{\partial f}{\partial \boldsymbol{\sigma}'}^T \mathbf{D}^{\mathrm{e}} \dfrac{\partial g}{\partial \boldsymbol{\sigma}'} + H} \right] \delta \boldsymbol{\varepsilon} = \mathbf{D}^{\mathrm{ep}} \delta \boldsymbol{\varepsilon} \tag{3.16}$$

where

$$H = -\frac{\partial f}{\partial \chi} \frac{\partial \chi}{\partial \boldsymbol{\varepsilon}^{\mathrm{p}}}^T \frac{\partial g}{\partial \boldsymbol{\sigma}'} \tag{3.17}$$

The most well-known hardening plastic model for soils is the Cam clay model. It was originally introduced in the early 1960s. Later, the model was modified by Roscoe and Burland (1968), known as the modified Cam clay model. It has been widely and successfully used for the analysis of soft clays under loading. The model has all ingredients of a hardening plasticity model, i.e. elastic properties, yield criterion, an associated flow rule and a hardening rule.

1- Elastic properties

The elastic behaviour of the soil is assumed isotropic and nonlinear and defined similar to Equations (3.4) and (3.5).

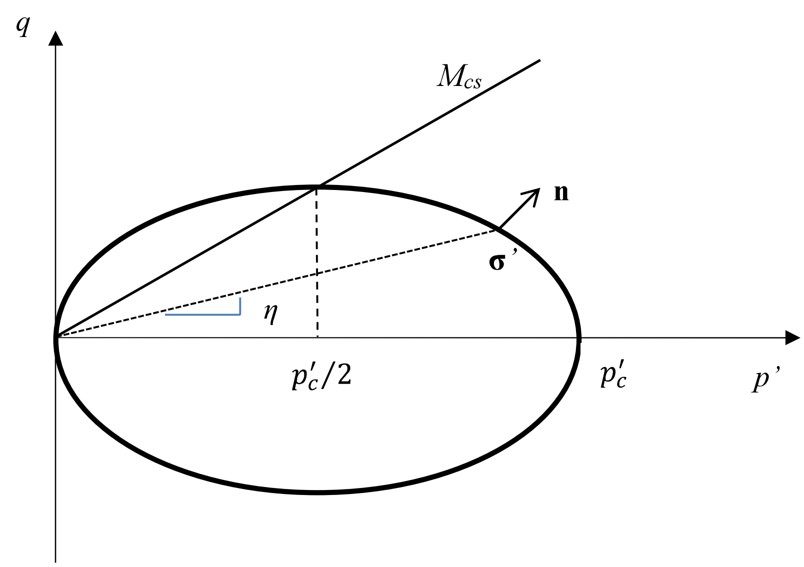

Figure 3.2 – Elliptical yield surface and plastic potential for the modified Cam Clay model

2- Yield criterion

A simple yield surface is assumed for the modified Cam clay model as an elliptical shape passing through the origin of the stress plane ($p'{\sim}q$), see Figure 3.2. The yield function f is defined as

$$f(\boldsymbol{\sigma}',p'_0)=\frac{q^2}{M_{cs}^2}-p'(p'_0-p') \tag{3.18}$$

where p'_0 is the size of the ellipse, i.e. the hardening parameter for the modified Cam clay model and M_{cs} is the slope of the critical state line (CSL) in the ($p'{\sim}q$) plane, the subscript cs indicates conditions at the critical state line.

3- Flow rule

The modified Cam Clay model obeys the associated flow rule so that the plastic strain increment vector is assumed to be normal to the yield surface at the current stress state. The plastic potential has the same form as the yield criterion

$$g(\boldsymbol{\sigma}')=f(\boldsymbol{\sigma}',p'_0)=\frac{q^2}{M^2}-p'\left(p'_0-p'\right)=0 \tag{3.19}$$

4- Hardening rule

The hardening rule describes the dependence of p'_0 on the plastic strain. For the modified Cam clay model, the size of the yield locus depends only on the plastic volumetric strain

$$\begin{pmatrix}\partial p'_0/\partial\varepsilon_p^p\\ \partial p'_0/\partial\varepsilon_q^p\end{pmatrix}=\begin{pmatrix}\upsilon p'_0/(\lambda-\kappa)\\ 0\end{pmatrix} \tag{3.20}$$

Based on the critical state theory, there exists a unique line in the $(\upsilon \sim p' \sim q)$ space where all stress states approach before failure irrespective of their initial conditions and the type of loading. The critical state is associated with continuous shear deformation without change in volume or effective stress. The conditions at the critical state are expressed by

$$\frac{\partial p'}{\partial \varepsilon_q} = \frac{\partial q}{\partial \varepsilon_q} = \frac{\partial \upsilon}{\partial \varepsilon_q} = 0 \tag{3.21}$$

with the effective stress ratio reaching its limit value at the critical state given by

$$\frac{q_{cs}}{p'_{cs}} = \eta_{cs} = M_{cs} \tag{3.22}$$

The projection of the critical state line (CSL) in the $(\upsilon \sim \ln p')$ plane is a straight line parallel to the isotropic compression line (ISL). The CSL and ISL together with the elastic unloading and reloading lines are shown in Figure 3.3. The equation of the critical state line in the $(\upsilon \sim \ln p')$ plane is given by

$$\upsilon_{cs} = \Gamma - \lambda \ln\left(\frac{p'_c}{2}\right) \tag{3.23}$$

where Γ is the specific volume intercept of the critical state line at a reference stress of p' = 1kPa and λ is the slope of the critical state line in the $(\upsilon \sim \ln p')$ plane.

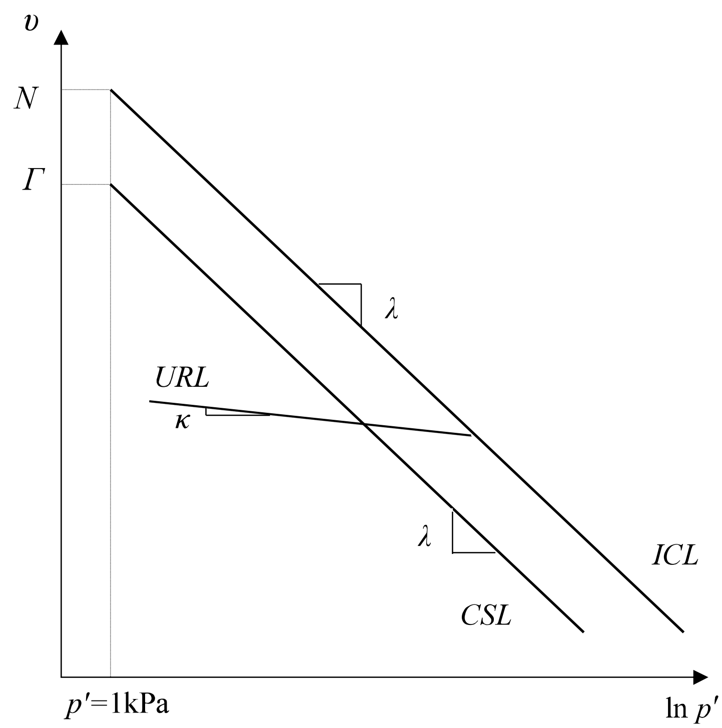

Figure 3.3 – Isotropic compression line (ICL), critical state line (CSL) and elastic unloading-reloading line (URL) for Cam clay model

The isotropic compression line represents the normally consolidated states of clays and enters the plasticity formulation as the basis for derivation of the isotropic volumetric hardening. The isotropic compression line is expressed as

$$\upsilon_{ICL} = N - \lambda \ln p'_c \tag{3.24}$$

where N is the intercept of the isotropic compression line at p' = 1kPa and p'_c is the preconsolidation stress. The isotropic compression line controls the variation of preconsolidation stress with change in plastic volumetric deformation. The isotropic hardening rule assumes the yield surface retains the same shape but changes in size with the change in plastic deformation. Isotropic volumetric hardening relationship is expressed by

$$\frac{\partial p'_c}{\partial \varepsilon_v^p} = \frac{\upsilon p'_c}{\lambda - \kappa} \tag{3.25}$$

where ε_v^p is the plastic volumetric strain, κ is the slope of elastic swelling and recompression line in the (υ~lnp') plane.

Although the modified Cam clay model is suitable and has widely been applied for the analysis of normally consolidated clays, it has been deficient in describing certain aspects of soil behaviour. The modified Cam clay model predictions have been found to overestimate the peak strength of overconsolidated clays and dense sands. Another major limitation of the modified Cam clay model is an abrupt change from elastic to elastoplastic behaviour, while the real soil behaviour shows smooth transition from elastic to elastoplastic state.

It is also clear that the conventional plasticity models are not capable of simulating viscoplastic response of soils such as creep or rate-dependency. Based on the well-established conventional plasticity theory, this research aims to develop a time-dependent constitutive model to capture the time and rate effects on the strength and deformation of soils.

3.3. Elasto-Viscoplastic Models for Time-Dependent Behaviour of Soils

There are two common approaches for modelling the time-dependent behaviour of geomaterials: the Perzyna's overstress approach and the consistency theory approach. The main feature of the Perzyna type models is that the viscoplastic strain develops when the yield function becomes larger than zero, i.e. the current stress state lies outside of the yield surface, which is known as 'overstress'. In the consistency approach models, the consistency condition is satisfied and the viscous behaviour is captured by defining the yield surface as a function of the strain rate. The details of these two approaches are further discussed in the following sections.

3.3.1. Overstress Models

The concept of overstress model was first introduced by Ludwick (1922), Prandtl (1928) and then Malvern (1951) as reported by Satake (1989). The Perzyna's overstress model (Perzyna, 1963, 1966) is a comprehensive three-dimensional version of Malvern's one-dimensional constitutive model (Liingaard *et al.*, 2004). In the overstress theory, it is assumed that no viscous strain occurs in the elastic region, i.e. when the current stress state is within the static yield surface. This is similar to the assumption of the elastic region in the conventional plasticity theory. Hence, the elastic strains are assumed to be time-independent, while the inelastic (or viscoplastic) strains are time-dependent.

In the Perzyna's models, the elastic strain rate $\dot{\boldsymbol{\varepsilon}}^{\mathrm{e}}$ is described by the generalised Hooke's law, whereas the inelastic strain rate $\dot{\boldsymbol{\varepsilon}}^{\mathrm{vp}}$, which combines viscous and plastic effects, is assumed to obey the following flow rule. The evolution of the viscoplastic strain rate is defined as

$$\dot{\boldsymbol{\varepsilon}}^{\mathrm{vp}} = \gamma\langle\Phi(F)\rangle\,\frac{\partial g}{\partial \boldsymbol{\sigma}'} \tag{3.26}$$

where γ is the viscoplastic parameters, Φ is the overstress function that depends on the static yield function $F(\boldsymbol{\sigma}', \Phi)$ which is considered as the rate-independent yield surface, g is a potential function, $\boldsymbol{\sigma}'$ is the effective stress, $\langle\rangle$ are the McCauley brackets, such that

$$\langle\Phi(F)\rangle = \begin{cases} \Phi(F)\ if\ \ F \geq 0, \\ 0 \quad if\ \ F < 0 \end{cases} \tag{3.27}$$

where $\Phi(F)$ is an arbitrary positive function which controls the magnitude of the viscoplastic strain rate and is commonly expressed in terms of the yield function F using either a power or exponential expression. The overstress theory differs from the general plasticity theory in the way of derivation, where it does not meet the consistency rule.

$\Phi(F)$ is a monotonically increasing function of F. Generally, the overstress function is defined in the form of

$$\Phi(F) = \left(\frac{f}{f_0}\right)^n \quad \text{or} \quad \Phi(F) = exp\left(\frac{f}{f_0}\right)^n - 1 \tag{3.28}$$

where n is a material parameter and f_0 is a normalising constant. The appropriate form of $\Phi(F)$ and magnitude of the material parameter n are determined from experimental observations.

Perzyna (1966) introduced several overstress functions $\Phi(F)$ as

$$\begin{gathered} \Phi(F) = F^{\delta}; \quad \Phi(F) = F; \quad \Phi(F) = \exp(F) - 1 \\ \Phi(F) = \textstyle\sum_{\alpha=1}^{N} A_\alpha[\exp(F^\alpha) - 1]; \quad \Phi(F) = \textstyle\sum_{\alpha=1}^{N} B_\alpha F^\alpha \end{gathered} \tag{3.29}$$

whereas $\delta, A_\alpha, B_\alpha$ $(\alpha = 1,2,..N)$ are constants.

Later, Akai *et al.* (1977) and Adachi and Okano (1974) suggested two of the most used forms of $\Phi(F)$ as

$$\Phi(F) = aF^6; \quad \Phi(F) = c\exp(jF^k) - 1 \tag{3.30}$$

where a, c, j and k are viscoplastic constants.

The main difficulty in Perzyna type models is the arbitrariness of the overstress function $\Phi(F)$. In addition, they do not satisfy the consistency condition and cannot be reduced to the rate independent elasto-viscoplastic formulation for the limiting case of the fluidity parameter approaching infinity (Simo *et al.*, 1988). The overstress models are limited in describing the tertiary creep (Oka *et al.*, 1994), i.e. creep at an accelerating strain rate leading to creep failure, unless by introducing a stress-state-dependent viscoplastic parameter, damage effect, or de-structure due to straining (Adachi *et al.*, 1987; Al-Shamrani and Sture, 1998; Yin *et al.*, 2011; Jiang *et al.*, 2017).

3.3.2. Consistency Approach Models

The consistency condition plays an important role in the conventional plasticity theory. Only by applying the consistency condition into the yield surface, a relationship between stress and strain is derived. The consistency condition states that the stress state must remain on the yield surface when (visco)plastic strains are being generated. It shows big advantages and conveniences in numerical implementation where the consistency condition appears in the form of a differential equation (Potts and Zdravković, 1999). Therefore, there is a challenge to incorporate the consistency condition in formulating a stress-strain relationship for time-dependent behaviour of geomaterials, which is not satisfied in the overstress type models.

The nonstationary flow surface (NSFS) theory (Naghdi and Murch, 1963; Sekiguchi, 1984; Matsui and Abe, 1985) developed for the viscoplastic modelling of soils satisfies the consistency requirement. NSFS theory is a further development of the inviscid elastoplastic theory and the yield surface is assumed to flow with time. The models based on NSFS theory achieve a higher convergence rated compared to overstress based models (Heeres *et al.*, 2002). The nonstationary-type model developed by Sekiguchi (1984) is able to predict undrained creep rupture in normally consolidated clays. However, it predicts an infinite deformation when the time is infinite and has a limitation in describing the transition between the inviscid and the viscous behaviour (Qiao *et al.*, 2016).

There was also a consistency viscoplastic approach presented by Wang *et al.* (1997). They introduced a solution for the viscoplastic tangent operator, which provides a smooth transition from rate-independent plasticity to rate-dependent viscoplasticity. Several simulation results were provided by Wang *et al.* (1997) and Carosio *et al.* (2000), which demonstrated the capability of consistency model in modelling the time-dependent behaviour of metal.

In the consistency approach, the viscoplastic flow direction is defined in the same way as in the Perzyna theory

$$\Delta\boldsymbol{\varepsilon}^{\mathrm{vp}} = \Delta\lambda\mathbf{m} \tag{3.31}$$

However, the viscoplastic multiplier $\Delta\lambda$ is determined using the consistency condition developed by Wang *et al.* (1997) and Carosio *et al.* (2000) as

$$f(\sigma,\lambda,\dot{\lambda}) = f + \mathbf{n}^T\delta\sigma + \frac{\partial f}{\partial\lambda}\partial\lambda + \frac{\partial f}{\partial\dot{\lambda}}\partial\dot{\lambda} \tag{3.32}$$

The time-dependency of the material response is represented through defining the yield surface as a function of viscoplastic strain and viscoplastic strain rate. Following the consistency rule, the stress point is either on or inside the yield surface and viscoplastic deformation occurs when the stress point lies on the yield surface. The consistency viscoplastic theory follows the mathematical framework of the conventional plasticity theory in the form of differential equation, which can be solved numerically. In the next sections, a viscoplastic bounding surface constitutive model is developed based on the consistency approach for describing time-dependent behaviour of soils with particular reference to tertiary creep.

3.4. A Bounding Surface Viscoplasticity Model for Time-Dependent Behaviour of Soils

3.4.1. Background of Bounding Surface Models

The concept of the "Bounding Surface" in a stress space was first introduced within the framework of critical state soil plasticity by Dafalias and Herrmann (1980). They used a three segmented bounding surface with a simple radial projection rule to describe the soil behaviour under monotonic and cyclic loading conditions. Mathematical foundation of the general bounding surface theory and its application to isotropic cohesive soils was presented by Dafalias (1986) and Dafalias and Hermann (1986). In this model, the loading surface and the bounding surface were the same shape, defined by a complicated split function comprising a hyperbolic and two elliptical components. An associative flow rule was also assumed, i.e. the plastic potential was of the same shape as the bounding surface. In the same year, Bardet (1986) developed a bounding surface plasticity model to describe the nonlinear irreversible behaviour of sands. The model was based on the critical state framework and associative flow rule and was able to simulate strain softening and stress dilatancy in dense sands. Crouch *et al.* (1994) extended the application of the bounding surface plasticity model to sands using a combined radial and deviatoric mapping, non-associative flow rule, a bilinear critical state line and an apparent normal consolidation line. Later, Gajo and Muir Wood (1999) and Dafalias and Manzari (2004) presented Mohr-Coulomb type bounding surface models for deviatoric response in sands.

More recently, Russell and Khalili (2004) and Khalili *et al.* (2005) introduced the bounding surface plasticity model at the University of New South Wales (UNSW) for granular soils based on the concept of the critical-state soil mechanics. The model is suited to a wide range of stresses with a uniquely three-part shaped critical state line to capture the three modes of plastic deformation including particle rearrangement, particle crushing and pseudoelastic deformation. Later, Russell and Khalili (2006) extended this model for unsaturated soils. The UNSW bounding surface plasticity model has been demonstrated to be able to accurately reproduce the stress-strain behaviour of many soil types in different testing conditions under monotonic and cyclic loadings. However, the model cannot describe the time-dependent behaviour of soils such as creep, stress relaxation and strain rate dependency.

In this section, a bounding surface viscoplasticity model is developed for describing the time-dependent behaviour of soils. The model meets the consistency condition and allows a seamless transition from rate-independent plasticity to rate-dependent viscoplasticity. The rate-dependency is achieved through defining the bounding surface as a function of both viscoplastic volumetric strain and strain rate.

In the proposed model, the total strain increment is decomposed into the elastic part (e) and the viscoplastic part (vp) as,

$$\delta\boldsymbol{\varepsilon} = \delta\boldsymbol{\varepsilon}^{\mathrm{e}} + \delta\boldsymbol{\varepsilon}^{\mathrm{vp}} \tag{3.33}$$

In the following parts, the essential elements of the model, i.e. the elastic properties, the bounding surface, the flow rule, and the hardening rule are described.

3.4.2. The Elastic Properties

For nonlinear materials, the elastic response can be described using an incremental stress-strain relationship as

$$\delta\boldsymbol{\sigma} = \mathbf{D}^{\mathrm{e}}\delta\boldsymbol{\varepsilon}^{\mathrm{e}} \tag{3.34}$$

where $\delta\boldsymbol{\varepsilon}^{\mathrm{e}}$ is the elastic strain increment, $\delta\boldsymbol{\sigma}$ is the stress increment, $\mathbf{D}^{\mathrm{e}}$ is the elastic stiffness matrix. In the $(p'{\sim}q)$ plane, $\mathbf{D}^{\mathrm{e}}$ is defined as,

$$\mathbf{D}^{\mathrm{e}} = \begin{bmatrix} K & 0 \\ 0 & 3G \end{bmatrix} \tag{3.35}$$

in which K and G are tangential bulk and shear moduli, respectively, as defined in Equation (3.5). The elastic moduli are calculated assuming that unloading/reloading occurs along the κ line in the $(\upsilon{\sim}lnp')$ plane.

In the bounding surface theory, it is common to define a purely elastic region as a region bounded by the loading surface. If the current stress state $\boldsymbol{\sigma}'$ lies inside the loading surface, the elastic behaviour occurs. However, deformation of soils is not purely elastic. Thus, in this study, a purely elastic region is omitted such that all deformations are elasto-viscoplastic.

3.4.3. The Viscoplastic Properties

In this model, the viscoplastic deformation occurs when the stress state lies within or on the bounding surface. The essential elements of this bounding surface viscoplastic model are: the critical state and limiting isotropic compression lines which are *a priori* functions of strain rate and define failure and hardening/softening characteristics of soil, respectively; the bounding surface which defines the limit of admissible states of stress; the loading surface on which the current stress state lies; the viscoplastic potential which determines the direction of viscoplastic strain increment vector; and the hardening rules which control the evolution of the bounding and loading surfaces with respect to the variation of viscoplastic strain and viscoplastic strain rate.

3.4.3.1. The Critical State and Isotropic Compression Lines

The critical state is an ultimate condition in which viscoplastic shear strain continues indefinitely without any changes in volumetric strain and effective stresses. The critical state line (CSL) in the $(\upsilon - \ln p')$ plane in Figure 3.4 can be expressed as

$$\upsilon_{cs} = \Gamma\left(\dot{\varepsilon}_p^{vp}\right) - \lambda\, ln(\,p'_{cs}) \tag{3.36}$$

where υ_{cs} is the critical state specific volume at a mean normal stress p_{cs}, $\Gamma\left(\dot{\varepsilon}_p^{vp}\right)$ is the specific volume intercept of the critical state line at p' = 1.0 kPa, and λ is the slope of the critical state line on $(\upsilon - \ln p')$ plane. The slope of the CSL in the $(q-p')$ plane, denoted by M_{cs}, is linked to the critical state friction angle, ϕ'_{cs}, through

$$M_{cs} = \left(\frac{q}{p'}\right)_{cs} = \frac{6\sin\phi'_{cs}}{3\tilde{t} - \sin\phi'_{cs}} \tag{3.37}$$

where $\tilde{t}$ is the loading direction multiplier with $\tilde{t} = +1$ for compression and $\tilde{t} = -1$ for extension.

In the three-dimensional general stress space, the slope of the critical state line (M_{cs}) is expressed as a function of the Lode angle θ. The Lode angle is defined by

$$\theta = \frac{1}{3}\sin^{-1}\left[-\frac{3\sqrt{3}}{2}\frac{J_3}{\sqrt{(J_2)^3}}\right] \tag{3.38}$$

where J_2 and J_3 are the second and the third invariants of the deviator stress vector. The Lode angle ranges from $\theta = -\pi/6$ for triaxial extension to $\theta = +\pi/6$ for triaxial compression. Lode angle dependency of M_{cs} determines the shapes of the yield and failure surfaces in the deviatoric (π) plane of the principle stress space. Several expressions have been proposed for modelling the shape of the failure surface in the deviatoric plane. A convenient expression for the variation of M_{cs} with θ is given by Sheng *et al.* (2000) as

$$M_{cs}(\theta) = M_{max}\left(\frac{2\alpha^4}{1+\alpha^4-(1-\alpha^4)\sin 3\theta}\right)^{1/4} \tag{3.39}$$

where α is given by

$$\alpha = \frac{M_{min}}{M_{max}} = \frac{3-\sin\phi'_{cs}}{3+\sin\phi'_{cs}} \tag{3.40}$$

in which M_{max} is the value of M_{cs} for triaxial compression and M_{min} is the value of M_{cs} for triaxial extension.

The limiting isotropic compression line (LICL) is defined to be parallel to the critical state line and at a constant shift along the κ line from the CSL in the $(\upsilon - \ln p')$ plane, see Figure 3.4. The LICL can be expressed as

$$\upsilon_{LICL} = N_{LICL}\left(\dot{\varepsilon}_p^{vp}\right) - \lambda \ln(\bar{p}_c') \tag{3.41}$$

where υ_{LICL} is the specific volume on the LICL at an isotropic stress $\bar{p}_c'$ and $N_{LICL}\left(\dot{\varepsilon}_p^{vp}\right)$ is the specific volume intercept of the LICL at p' = 1.0 kPa.

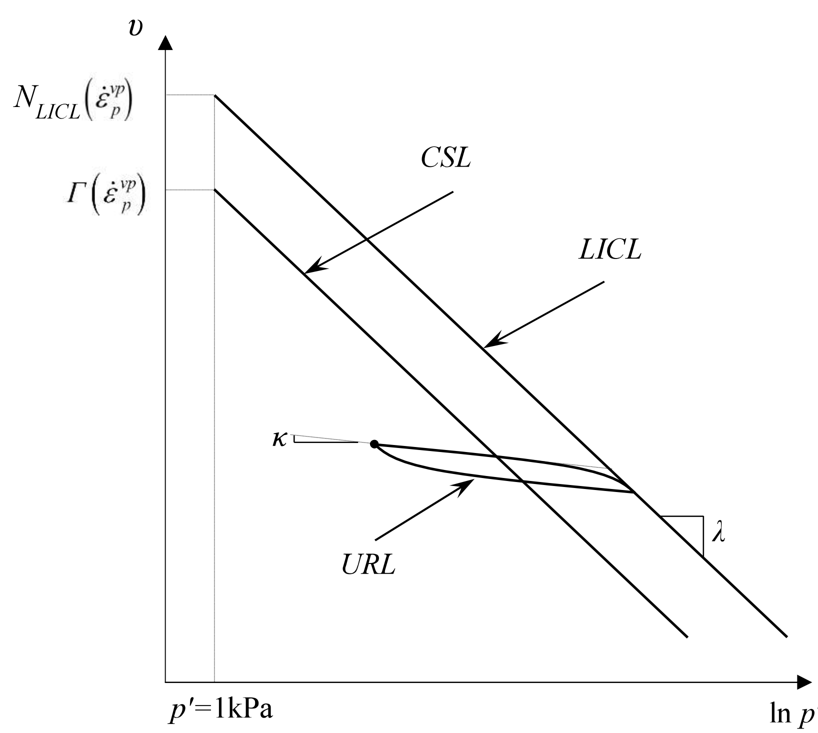

Figure 3.4 – The limiting isotropic compression line (LICL), critical state line (CSL), and unloading-reloading line (URL) in the (υ-lnp') plane.

3.4.3.2. *The Bounding Surface*

For the bounding surface, the simple yet versatile function proposed by Khalili *et al.* (2005) is adopted and extended to include the strain rate effect

$$F(\bar{p}', \bar{q}, \bar{p}'_c) = \left(\frac{\bar{q}}{M_{cs}\bar{p}'}\right)^N - \frac{\ln(\bar{p}'_c/\bar{p}')}{\ln R} = 0 \qquad (3.42)$$

in which parameter $\bar{p}'_c(\varepsilon_p^{vp}, \dot{\varepsilon}_p^{vp})$ controls the size of F and depends *a priori* on viscoplastic volumetric strain ε_p^{vp} and viscoplastic volumetric strain rate $\dot{\varepsilon}_p^{vp}$. The material constant R represents the ratio between $\bar{p}'_c$ and the value of $\bar{p}'$ at the intercept of F with the CSL in the $(q{-}p')$ plane, the material constant N controls the curvature of the surface, and the superimposed bar denotes stress conditions on the bounding surface.

3.4.3.3. *The Loading Surface*

The current effective stress $\boldsymbol{\sigma}'$ is always located on the loading surface. The loading surface adopted is of the same shape and is homologous to the bounding surface about the centre of homology. The centre of homology is defined at the origin of stresses in the $(q{-}p')$ plane for first time loading (Figure 3.5). For unloading/reloading, the centre of homology moves to the last point of stress reversal. The maximum loading surface through the point of stress reversal acts as a local bounding surface for the loading surfaces within the maximum surface (Khalili *et al.*, 2005). The loading surfaces undergo kinematic hardening during loading and unloading such that they are tangent to the local bounding surface at the centre of homology and their local coordinate system remains parallel to the global coordinates system (Figure 3.6). Thus, the loading surface function, f, takes the form

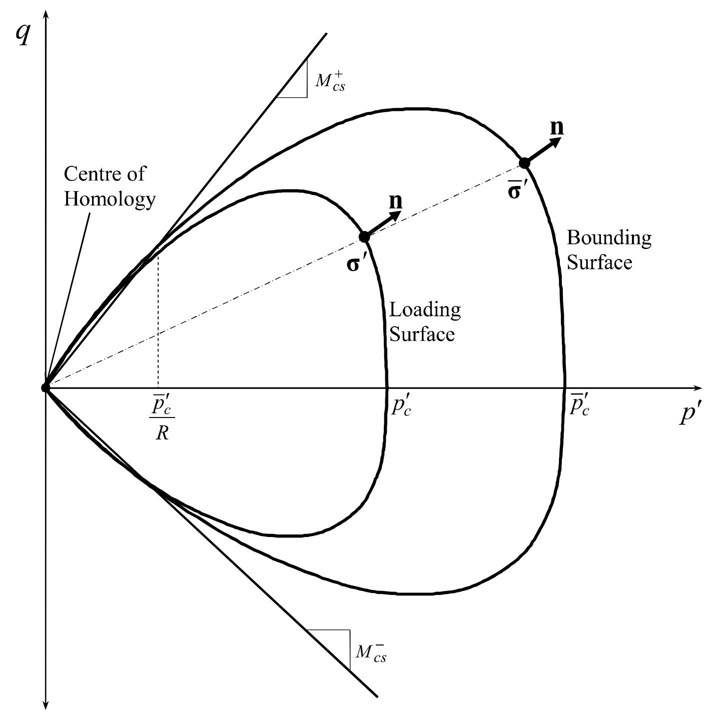

Figure 3.5 – Bounding surface, loading surface, mapping rule and image point in the (q-p') plane for first time loading

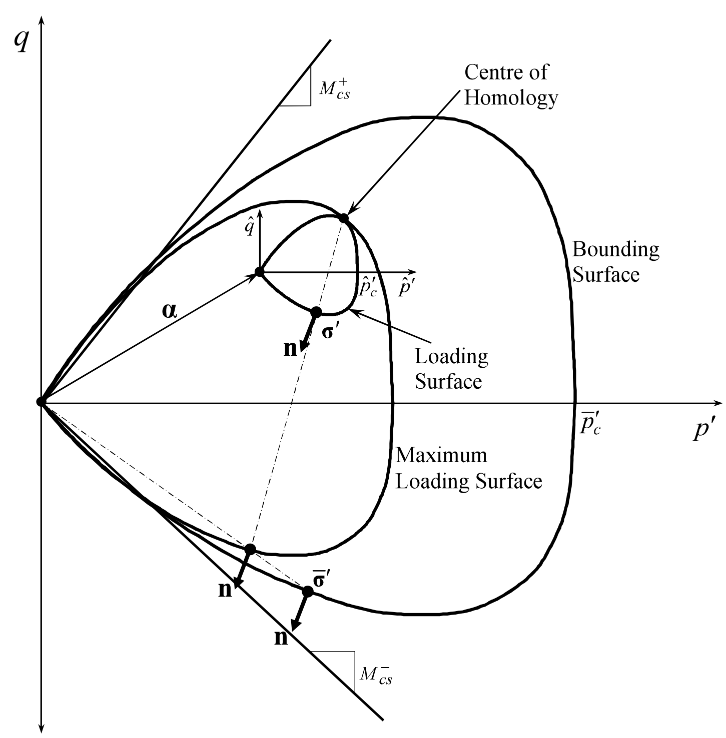

Figure 3.6 – Mapping rule and the evolution of loading surface in the (q-p') plane for unloading/reloading

$$f(\hat{p}', \hat{q}, \hat{p}'_c) = \left(\frac{\hat{q}}{M_{cs}\hat{p}'}\right)^N - \frac{\ln(\hat{p}'_c/\hat{p}')}{\ln R} = 0 \tag{3.43}$$

where $\hat{p}_c' = p_c' - \alpha_p$ is an isotropic hardening parameter controlling the size of the loading surface, $\boldsymbol{\alpha} = [\alpha_p, \alpha_q]^T$ is the kinematic hardening vector controlling the position of the loading surface, $\hat{q} = q - \alpha_q$, and $\hat{p}' = p' - \alpha_p$.

3.4.3.4. The Image Point

The image point for the first time loading is obtained using a mapping rule such that a straight line passing through the centre of homology and $\boldsymbol{\sigma}'$ intersects the bounding surface at $\bar{\boldsymbol{\sigma}}'$ having the same unit normal vector as $\boldsymbol{\sigma}'$ on the loading surface. For unloading/reloading, the image point is located sequentially by projecting the stress point onto a series of intermediate image points on successive local bounding surfaces passing through each point of stress reversal. The loading history of the material is captured through the stress reversal points and the corresponding maximum loading surfaces. The point of stress reversal is identified by $\mathbf{n}^T\delta\boldsymbol{\sigma}'^{\mathrm{e}} < 0$ where $\mathbf{n}$ is the unit normal vector at the image point defining the direction of loading and $\delta\boldsymbol{\sigma}'^{\mathrm{e}} = \mathbf{D}^{\mathrm{e}}\delta\boldsymbol{\varepsilon}$ is the elastic stress increment (Mroz *et al.*, 1981). The unit vector of loading $\mathbf{n}$ is given by

$$\mathbf{n} = \frac{\partial F/\partial\bar{\boldsymbol{\sigma}}'}{\|\partial F/\partial\bar{\boldsymbol{\sigma}}'\|} = \frac{\partial f/\partial\boldsymbol{\sigma}'}{\|\partial f/\partial\boldsymbol{\sigma}'\|} \tag{3.44}$$

where

$$\frac{\partial F}{\partial\bar{\boldsymbol{\sigma}}'} = \left[-\frac{N}{\bar{p}'}\left(\frac{\bar{q}}{M_{cs}\bar{p}'}\right)^N + \frac{1}{\bar{p}'\ln R} \qquad N\left(\frac{1}{M_{cs}\bar{p}'}\right)^N \bar{q}^{N-1}\right]^T \tag{3.45}$$

For three-dimensional stress state, the vector $\partial F/\partial\bar{\boldsymbol{\sigma}}'$ is written as

$$\frac{\partial F}{\partial \bar{\boldsymbol{\sigma}}'} = \frac{\partial F}{\partial \bar{p}'}\frac{\partial \bar{p}'}{\partial \bar{\boldsymbol{\sigma}}'} + \frac{\partial F}{\partial \bar{q}}\frac{\partial \bar{q}}{\partial \bar{\boldsymbol{\sigma}}'} + \frac{\partial F}{\partial \bar{\theta}}\frac{\partial \bar{\theta}}{\partial \bar{\boldsymbol{\sigma}}'} \tag{3.46}$$

where $\partial F/\partial \bar{p}'$, $\partial F/\partial \bar{q}$ and $\partial F/\partial \bar{\theta}$ are determined by differentiating the generalized form of Equation (3.42) with respect to $\bar{p}', \bar{q}$ and $\bar{\theta}$ as

$$\frac{\partial F}{\partial \bar{p}'} = -\frac{N}{\bar{p}'}\left(\frac{\bar{q}}{M_{cs}(\bar{\theta})\bar{p}'}\right)^{N} + \frac{1}{\bar{p}'\ln R} \tag{3.47}$$

$$\frac{\partial F}{\partial \bar{q}} = \frac{N}{M_{cs}(\bar{\theta})\bar{p}'}\left(\frac{\bar{q}}{M_{cs}(\bar{\theta})\bar{p}'}\right)^{N-1} \tag{3.48}$$

$$\frac{\partial F}{\partial \bar{\theta}} = \frac{\partial F}{\partial M_{cs}(\bar{\theta})}\frac{\partial M_{cs}(\bar{\theta})}{\partial \bar{\theta}} = -\frac{3N}{4}\left(\frac{\bar{q}}{M_{cs}(\bar{\theta})\bar{p}'}\right)^{N}\left(\frac{(1-\alpha^4)\cos 3\bar{\theta}}{1+\alpha^4-(1-\alpha^4)\sin 3\bar{\theta}}\right) \tag{3.49}$$

3.4.3.5. The Viscoplastic Potential

In this model, the viscoplastic potential is defined using a non-associated viscoplastic flow rule relating the viscoplastic dilatancy *d* to the stress ratio $\eta = q/p'$. In triaxial stress state, the stress-dilatancy relationship can be written as

$$d = \tilde{t}\frac{\delta\varepsilon_p^{vp}}{\delta\varepsilon_q^{vp}} = \tilde{t}A\left(M_{cs} - \frac{q}{p'}\right) \tag{3.50}$$

where A is a material constant dependent on the mechanism and amount of energy dissipation. The viscoplastic potential g is obtained by integrating with respect to p' and q as

$$g(p', q, p_0) = \tilde{t}\left[q + M_{cs}p'\ln\left(\frac{p'}{p_0}\right)\right] \quad \text{for } A = 1 \tag{3.51}$$

$$g(p', q, p_0) = \tilde{t}\left[q + \frac{AM_{cs}p'}{A-1}\left(\left(\frac{p'}{p_0}\right)^{A-1} - 1\right)\right] \quad \text{for } A \neq 1 \tag{3.52}$$

in which p_0 is the variable controlling the size of the viscoplastic potential. A graphical depiction of the viscoplastic potential is shown in Figure 3.7. This function has been successfully applied and verified for a wide range of geomaterials (Russell and Khalili, 2004; Khalili *et al.*, 2005; Russell and Khalili, 2006; Khalili *et al.*, 2008; Kan *et al.*, 2014; Mac *et al.*, 2014; Mac *et al.*, 2017; Shahbodagh *et al.*, 2017; Mac *et al.*, 2019).

The direction of viscoplastic flow is defined as

$$\mathbf{m} = \frac{\partial g/\partial \boldsymbol{\sigma}'}{\|\partial g/\partial \boldsymbol{\sigma}'\|} \tag{3.53}$$

Using Equation (3.53), two vectors of viscoplastic flow are identified at any stress point: $\mathbf{m}^+$ for compressive loading ($\tilde{t} = +1$) and $\mathbf{m}^-$ for extensive loading ($\tilde{t} = -1$).

In the general three-dimensional stress space, the viscoplastic potential equations (3.51) and (3.52) are expressed as

For $A = 1$:

$$g(p', q, \bar{\theta}, p_0) = \bar{\tilde{t}}q + M_{cs}(\bar{\theta})p'\ln\left(\frac{p'}{p_0}\right) \tag{3.54}$$

For $A \neq 1$:

$$g(p', q, \bar{\theta}, p_0) = \bar{\tilde{t}}q + \frac{AM_{cs}(\bar{\theta})p'}{A-1}\left(\left(\frac{p'}{p_0}\right)^{A-1} - 1\right) \tag{3.55}$$

In addition, the vector $\partial g/\partial \boldsymbol{\sigma}'$ is evaluated by applying the chain rule of differentiation

$$\frac{\partial g}{\partial \boldsymbol{\sigma}'} = \frac{\partial g}{\partial p'}\frac{\partial p'}{\partial \boldsymbol{\sigma}'} + \frac{\partial g}{\partial q}\frac{\partial q}{\partial \boldsymbol{\sigma}'} + \frac{\partial g}{\partial \bar{\theta}}\frac{\partial \bar{\theta}}{\partial \boldsymbol{\sigma}'} \tag{3.56}$$

where $\partial g/\partial p'$, $\partial g/\partial q$ and $\partial g/\partial \bar{\theta}$ are determined by differentiating the generalized form of Equations (3.54) or (3.55) with respect to p', q and $\bar{\theta}$

$$\frac{\partial g}{\partial p'} = A\left(M_{cs}(\bar{\theta}) - \bar{\bar{t}}\frac{q}{p'}\right) \tag{3.57}$$

$$\frac{\partial g}{\partial q} = \bar{\bar{t}} \tag{3.58}$$

$$\frac{\partial g}{\partial \bar{\theta}} = \frac{\partial g}{\partial M_{cs}(\bar{\theta})}\frac{\partial M_{cs}(\bar{\theta})}{\partial \bar{\theta}} = -\bar{\bar{t}}\frac{3q}{4}\left(\frac{(1-\alpha^4)\cos 3\bar{\theta}}{1+\alpha^4-(1-\alpha^4)\cos 3\bar{\theta}}\right) \tag{3.59}$$

3.4.3.6. The Hardening Rule

Following the conventional approach in the bounding surface plasticity, the strain hardening modulus h can be divided into two components

$$h = h_b + h_f \tag{3.60}$$

where h_b is the viscoplastic strain hardening modulus at the image point $\bar{\boldsymbol{\sigma}}'$ on the bounding surface, and h_f is some arbitrary modulus at $\boldsymbol{\sigma}'$, defined as a function of the distance between $\bar{\boldsymbol{\sigma}}'$ and $\boldsymbol{\sigma}'$.

Applying the consistency condition to the bounding surface yields

$$\delta F = \left(\frac{\partial F}{\partial \bar{\boldsymbol{\sigma}}'}\right)^T \delta\bar{\boldsymbol{\sigma}}' + \frac{\partial F}{\partial \bar{p}'_c}\frac{\partial \bar{p}'_c}{\partial \varepsilon_p^{vp}}\delta\varepsilon_p^{vp} + \frac{\partial F}{\partial \bar{p}'_c}\frac{\partial \bar{p}'_c}{\partial \dot{\varepsilon}_p^{vp}}\delta\dot{\varepsilon}_p^{vp} = 0 \tag{3.61}$$

Equation (3.61) can also be rewritten as

$$\mathbf{n}^T \delta\bar{\boldsymbol{\sigma}}' m_p - h_b \delta\varepsilon_p^{vp} - \xi \delta\dot{\varepsilon}_p^{vp} = 0 \tag{3.62}$$

where

$$h_b = -\frac{\partial F}{\partial \bar{p}'_c} \frac{\partial \bar{p}'_c}{\partial \varepsilon_p^{vp}} \frac{m_p}{\|\partial F/\partial \bar{\boldsymbol{\sigma}}'\|} \tag{3.63}$$

and ξ is the viscoplastic strain rate hardening modulus,

$$\xi = -\frac{\partial F}{\partial \bar{p}'_c} \frac{\partial \bar{p}'_c}{\partial \dot{\varepsilon}_p^{vp}} \frac{m_p}{\|\partial F/\partial \bar{\boldsymbol{\sigma}}'\|} \tag{3.64}$$

whereas

$$m_p = \partial g/\partial p' / \|\partial g/\partial \boldsymbol{\sigma}'\| \tag{3.65}$$

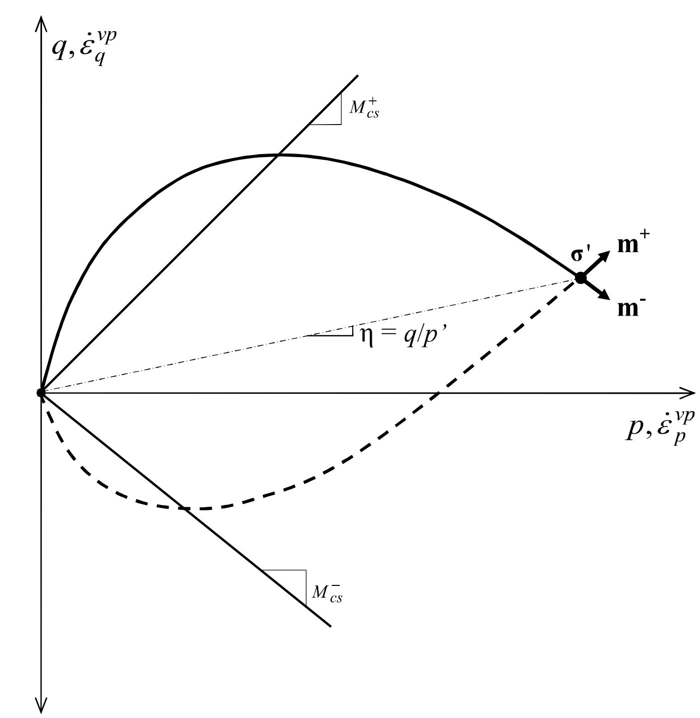

Figure 3.7 – Viscoplastic potential for triaxial compression and extension loadings in the (*q*-*p'*) plane

The differential terms of Equation (3.42) are expressed as

$$\frac{\partial F}{\partial \bar{p}'_c} = -\frac{1}{\bar{p}'_c lnR} \tag{3.66}$$

$$\frac{\partial \bar{p}'_c}{\partial \varepsilon_p^{vp}} = \frac{\upsilon \bar{p}'_c}{\lambda - \kappa} \tag{3.67}$$

Substituting Equations (3.66) and (3.67) back to Equation (3.63), we have:

$$h_b = \frac{\upsilon}{(\lambda - \kappa)\ln R} \frac{m_p}{\|\partial F/\partial \bar{\boldsymbol{\sigma}}'\|} \tag{3.68}$$

The strain hardening modulus h_f is defined such that it is zero on the bounding surface and infinity at the point of stress reversal. Following Khalili *et al.* (2005), h_f is assumed to be of the form

$$h_f = \tilde{t}\, \frac{\partial \bar{p}'_c}{\partial \varepsilon_p^{vp}} \frac{p'}{\bar{p}'_c} \left[\frac{\bar{p}'_c}{\hat{p}'_c} - 1\right] k_m(\eta_p - \eta) \tag{3.69}$$

where $\eta_p = M_{cs}\big(1 - 2(\upsilon - \upsilon_{cs})\big)$ is the slope of the peak strength line in the $(q - p')$ plane and k_m is a material parameter controlling the steepness of the response in the $(q - \varepsilon_q)$ plane.

To derive the evolution of $\bar{p}'_c$ with the rate of viscoplastic volumetric strain, we start from the classical equation of secondary compression

$$\Delta e = -C_\alpha \Delta \log(t) \tag{3.70}$$

where C_α is the secondary compression index, Δe is the change of void ratio, and t is time.

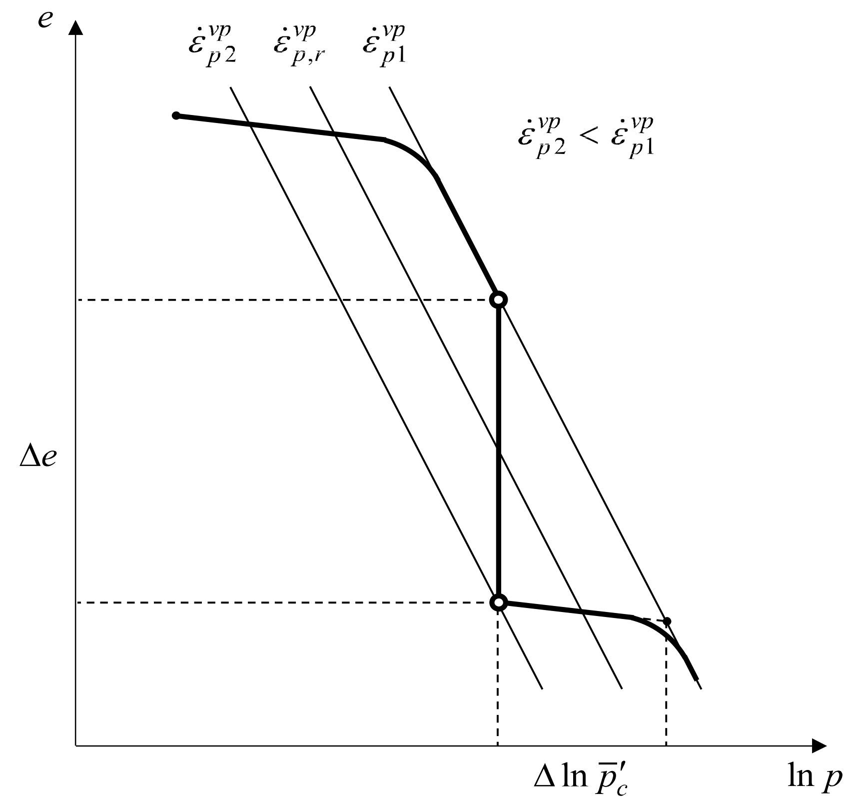

Figure 3.8 – Effect of secondary compression on the evolution of the compression line in the (*e*-ln*p'*) plane

During secondary compression of normally consolidated clay, the void ratio and the rate of viscoplastic volumetric strain progressively decrease, and the state of the soil in the $(e - \ln p')$ plane moves towards lower constant rate of strain (CRS) compression lines, see Figure 3.8. The rate of viscoplastic volumetric strain is obtained from the time derivative of the secondary compression equation as

$$\dot{\varepsilon}_p^{vp} = -\frac{\dot{e}}{v} = \frac{C_\alpha}{v \ln(10)} \frac{1}{t} \tag{3.71}$$

Combining Equations (3.70) and (3.71), the relationship between the change of void ratio and the change of viscoplastic strain rate during secondary compression is expressed as

$$\Delta e = \frac{C_\alpha}{\ln(10)} \Delta \ln\left(\dot{\varepsilon}_p^{vp}\right) \tag{3.72}$$

The secondary compression results in the stiffening of the soil and the increase of pre-consolidation pressure of the soil under subsequent loading (Figure 3.8). The change of pre-consolidation pressure due to the secondary compression is obtained from

$$\Delta \ln(\bar{p}_c') = \frac{\Delta e}{(\lambda - \kappa)} \tag{3.73}$$

Combining Equations (3.72) and (3.73), the evolution of $\bar{p}'_c$ with the viscoplastic volumetric strain rate $\dot{\varepsilon}_p^{vp}$ is expressed as

$$\Delta \ln(\bar{p}_c') = \frac{C_\alpha}{(\lambda - \kappa)\ln(10)} \Delta \ln\left(\dot{\varepsilon}_p^{vp}\right) \tag{3.74}$$

Equation (3.74) can be rewritten as

$$\bar{p}_c' = \bar{p}_{c,r}' \left(\frac{\dot{\varepsilon}_p^{vp}}{\dot{\varepsilon}_{p,r}^{vp}}\right)^{c_\beta} \tag{3.75}$$

where

$$c_\beta = \frac{C_\alpha}{(\lambda - \kappa)\ln(10)} \tag{3.76}$$

is the viscoplastic parameter controlling the evolution of the strain rate hardening and $\bar{p}_{c,r}'$ is the hardening parameter on a reference CRS compression line with the viscoplastic volumetric strain rate $\dot{\varepsilon}_{p,r}^{vp}$. The parameter c_β is nearly constant in a range of strain rates experienced by the soil during secondary compression in laboratory consolidation tests. However, based on the experimental evidence (Leroueil *et al.*, 1988; Leroueil, 2006; Watabe *et al.*, 2012), c_β depends *a priori* on strain rate and decreases with the decrease in the rate. The position of the CRS compression line in the $(e - \ln p')$ plane depends on the magnitude of the volumetric strain rate, and hence the absolute strain rate is used in Equation (3.75) as

$$\bar{p}'_c = \bar{p}'_{c,r} \left| \frac{\dot{\varepsilon}_p^{vp}}{\dot{\varepsilon}_{p,r}^{vp}} \right|^{c_\beta} \tag{3.77}$$

It can be assumed that below a certain limit to the strain rate, further decrease in rate does not affect the hardening parameter $\bar{p}'_c$ and the material behaviour becomes rate-independent. Hence, a viscoplastic volumetric strain rate threshold $\dot{\varepsilon}_{p,th}^{vp}$ can be defined in the model as the lower limit to the strain rate effect on the size of the bounding surface, i.e. if $\left|\dot{\varepsilon}_p^{vp}\right| < \dot{\varepsilon}_{p,th}^{vp}$, $\left|\dot{\varepsilon}_p^{vp}\right| = \dot{\varepsilon}_{p,th}^{vp}$ is considered in Equation (3.75). This is consistent with the concept of the static yield surface in the overstress theory. The threshold strain rate is assumed to be very small, or ideally equal to zero. For axial strain rates less than the threshold value, the viscoplastic model becomes rate-independent, i.e. no viscous behaviour exists, and the soil reaches to the final stable state. For axial strain rates exceeding the threshold value, the yield stress becomes rate-sensitive. The concept of the threshold strain rate is also considered in the works of Sheahan *et al.* (1994), Zhen-Yu *et al.* (2010), Qu *et al.* (2010) and Qiao *et al.* (2016). Qiao *et al.* (2016) recommended that the threshold strain rate can be considered in the range of $1 \times 10^{-5}\text{min}^{-1}$ to $1 \times 10^{-9}\text{min}^{-1}$ for soft clays.

Using Equations (3.63) – (3.64), (3.66) and (3.77), the relationship between the strain rate hardening modulus ξ and the strain hardening modulus h_b is obtained as

$$\xi = \frac{c_\beta(\lambda - \kappa)}{\upsilon\left(\dot{\varepsilon}_p^{vp} + \dot{\varepsilon}_{p,thr}^{vp}\right)} |h_b| \tag{3.78}$$

Note that the position of the CRS compression line in the $(e - \ln p')$ plane depends on the absolute value of the volumetric strain rate, and hence the absolute strain rate is used in Equations (3.76), (3.77) and (3.78).

3.4.4. Elasto-Viscoplastic Stress-Strain Relationship

Recalling the basic assumption of the bounding surface theory, the equivalent consistency condition at the current stress state $\boldsymbol{\sigma}'$ can be written as

$$\mathbf{n}^T \delta\boldsymbol{\sigma}' m_p - h\delta\varepsilon_p^{vp} - \xi\delta\dot{\varepsilon}_p^{vp} = 0 \tag{3.79}$$

The increment of viscoplastic volumetric strain rate can be approximated by

$$\delta\dot{\varepsilon}_p^{vp} \cong \frac{\delta\varepsilon_p^{vp\,t+\Delta t} - \delta\varepsilon_p^{vp\,t}}{\delta t} \tag{3.80}$$

in which δt is the time increment and $\delta\varepsilon_p^{vp\,t}$ and $\delta\varepsilon_p^{vp\,t+\Delta t}$ are the viscoplastic volumetric strain increments at the previous and current time steps, respectively. Substituting Equation (3.80) into the consistency equation (3.79) yields

$$\mathbf{n}^T \delta\boldsymbol{\sigma}' m_p - \left(h + \frac{\xi}{\delta t}\right)\delta\varepsilon_p^{vp\,t+\Delta t} + \xi\dot{\varepsilon}_p^{vp\,t} = 0 \tag{3.81}$$

The viscoplastic strain increment is given by

$$\delta\boldsymbol{\varepsilon}^{\mathrm{vp}} = \delta\lambda\mathbf{m} \tag{3.82}$$

where $\delta\lambda$ is the viscoplastic multiplier. Rewriting Equation (3.2) as

$$\delta\boldsymbol{\sigma}' = \mathbf{D}^{\mathrm{e}}(\delta\boldsymbol{\varepsilon} - \delta\boldsymbol{\varepsilon}^{\mathrm{vp}}) = \mathbf{D}^{\mathrm{e}}(\delta\boldsymbol{\varepsilon} - \delta\lambda\mathbf{m}) \tag{3.83}$$

and substituting Equations (3.82) and (3.83) into Equation (3.81) yields

$$\delta\lambda^{t+\Delta t} = \frac{\mathbf{n}^T\mathbf{D}^{\mathrm{e}}\delta\boldsymbol{\varepsilon} + \xi^*\dot{\varepsilon}_p^{vp\,t}}{\left(h + \frac{\xi}{\delta t} + \mathbf{n}^T\mathbf{D}^{\mathrm{e}}\mathbf{m}\right)} \tag{3.84}$$

in which

$$\xi^* = \frac{\xi}{m_p} = -\frac{\partial F}{\partial \bar{p}_c'}\frac{\partial \bar{p}_c'}{\partial \dot{\varepsilon}_p^{vp}}\frac{1}{\|\partial F/\partial \bar{\boldsymbol{\sigma}}'\|} \tag{3.85}$$

Substituting Equation (3.84) into (3.83) the elasto-viscoplastic stress-strain relation is expressed as

$$\delta\boldsymbol{\sigma}' = \mathbf{D}^{\mathrm{evp}}\delta\boldsymbol{\varepsilon} - \frac{\mathbf{D}^{\mathrm{e}}\mathbf{m}\xi^*\dot{\varepsilon}_p^{vp\,t}}{h + \frac{\xi}{\delta t} + \mathbf{n}^T\mathbf{D}^{\mathrm{e}}\mathbf{m}} = \mathbf{D}^{\mathrm{evp}}\delta\boldsymbol{\varepsilon} - \boldsymbol{\sigma}'^{\mathrm{vp}} \tag{3.86}$$

where $\mathbf{D}^{\mathrm{evp}}$ is the elasto-viscoplastic stiffness matrix given by

$$\mathbf{D}^{\mathrm{evp}} = \mathbf{D}^{\mathrm{e}} - \frac{\mathbf{D}^{\mathrm{e}}\mathbf{m}\mathbf{n}^T\mathbf{D}^{\mathrm{e}}}{h + \frac{\xi}{\delta t} + \mathbf{n}^T\mathbf{D}^{\mathrm{e}}\mathbf{m}} \tag{3.87}$$

3.4.5. Hardening Rule for Unsaturated Soils

For unsaturated soils, the hardening parameter is defined as a function of the viscoplastic strain, the viscoplastic strain rate and the matric suction, i.e. $\chi(\varepsilon^{vp}, \dot{\varepsilon}^{vp}, s)$ (Mac *et al.*, 2017).

Following the conventional approach in the bounding surface plasticity, the strain hardening modulus h can be divided into two components

$$h = h_b + h_f \tag{3.88}$$

where h_b is the strain hardening modulus us at stress point $\bar{\boldsymbol{\sigma}}'$ on the bounding surface, and h_f is the arbitrary moduli at $\boldsymbol{\sigma}'$, defined as functions of the distance between $\bar{\boldsymbol{\sigma}}'$ and $\boldsymbol{\sigma}'$.

Applying the consistency condition at the bounding surface, and incorporating the hardening effects of viscoplastic volumetric strain, viscoplastic volumetric strain rate and matric suction yields

$$\delta F = \left(\frac{\partial F}{\partial \bar{\boldsymbol{\sigma}}'}\right)^T \delta \bar{\boldsymbol{\sigma}}' + \frac{\partial F}{\partial \bar{p}'_c} \frac{\partial \bar{p}'_c}{\partial \varepsilon_p^{vp}} \delta \varepsilon_p^{vp} + \frac{\partial F}{\partial \bar{p}'_c} \frac{\partial \bar{p}'_c}{\partial \dot{\varepsilon}_p^{vp}} \delta \dot{\varepsilon}_p^{vp} + \frac{\partial F}{\partial \bar{p}'_c} \frac{\partial \bar{p}'_c}{\partial s} \delta s = 0 \tag{3.89}$$

Equation (3.89) can also be rewritten as

$$\mathbf{n}^T \delta \bar{\boldsymbol{\sigma}}' m_p - h_b \delta \varepsilon_p^{vp} - \xi \delta \dot{\varepsilon}_p^{vp} = 0 \tag{3.90}$$

where

$$h_b = -\frac{\partial F}{\partial \bar{p}'_c}\left(\frac{\partial \bar{p}'_c}{\partial \varepsilon_p^{vp}} + \frac{\partial \bar{p}'_c}{\partial s}\frac{\partial s}{\partial \varepsilon_p^{vp}}\right)\frac{m_p}{\|\partial F / \partial \bar{\boldsymbol{\sigma}}'\|} \tag{3.91}$$

and ξ is the viscoplastic strain rate hardening modulus,

$$\xi = -\frac{\partial F}{\partial \bar{p}'_c}\frac{\partial \bar{p}'_c}{\partial \dot{\varepsilon}_p^{vp}}\frac{m_p}{\|\partial F / \partial \bar{\boldsymbol{\sigma}}'\|} \tag{3.92}$$

in which

$$m_p = \partial g / \partial p' / \|\partial g / \partial \boldsymbol{\sigma}'\| \tag{3.93}$$

The strain hardening modulus h_f is defined such that it is zero on the bounding surface and infinity at the point of stress reversal. Following Khalili *et al.* (2005), h_f is assumed to be of the form

$$h_f = \bar{\bar{t}}\left(\frac{\partial \bar{p}'_c}{\partial \varepsilon_p^{vp}} + \frac{\partial \bar{p}'_c}{\partial s}\frac{\partial s}{\partial \varepsilon_p^{vp}}\right)\frac{p'}{\bar{p}'_c}\left[\frac{\bar{p}'_c}{p'_c} - 1\right]k_m(\eta_p - \eta) \tag{3.94}$$

where $\eta_p = M_{cs}\big(1 - 2(v - v_{cs})\big)$ is the slope of the peak strength line in the $(q - p')$ plane and k_m is a material parameter controlling the steepness of the response in the $(q - \varepsilon_q)$ plane.

Solving Equation (3.90) similarly to section 3.4.4, the increment of viscoplastic volumetric strain rate can be approximated by

$$\delta\dot{\varepsilon}_p^{vp} \cong \frac{\delta\varepsilon_p^{vp\,t+\Delta t} - \delta\varepsilon_p^{vp\,t}}{\delta t} \tag{3.95}$$

The consistency equation (3.90) yields

$$\mathbf{n}^T\delta\boldsymbol{\sigma}' m_p - \left(h + \frac{\xi}{\delta t}\right)\delta\varepsilon_p^{vp\,t+\Delta t} + \xi\dot{\varepsilon}_p^{vp\,t} = 0 \tag{3.96}$$

The viscoplastic strain increment is given by

$$\delta\boldsymbol{\varepsilon}^{\mathrm{vp}} = \delta\lambda\mathbf{m} \tag{3.97}$$

where $\delta\lambda$ is the viscoplastic multiplier. Rewriting Equation (3.2) as

$$\delta\boldsymbol{\sigma}' = \mathbf{D}^{\mathrm{e}}(\delta\boldsymbol{\varepsilon} - \delta\boldsymbol{\varepsilon}^{\mathrm{vp}}) = \mathbf{D}^{\mathrm{e}}(\delta\boldsymbol{\varepsilon} - \delta\lambda\mathbf{m}) \tag{3.98}$$

and substituting Equations (3.97) and (3.98) into Equation (3.96) yields

$$\delta\lambda^{t+\Delta t} = \frac{\mathbf{n}^T \mathbf{D}^{\mathrm{e}} \delta\boldsymbol{\varepsilon} + \xi^* \dot{\varepsilon}_p^{vp\,t}}{\left(h + \frac{\xi}{\delta t} + \mathbf{n}^T \mathbf{D}^{\mathrm{e}} \mathbf{m}\right)} \tag{3.99}$$

where

$$\xi^* = \frac{\xi}{m_p} = -\frac{\partial F}{\partial \bar{p}'_c} \frac{\partial \bar{p}'_c}{\partial \dot{\varepsilon}_p^{vp}} \frac{1}{\left\| \frac{\partial F}{\partial \bar{\boldsymbol{\sigma}}'} \right\|} \tag{3.100}$$

Substituting Equation (3.99) into (3.98) the elasto-viscoplastic stress-strain relation is expressed as

$$\delta\boldsymbol{\sigma}' = \mathbf{D}^{\mathrm{evp}} \delta\boldsymbol{\varepsilon} - \frac{\mathbf{D}^{\mathrm{e}} \mathbf{m} \xi^* \dot{\varepsilon}_p^{vp\,t}}{h + \frac{\xi}{\delta t} + \mathbf{n}^T \mathbf{D}^{\mathrm{e}} \mathbf{m}} = \mathbf{D}^{\mathrm{evp}} \delta\boldsymbol{\varepsilon} - \boldsymbol{\sigma}'^{\mathrm{vp}} \tag{3.101}$$

where $\mathbf{D}^{\mathrm{evp}}$ is the elasto-viscoplastic stiffness matrix given by

$$\mathbf{D}^{\mathrm{evp}} = \mathbf{D}^{\mathrm{e}} - \frac{\mathbf{D}^{\mathrm{e}} \mathbf{m} \mathbf{n}^T \mathbf{D}^{\mathrm{e}}}{h + \frac{\xi}{\delta t} + \mathbf{n}^T \mathbf{D}^{\mathrm{e}} \mathbf{m}} \tag{3.102}$$

3.4.5.1. Suction Hardening

The general effect of suction is to increase the effective stress and hardens the soil response. The increase in the soil stiffness leads to an increase in both the intercept $N(s)$ and $\lambda(s)$ of the isotropic compression line, which will have a net effect of increasing the size of the bounding surface ($\bar{p}'_c$). There are two approaches for incorporating the hardening effect of suction; a coupled influence where suction has a multiplicative effect to the viscoplastic volumetric hardening; or a decoupled influence where suction has an additive effect on the hardening parameter. In the formulation presented here, the approach proposed by Loret and Khalili (2002) which considers a coupled effect of suction hardening is adopted. For the coupled approach, the general expression for the hardening rule is given by

$$\bar{p}'_c(\varepsilon_p^{vp}) = \bar{p}'_{ci}\gamma(s)\exp\left(\frac{v_i\Delta\varepsilon_p^{vp}}{\lambda(s)-\kappa}\right) \tag{3.103}$$

where v_i is the initial specific volume, $\bar{p}'_{ci}$ is the initial value of the hardening parameter, $\Delta\varepsilon_p^{vp}$ is the increment of viscoplastic volumetric strain, $\gamma(s)$ is a function representing the coupled effect of suction hardening and can be determined considering the shift in the limiting isotropic compression line (LICL) due to suction change

$$\gamma(s) = \exp\left(\frac{N(s)-N(s_i)}{\lambda(s)-\kappa} - \frac{\lambda(s)-\lambda(s_i)}{\lambda(s)-\kappa}\ln(\bar{p}'_{ci})\right) \tag{3.104}$$

in which $N(s_i)$ and $\lambda(s_i)$ are intercept and slope of the LICL at the initial suction s_i, while $N(s)$ and $\lambda(s)$ are intercept and slope of the LICL at the final suction *s* (Figure 3.9)

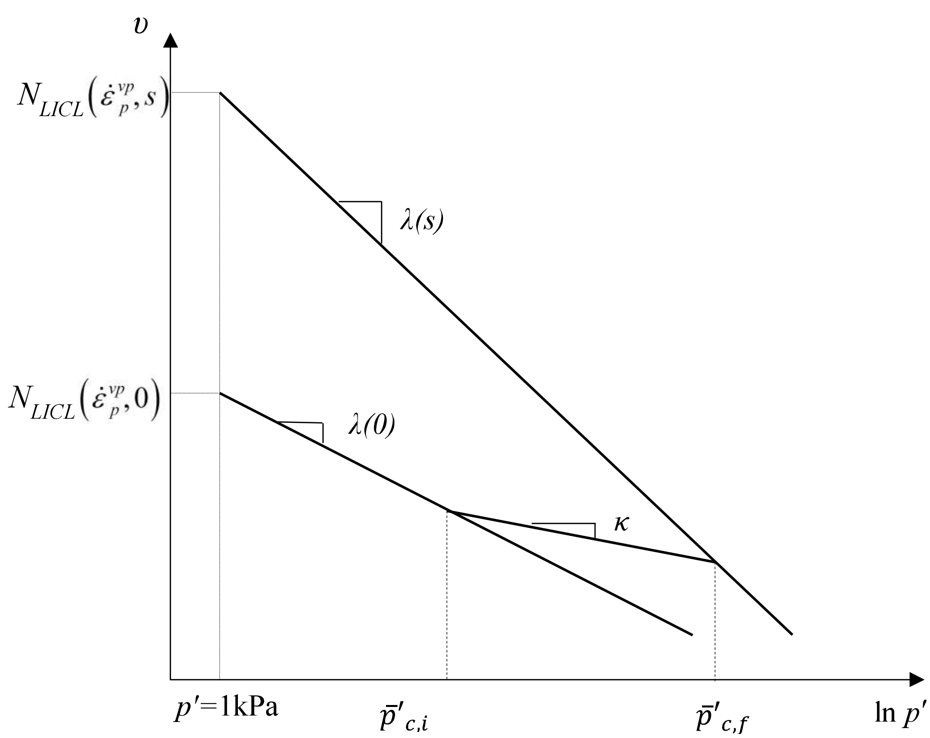

Figure 3.9 – Schematic diagram illustrating the hardening effect of suction

3.4.6. Parameter Identification

The constitutive parameters used in the model can be summarised as follows: κ and ν to describe the elastic behaviour; M_{cs}, λ, Γ to define the reference critical state line; N and R to define the shape of the bounding surface; A to describe the stress-dilatancy relationship; k_m to calibrate the hardening modulus; and c_β, $\dot{\varepsilon}_{p,r}^{vp}$, $\dot{\varepsilon}_{p,thr}^{vp}$ to describe the strain rate hardening. A series of laboratory tests at different stress paths and strain rates is required in order to calibrate the model parameters.

The elastic parameters κ and ν are determined from isotropic loading and unloading tests. κ is the initial slope of elastic unloading-reloading line in the $(\upsilon - \ln p')$ plane. ν is the Poisson's ratio, which can be obtained from the unloading stage of the same test by measuring the ratio of the radial strain to the axial strain. The Poisson's ratio can also be determined indirectly using measured values of the tangential bulk and shear moduli. The critical state parameters M_{cs}, λ, Γ are best determined from a series of standard triaxial and isotropic compression tests. M_{cs} is the slope of the critical state line in the $(q - p')$ plane, λ is the slope of the critical state line in the $(\upsilon - \ln p')$ plane, and Γ is the reference specific volume at the critical state at a unit confining pressure. λ can also be obtained from isotropic compression tests as the slope of the limiting isotropic compression line. The parameters N and R defining the shape of bounding surface can be determined by fitting the equation of the bounding surface to the effective stress path of undrained deviatoric response on very loose samples. R is the distance between the CSL and LICL along the κ-line and can be determined from isotropic consolidation test data. The material parameter k_m is obtained by fitting, using the initial slope of drained deviatoric loading and unloading responses in the $(q - \varepsilon_q)$ plane. The dilatancy coefficient *A* can be determined by plotting the stress ratio η against the measured total dilatancy in standard drained triaxial compression tests, assuming elastic strains are negligible in comparison to viscoplastic strains.

Strain rate hardening parameters c_β and $\dot{\varepsilon}_{p,r}^{vp}$ can be determined from secondary compression tests. The reference viscoplastic strain rate corresponding to a secondary compression test at time *t* can be obtained from

$$\dot{\varepsilon}_{p,r}^{vp} = \frac{C_\alpha}{t\upsilon_0 \ln(10)} \tag{3.105}$$

where υ_0 is the initial specific volume. Strain rate hardening parameters c_β and $\dot{\varepsilon}_{p,r}^{vp}$ can also be determined from constant rate of strain tests by measuring Γ and $\bar{p}_c'$ at a range of strain rates. The threshold viscoplastic volumetric strain rate $\dot{\varepsilon}_{p,thr}^{vp}$ depending on the variation of c_β with strain rate can be determined by fitting Equation (3.77) to the results of oedometer and CRS tests in the $\left(\ln(\bar{p}_c'/\bar{p}_{c,r}') \sim \ln\left(\dot{\varepsilon}_p^{vp}/\dot{\varepsilon}_{p,r}^{vp}\right)\right)$ plane.

3.5. Tertiary Creep

Tertiary creep is associated with increasing strain rate leading to failure of soil. This is of particular relevance to natural and excavated slopes in which creep failures are most common. In this section, the capability of the model to predict tertiary creep in drained and undrained conditions is demonstrated.

3.5.1. Drained Creep Rupture

During the drained creep process, the effective stresses remain constant. This corresponds to a single stress point in the $(p' - q)$ plane, i.e.

$$\delta\boldsymbol{\sigma}' = \{\delta p', \delta q\}^T = 0 \tag{3.106}$$

Applying the stress condition (3.106) to Equations (3.2) and (3.50) gives

$$\delta\boldsymbol{\varepsilon}^{\mathrm{e}} = \left\{\delta\varepsilon_p^e, \delta\varepsilon_q^e\right\}^T = 0 \tag{3.107}$$

$$\dot{d} = \frac{d}{dt}\left(\frac{\delta\varepsilon_p^{vp}}{\delta\varepsilon_q^{vp}}\right) = 0 \tag{3.108}$$

The consistency condition at this constant effective stress state is expressed as

$$h\delta\varepsilon_p^{vp} + \xi\delta\dot{\varepsilon}_p^{vp} = 0 \tag{3.109}$$

Using Equations (3.106)-(3.109) the rate of strain increment is related to the strain increment by

$$\{\delta\dot{\varepsilon}_p \quad \delta\dot{\varepsilon}_q\} = -\frac{h}{\xi}\{\delta\varepsilon_p \quad \delta\varepsilon_q\} \tag{3.110}$$

During creep under loading with the stress point is below the critical state line in the $(p' - q)$ plane,

$$h > 0; \quad \xi > 0; \quad \delta\boldsymbol{\varepsilon} = \{\delta\varepsilon_p \quad \delta\varepsilon_q\}^T > \mathbf{0} \tag{3.111}$$

Applying the conditions (3.111) to Equation (3.110) results in

$$\delta\dot{\boldsymbol{\varepsilon}} = \{\delta\dot{\varepsilon}_p \quad \delta\dot{\varepsilon}_q\}^T < \mathbf{0} \tag{3.112}$$

This is associated with the primary phase of creep with decreasing strain rate, and is consistent with the experimental evidence demonstrating that the drained creep rupture cannot occur in normally consolidated soils.

For over-consolidated soils, when the stress point is above the critical state line in the $(p' - q)$ plane,

$$h_f \geq 0; \quad h_b < 0; \quad \xi > 0; \quad \delta\varepsilon_p < 0; \quad \delta\varepsilon_q > 0 \tag{3.113}$$

The creep-induced instability in over-consolidated soils often occurs at stress levels below the peak strength (Murayama and Shibata, 1958; Bishop and Lovenbury, 1969; Snead, 1970; Tavenas *et al.*, 1978; Lefebvre, 1981). In this case, in the early stage of creep

$$h = h_f + h_b > 0 \tag{3.114}$$

Applying the conditions (3.113) and (3.114) to Equation (3.110) results in

$$\delta\dot{\varepsilon}_p > 0, \qquad \delta\dot{\varepsilon}_q < 0 \tag{3.115}$$

This is associated with the primary phase of drained creep in over-consolidated soils with decreasing strain rate. During the primary phase, the bounding surface shrinks due to both increase in void ratio and decrease in viscoplastic volumetric strain rate. This results in the reduction of h_f of over time, and can lead the process into the secondary phase of creep with constant strain rate, i.e.

$$h = h_f + h_b = 0 \tag{3.116}$$

Applying Equation (3.116) into Equation (3.110) yields

$$\delta\dot{\varepsilon}_p = 0; \qquad \delta\dot{\varepsilon}_q = 0 \tag{3.117}$$

By further shrinkage of the bounding surface due to increase in void ratio, the distance between the current stress $\boldsymbol{\sigma}'$ and the image of the stress point on the bounding surface $\overline{\boldsymbol{\sigma}}'$ decreases, which results in h_f approaching zero. This yields

$$h = h_f + h_b < 0 \tag{3.118}$$

Applying Equation (3.116) into Equation (3.110) yields

$$\delta\dot{\varepsilon}_p < 0; \qquad \delta\dot{\varepsilon}_q > 0 \tag{3.119}$$

This is associated with the tertiary phase of drained creep with increasing strain rate, which leads to creep failure of over-consolidated soil. It is worth noting that when the bounding surface reaches the stress point, i.e. $h_f = 0$, the rate of shrinkage of bounding surface due to increase in void ratio becomes equal to the rate of its expansion due to increase in viscoplastic volumetric strain rate, and hence $\delta\bar{p}_c{}' = 0$. This is captured in the model by using Equation (3.77).

As demonstrated, the bounding surface framework enables the model to capture all the three phases of drained creep in over-consolidated soils. In single yield surface viscoplastic models, the creep process cannot be initiated from a stress state inside the yield surface and only begins when the stress point lies on the yield surface. In this case, the hardening modulus h is always negative, and hence the primary and secondary phases of creep cannot be captured. This is particularly important in the stability analysis of clayey slopes in which the creep-induced instability generally occurs at strengths less than the peak strength (Shahbodagh *et al.*, 2020).

3.5.2. Undrained Creep Rupture

During the undrained creep process, the deviatoric stress and the void ratio remain constant, i.e.

$$\delta q = 0; \quad \delta \varepsilon_p = 0 \tag{3.120}$$

The change in deviatoric strain due to creep, however, affects the pore water pressure and consequently changes the mean effective stress. Under this condition, the viscoplastic volumetric strain rate is related to the rate of mean effective stress by

$$\dot{\varepsilon}_p^{vp} = -\dot{\varepsilon}_p^{e} = -\frac{\dot{p}'}{K} \tag{3.121}$$

The time derivative of the dilatancy Equation (3.50) gives

$$\delta \dot{\varepsilon}_q = \tilde{t}\frac{\delta \dot{\varepsilon}_p^{vp}}{d} - \frac{\dot{d}}{d}\delta \varepsilon_q \tag{3.122}$$

where
$$\dot{d} = \tilde{t}A\frac{q\dot{p}'}{p'^2} \tag{3.123}$$

Substituting Equations (3.121) and (3.123) into (3.122) yields

$$\delta \dot{\varepsilon}_q = \tilde{t}\frac{\delta \dot{\varepsilon}_p^{vp}}{d} + AK\frac{q}{p'^2}\left(\dot{\varepsilon}_q \delta \varepsilon_q\right) \tag{3.124}$$

The consistency condition at the current stress state during the undrained creep process is expressed as

$$\delta p' n_p m_p - h\delta \varepsilon_p^{vp} - \xi \delta \dot{\varepsilon}_p^{vp} = 0 \tag{3.125}$$

Using Equations (3.121), (3.125) and (3.50), the rate of viscoplastic volumetric strain increment is related to the deviatoric strain increment by

$$\delta \dot{\varepsilon}_p^{vp} = \frac{-\left(Kn_p m_p + h\right)\tilde{t}d}{\xi}\delta \varepsilon_q \tag{3.126}$$

Substituting Equation (3.124) into Equation (3.122) yields

$$\delta\dot{\varepsilon}_q = AK\frac{q}{p'^2}\left(\dot{\varepsilon}_q\delta\varepsilon_q\right) - \frac{Kn_p m_p + h}{\xi}\delta\varepsilon_q \tag{3.127}$$

During the undrained creep due to loading, the first term in Equation (3.127) remains always positive (or zero when $q = 0$). The sign of the second term depends on the effective stress state. By progress of creep, the current stress point moves towards the critical state line in the $(p' - q)$ plane. At low shear stress levels, i.e. when $q << q_{ultimate}$, the term $\delta\varepsilon_q\left(Kn_p m_p + h\right)/\xi$ is positive and larger than the first term. Thus, $\delta\dot{\varepsilon}_q < 0$ while $\delta\varepsilon_q > 0$, which is associated with the primary phase of undrained creep with decreasing strain rate. In this case, $\delta\varepsilon_q$ approaches zero before the stress reaches the critical state, and hence no creep-induced instability occurs. At high shear stress levels, however, the current stress point can approach the critical state line, which results in the second term in approaching zero, and hence $\delta\dot{\varepsilon}_q > 0$. This is associated with the undrained creep rupture leading to failure of the soil.

3.6. Conclusions

A unified bounding surface viscoplasticity model was developed to describe the time-dependent stress-strain behaviour of both saturated and unsaturated soils. The main features of the conventional plasticity models, the methods used for the derivation of the stress-strain relationship for an elasto-(visco)plastic constitutive model, and the approaches widely used for the development of viscoplastic constitutive models were introduced. All ingredients of the proposed bounding surface viscoplasticity model were described in details. The capability of the model to predict tertiary creep in drained and undrained conditions was demonstrated.

CHAPTER 4

GOVERNING EQUATIONS AND NUMERICAL IMPLEMENTATION

4.1. Introduction

This chapter presents the governing equations of multiphase porous media and their finite element approximations. The governing differential equations are derived using a macroscopic approach and based on the model proposed by Khalili *et al.* (2008) for a fully coupled flow-deformation analysis of unsaturated porous media. The coupling between solid and fluid phases is enforced according to the effective stress principle taking suction dependency of the effective stress parameter into account. The effect of hydraulic hysteresis on the effective stress parameter and soil water characteristic curve is also taken into account. The governing equations will be presented in Sections 4.3 and 4.4, and the numerical implementation is presented in Section 4.5. Both global and local solution schemes are required to numerically solve a boundary value problem. The global solution scheme involves solving the governing equations for the unknown primary variables such as displacements and pore pressures, while the local solution scheme involves integration of the constitutive equations to compute internal variables including strains and stresses. Both global and local solution procedures must satisfy the basic requirements of equilibrium, compatibility, constitutive behaviour and boundary conditions, at the same time maintaining accuracy, simplicity, efficiency and robustness.

4.2. Notation and Sign Convention

The sign convention of continuum mechanics is adopted throughout, i.e. tension taken as positive and compression as negative. Compact matrix-vector notation is used throughout. Bold face letters indicate matrices and vectors. $\nabla(.) = \partial(.)/\partial x$ is the spatial gradient and $div(.)$ is the divergence operator. The identity vector is identified as $\boldsymbol{\delta} = \{1,1,1,0,0,0\}^T$.

Following the soil mechanics convention, pore water and pore air pressures are considered positive in compression. The mean normal stress and the volumetric strain (p and ε_v) are defined as $p = -\frac{1}{3}\boldsymbol{\delta}^T\boldsymbol{\sigma}$ and $\varepsilon_v = -\boldsymbol{\delta}^T\boldsymbol{\varepsilon}$ so that they are positive in compression.

Unsaturated soils consist of three phases: solid particles (s) and a pore space filled with water (w) and air (a). Within the context of theory of mixtures, each phase is endowed with its own kinematics, mass and momentum, occupying the entire volume of the unsaturated porous medium, V. Each constituent has a mass M_α and a volume V_α ($\alpha = s, w, a$). The total volume V is $V = V_s + V_w + V_a$, while the total mass M is $M = M_s + M_w + M_a$.

Intrinsic quantities are defined using subscripts and apparent quantities using superscripts. Hence, the intrinsic mass density of phase α is denoted as $\rho_\alpha = M_\alpha / V_\alpha$, whereas the apparent mass density is written as $\rho^\alpha = M_\alpha / V$. Therefore, $\rho^\alpha = n^\alpha \rho_\alpha$, where $n^\alpha = V_\alpha / V$ is the apparent volume fraction of phase α. The apparent volume fractions satisfy the constraint $n^s + n^w + n^a = 1$. All measurements are made from configuration at time $t = 0$. The initial configuration is assumed to be free of strain. Finally, $d_\alpha()/dt = \partial()/\partial t + \nabla().\mathbf{v}_\alpha$ is used to denote the material time derivative with respect to phase α, with $\mathbf{v}_\alpha$ representing the velocity field of constituent α.

4.3. Effective Stress Theory

The effective stress concept was first introduced by Terzaghi, and then has been widely applied for saturated soils to solve many geotechnical engineering problems. If the soil constituent is assumed to be incompressible, the effective stress for saturated soils is defined by Terzaghi (1936) as

$$\boldsymbol{\sigma}' = \boldsymbol{\sigma} + p_w \boldsymbol{\delta} \tag{4.1}$$

where $\boldsymbol{\sigma}'$ is the effective stress, p_w is the pore water pressure and $\boldsymbol{\delta}$ is the identity vector.

For unsaturated soils, the effective stress is expressed by Bishop (1959) as

$$\boldsymbol{\sigma}' = \boldsymbol{\sigma} + p_a \boldsymbol{\delta} - \chi (p_a - p_w) \boldsymbol{\delta} \tag{4.2}$$

where p_a is the pore air pressure, χ is the effective stress parameter, attaining a value of one for saturated soils and zero for dry soils. Equation (4.2) can be rewritten as

$$\boldsymbol{\sigma}' = \boldsymbol{\sigma}_{net} - \chi s \boldsymbol{\delta} \tag{4.3}$$

where $\boldsymbol{\sigma}_{net} = \boldsymbol{\sigma} + p_a \boldsymbol{\delta}$ is the net stress and $s = p_a - p_w$ is the matric suction. Constitutive relations for soils are highly nonlinear, and hence they are generally expressed in the incremental format (Shahbodagh *et al.*, 2014; Mac *et al.*, 2014; Shahbodagh *et al.*, 2015; Mac *et al.*, 2017; Shahbodagh *et al.*, 2019; Ghaffaripour *et al.*, 2019; Mac *et al.*, 2019; Oka *et al.*, 2019). The incremental form of the effective stress equation is obtained through a simple differentiation of Equation (4.3) as

$$\dot{\boldsymbol{\sigma}}' = \dot{\boldsymbol{\sigma}}_{net} - \psi \dot{s} \boldsymbol{\delta} \tag{4.4}$$

where the superimposed dot indicates the rate of change, $\dot{\boldsymbol{\sigma}}_{net} = \dot{\boldsymbol{\sigma}} + \dot{p}_a \boldsymbol{\delta}$ is the incremental net stress, $\dot{s} = \dot{p}_a - \dot{p}_w$ is the incremental suction, and $\psi = d(\chi s)/ds$ is the incremental effective stress parameter.

4.3.1. Effective Stress Parameter

The effective stress parameter, χ, represents the contribution of suction to the effective stress. It is linked to the soil structure through an experimentally obtained correlation between soil suction and the effective stress parameter. Following Khalili and Khabbaz (1998) and Khalili *et al.* (2004), the effective stress parameter is defined as

$$\chi = \begin{cases} 1 & \text{for } \dfrac{s}{s_e} \leq 1 \\ \left(\dfrac{s}{s_e}\right)^{-\Omega} & \text{for } \dfrac{s}{s_e} > 1 \end{cases} \tag{4.5}$$

where Ω is a material parameter with the best fit value of 0.55, and s_e is the suction value marking the transition between saturated and unsaturated states. For the wetting process, $s_e = s_{ex}$, and for the drying process, $s_e = s_{ae}$, in which s_{ex} is the air expulsion value and s_{ae} is the air entry value. s_{ex} and s_{ae} are functions of the specific volume (density) of the soil. This leads to a shift to the right of the effective stress parameter curve with increasing density (Figure 4.1). Khalili and Zargarbashi (2010) experimentally studied the effects of hydraulic hysteresis on the effective stress parameter, and established the following correlation for suction reversals:

$$\chi = \begin{cases} \left(\dfrac{s_{rd}}{s_{ae}}\right)^{-\Omega} \left(\dfrac{s}{s_{rd}}\right)^{\zeta} & \text{for drying path reversal } \left(\dfrac{s_{ex}}{s_{ae}}\right)^{\frac{\Omega}{\Omega-\zeta}} s_{rd} \leq s \leq s_{rd} \\ \left(\dfrac{s_{rw}}{s_{ex}}\right)^{-\Omega} \left(\dfrac{s}{s_{rw}}\right)^{\zeta} & \text{for wetting path reversal } s_{rw} \leq s \leq \left(\dfrac{s_{ae}}{s_{ex}}\right)^{\frac{\Omega}{\Omega-\zeta}} s_{rw} \end{cases} \tag{4.6}$$

where ζ is the slope of the transition line between the main wetting and main drying paths in the $(ln\chi{\sim}lns)$ plane, and s_{rw} and s_{rd} are the points of suction reversal on the main wetting and the main drying paths, respectively. The variation of the value of χ upon suction reversal is due to a change in the contact angle between the air-water interface and the solid grains. s_{ex} and s_{ae} are functions of the specific volume (density) of the soil.

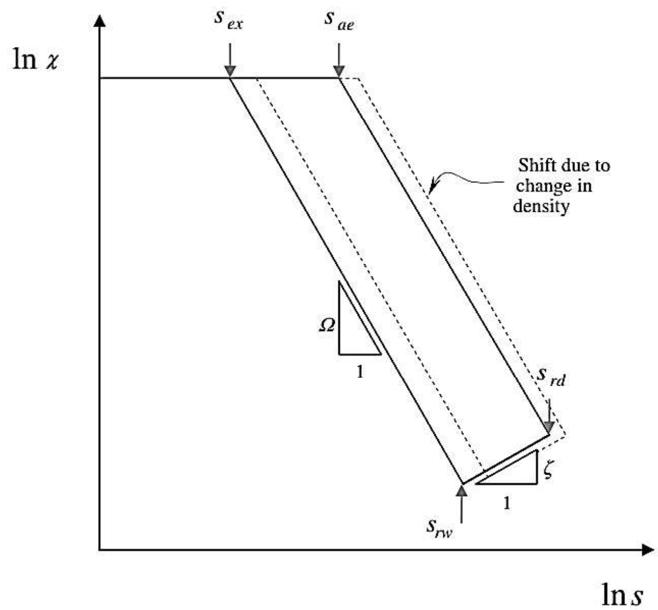

Figure 4.1 – Evolution of the effective stress parameter with hydraulic hysteresis and with change in density (after Khalili *et al.*, 2008)

4.3.2. Soil Water Characteristic Curve (SWCC)

The soil water characteristic curve (SWCC) determines the volumetric deformation of the water phase with respect to change in matric suction. In this formulation, the SWCC model proposed by Brooks and Corey (1964), extended by Khalili *et al.* (2008) to include hydraulic hysteresis effects, is adopted as

$$S_{\text{eff}} = \begin{cases} 1 & \text{for } \dfrac{s}{s_e} \leq 1 \\ \left(\dfrac{s_e}{s}\right)^{\lambda_p} & \text{for } \dfrac{s}{s_e} > 1 \end{cases} \tag{4.7}$$

$$S_{\text{eff}} = \begin{cases} \left(\dfrac{s_{ae}}{s_{rd}}\right)^{\lambda_p} \left(\dfrac{s_{rd}}{s}\right)^{\xi} & \text{for drying path reversal } \left(\dfrac{s_{ex}}{s_{ae}}\right)^{\frac{\lambda_p}{\lambda_p - \xi}} s_{rd} \leq s \leq s_{rd} \\ \left(\dfrac{s_{ex}}{s_{rw}}\right)^{\lambda_p} \left(\dfrac{s_{rw}}{s}\right)^{\xi} & \text{for wetting path reversal } s_{rw} \leq s \leq \left(\dfrac{s_{ae}}{s_{ex}}\right)^{\frac{\lambda_p}{\lambda_p - \xi}} s_{rw} \end{cases} \tag{4.8}$$

where λ_p is the pore size distribution index, $S_{\text{eff}} = (S_r - S_{res})/(1 - S_{res})$ is the effective degree of saturation, S_{res} is the residual degree of saturation, ξ is the slope of the transition line between the main wetting and drying paths in the ($\ln S_{\text{eff}} \sim \ln s$) plane, and s_{rd} and s_{rw} are the points of suction reversal on the main drying and main wetting paths, respectively. A schematic representation of the model is shown in Figure 4.2, where the shift to the right of the soil water characteristic curve commonly observed in soils due to density dependency of the air entry and air expulsion values.

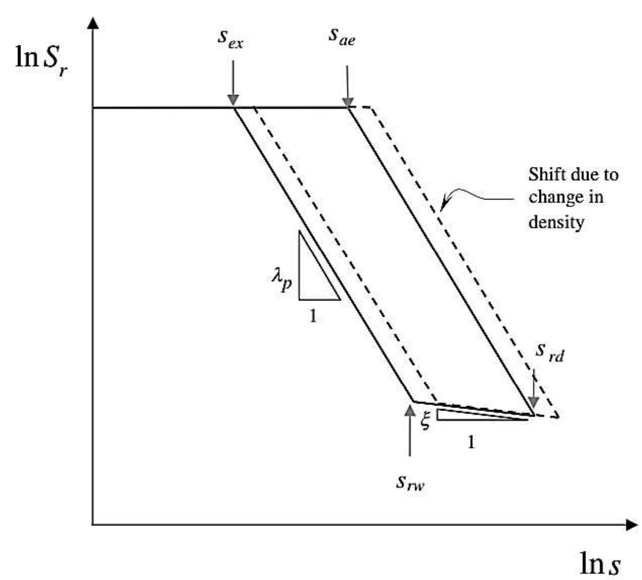

Figure 4.2 – Soil water characteristic curve including the effects of hydraulic hysteresis and change in density (after Khalili *et al.*, 2008)

4.3.3. Coefficient of Permeability

The coefficient of permeability for unsaturated soils is not a constant, and is significantly affected by changes in the void ratio and the degree of saturation.

The variation of permeability with void ratio, *e*, is accounted for using the empirical equation proposed by Taylor

$$k_{\beta s} = k_{\beta s0} \exp\left(\frac{e - e_0}{C_k}\right) \qquad (\beta = w, a) \tag{4.9}$$

where k_{ws} is the water permeability under saturated conditions, k_{as} is the gas permeability under fully dry conditions, $k_{\beta s0}$ is the initial value of $k_{\beta s}$, e_0 is the initial void ratio, and C_k is the material constant.

The dependency of the permeability coefficient on the degree of saturation can be captured using the model proposed by Brooks and Corey (1964) as

$$k_{rW} = S_{eff}^{\delta_1} \tag{4.10}$$

$$k_{ra} = \left(1 - S_{eff}\right)^2 \left(1 - S_{eff}^{\delta_2}\right) \tag{4.11}$$

where $\delta_1 = (2 + 3\lambda_p)/\lambda_p$ and $\delta_2 = (2 + \lambda_p)/\lambda_p$ are the fitting parameters determined empirically.

4.4. Governing Equations

The governing equations for fully coupled analysis of flow and deformation in partially saturated soils are formulated within the context of theory of mixtures using a systematic macroscopic approach satisfying the conservation equations of mass and momentum. Three phases (solid, water and air) are identified. Each phase is viewed as an independent continuum, endowed with its own kinematics, mass and momentum (Habte *et al.*, 2006; Khalili *et al.*, 2008).

The differential governing equations consist of two separate models: the fluid flow model and the deformation model. The flow model involves two phases, water phase and air phase, which are connected through the soil water characteristic curve. The deformation model is based on viscoplastic constitutive model, satisfying equation of total stress equilibrium, the compatibility and the consistency. The coupling between the flow model and the deformation model is derived using the concept of effective stress and the compatibility of the volumetric deformation of the three phases.

4.4.1. Flow Model

4.4.1.1. Water Phase

The water phase model is described by combining the equation of linear momentum balance for the liquid phase and the mass balance equation of the fluid. Neglecting the inertial and viscous effects, the equation of linear momentum balance for the water phase can be written as

$$\mathbf{v}_w^r = -\frac{k_{rw}\mathbf{k}}{\mu_w}(\nabla p_w + \rho_w \mathbf{g}) \tag{4.12}$$

where $\mathbf{v}_w^r$ is the relative velocity vector for the water phase, $\mathbf{k}$ is the intrinsic permeability of the soil**,** k_{rw} is the relative permeability with respect to the water phase, μ_w is the dynamic viscosity of water, $\mathbf{g}$ is the vector of gravitational acceleration. The relative velocity of the water with respect to a moving solid is given by

$$\mathbf{v}_w^r = n_w(\mathbf{v}_w - \mathbf{v}_s) = n_w\left(\frac{\partial \mathbf{u}_w}{\partial t} - \frac{\partial \mathbf{u}}{\partial t}\right) \tag{4.13}$$

where n_w is the volumetric water content, $\mathbf{v}_w$ is the absolute water velocity, $\mathbf{v}_s$ is the solid skeleton velocity, and $\mathbf{u}_w$ and $\mathbf{u}$ are the displacement vectors of the fluid and solid, respectively.

Excluding mass exchange between the phases due to vaporisation and condensation, the mass balance equation for the water phase is given by

$$\mathrm{div}(\rho_w n_w \mathbf{v}_w) + \frac{\partial}{\partial t}(\rho_w n_w) = 0 \tag{4.14}$$

Substituting Equation (4.13) into Equation (4.14) yields,

$$-\mathrm{div}(\rho_w \mathbf{v}_w^r) - \mathrm{div}(\rho_w n_w \mathbf{v}_s) = \frac{\partial}{\partial t}(\rho_w n_w) \tag{4.15}$$

Applying the Lagrangian total derivative with respect to a moving solid $d_s(.)/dt = \partial(.)/\partial t + \nabla(.)\mathbf{v}_s$, and a moving fluid $d_w(.)/dt = \partial(.)/\partial t + \nabla(.)\mathbf{v}_w$, with the vector identify $\mathrm{div}((.)\mathbf{v}_\alpha) = (.)\mathrm{div}(\mathbf{v}_\alpha) + \nabla(.)\mathbf{v}_\alpha$, Equation (4.15) can be rearranged to

$$-\rho_w \mathrm{div}(\mathbf{v}_w^r) = n_w \frac{d_w \rho_w}{dt} + \rho_w \frac{d_s n_w}{dt} + \rho_w n_w \mathrm{div}(\mathbf{v}_s) \tag{4.16}$$

If the fluid constituent is assumed to be barotropic, the coefficient of water compressibility (c_w) can be obtained from

$$\frac{d_w \rho_w}{dt} = \rho_w c_w \frac{d_w p_w}{dt} \tag{4.17}$$

From the definition of the volumetric water content, $n_w = V_w/V$

$$\frac{d_s n_w}{dt} = \frac{1}{V}\left(\frac{d_s V_w}{dt} - n_w \frac{d_s \mathrm{V}}{dt}\right) \tag{4.18}$$

Substituting Equations (4.12), (4.17) and (4.18) into Equation (4.16) and noting $(d_s V/dt)/V = \mathrm{div}(\mathbf{v}_s)$ yields the governing equation for the water flow in partially saturated soils

$$\mathrm{div}\left(\frac{k_{rw}\mathbf{k}}{\mu_w}(\nabla p_w + \rho_w \mathbf{g})\right) = n_w c_w \frac{d_w p_w}{dt} + \frac{1}{V}\frac{d_s V_w}{dt} \tag{4.19}$$

4.4.1.2. Air Phase

The equivalent form of the momentum balance equation for the air phase can be written as (Khalili *et al.*, 2000)

$$\mathbf{v}_a^r = -\frac{k_{ra}\mathbf{k}}{\mu_a}\nabla p_w \tag{4.20}$$

where $\mathbf{v}_a^r$ is the relative velocity vector for the air phase, k_{ra} is the relative permeability of the air phase, μ_a is the dynamic viscosity of air.

Similar to the water phase, the relative velocity of air is given by

$$\mathbf{v}_a^r = n_a(\mathbf{v}_a - \mathbf{v}_s) \tag{4.21}$$

where n_a and $\mathbf{v}_a$ are the volumetric content and the absolute velocity of the gas phase.

The balance equation for the conservation of air mass is

$$\mathrm{div}(\rho_a n_a \mathbf{v}_a) + \frac{\partial}{\partial t}(\rho_a n_a) = 0 \tag{4.22}$$

Following the same procedure as for the water phase, Equation (4.22) can be rearranged to

$$-\rho_a \mathrm{div}(\mathbf{v}_a^r) = n_a \frac{d_a \rho_a}{dt} + \rho_a \frac{d_s n_a}{dt} + \rho_a n_a \mathrm{div}(\mathbf{v}_s) \tag{4.23}$$

For the isothermal conditions, the density of air is given by

$$\rho_a = \frac{P_a \omega}{RT} \tag{4.24}$$

where ω is the molecular mass of gas, $P_a = p_a + p_{atm}$ is the absolute air pressure, p_{atm} is the atmospheric pressure, R is the universal gas constant and T is the absolute temperature. The derivative of ρ_a with respect to a moving gas phase is given by

$$\frac{d_a \rho_a}{dt} = \rho_a c_a \frac{d_a p_a}{dt} \tag{4.25}$$

in which $c_a = 1/P_a$ is the compressibility of air and is obtained by differentiating Equation (4.24). Substituting Equations (4.20) and (4.25) into Equation (4.23) results in the governing equation for the flow of air in partially saturated soils

$$\operatorname{div}\left(\frac{k_{ra}\mathbf{k}}{\mu_a}(\nabla p_a + \rho_a \mathbf{g})\right) = n_a c_a \frac{d_a p_a}{dt} + \frac{1}{V}\frac{d_s V_a}{dt} \tag{4.26}$$

4.4.2. Deformation Model

The deformation model of the solid phase is expressed using the condition of equilibrium on a representative volume of the soil element. Neglecting inertial effects, the linear momentum balance equation for an elemental volume is given by

$$\operatorname{div}\boldsymbol{\sigma} + \mathbf{F} = 0 \tag{4.27}$$

where $\boldsymbol{\sigma}$ is the total external stress and $\mathbf{F}$ is the body force per unit volume. Rewriting the incremental form of the effective stress equation (4.4) as

$$\dot{\boldsymbol{\sigma}}' = \dot{\boldsymbol{\sigma}} + \psi \dot{p}_w \boldsymbol{\delta} + (1-\psi)\dot{p}_a \boldsymbol{\delta} \tag{4.28}$$

and expressing stress-strain relationship

$$\dot{\boldsymbol{\sigma}}' = \mathbf{D}^{\mathrm{evp}}\dot{\boldsymbol{\varepsilon}} - \boldsymbol{\sigma}'^{\mathrm{vp}} \tag{4.29}$$

where $\mathbf{D}^{\mathrm{evp}}$ is the drained stiffness matrix of the soil and $\dot{\boldsymbol{\varepsilon}}$ is the soil skeleton strain.

Assuming infinitesimal strain theory, the relationship between strain and displacement is expressed as

$$\boldsymbol{\varepsilon} = \overline{\nabla}\mathbf{u} \tag{4.30}$$

where $\mathbf{u}$ denotes the displacement vector of the soil skeleton and $\overline{\nabla}$ is a differential operator for the displacement-strain relationships used in the current formulation

$$\overline{\nabla}=\begin{bmatrix}\frac{\partial}{\partial x} & 0 & 0\\ 0 & \frac{\partial}{\partial y} & 0\\ 0 & 0 & \frac{\partial}{\partial z}\\ \frac{\partial}{\partial y} & \frac{\partial}{\partial x} & 0\\ 0 & \frac{\partial}{\partial z} & \frac{\partial}{\partial y}\\ \frac{\partial}{\partial z} & 0 & \frac{\partial}{\partial x}\end{bmatrix} \tag{4.31}$$

Combining Equations (4.27) – (4.30) yields the governing equation for the deformation model

$$\mathrm{div}[\mathbf{D}^{\mathrm{evp}}(\overline{\nabla}\dot{\mathbf{u}}) - \boldsymbol{\sigma}'^{\mathrm{vp}} - \psi\dot{p}_w\boldsymbol{\delta} - (1-\psi)\dot{p}_a\boldsymbol{\delta}] + \dot{\mathbf{F}} = \mathbf{0} \tag{4.32}$$

4.4.3. Constitutive Relationships

The constitutive equations complement the governing equations by providing additional relationships between the deformation and stress variables. Two classes of constitutive relationships are presented in this section; the constitutive equations for volumetric deformations of the fluid phases to supplement the flow model, and the constitutive equations for the stress-strain relationship of the soil skeleton to supplement the deformation model.

4.4.3.1. Elastic Formulation

For elastic formulation, the elastic strain components ($\dot{\boldsymbol{\varepsilon}}^e$; $\dot{V}_w^e/V$; $\dot{V}_a^e/V$) are related to stress components ($\dot{\boldsymbol{\sigma}}$; $\dot{p}_w$; $\dot{p}_a$) such as

$$\dot{\boldsymbol{\varepsilon}}^e = \mathbf{D}^{\mathrm{e}-1}[\dot{\boldsymbol{\sigma}} + \psi\dot{p}_w\boldsymbol{\delta} + (1-\psi)\dot{p}_a\boldsymbol{\delta}] \tag{4.33}$$

$$-\frac{\dot{V}_{\mathrm{w}}^e}{V} = \psi\dot{\varepsilon}_{\mathrm{v}}^e + a_{11}^e\dot{p}_{\mathrm{w}} + a_{12}^e\dot{p}_{\mathrm{a}} \tag{4.34}$$

$$-\frac{\dot{V}_{\mathrm{a}}^e}{V} = (1-\psi)\dot{\varepsilon}_{\mathrm{v}}^e + a_{21}^e\dot{p}_{\mathrm{w}} + a_{22}^e\dot{p}_{\mathrm{a}} \tag{4.35}$$

where a_{11}^e , a_{22}^e and $a_{12}^e = a_{21}^e$ are the elastic constitutive coefficients relating incremental pore-water and pore-air volumetric deformations to changes in pore-air and pore-water pressures, and $\mathbf{D}^{\mathrm{e}}$ is the elastic stiffness matrix of the solid skeleton.

4.4.3.2. Viscoplastic Formulation

For viscoplastic formulation, the total strain rate and the fluid volume contents are decomposed into their corresponding elastic and viscoplastic components

$$\dot{\boldsymbol{\varepsilon}} = \dot{\boldsymbol{\varepsilon}}^{\mathrm{e}} + \dot{\boldsymbol{\varepsilon}}^{\mathrm{vp}} \tag{4.36}$$

$$\frac{\dot{V}_w}{V} = \frac{\dot{V}_w^e}{V} + \frac{\dot{V}_w^{vp}}{V} \tag{4.37}$$

$$\frac{\dot{V}_a}{V} = \frac{\dot{V}_a^e}{V} + \frac{\dot{V}_a^{vp}}{V} \tag{4.38}$$

where superscripts *e* and *vp* refer to the elastic and viscoplastic parts.

The viscoplastic deformation of the solid skeleton is obtained from the existence of viscoplastic potential $g(\boldsymbol{\sigma}')$

$$\dot{\boldsymbol{\varepsilon}}^{\mathrm{vp}} = \dot{\Lambda}\frac{\partial g}{\partial \boldsymbol{\sigma}} = \dot{\Lambda}\frac{\partial g}{\partial \boldsymbol{\sigma}'} \tag{4.39}$$

in which $\dot{\Lambda}$ is the viscoplastic multiplier.

The viscoplastic deformation of the pore fluid consists of two components

$$\frac{\dot{V}_{\alpha}^{vp}}{V} = \frac{\dot{V}_{\alpha}^{vp-s}}{V} + \frac{\dot{V}_{\alpha}^{vp-f}}{V} \tag{4.40}$$

where $\frac{\dot{V}_{\alpha}^{vp-s}}{V}$ and $\frac{\dot{V}_{\alpha}^{vp-f}}{V}$ represent the irrecoverable changes in the pore fluid content from a change in the viscoplastic deformation of the solid skeleton and from the hydraulic hysteresis, respectively.

The first component, $\frac{\dot{V}_{\alpha}^{vp-s}}{V}$, representing the change in the viscoplastic deformation of the solid skeleton, is obtained from the viscoplastic potential $g(\boldsymbol{\sigma}')$ and the definition of the effective stress as

$$\frac{\dot{V}_{w}^{vp-s}}{V} = \dot{\Lambda}\frac{\partial g}{\partial p_w} = \psi\dot{\Lambda}\boldsymbol{\delta}^{T}\frac{\partial g}{\partial \boldsymbol{\sigma}'} \tag{4.41}$$

$$\frac{\dot{V}_{a}^{vp-s}}{V} = \dot{\Lambda}\frac{\partial g}{\partial p_a} = (1-\psi)\dot{\Lambda}\boldsymbol{\delta}^{T}\frac{\partial g}{\partial \boldsymbol{\sigma}'} \tag{4.42}$$

The second component, $\frac{\dot{V}_{\alpha}^{vp-f}}{V}$, representing the change in hydraulic hysteresis, is related to changes in pore-air and pore-water pressures as

$$\frac{\dot{V}_w^{vp-f}}{V} = a_{11}^{vp}\dot{p}_{\mathrm{w}} + a_{12}^{vp}\dot{p}_{\mathrm{a}} \tag{4.43}$$

$$\frac{\dot{V}_a^{vp-f}}{V} = a_{21}^{vp}\dot{p}_{\mathrm{w}} + a_{22}^{vp}\dot{p}_{\mathrm{a}} \tag{4.44}$$

Combining Equations (4.35) – (4.40), and making use of Equations (4.32) – (4.34) yields

$$-\frac{\dot{V}_w}{V} = \psi\dot{\varepsilon}_{\mathrm{v}} + a_{11}\dot{p}_{\mathrm{w}} + a_{12}\dot{p}_{\mathrm{a}} \tag{4.45}$$

$$-\frac{\dot{V}_a}{V} = (1-\psi)\dot{\varepsilon}_{\mathrm{v}} + a_{21}\dot{p}_{\mathrm{w}} + a_{22}\dot{p}_{\mathrm{a}} \tag{4.46}$$

The constitutive coefficients a_{11}, a_{21}, a_{12} and a_{22} can be determined by subjecting an element of the unsaturated porous medium to perturbations of pore-air and pore-water pressure and measuring the resulting changes in the volume of the pore-water content and the volume of the soil skeleton. Alternatively, they can be obtained from the soil water characteristic curve, exploiting the following constraints

$$\frac{\dot{V}_w}{V} = S_r\frac{\dot{V}_{\mathrm{v}}}{V} + n\dot{S}_r = -S_r\dot{\varepsilon}_{\mathrm{v}} + n\dot{S}_r \tag{4.47}$$

$$\frac{\dot{V}_a}{V} = (1-S_r)\frac{\dot{V}_{\mathrm{v}}}{V} - n\dot{S}_r = -(1-S_r)\dot{\varepsilon}_{\mathrm{v}} - n\dot{S}_r \tag{4.48}$$

in which V_v is the volume of voids and n is the porosity.

In the other hand, we have

$$\dot{S}_r = \frac{\partial S_r}{\partial s}\dot{s} + \frac{\partial S_r}{\partial \varepsilon_{\mathrm{v}}}\dot{\varepsilon}_{\mathrm{v}} \tag{4.49}$$

in which, $\frac{\partial S_r}{\partial \varepsilon_\mathrm{v}}\dot{\varepsilon}_\mathrm{v}$ represents the change in the pore degree of saturation due to a change in the volume of the pore at the constant suction.

Substituting Equation (4.45) into Equations (4.43) and (4.44) yields

$$\frac{\dot{V}_w}{V} = -\left(S_r - n\frac{\partial S_r}{\partial \varepsilon_\mathrm{v}}\right)\dot{\varepsilon}_\mathrm{v} + n\frac{\partial S_r}{\partial s}\dot{s} \tag{4.50}$$

$$\frac{\dot{V}_a}{V} = -\left(1 - S_r + n\frac{\partial S_r}{\partial \varepsilon_\mathrm{v}}\right)\dot{\varepsilon}_\mathrm{v} - n\frac{\partial S_r}{\partial s}\dot{s} \tag{4.51}$$

We obtain

$$\psi = S_r - n\frac{\partial S_r}{\partial \varepsilon_\mathrm{v}} \tag{4.52}$$

$$a_{11} = a_{22} = -a_{21} = -a_{12} = n\frac{\partial S_r}{\partial s} \tag{4.53}$$

4.4.4. Final Form of the Fully Coupled Equations

The fully coupled equations are obtained by combining the governing equations for the flow and deformation models, Equations (4.19), (4.26) and (4.32), with the constitutive equations (4.45) – (4.46)

$$\mathrm{div}\left(\frac{k_{rw}\mathbf{k}}{\mu_w}(\nabla p_w + \rho_w\mathbf{g})\right) = n_w c_w\frac{d_w p_w}{dt} - \psi\frac{d_s\varepsilon_\mathrm{v}}{dt} - a_{11}\frac{d_s p_w}{dt} - a_{12}\frac{d_s p_a}{dt} \tag{4.54}$$

$$\mathrm{div}\left(\frac{k_{ra}\mathbf{k}}{\mu_a}(\nabla p_a + \rho_a\mathbf{g})\right) = n_a c_a\frac{d_a p_a}{dt} - (1-\psi)\frac{d_s\varepsilon_\mathrm{v}}{dt} - a_{21}\frac{d_s p_w}{dt} - a_{22}\frac{d_s p_a}{dt} \tag{4.55}$$

Noting ($\boldsymbol{\varepsilon}_{\mathrm{v}} = -\boldsymbol{\delta}^T\boldsymbol{\varepsilon} = -\mathrm{div}\mathbf{u}$) and applying the approximation $d_\alpha(.)/dt \approx \partial(.)/\partial t$ and $\nabla(.).\mathbf{v}_s/dt \ll \partial(.)/\partial t$, the fully coupled differential equation governing the flow of water and gas through an unsaturated porous medium can be written as

$$\mathrm{div}\left(\frac{k_{rw}\mathbf{k}}{\mu_w}(\nabla p_w + \rho_w\mathbf{g})\right) = \psi\mathrm{div}\dot{\mathbf{u}} + \bar{a}_{11}\dot{p}_w - a_{12}\dot{p}_a \tag{4.56}$$

$$\mathrm{div}\left(\frac{k_{ra}\mathbf{k}}{\mu_a}(\nabla p_a + \rho_a\mathbf{g})\right) = (1-\psi)\mathrm{div}\dot{\mathbf{u}} - a_{21}\dot{p}_w + \bar{a}_{22}\dot{p}_a \tag{4.57}$$

with

$$\begin{aligned} \bar{a}_{11} &= n_w c_w + a_{12} \\ \bar{a}_{22} &= n_a c_a + a_{21} \\ a_{12} = a_{21} &= -n\frac{\partial S_r}{\partial s} \end{aligned} \tag{4.58}$$

Equations (4.57), (4.58) and (4.32) form the general set of differential equations governing flow and deformation phenomena in unsaturated porous media.

The governing equation for the deformation model is rewritten as

$$\overline{\nabla}^{\mathrm{T}}[\mathbf{D}^{\mathrm{evp}}(\overline{\nabla}\dot{\mathbf{u}}) - \boldsymbol{\sigma}'^{\mathrm{vp}} - \psi\dot{p}_w\boldsymbol{\delta} - (1-\psi)\dot{p}_a\boldsymbol{\delta}] + \dot{\mathbf{F}} = \mathbf{0} \tag{4.59}$$

4.5. Finite Element Formulation

The solutions to most of differential equations are too complex and are commonly obtained by using approximate numerical techniques. The finite element method has a wide range of applications for numerically solving various problems in many branches of science and engineering. It is the most powerful technique widely adopted to derive the numerical solution of the differential equations governing the problems. The solution procedure for a continuum problem based on the finite element method involves the following basis steps:

1 – Element discretisation

This is the process of modelling the geometry of the problems using finite elements.

2 – Primary variable approximation

A primary variable must be selected and rules as to how it should vary over a finite element established. This variation is expressed in terms of nodal values. Nodal displacements, pore water pressure and pore air pressure are considered as the primary variables in this formulation.

3 – Element equations

Use an appropriate principle to derive element equations: $[\boldsymbol{K}_E]\{\Delta\boldsymbol{d}_E\} = \{\Delta\boldsymbol{R}_E\}$

where $[\boldsymbol{K}_E]$ is the element stiffness matrix, $\{\Delta\boldsymbol{d}_E\}$ is the vector of incremental element nodal displacements and $\{\Delta\boldsymbol{R}_E\}$ is the vector of incremental element nodal forces.

4 – Global equations

Combine element equations to form the global equations: $[\boldsymbol{K}_G]\{\Delta\boldsymbol{d}_G\} = \{\Delta\boldsymbol{R}_G\}$

where $[\boldsymbol{K}_G]$ is the global stiffness matrix, $\{\Delta\boldsymbol{d}_G\}$ is the vector of incremental global nodal displacements and $\{\Delta\boldsymbol{R}_G\}$ is the vector of incremental global nodal forces.

5 – Boundary conditions

Formulate boundary conditions and modify global equations.

6 – Solve the global equations

Solving the system of the linearised equations for the unknown nodal variables.

4.5.1. Spatial Discretisation of the Governing Equations

The governing equations for the fully coupled analysis of flow and deformation in unsaturated soils, established in Section 4.4, can be rewritten as

$$\overline{\nabla}^{\mathrm{T}}[\mathbf{D}^{\mathrm{evp}}(\overline{\nabla}\dot{\mathbf{u}}) - \boldsymbol{\sigma}'^{\mathrm{vp}} - \psi\dot{p}_w\boldsymbol{\delta} - (1-\psi)\dot{p}_a\boldsymbol{\delta}] + \dot{\mathbf{F}} = 0 \tag{4.60}$$

$$\mathrm{div}\left(\frac{k_{rw}\mathbf{k}}{\mu_w}(\nabla p_w + \rho_w\mathbf{g})\right) = \psi\mathrm{div}\dot{\mathbf{u}} + \bar{a}_{11}\dot{p}_w - a_{12}\dot{p}_a \tag{4.61}$$

$$\mathrm{div}\left(\frac{k_{ra}\mathbf{k}}{\mu_a}(\nabla p_a + \rho_a\mathbf{g})\right) = (1-\psi)\mathrm{div}\dot{\mathbf{u}} - a_{21}\dot{p}_w + \bar{a}_{22}\dot{p}_a \tag{4.62}$$

For ease of convenience of the finite element formulation, these equations are rearranged and rewritten as

$$\overline{\nabla}^{\mathrm{T}}([\mathrm{D}^{\mathrm{evp}}]\overline{\nabla}\{\dot{\mathrm{u}}\}) - \overline{\nabla}^{\mathrm{T}}\{\sigma'^{\mathrm{vp}}\} - \psi\overline{\nabla}^{\mathrm{T}}\{\delta\}\dot{p}_w - (1-\psi)\overline{\nabla}^{\mathrm{T}}\{\delta\}\dot{p}_a + \{\dot{\mathrm{F}}\} = \{0\} \tag{4.63}$$

$$\nabla^{\mathrm{T}}\left(\frac{k_{rw}[\mathrm{k}]}{\mu_w}(\{\nabla p_w\} + \rho_w\{\mathrm{g}\})\right) - \psi\{\delta\}^{\mathrm{T}}\overline{\nabla}\{\dot{\mathrm{u}}\} - \bar{a}_{11}\dot{p}_w + a_{12}\dot{p}_a = 0 \tag{4.64}$$

$$\nabla^{\mathrm{T}}\left(\frac{k_{ra}[\mathrm{k}]}{\mu_a}(\{\nabla p_a\} + \rho_a\{\mathrm{g}\})\right) - (1-\psi)\{\delta\}^{\mathrm{T}}\overline{\nabla}\{\dot{\mathrm{u}}\} + a_{21}\dot{p}_w - \bar{a}_{22}\dot{p}_a = 0 \tag{4.65}$$

where $\overline{\nabla}$ is the differential operator corresponding to definition of engineering strains; $\boldsymbol{\delta} = \{\delta\}$ is the identity vector and is defined as $\boldsymbol{\delta} = \{\delta\} = \{1,1,1,0,0,0\}^{\mathrm{T}}$. The vector format of the gradient operator is $\nabla^{\mathrm{T}} = \{\partial/\partial x, \partial/\partial y, \partial/\partial z\}$.

Applying Galerkin's approach to (4.63) – (4.65) results in

$$\int_{\Omega} [\mathrm{N}]^{T}\left(\overline{\nabla}^{\mathrm{T}}\left([\mathrm{D}^{\mathrm{evp}}]\overline{\nabla}\{\dot{\tilde{\mathrm{u}}}\}\right) - \overline{\nabla}^{\mathrm{T}}\{\sigma'^{\mathrm{vp}}\} - \psi\overline{\nabla}^{\mathrm{T}}\{\delta\}\dot{\tilde{p}}_{w} - (1-\psi)\overline{\nabla}^{\mathrm{T}}\{\delta\}\dot{\tilde{p}}_{a} + \{\dot{\mathrm{F}}\}\right) d\Omega = \{0\} \quad (4.66)$$

$$\int_{\Omega} [\mathrm{N}]^{T}\left(\nabla^{\mathrm{T}}\left(\frac{k_{rw}[\mathrm{k}]}{\mu_{w}}(\{\nabla\tilde{p}_{w}\} + \rho_{w}\{\mathrm{g}\})\right) - \psi\{\delta\}^{\mathrm{T}}\overline{\nabla}\{\dot{\tilde{\mathrm{u}}}\} - \bar{a}_{11}\dot{\tilde{p}}_{w} + a_{12}\dot{\tilde{p}}_{a}\right) d\Omega = 0 \quad (4.67)$$

$$\int_{\Omega} [\mathrm{N}]^{T}\left(\nabla^{\mathrm{T}}\left(\frac{k_{ra}[\mathrm{k}]}{\mu_{a}}(\{\nabla\tilde{p}_{a}\} + \rho_{a}\{\mathrm{g}\})\right) - (1-\psi)\{\delta\}^{\mathrm{T}}\overline{\nabla}\{\dot{\tilde{\mathrm{u}}}\} + a_{21}\dot{\tilde{p}}_{w} - \bar{a}_{22}\dot{\tilde{p}}_{a}\right) d\Omega = 0 \quad (4.68)$$

in which $\tilde{\mathbf{u}}$, $\tilde{p}_{w}$ and $\tilde{p}_{a}$ are the approximate solutions, $[\mathrm{N}]$ is the shape function and Ω is the element domain.

The approximate solutions are related to the nodal values of the field variables through

$$\tilde{\mathbf{u}} = [\mathrm{N}]\{\mathrm{u}\} \quad (4.69)$$

$$\tilde{p}_{w} = [\mathrm{N}]\{\mathrm{p}_{w}\} \quad (4.70)$$

$$\tilde{p}_{a} = [\mathrm{N}]\{\mathrm{p}_{a}\} \quad (4.71)$$

where $\{\mathrm{u}\}$, $\{\mathrm{p}_{w}\}$and $\{\mathrm{p}_{a}\}$ are vectors of the nodal values of soil matrix displacement, pore water pressure and pore air pressure, respectively.

Expanding Equations (4.66) – (4.68) by using Green's theorem and substituting the nodal values of the field variables yields

$$
\begin{aligned}
&-\int_{\Omega} [\overline{\nabla}\mathrm{N}]^T [\mathrm{D}^{\mathrm{evp}}][\overline{\nabla}\mathrm{N}]\{\dot{\mathrm{u}}\}d\Omega + \int_{\Gamma} [\mathrm{N}]^T[\mathrm{D}^{\mathrm{evp}}][\overline{\nabla}\mathrm{N}]\{\dot{\mathrm{u}}\}d\Gamma + \int_{\Omega} [\overline{\nabla}\mathrm{N}]^T\{\sigma'^{\mathrm{vp}}\}d\Omega \\
&\quad - \int_{\Gamma} [\mathrm{N}]^T\{\sigma'^{\mathrm{vp}}\}d\Gamma + \int_{\Omega} \psi[\overline{\nabla}\mathrm{N}]^T\{\delta\}[\mathrm{N}]\{\dot{\mathrm{p}}_w\}d\Omega \\
&\quad - \int_{\Gamma} \psi[\mathrm{N}]^T\{\delta\}[\mathrm{N}]\{\dot{\mathrm{p}}_w\}d\Gamma + \int_{\Omega} (1-\psi)[\nabla\mathrm{N}]^T\{\delta\}[\mathrm{N}]\{\dot{\mathrm{p}}_a\}d\Omega \\
&\quad - \int_{\Gamma} (1-\psi)[\mathrm{N}]^T\{\delta\}[\mathrm{N}]\{\dot{\mathrm{p}}_a\}d\Gamma + \int_{\Omega} [\mathrm{N}]^T\{\dot{\mathrm{F}}\}d\Omega = \{0\}
\end{aligned}
\tag{4.72}
$$

$$
\begin{aligned}
&-\int_{\Omega} \psi[\mathrm{N}]^T\{\delta\}^T[\overline{\nabla}\mathrm{N}]\{\dot{\mathrm{u}}\}d\Omega - \int_{\Omega} \bar{a}_{11}[\mathrm{N}]^T[\mathrm{N}]\{\dot{\mathrm{p}}_w\}d\Omega \\
&\quad - \int_{\Omega} [\nabla\mathrm{N}]^T \frac{k_{rw}[\mathrm{k}]}{\mu_w}[\nabla\mathrm{N}]\{\mathrm{p}_w\}d\Omega + \int_{\Gamma} [\mathrm{N}]^T \frac{k_{rw}[\mathrm{k}]}{\mu_w}[\nabla\mathrm{N}]\{\mathrm{p}_w\}d\Gamma \\
&\quad + \int_{\Omega} a_{12}[\mathrm{N}]^T[\mathrm{N}]\{\dot{\mathrm{p}}_a\}d\Omega = 0
\end{aligned}
\tag{4.73}
$$

$$
\begin{aligned}
&-\int_{\Omega} (1-\psi)[\mathrm{N}]^T\{\delta\}^T[\overline{\nabla}\mathrm{N}]\{\dot{\mathrm{u}}\}d\Omega + \int_{\Omega} a_{21}[\mathrm{N}]^T[\mathrm{N}]\{\dot{\mathrm{p}}_w\}d\Omega \\
&\quad - \int_{\Omega} [\nabla\mathrm{N}]^T \frac{k_{ra}[\mathrm{k}]}{\mu_a}[\nabla\mathrm{N}]\{\mathrm{p}_a\}d\Omega + \int_{\Gamma} [\mathrm{N}]^T \frac{k_{ra}[\mathrm{k}]}{\mu_a}[\nabla\mathrm{N}]\{\mathrm{p}_a\}d\Gamma \\
&\quad - \int_{\Omega} \bar{a}_{22}[\mathrm{N}]^T[\mathrm{N}]\{\dot{\mathrm{p}}_a\}d\Omega = 0
\end{aligned}
\tag{4.74}
$$

where Γ is the element boundary.

Rearranging these equations and substituting the boundary conditions

$$\begin{aligned}
&\int_{\Omega} [\overline{\nabla}\mathrm{N}]^{T}\,[\mathrm{D}^{\mathrm{evp}}][\overline{\nabla}\mathrm{N}]\{\dot{\mathrm{u}}\}d\Omega - \int_{\Omega} [\overline{\nabla}\mathrm{N}]^{T}\{\sigma'^{\mathrm{vp}}\}d\Omega - \int_{\Omega} \psi[\overline{\nabla}\mathrm{N}]^{T}\{\delta\}[\mathrm{N}]\{\dot{\mathrm{p}}_{w}\}d\Omega \\
&\quad - \int_{\Omega} (1-\psi)[\nabla\mathrm{N}]^{T}\{\delta\}[\mathrm{N}]\{\dot{\mathrm{p}}_{a}\}d\Omega \\
&\quad = \int_{\Gamma} [\mathrm{N}]^{T}\{\dot{\mathrm{T}}\}d\Gamma + \int_{\Omega} [\mathrm{N}]^{T}\{\dot{\mathrm{F}}\}d\Omega
\end{aligned} \tag{4.75}$$

$$\begin{aligned}
&-\int_{\Omega} \psi[\mathrm{N}]^{T}\{\delta\}^{T}[\overline{\nabla}\mathrm{N}]\{\dot{\mathrm{u}}\}d\Omega - \int_{\Omega} \bar{a}_{11}[\mathrm{N}]^{T}[\mathrm{N}]\{\dot{\mathrm{p}}_{w}\}d\Omega \\
&\quad - \int_{\Omega} [\nabla\mathrm{N}]^{T}\frac{k_{rw}[\mathrm{k}]}{\mu_{w}}[\nabla\mathrm{N}]\{\mathrm{p}_{w}\}d\Omega + \int_{\Omega} a_{12}[\mathrm{N}]^{T}[\mathrm{N}]\{\dot{\mathrm{p}}_{a}\}d\Omega \\
&\quad = -\int_{\Gamma} [\mathrm{N}]^{T}\{q_{w}\}d\Gamma
\end{aligned} \tag{4.76}$$

$$\begin{aligned}
&-\int_{\Omega} (1-\psi)[\mathrm{N}]^{T}\{\delta\}^{T}[\overline{\nabla}\mathrm{N}]\{\dot{\mathrm{u}}\}d\Omega + \int_{\Omega} a_{21}[\mathrm{N}]^{T}[\mathrm{N}]\{\dot{\mathrm{p}}_{w}\}d\Omega \\
&\quad - \int_{\Omega} [\nabla\mathrm{N}]^{T}\frac{k_{ra}[\mathrm{k}]}{\mu_{a}}[\nabla\mathrm{N}]\{\mathrm{p}_{a}\}d\Omega - \int_{\Omega} \bar{a}_{22}[\mathrm{N}]^{T}[\mathrm{N}]\{\dot{\mathrm{p}}_{a}\}d\Omega \\
&\quad = -\int_{\Gamma} [\mathrm{N}]^{T}\{q_{a}\}d\Gamma
\end{aligned} \tag{4.77}$$

in which the boundary tractions and fluid influxes are given by

$$\{\dot{\mathrm{T}}\} = [\mathrm{D^{evp}}][\overline{\nabla}\mathrm{N}]\{\dot{\mathrm{u}}\} - \{\sigma'^{\mathrm{vp}}\} - \psi\{\delta\}[\mathrm{N}]\{\dot{\mathrm{p}}_w\} - (1-\psi)\{\delta\}[\mathrm{N}]\{\dot{\mathrm{p}}_a\} \tag{4.78}$$

$$\{q_w\} = -\frac{k_{rw}[\mathrm{k}]}{\mu_w}[\nabla\mathrm{N}]\{\mathrm{p}_w\} \tag{4.79}$$

$$\{q_a\} = -\frac{k_{ra}[\mathrm{k}]}{\mu_a}[\nabla\mathrm{N}]\{\mathrm{p}_a\} \tag{4.80}$$

where $\{\dot{\mathrm{T}}\}$, $\{q_w\}$ and $\{q_a\}$ are vectors of the nodal traction force, water influx and air influx at the element boundary, respectively. Denoting derivatives of the shape function as $[\mathrm{B}_1] = [\overline{\nabla}\mathrm{N}]$, $[\mathrm{B}_2] = \{\delta\}^T[\overline{\nabla}\mathrm{N}]$, $[\mathrm{B}_3] = [\nabla\mathrm{N}]$, and substituting them into Equations (4.75) – (4.77) yield

$$\begin{aligned}&\int_\Omega [\mathrm{B}_1]^T [\mathrm{D^{evp}}][\mathrm{B}_1]\{\dot{\mathrm{u}}\}d\Omega - \psi\int_\Omega [\mathrm{B}_2]^T[\mathrm{N}]\{\dot{\mathrm{p}}_w\}d\Omega - (1-\psi)\int_\Omega [\mathrm{B}_2]^T[\mathrm{N}]\{\dot{\mathrm{p}}_a\}d\Omega \\ &= \int_\Gamma [\mathrm{N}]^T\{\dot{\mathrm{T}}\}d\Gamma + \int_\Omega [\mathrm{N}]^T\{\dot{\mathrm{F}}\}d\Omega + \int_\Omega [\mathrm{B}_1]^T\{\dot{\sigma}'^{\mathrm{vp}}\}d\Omega\end{aligned} \tag{4.81}$$

$$\begin{aligned}&-\psi\int_\Omega [\mathrm{N}]^T[\mathrm{B}_2]\{\dot{\mathrm{u}}\}d\Omega - \bar{a}_{11}\int_\Omega [\mathrm{N}]^T[\mathrm{N}]\{\dot{\mathrm{p}}_w\}d\Omega - \frac{k_{rw}}{\mu_w}\int_\Omega [\mathrm{B}_3]^T[\mathrm{k}][\mathrm{B}_3]\{\mathrm{p}_w\}d\Omega \\ &+ a_{12}\int_\Omega [\mathrm{N}]^T[\mathrm{N}]\{\dot{\mathrm{p}}_a\}d\Omega = \int_\Gamma [\mathrm{N}]^T\{q_w\}d\Gamma\end{aligned} \tag{4.82}$$

$$\begin{aligned}&-\int_\Omega (1-\psi)[\mathrm{N}]^T[\mathrm{B}_2]\{\dot{\mathrm{u}}\}d\Omega + a_{21}\int_\Omega [\mathrm{N}]^T[\mathrm{N}]\{\dot{\mathrm{p}}_w\}d\Omega - \frac{k_{ra}}{\mu_a}\int_\Omega [\mathrm{B}_3]^T[\mathrm{k}][\mathrm{B}_3]\{\mathrm{p}_a\}d\Omega \\ &- \bar{a}_{22}\int_\Omega [\mathrm{N}]^T[\mathrm{N}]\{\dot{\mathrm{p}}_a\}d\Omega = \int_\Gamma [\mathrm{N}]^T\{q_a\}d\Gamma\end{aligned} \tag{4.83}$$

in which $[\mathrm{D^{evp}}]$ is the elasto-viscoplastic stiffness matrix. By integrating Equations (4.81), (4.82) and (4.83) numerically, the resulting system of equations becomes

$$[\mathrm{K}]\{\dot{\mathrm{u}}\}-\psi[\mathrm{C}]\{\dot{\mathrm{p}}_w\}-(1-\psi)[\mathrm{C}]\{\dot{\mathrm{p}}_a\}=\{\dot{\mathrm{P}}\} \tag{4.84}$$

$$-\psi[\mathrm{C}]^T\{\dot{\mathrm{u}}\}-\bar{a}_{11}[\mathrm{M}]\{\dot{\mathrm{p}}_w\}-[\mathrm{H}_w]\{\mathrm{p}_w\}+a_{12}[\mathrm{M}]\{\dot{\mathrm{p}}_a\}=\{\mathrm{Q}_w\} \tag{4.85}$$

$$-(1-\psi)[\mathrm{C}]^T\{\dot{\mathrm{u}}\}+a_{21}[\mathrm{M}]\{\dot{\mathrm{p}}_w\}-[\mathrm{H}_a]\{\mathrm{p}_a\}-\bar{a}_{22}[\mathrm{M}]\{\dot{\mathrm{p}}_a\}=\{\mathrm{Q}_a\} \tag{4.86}$$

in which [K] is the element stiffness matrix, [C] is the coupling matrix, [M] is the mass matrix, $[\mathrm{H}_w]$ and $[\mathrm{H}_a]$ are flow matrices corresponding to the permeabilities of the water and air phases respectively, {u} is the vector of nodal displacements, $\{\mathrm{p}_w\}$ is the vector of nodal pore water pressures, $\{\mathrm{p}_a\}$ is the vector of nodal pore air pressures, {P} is the vector of nodal forces, $\{\mathrm{Q}_w\}$ and $\{\mathrm{Q}_a\}$ are vectors of nodal fluxes of the water and air flows respectively. The element matrices are evaluated using

$$[\mathrm{K}]=\int_\Omega [\mathrm{B}_1]^T\,[\mathrm{D}^{\mathrm{evp}}][\mathrm{B}_1]d\Omega \tag{4.87}$$

$$[\mathrm{M}]=\int_\Omega [\mathrm{N}]^T[\mathrm{N}]\,d\Omega \tag{4.88}$$

$$[\mathrm{C}]=\int_\Omega [\mathrm{B}_2]^T[\mathrm{N}]\,d\Omega \tag{4.89}$$

$$[\mathrm{H}_w]=\frac{k_{rw}}{\mu_w}\int_\Omega [\mathrm{B}_3]^T[\mathrm{k}][\mathrm{B}_3]d\Omega \tag{4.90}$$

$$[\mathrm{H}_a]=\frac{k_{ra}}{\mu_a}\int_\Omega [\mathrm{B}_3]^T[\mathrm{k}][\mathrm{B}_3]d\Omega \tag{4.91}$$

The nodal forces and nodal fluxes are given by

$$\{\dot{\mathrm{P}}\} = \int_{\Gamma} [\mathrm{N}]^T \{\dot{\mathrm{T}}\} d\Gamma + \int_{\Omega} [\mathrm{N}]^T \{\dot{\mathrm{F}}\} d\Omega + \int_{\Omega} [\mathrm{B}_1]^T \{\sigma'^{\mathrm{vp}}\} d\Omega \tag{4.92}$$

$$\{\mathrm{Q}_w\} = \int_{\Gamma} [\mathrm{N}]^T \{q_w\} d\Gamma \tag{4.93}$$

$$\{\mathrm{Q}_a\} = \int_{\Gamma} [\mathrm{N}]^T \{q_a\} d\Gamma \tag{4.94}$$

4.5.2. Discretisation in Time Domain

The rate forms of the discretised equations are used to be integrated over the time domain. Using the finite difference approach, integration of an arbitrary function *y* over a time interval Δt is given by

$$\int_{t}^{t+\Delta t} y(t)dt = [(1-\beta)y_t + \beta y_{t+\Delta t}]\Delta t = (\beta \Delta y + y_t)\Delta t \tag{4.95}$$

where y_t is the value of y at time *t,* and β is a parameter controlling the type of interpolation.

Applying Equation (4.90) into Equations (4.84), (4.85) and (4.86) results in the following linearised form of the governing equations

$$[\mathrm{K}]\{\Delta \mathrm{u}\} - \psi[\mathrm{C}]\{\Delta \mathrm{p}_w\} - (1-\psi)[\mathrm{C}]\{\Delta \mathrm{p}_a\} = \{\Delta \mathrm{R}\} \tag{4.96}$$

$$-\psi[\mathrm{C}]^T\{\Delta\mathrm{u}\} - \bar{a}_{11}[\mathrm{M}]\{\Delta\mathrm{p}_w\} - [\mathrm{H}_w](\beta\{\Delta\mathrm{p}_w\} + \{\mathrm{p}_w\}_t)\Delta t + a_{12}[\mathrm{M}]\{\Delta\mathrm{p}_a\} = (\{\mathrm{Q}_w\}_t + \beta\{\Delta\mathrm{Q}_w\})\Delta t \tag{4.97}$$

$$-(1-\psi)[\mathrm{C}]^T\{\Delta\mathrm{u}\} + a_{21}[\mathrm{M}]\{\Delta\mathrm{p}_w\} - [\mathrm{H}_a](\beta\{\Delta\mathrm{p}_a\} + \{\mathrm{p}_a\}_t)\Delta t - \bar{a}_{22}[\mathrm{M}]\{\Delta\mathrm{p}_a\} = (\{\mathrm{Q}_a\}_t + \beta\{\Delta\mathrm{Q}_a\})\Delta t \tag{4.98}$$

In the compact matrix-vector form, these equations are summarised as

$$\begin{bmatrix} [\mathrm{K}] & -\psi[\mathrm{C}] & -(1-\psi)[\mathrm{C}] \\ -\psi[\mathrm{C}]^T & -\bar{a}_{11}[\mathrm{M}] - \beta\Delta t[\mathrm{H}_w] & a_{12}[\mathrm{M}] \\ -(1-\psi)[\mathrm{C}]^T & a_{21}[\mathrm{M}] & -\bar{a}_{22}[\mathrm{M}] - \beta\Delta t[\mathrm{H}_a] \end{bmatrix} \begin{Bmatrix} \{\Delta\mathrm{u}\} \\ \{\Delta\mathrm{p}_w\} \\ \{\Delta\mathrm{p}_a\} \end{Bmatrix} = \begin{Bmatrix} \{\Delta\mathrm{P}\} \\ 0 \\ 0 \end{Bmatrix} + (1-\beta)\Delta t \begin{Bmatrix} 0 \\ \{\mathrm{Q}_w\}_t \\ \{\mathrm{Q}_a\}_t \end{Bmatrix} + \beta\Delta t \begin{Bmatrix} 0 \\ \{\mathrm{Q}_w\}_{t+\Delta t} \\ \{\mathrm{Q}_a\}_{t+\Delta t} \end{Bmatrix} + \Delta t \begin{Bmatrix} 0 \\ [\mathrm{H}_w]\{\mathrm{p}_w\}_t \\ [\mathrm{H}_a]\{\mathrm{p}_a\}_t \end{Bmatrix} \tag{4.99}$$

4.5.3. Solution Procedure

The global solution procedure for nonlinear finite element analysis is generally either iterative or incremental schemes. Iterative solutions are based on the concept of solving repetitively a system of nonlinear equations until the unbalanced residual forces become negligible. The scheme is highly accurate, satisfy the equilibrium condition automatically. However, iterative scheme may not converge for strongly nonlinear equations, and can be highly computationally expensive. Incremental solution procedures involve solving a system of ordinary differential equations using a series of linear approximations of the governing equations. In this approach, the global stiffness matrix is computed at the beginning of each increment and is assumed to remain constant over the increment. The incremental scheme is simple because they do not involve iterations.

This method is robust and useful for highly nonlinear problems involving complex constitutive behaviour (Sloan *et al.*, 2001). In this study, the incremental scheme is selected as the most suitable procedure to solve the complex governing equations.

In non-linear finite element analysis, integrating the constitutive relations to obtain the unknown increment in the stresses requires implicit or explicit methods. In implicit method, the gradients and hardening law are evaluated at unknown stress states and the resulting system of non-linear equations must be solved iteratively. The resulting stresses automatically satisfy the yield criterion to a specified tolerance. They do not require the intersection with the yield surface to be computed if the stress point changes from an elastic state to a plastic state. However, it is difficult to implement for complex constitutive relations because it requires second order derivatives of the yield function and plastic potential. Explicit methods have the advantage of being more straightforward to implement. Since explicit schemes employ the standard elastoplastic constitutive law and require only first derivatives of the yield function and plastic potential, they can be used to design a general purpose integrator that can be used for a wide range of models. In this study, the explicit scheme rather than the implicit scheme is used to solve the complex differential equations.

This combination assures efficiency, accuracy and robustness of the numerical solutions at both the global and local levels. The tendency to drift from the global equilibrium condition is minimised by ensuring the unbalanced residual forces at the end of each load or strain increment remain below a prescribed error limit. The accuracy and efficiency of explicit methods is significantly enhanced by combining them with automatic sub-stepping and error control. Such schemes limit the error in the computed stresses, and are best employed in conjunction with a correction to restore the stresses to the yield surface during the integration process. The integration algorithms use the modified Euler scheme to estimate the local error in the computed stresses and control the sub-incrementation of the applied strain increment. An appropriate size for each sub-step using the modified Euler method provide an estimate of the local error. For a given load path, the modified Euler scheme is able to control the integration error to lie near a prescribed error tolerance. If the unbalanced forces exceed the error tolerance, the global solution procedure is repeated iteratively using the modified Newton-Raphson method until the residual forces become less than the prescribed error tolerance.

4.6. Conclusions

In this chapter, the governing equations for the fully coupled analysis of flow and deformation in variably saturated porous media were developed. The governing differential equations are derived based on the concept of effective stress and the theory of multiphase mixtures. The equations governing the flow of water and air were established from the conservation equations of mass and momentum. The deformation equations were derived by satisfying the equations of equilibrium and compatibility. The coupling between the flow and viscoplastic deformation models was obtained through the effective stress parameter. Finally, for numerical implementation, both global and local solution schemes were successfully obtained using the finite element method.

CHAPTER 5

MODEL VALIDATIONS AND APPLICATIONS

5.1. Introduction

In this chapter, the capability of the proposed bounding surface viscoplasticity model to capture the time-dependent behaviour of soils is demonstrated. First, the essential elements of the model are validated by comparing the numerical results with the experimental data from the literature. The application of the bounding surface viscoplasticity model to predict the time-dependent behaviour of fully saturated soils is illustrated in Section 5.2 for creep tests, in Section 5.3 for constant strain rate tests and in Section 5.4 for undrained loading, unloading and relaxation tests. Several numerical examples are also presented in Section 5.3 to show the capability of the model to capture the time-dependent behaviour of cohesive soils under both drained and undrained loading conditions. Application of the fully coupled elasto-viscoplastic model to the time-dependent behaviour of unsaturated soils is then presented in Section 5.5. In Section 5.6, the experimental results from the literature for drained and undrained triaxial creep tests are used to highlight the capability of the proposed model to predict the creep rupture in clay. Finally, several boundary value problems are presented in Sections 5.7 and then solved using the fully coupled hydro-mechanical model proposed in Chapter 4 and the bounding surface viscoplastic constitutive model presented in Chapter 3.

A summary of simulation results is presented in Table 5.1.

Table 5.1 – Summary of simulated tests

Type of Simulated test	**Material**	**Material type**	**Test conditions**	**Saturated/ Unsaturated soils**	**Simulation Results**
Creep Test	San Francisco Bay Mud	Normally consolidated	Undrained	Saturated	Figure 5.1
	Remoulded Fukakusa Clay	Normally consolidated	Undrained	Saturated	Figure 5.2
Constant Strain Rate Test	Remoulded Fukakusa Clay	Normally consolidated	Undrained	Saturated	Figure 5.3 Figure 5.4
	San Francisco Bay Mud	Normally consolidated	Undrained	Saturated	Figure 5.5 Figure 5.6
	Weald Clay	Normally consolidated	Drained	Saturated	Figure 5.7 Figure 5.8
		Heavily Over consolidated	Drained	Saturated	Figure 5.7 Figure 5.8
	Cardiff Kaolin Clay	Normally consolidated	Undrained	Saturated	Figure 5.9 Figure 5.10
		Lightly Over consolidated	Undrained	Saturated	Figure 5.11 Figure 5.12
		Heavily Over consolidated	Undrained	Saturated	Figure 5.13 Figure 5.14
	Bourke Silt	Normally consolidated	Undrained	Unsaturated	Figure 5.18 Figure 5.19
Stress Relaxation Test	Hong Kong Marine Deposits	Normally consolidated	Undrained	Saturated	Figure 5.15 Figure 5.16 Figure 5.17
Tertiary Creep and Creep Rupture Test	San Francisco Bay Mud	Normally consolidated	Undrained	Saturated	Figure 5.20 Figure 5.21 Figure 5.22
	Haney Clay	Normally consolidated	Drained	Saturated	Figure 5.23 Figure 5.24

5.2. Application of Bounding Surface Viscoplasticity Model to Creep Tests

Creep is the development of time-dependent shear and/or volumetric strains at constant stress (Mitchell and James Kenneth, 2005). One of the important aspects in modelling soil creep is the dependency of the creep rate on the effective stress. In a conventional creep test, soil sample is usually loaded to a specific effective stress and then allowed to creep at constant stress. In most of triaxial creep tests, it has been observed that the higher the deviatoric stress, the higher the rate of creep deformation (Singh and Mitchell, 1968; Tavenas *et al.*, 1978).

In this section, application of the proposed bounding surface viscoplasticity model to reproduce the creep behaviour of geomaterials is demonstrated by comparing numerical simulations with experimental results of undrained creep tests for Remoulded Fukakusa clay and San Francisco Bay Mud. It is noted that although the model proposed is capable of describing both shear and compression creeps, the numerical examples presented mainly focus on triaxial creep, i.e. creep under shear.

5.2.1. Remoulded Fukakusa Clay

The physical properties and experimental data for Remoulded Fukakusa clay were published by Adachi and Oka (1982). The Remoulded Fukakusa clay specimens were isotropically consolidated to 392kN/m^2 and undrained creep tests were performed after shearing up to a prescribed deviatoric stress. All creep tests were conducted for about 10,000 minutes at each stress level. The undrained creep tests were conducted after the samples were sheared up to prescribed deviatoric stress levels of 0.2, 0.3, 0.4, 0.5 and 0.6 times of the stress state at the end of consolidation (σ'_{me}).

5.2.1.1. Model Parameters

The material parameters used in the simulations were calibrated using the experimental data. The parameters $\kappa = 0.02$ and $\lambda = 0.1$ were obtained from the consolidation and swelling test results; $G = 36300$kPa, $M_{cs} = 1.5$, $\Gamma = 2.263$ were determined from the triaxial compression test results. The bounding surface material constants used in the simulations were $N = 1.1$, $R = 2.4$, $A = 1.0$, and $k_m = 1.0$. The initial conditions of the samples were $p'_0 = 392$kPa and $e_0 = 0.74$. The viscoplastic parameter was taken as $c_\beta = 0.06$ with the reference strain rate $\dot{\varepsilon}^{vp}_{p,r} = 5.0 \times 10^{-2}/\text{min}$ and the threshold strain rate $\dot{\varepsilon}^{vp}_{p,th} = 10^{-10}/\text{min}$.

5.2.1.2. Simulation Results

Figure 5.1 shows the model simulations and experimental data of undrained creep tests on Remoulded Fukakusa clay with $p'_0 = 392$kPa. The results show that the rate of creep decreases with time and the instantaneous component of the axial deformation were much smaller than the time dependent deformation. Good agreement is observed between the numerical and experimental results, demonstrating the ability of the proposed bounding surface viscoplastic model to capture the creep behaviour of clay.

During the undrained creep, the deviatoric stress and the void ratio remain constant, while the change in deviatoric strain results in the pore pressure build-up and consequently the reduction of the mean effective stress. By progress of creep, the stress point moves towards the critical state line in the $(p' - q)$ plane. At low shear stress levels, the deviatoric strain rate approaches zero before the stress point reaches the critical state, and hence no creep-induced instability occurs. At high shear stress levels, however, the stress point can approach the critical state line leading to the undrained creep failure of the soil. The samples subjected to the creep loads of $q/\sigma'_{me} = 0.2, 0.3,$ and 0.4 show only a small increase in axial strain, whereas the samples subjected to the creep loads of $q/\sigma'_{me} = 0.5$ and 0.6 show a large increase of strain after the initial deformation.

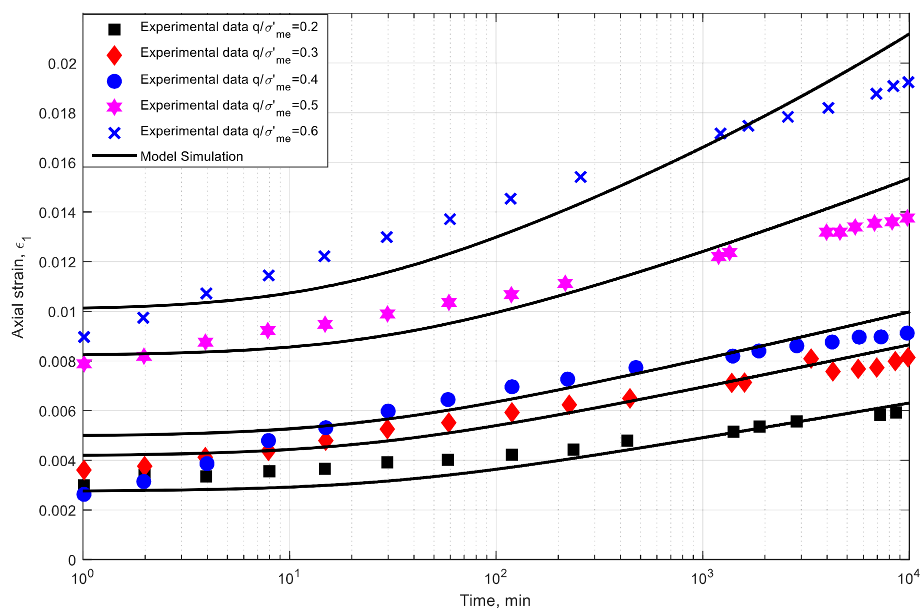

Figure 5.1 – Model simulation and experimental data of undrained creep tests on Remoulded Fukakusa clay with p'_0 = 392 kPa and creep loads of 0.2, 0.3, 0.4, 0.5 and 0.6 times of σ'_{me}: Axial strain versus Time

5.2.2. San Francisco Bay Mud

The experimental data of San Francisco Bay Mud, a normally-consolidated silty coastal organic clay, were provided by Arulanandan *et al.* (1971). Undisturbed samples were obtained at depths of 12-15ft (3.576-4.572m) below the ground surface using a piston sampler that takes samples of 3ft (0.9144m) long and 2in (0.0508m) in diameter. Tests were carried out with triaxial equipment built at the University of California at Davis. The tests were carried out in a constant temperature room at the temperature of $73 \pm \frac{1}{2}$°F (22.778 ± 0.278ºC). First, the normal strength tests were carried out to determine the ultimate deviator stress. Then the series of creep tests were undertaken.

Arulanandan *et al.* (1971) conducted a series of undrained triaxial creep tests on San Francisco Bay Mud. The stress-controlled undrained triaxial tests were performed at different isotropic consolidation pressures and stress levels. In the set of tests selected for the simulation, the sustained deviatoric stress levels maintained during creep were 30%, 50%, and 70% of the ultimate deviatoric stress $q_{ult} = 77.5$ kPa (or $0.79 kg/cm^2$) for the creep test with $p'_0 = 98kPa$ (or $1 kg/cm^2$). The ultimate deviatoric stress was determined from normal strength tests. The creep tests were continued for a period of two-weeks, i.e. roughly 20,000 minutes, unless prior failure occurred.

5.2.2.1. Model Parameters

The material parameters used in the simulations were calibrated using the experimental data. The parameters $\kappa = 0.01$ and $\lambda = 0.29$ were obtained from the consolidation and swelling test results; $G = 14710$kPa, $M_{cs} = 1.44$, $\Gamma = 4.3516$ were determined from the triaxial compression test results. The bounding surface material constants obtained from back-calculation of the test results were $N = 1.02$, $R = 2.8043$,

$A = 0.4$, and $k_m = 1.0$. The initial conditions of the samples were $p'_0 = 98.1$kPa and $e_0 = 2.3$. The viscoplastic parameter $c_\beta = 0.06$ was used in the simulations with the reference strain rate $\dot{\varepsilon}^{vp}_{p,r} = 10^{-3}$/min and the threshold strain rate $\dot{\varepsilon}^{vp}_{p,th} = 0$/min.

5.2.2.2. Simulation Results

The simulation results and experimental data of the undrained creep tests on San Francisco Bay Mud are presented in Figure 5.2. Good agreement is observed between the measured data and the model simulations. The samples subjected to creep loads of 30% and 50% of q_{ult} show only a small increase in axial strain after the initial deformation, while samples subjected to creep loads of 70% show large axial strain leading to creep failure.

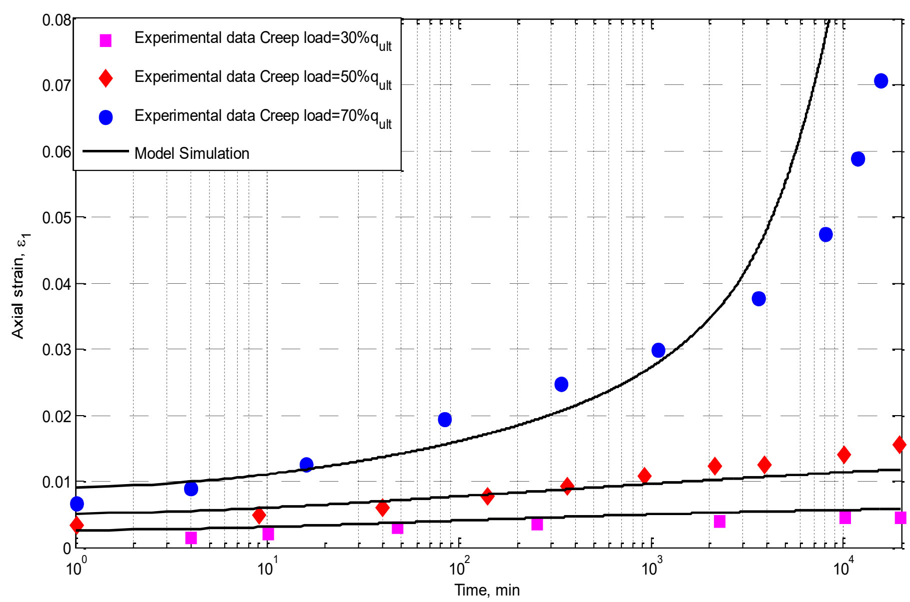

Figure 5.2 – Simulation results and experimental data of undrained creep tests on San Francisco Bay Mud with creep loading 30%, 50% and 70% of the ultimate deviator stress and initial cell pressure $p'_0 = 98.1$ kPa (1kg/cm^2): Axial strain versus Time

5.3. Application of Bounding Surface Viscoplasticity Model to Constant Strain Rate Triaxial Compression Tests

In a constant strain rate test, a total strain rate is enforced and kept constant throughout the experiment while the stress response is measured. An increase in strain rate during soil compression is manifested by increase in soil stiffness (Mitchell and James Kenneth, 2005), i.e. the larger the strain rate, the stiffer the soil. Many researchers have conducted extensive laboratory tests, mainly one-dimensional and triaxial tests, to investigate the time-dependent behaviour of soils (Vaid *et al.*, 1979; Adachi and Oka, 1982; Graham *et al.*, 1983; Leroueil *et al.*, 1985). In this section, the capability of the proposed bounding surface model to capture the strain rate dependent behaviour of two soft soils, i.e. Remoulded Fukakusa clay and San Francisco Bay Mud is demonstrated. Several numerical examples are also presented to show the application of the model to simulate the rate-dependent behaviour of normally consolidated as well as overconsolidated cohesive soils under both drained and undrained loading conditions.

5.3.1. Remoulded Fukakusa Clay

A series of undrained constant strain rate tests were conducted on Remoulded Fukakusa clay by Adachi & Oka (1982). The samples were initially consolidated isotropically for one day under the effective cell pressure of 392 kPa and the back pressure of 98 kPa. The constant axial strain rates imposed in the CRS tests were 0.0835%/min and 0.00817%/min.

5.3.1.1. Model Parameters

The material parameters used in the simulations were: $\kappa = 0.02$, $G = 36300$ kPa, $M_{cs} = 1.5$, $\lambda_0 = 0.1$, $\Gamma_0 = 2.3$; the bounding surface material constants: $N = 1.45$, $R = 1.85$ and $k = 2.0$, $k_d = 1.0$, $A = 1.0$, and $k_m = 0.0$. The initial conditions were $p'_0 = 392$ kN/m^2 and $e_0 = 0.72$. The viscoplastic parameters used in the simulations as obtained from back-calculation of the test results were $c_\beta = 0.1$ with the reference strain rate $\dot{\varepsilon}_{p,r}^{vp} = 2.0 \times 10^{-5}/\mathrm{min}$ and the threshold strain rate $\dot{\varepsilon}_{p,th}^{vp} = 10^{-7}/\mathrm{min}$.

5.3.1.2. Simulation Results

Figures 5.3 and 5.4 show the effect of strain rate on the stress-strain response and the effective stress paths for Remoulded Fukakusa clay, respectively. There is a good agreement between the experimental and numerical results for both constant strain rate tests. As observed, the stiffness and strength of the clay increase with the increase of the strain rate. It can be seen from Figure 5.3 that the maximum deviatoric stress increases with increase in the strain rate. Figure 5.4 shows that the lower the strain rate, the flatter the undrained stress path.

By increasing the strain rate, the CRS compression curve moves to the right in the $(e - \ln p')$ plane, resulting in the enlargement of the bounding surface and the increase of the over-consolidation degree of the soil. Due to the strain rate dependency of the pre-consolidation pressure, clay behaves like an overconsolidated soil under high strain rates, while it shows the characteristics of normally consolidated clay when the rate of loading is low.

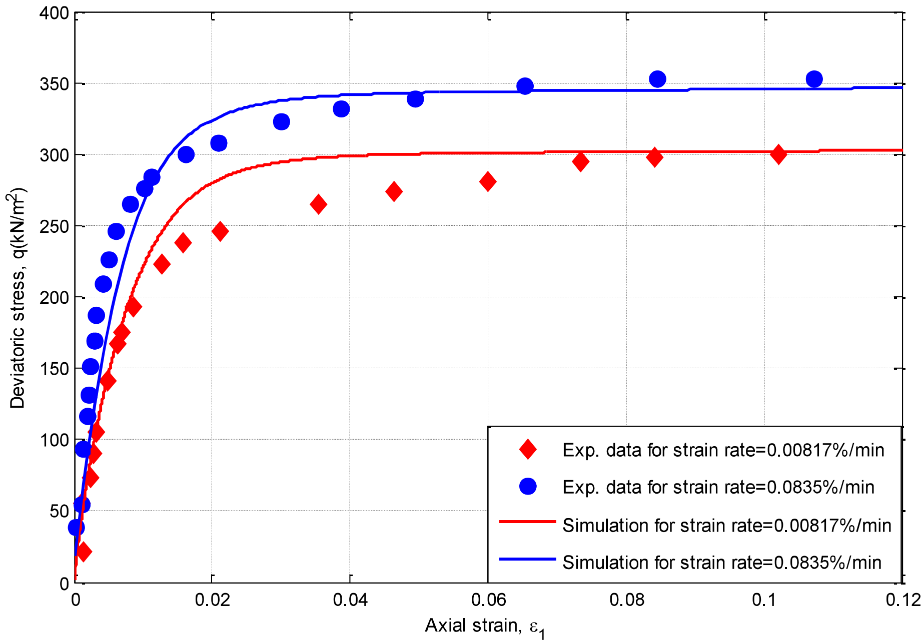

Figure 5.3 – Effect of strain rate on stress-strain response of Remoulded Fukakusa clay: Deviatoric stress versus Axial strain

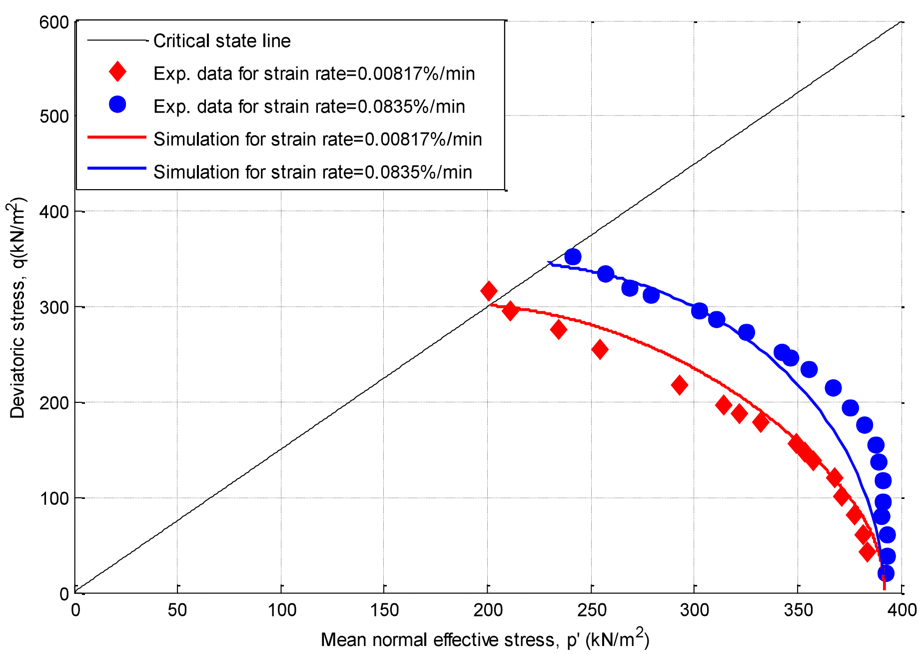

Figure 5.4 – Effect of strain rate on undrained stress path for Remoulded Fukakusa clay: Deviatoric stress versus Mean normal effective stress

5.3.2. San Francisco Bay Mud

The strain rate dependency behaviour was examined by using the strain rates 0.001%/min and 0.01%/min. The stress-strain relations and the stress paths are shown in Figures 5.5 and 5.6, respectively.

5.3.2.1. Model Parameters

The material parameters used in the simulations were calibrated using the experimental data. The parameters $\kappa = 0.01$ and $\lambda = 0.29$ were obtained from the consolidation and swelling test results; $G = 14710$kPa, $M_{cs} = 1.44$, $\Gamma = 4.3516$ were determined from the triaxial compression test results. The bounding surface material constants obtained from back-calculation of the test results were $N = 1.02$, $R = 2.8043$, $A = 0.4$, and $k_m = 8.0$. The initial conditions of the samples were $p'_0 = 98.1$kPa and $e_0 = 2.3$. The viscoplastic parameter $c_\beta = 0.06$ was used in the simulations with the reference strain rate $\dot{\varepsilon}_{p,r}^{vp} = 10^{-6}$/min and the threshold strain rate $\dot{\varepsilon}_{p,th}^{vp} = 0/\text{min}$.

5.3.2.2. Simulation Results

Figures 5.5 and 5.6 show the response of San Francisco Bay Mud at the strain rates of 0.001%/min and 0.01%/min and compare it with the rate-independent response. It is seen that the larger the strain rate, the stiffer the soil. In Figure 5.6, the undrained stress paths become flatter at lower rates of strain.

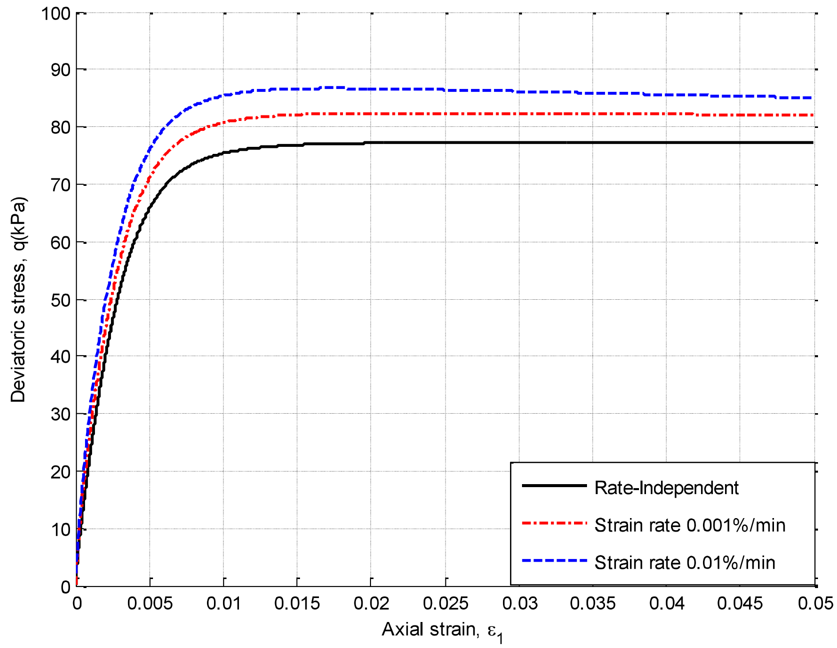

Figure 5.5 – Effect of strain rate on stress-strain response of normally consolidated San Francisco Bay Mud specimens ($p'_0 = 98.1$ kPa): Deviatoric stress versus Axial strain

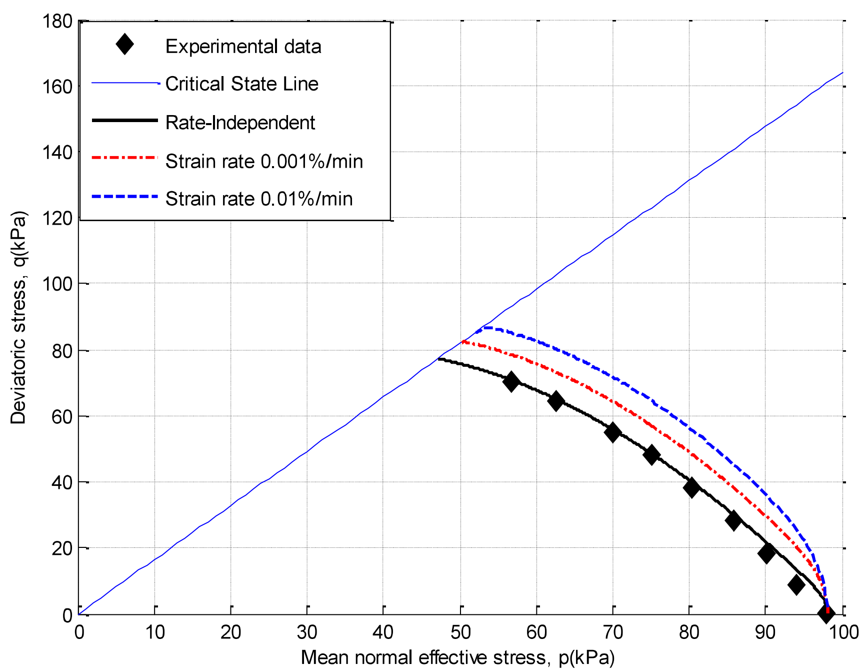

Figure 5.6 – Effect of strain rate on undrained stress path of normally consolidated San Francisco Bay Mud specimens ($p'_0 = 98.1$ kPa): Deviatoric stress versus Mean normal effective stress

5.3.3. Weald Clay – Drained Tests

Capability of the proposed bounding surface viscoplasticity model to capture the behaviour of cohesive soils during drained loading is demonstrated using the experimental results for Weald Clay. The results of the conventional triaxial tests on a normally consolidated and heavily overconsolidated soil samples were presented by Henkel (1956).

5.3.3.1. Model Parameters

The material parameters used in the simulations were calibrated using the experimental data. The parameters $\kappa = 0.025$ and $\lambda = 0.093$ were obtained from the consolidation and swelling test results; $\nu = 0.3$, $M_{cs} = 0.96$, $\Gamma_0 = 2.06$ were determined from the triaxial compression test results. The bounding surface material constants used in the simulations were $N = 4.5$, $R = 2.714$, $k = 2.0$, $A = 0.72$, and $k_m = 0.7$. The initial conditions were $p'_0 = 207kPa$ and $e_0 = 0.632$ for the normally consolidated and $p'_0 = 34.5kPa$ and $e_0 = 0.617$ for the heavily overconsolidated samples. The viscoplastic parameter used in the simulations were $c_\beta = 0.07$ with the reference strain rate $\dot{\varepsilon}^{vp}_{p,r} = 2.0 \times 10^{-5}/\text{min}$ and the threshold strain rate $\dot{\varepsilon}^{vp}_{p,th} = 0/\text{min}$.

5.3.3.2. Simulation Results

The influence of strain rate on deformation behaviour of both normally consolidated and heavily overconsolidated Weald Clay is demonstrated in Figures 5.7 and 5.8. It can be seen from these figures that the rate dependency is more pronounced in normally consolidated clay in comparison with the heavily overconsolidated clay. This is consistent with the results reported by Mitchell and James Kenneth (2005). This behaviour was also observed by Sheahan *et al.* (1996) in the results of the tests conducted on Boston blue clay, as the undrained stress path and the strength were much more strain rate dependent for lightly overconsolidated clay (OCR = 1 and 2) in comparison with heavily overconsolidated clay (OCR = 4 and 8).

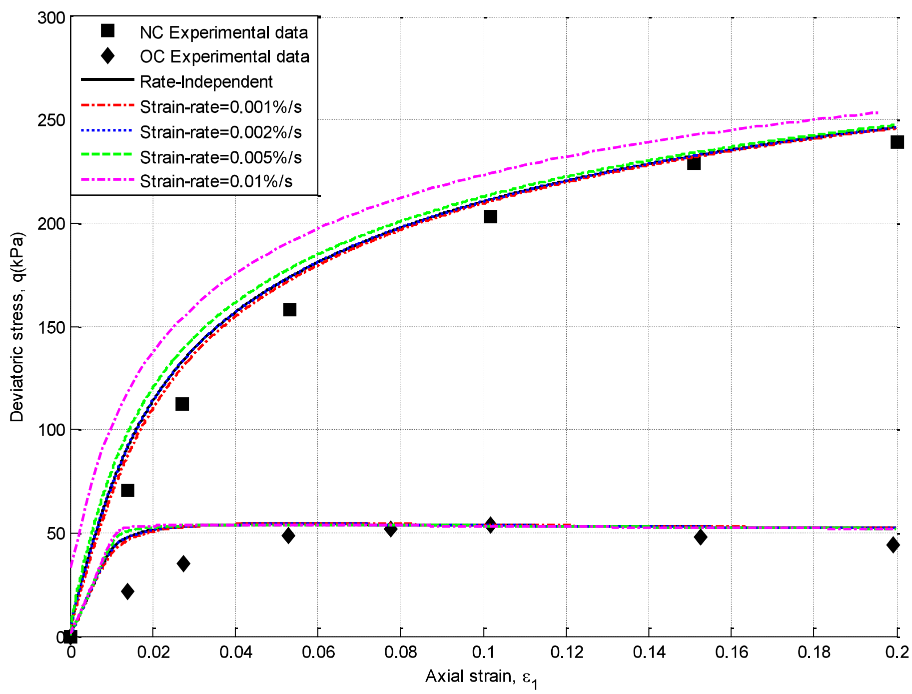

Figure 5.7 – Effect of strain rate on stress-strain response of normally and heavily overconsolidated Weald Clay: Deviatoric stress versus Axial strain

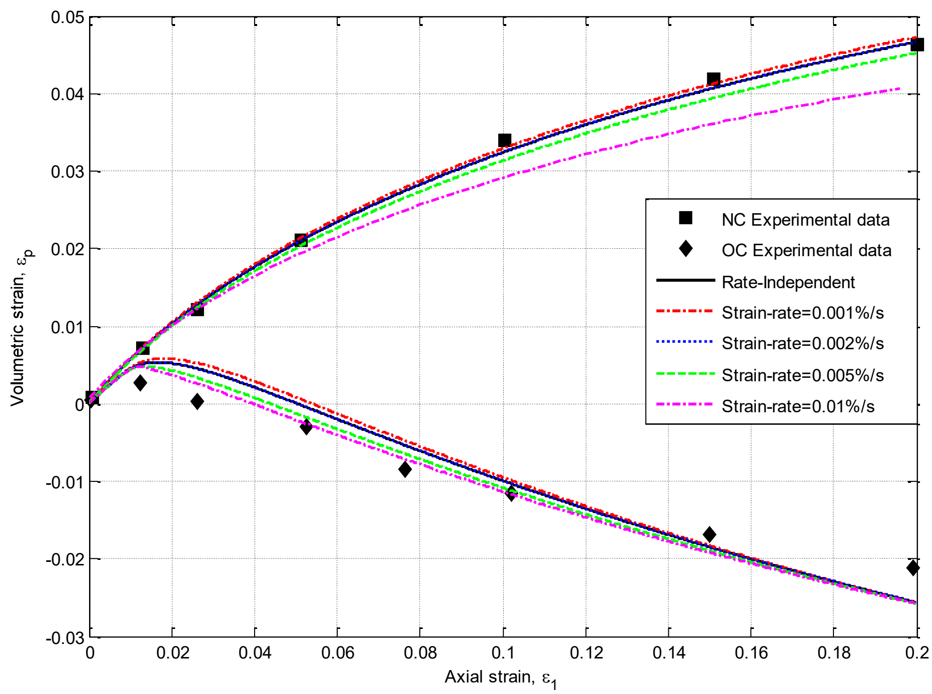

Figure 5.8 – Effect of strain rate on response of normally and heavily overconsolidated Weald Clay: Volumetric strain versus Axial strain

5.3.4. Cardiff Kaolin Clay – Undrained Tests with Different OCRs

Application of the proposed model to the undrained analysis of cohesive soils is demonstrated using the results of the undrained monotonic triaxial tests on soft kaolin clay conducted at Cardiff University. Details of the experimental tests including sample preparation, testing procedure and material parameters were reported by Banerjee and Stipho (1978). The tests with the over-consolidation ratios (OCR) of 1, 2 and 5 are presented below.

5.3.4.1. Model Parameters

The material parameters used in the simulations were calibrated using the experimental data. The parameters $\kappa = 0.05$ and $\lambda = 0.14$ were obtained from the consolidation and swelling test results; $\nu = 0.15$, $M_{cs} = 1.05$, $\Gamma_0 = 2.676$ were determined from the triaxial compression test results. The bounding surface material constants obtained from back-calculation of the test results were $N = 1.44$, $R = 2.9$, $k = 2.0$, $A = 0.4$, and $k_m = 1.0$. The initial conditions of the samples were $p'_0 =$ 98.1kPa and $e_0 = 2.3$. The viscoplastic parameter $c_\beta = 0.1$ was used in the simulations with the reference strain rate $\dot{\varepsilon}^{vp}_{p,r} = 10^{-6}/\text{min}$ and the threshold strain rate $\dot{\varepsilon}^{vp}_{p,th} = 10^{-10}/\text{min}$.

5.3.4.2. Simulation Results

The simulation results to capture rate-dependency behaviour for Cardiff Kaolin Clay with over-consolidation ratios of 1, 2 and 5 are presented in Figures 5.9 and 5.10, Figures 5.11 and 5.12, and Figures 5.13 and 5.14, respectively. From the results, it can be seen that the effect of strain rate on undrained response decreases with increase in over-consolidation ratio. The effect of strain rate is not significant for heavily over-consolidated clay. This conclusion is consistent with observations and simulation results of Weald Clay presented in Section 5.3.3.

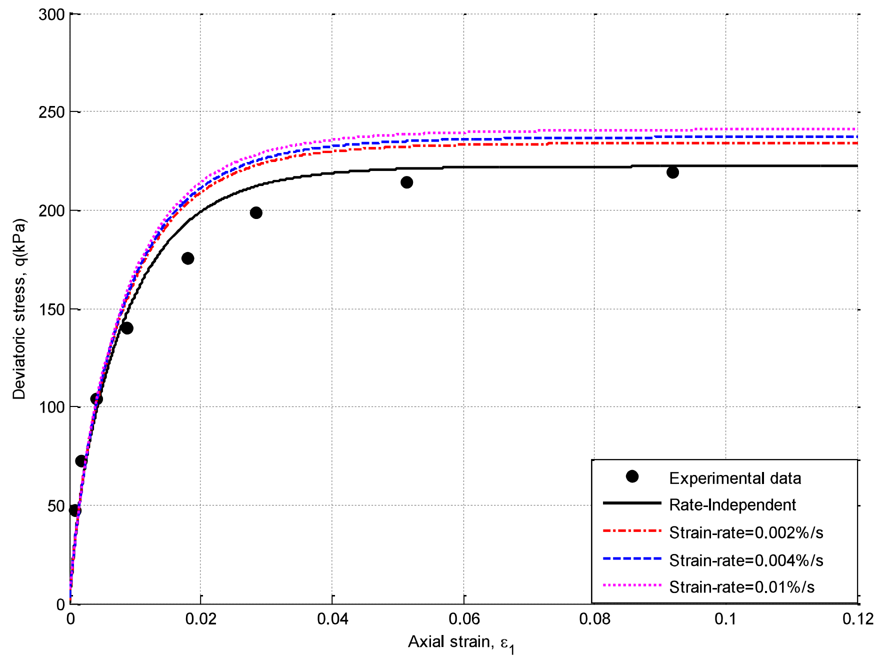

Figure 5.9 – Effect of strain rate on stress-strain response of Cardiff Kaolin Clay with $p'_0 = 414$ kPa, $e_0 = 0.93$ and OCR = 1: Deviatoric stress versus Axial strain

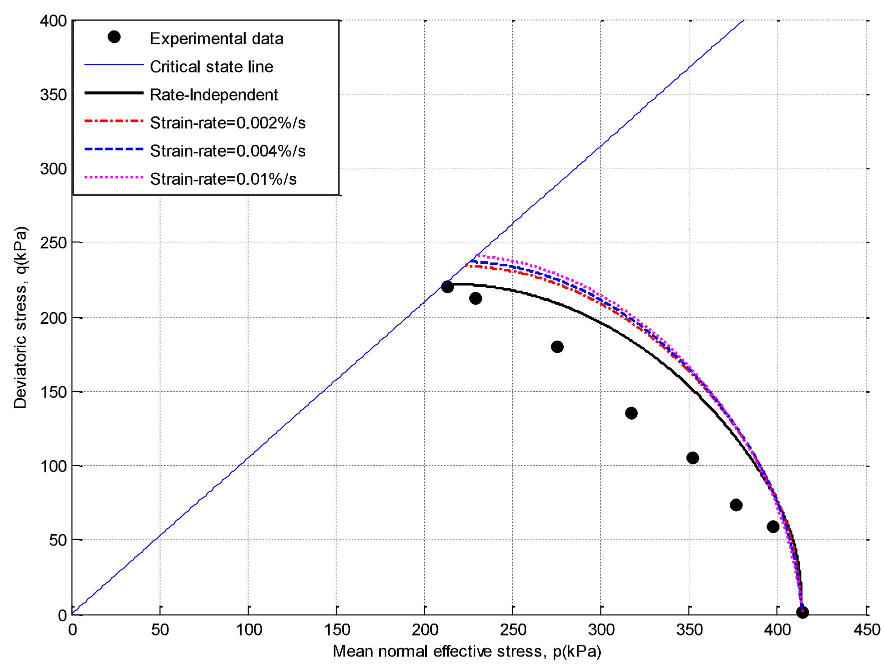

Figure 5.10 – Effect of strain rate on response of Cardiff Kaolin Clay with $p'_0 = 414$ kPa, $e_0 = 0.93$ and OCR = 1: Deviatoric stress versus Mean normal effective stress

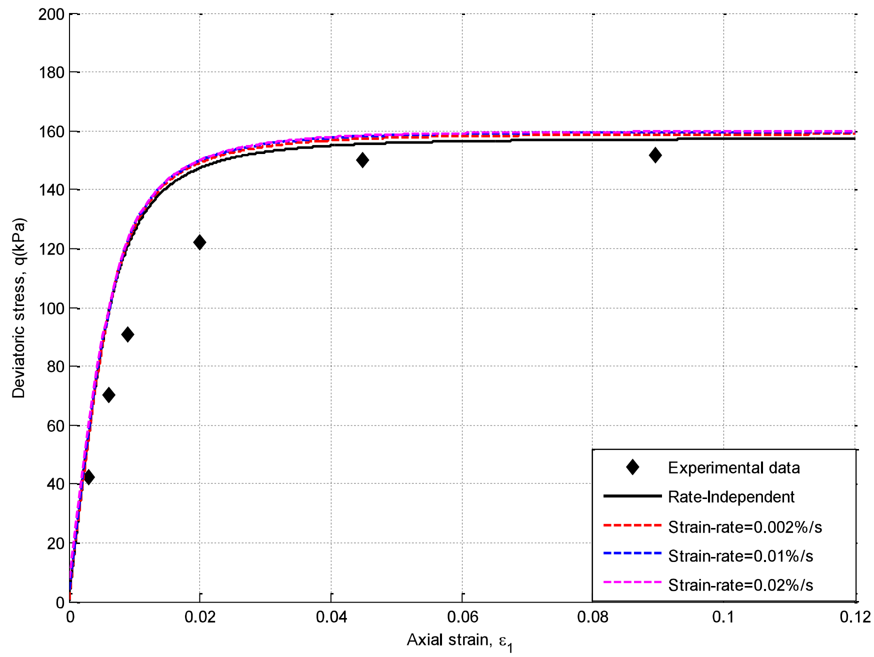

Figure 5.11 – Effect of strain rate on stress-strain response of Cardiff Kaolin Clay with $p'_0 = 193$ kPa, $e_0 = 0.97$ and OCR = 2: Deviatoric stress versus Axial strain

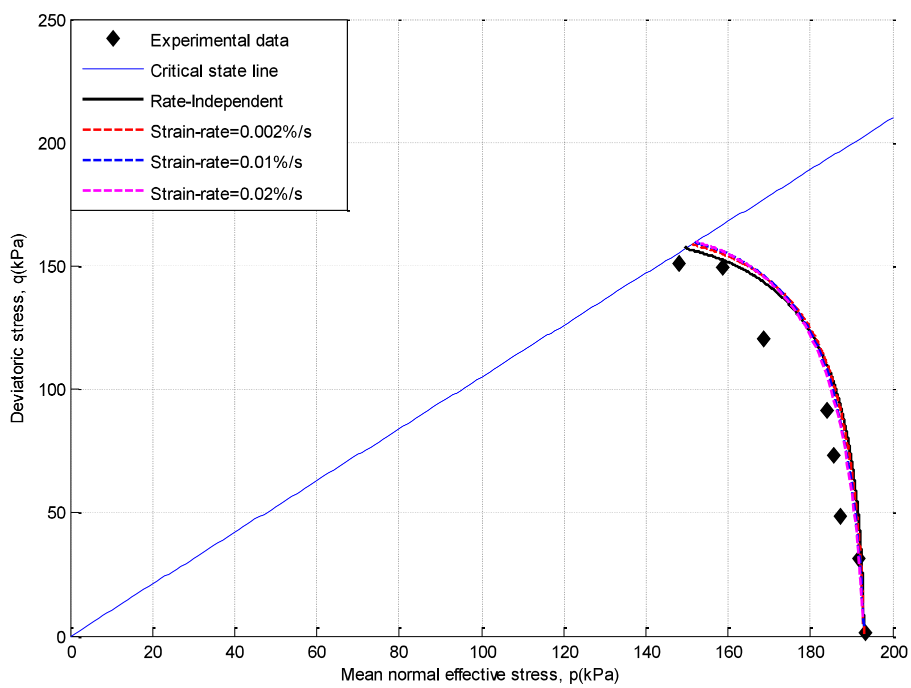

Figure 5.12 – Effect of strain rate on response of Cardiff Kaolin Clay with $p'_0 = 193$ kPa, $e_0 = 0.97$ and OCR = 2: Deviatoric stress versus Mean normal effective stress

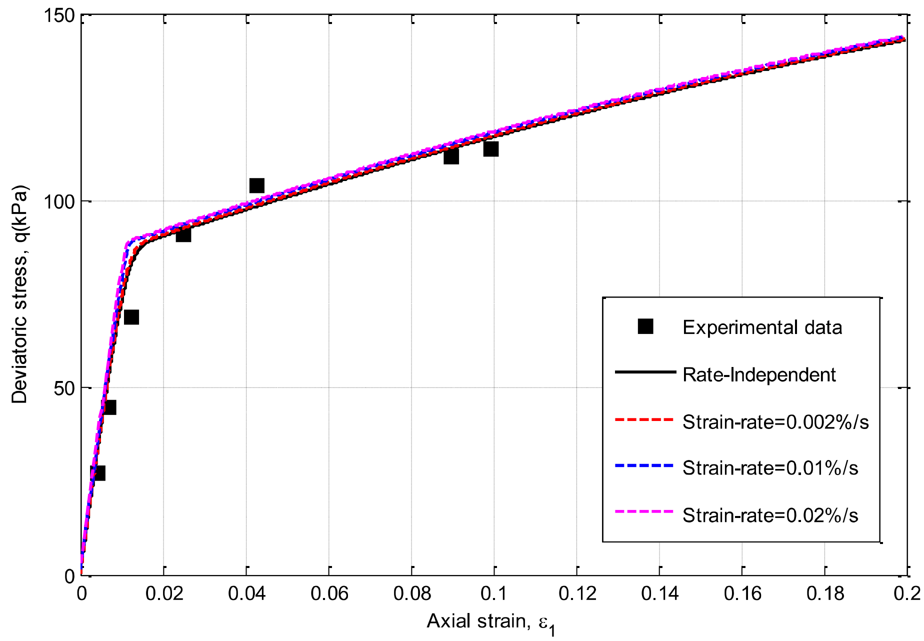

Figure 5.13 – Effect of strain rate on stress-strain response of Cardiff Kaolin Clay with $p'_0 = 76$ kPa, $e_0 = 0.94$ and OCR = 5: Deviatoric stress versus Axial strain

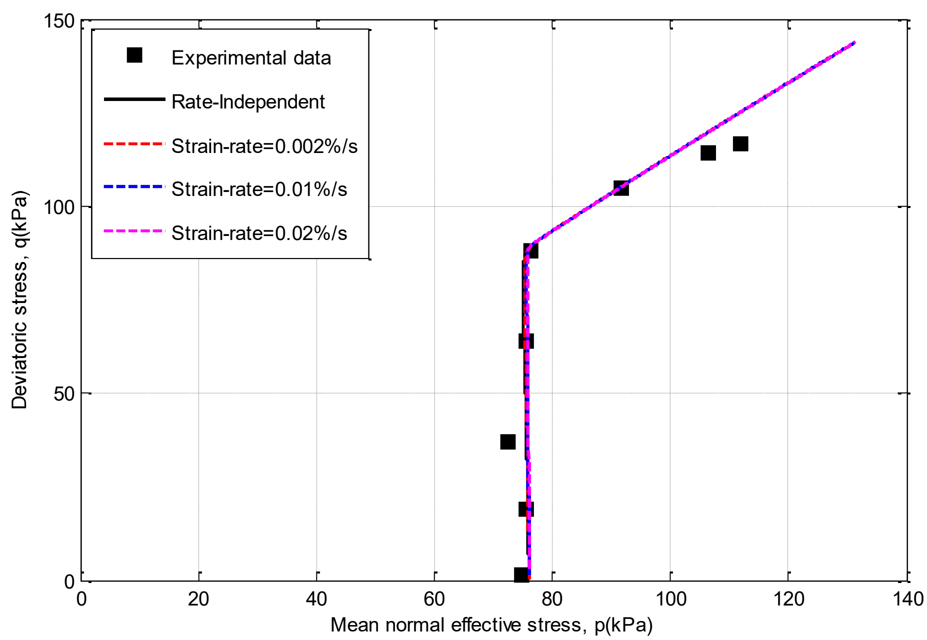

Figure 5.14 – Effect of strain rate on response of Cardiff Kaolin Clay with $p'_0 = 76$ kPa, $e_0 = 0.94$ and OCR = 5: Deviatoric stress versus Mean normal effective stress

5.4. Application of Bounding Surface Viscoplasticity Model to Undrained Loading, Unloading and Relaxation Tests

The stress relaxation is a drop in stress over time after a soil is subjected to a constant strain level. Although stress relaxation has been less studied than creep (Murayama and Shibata, 1961; Akai *et al.*, 1975; Lacerda and Houston, 1973; Lacerda, 1976), the observed stress relaxation behaviour is not in "correspondence" with the measured creep behaviour (Lade, 2009). Borja (1992) suggested that each of these two processes could bring about the other, and both deserve a thorough examination to better understand the stress – strain – time behaviour of soils.

In this section, the application of the proposed bounding surface viscoplasticity model to predict the stress relaxation behaviour of geomaterials is demonstrated by comparing the numerical simulations with the experimental results of cyclic undrained constant-rate triaxial and relaxation tests on Hong Kong marine deposits.

5.4.1. Hong Kong Marine Deposits

The application of the proposed bounding surface model to predict the loading-unloading and relaxation behaviour of soils is demonstrated using the results of a step-changed test conducted by Zhu (2000). The test is the combination of cyclic undrained constant-rate triaxial test and relaxation test on Hong Kong marine deposits.

5.4.1.1. Model Parameters

Details of the test's procedure are written in Table 5.2. Slopes of the isotropic compression line $\lambda = 0.195$ and unloading reloading line $\kappa = 0.049$ were obtained from the isotropic compression test data. The soil was normally consolidated to the confining pressure 300 kPa. Samples were saturated under back pressure of 200 kPa and then sheared under undrained conditions. The initial specific volume used for the simulation was $\upsilon = 1.89$. Slope of the critical state line was given as $M_{cs} = 1.265$. The other material constants used in these simulations as obtained from back-calculation of the test results were $\nu = 0.1$, $N_0 = 3.0168$, $N = 1.44$, $R = 2.90$, and $A = 1.0$.

Table 5.2 – Loading procedure for the combined test conducted on Hong Kong marine deposits

Stage	Axial strain rate $\dot{\varepsilon}$ (1/min)	Duration (min)
1 Loading	0.1%	29
2 Unloading	-0.1%	7
3 Reloading	0.1%	20
4 Relaxation	0	2540
5 Loading	0.01%	232
6 Relaxation	0	1320
7 Loading	0.001%	830
8 Relaxation	0	705

The viscoplastic parameter $c_\beta = 0.015$ was considered in the simulations with the reference strain rate $\dot{\varepsilon}_{p,r}^{vp} = 10^{-7}/\text{min}$ and the threshold strain rate $\dot{\varepsilon}_{p,th}^{vp} = 10^{-8}/\text{min}$. In cyclic tests, k_m parameter for first time loading (FTL) and next unloading/reloadings (URL) can be defined differently. In this simulation, the values considered for these two parameters were $k_m{}^{\mathrm{FTL}} = 0.0$ and $k_m{}^{\mathrm{URL}} = 40.0$.

5.4.1.2. Simulation Results

Figures 5.15 – 5.17 show the simulation results and laboratory test data which contain variation of shear stress versus axial strain, stress path curves, and variation of pore water pressure versus axial strain, respectively. It can be observed that the predicted results agree with the experimental data to an acceptable accuracy, demonstrating the capability of the model to capture stress relaxation as well as strain rate behaviour of the soil. As seen in the figures, applying the higher strain rate results in the increase of the undrained shear strength of the soil and consequently the decrease in the excess pore water pressure.

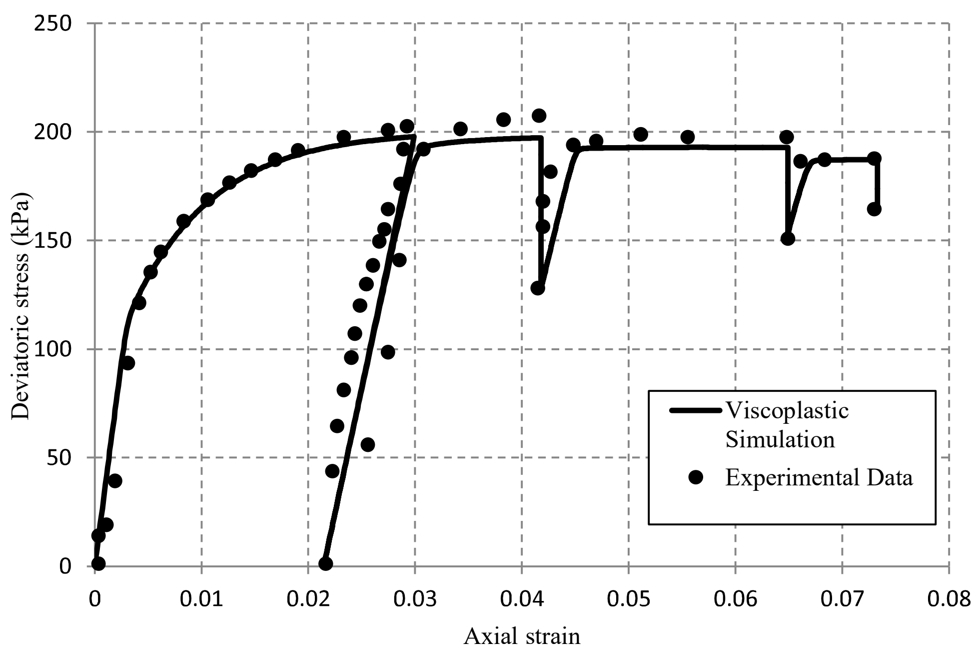

Figure 5.15 – Model simulation and experimental results of Hong Kong marine deposits under the combined triaxial and relaxation tests: Deviatoric stress versus Axial strain

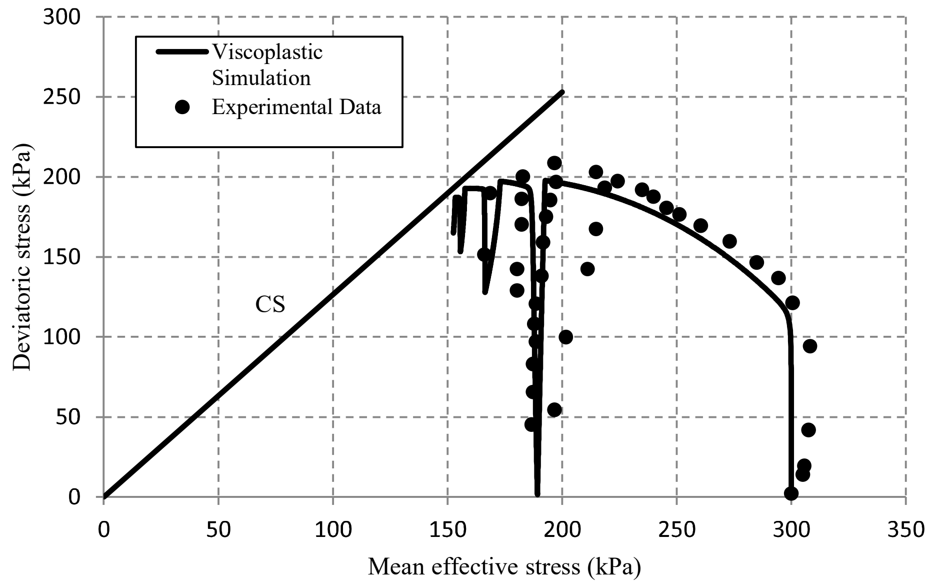

Figure 5.16 – Model simulation and experimental results of Hong Kong marine deposits under the combined triaxial and relaxation tests: Deviatoric stress versus Mean effective stress

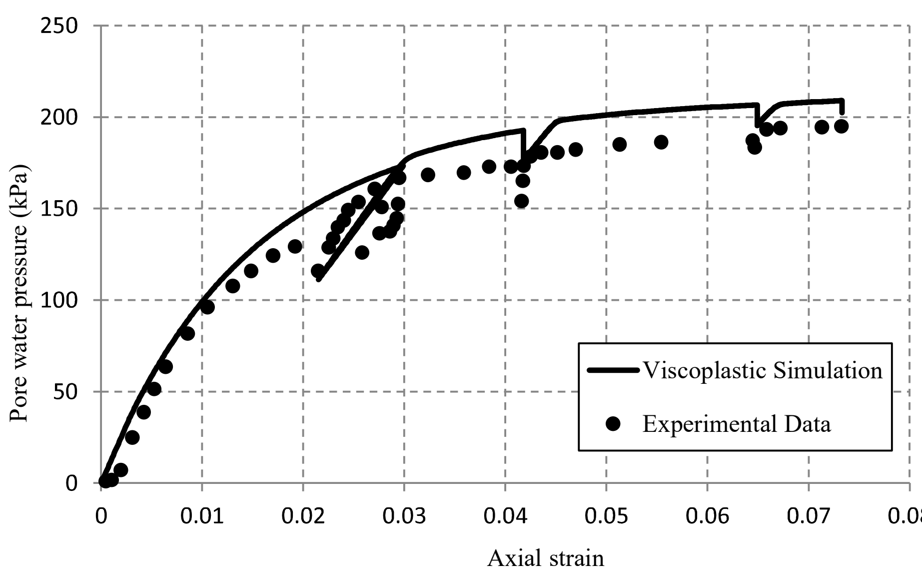

Figure 5.17 – Model simulation and experimental results of Hong Kong marine deposits under the combined triaxial and relaxation tests: Pore water pressure versus Axial strain

5.5. Application of Bounding Surface Viscoplasticity Model to Constant Strain Rate Tests for Unsaturated Soils

The time-dependent behaviour of soils has been investigated extensively through both one-dimensional and triaxial loading conditions. While most of the experimental studies in the literature have focused on determination of time-dependent behaviour of saturated soils, there are lack of experimental studies on creep, stress relaxation and strain-rate effects on unsaturated soils. There are also quite a large number of models developed to capture the time-dependent behaviour of soils as discussed in detail in Chapter 2. However, there are a few constitutive models which are able to simulate the time-dependent behaviour of unsaturated geomaterials. In this section, the capability of the proposed bounding surface viscoplasticity model to predict the time-dependent behaviour of unsaturated soils is demonstrated.

5.5.1. Bourke Silt

A series of suction controlled tests on Bourke Silt were conducted by Uchaipichat (2005). All tests were carried out in a modified Bishop-Wesley triaxial cell capable of independent measurement and control the pore air pressure, pore water pressure, water volume change and sample volume change. The triaxial tests are drained compression tests at constant suction. All the samples were preconsolidated to an isotropic preconsolidation stress of 200kPa.

5.5.1.1. Model Parameters

The material parameters used in the simulations were calibrated using the experimental data. The parameters $\kappa = 0.006$ and $\lambda = 0.1$ were obtained from the consolidation and swelling test results; $\nu = 0.25$, $M_{cs} = 1.17$, and $\Gamma = 2.3$ were determined from the triaxial compression test results. The bounding surface material constants obtained from back-calculation of the test results were $N = 3.0$, $R = 1.82$, $k = 2.0$, $k_d = 1.0$, $A = 1.0$, and $k_m = 1.0$. The initial conditions of the samples were $p'_0 = 98.1$kPa and $e_0 = 2.3$. The viscoplastic parameter $c_\beta = 0.03$ was used in the simulations with the reference strain rate $\dot{\varepsilon}_{p,r}^{vp} = 2.0\text{x}10^{-7}/\text{min}$ and the threshold strain rate $\dot{\varepsilon}_{p,th}^{vp} = 10^{-8}/\text{min}$.

5.5.1.2. Simulation Results

The effect of strain rate was simulated based on the data of the triaxial tests conducted under the drained compression condition with cell pressure of 50kPa at constant suction of 300kPa. The simulation results are presented in Figures 5.18 and 5.19. It is observed that the stiffness and strength of the soil increase with the increase of strain rate.

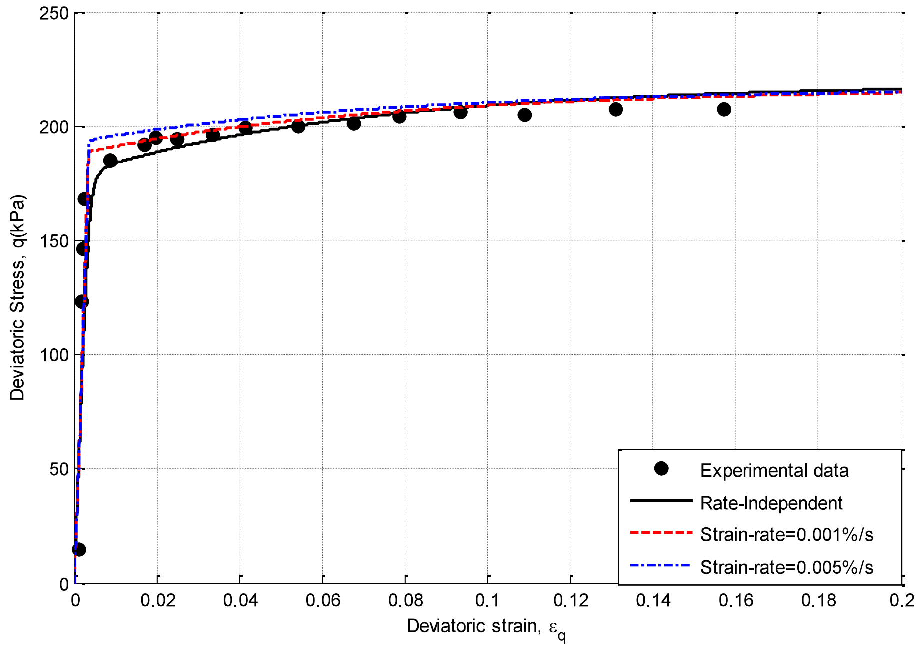

Figure 5.18 – Effect of strain rate on Bourke Silt at a cell pressure of 50 kPa and suction of 300 kPa: Deviatoric stress versus Deviatoric strain

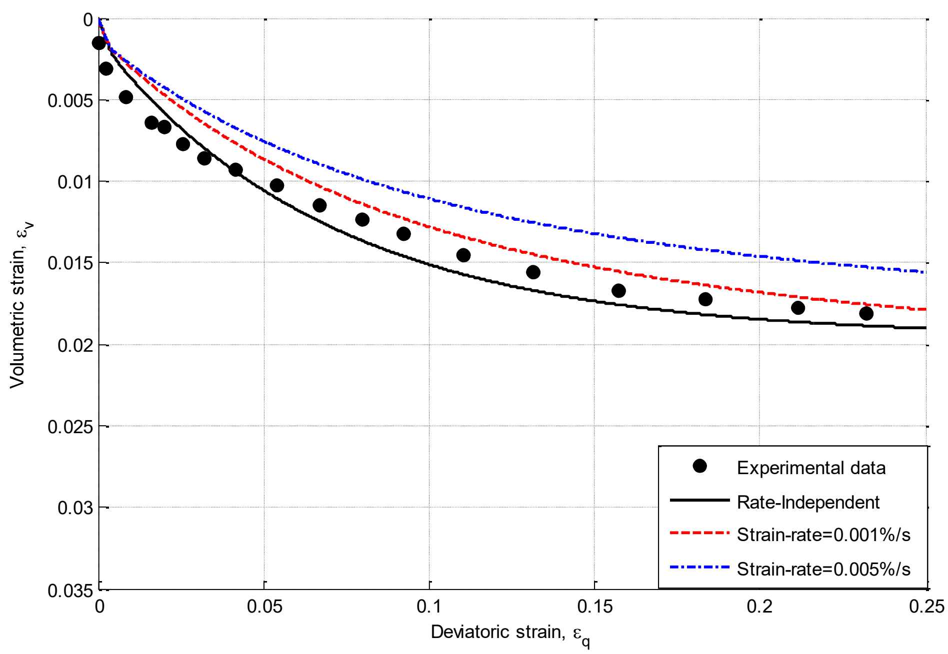

Figure 5.19 – Effect of strain rate on Bourke Silt at a cell pressure of 50 kPa and suction of 300 kPa: Volumetric strain versus Deviatoric strain

5.6. Application of Bounding Surface Viscoplasticity Model to Capture Tertiary Creep and Creep Rupture

Tertiary creep is the creep at the third phase of the creep process with an accelerating strain rate. Some soils may fail under creep stress levels less than the peak strength. This observation was reported by many researchers including Saito and Uezawa (1961), Singh and Mitchell (1969), Campanella and Vaid (1972), Tavenas and Leroueil (1981) and Sekiguchi (1984). In general, saturated soft sensitive clays under undrained conditions are most susceptible to strength loss during creep due to reduction in effective stress caused by increase in pore water pressure with time. Heavily over-consolidated clays under drained conditions are also susceptible to creep rupture due to softening associated with the increase in water content by dilation and swelling (Mitchell, 1993). In this section, the capability of the proposed model to capture tertiary creep and creep rupture is described both for undrained creep tests on normally consolidated soil and for drained creep tests on heavily over-consolidated clay.

5.6.1. San Francisco Bay Mud

The creep test on San Francisco Bay Mud presented in section 5.2 is taken into consideration. A series of stress-controlled undrained triaxial tests were performed by Arulanandan *et al.* (1971) on San Francisco Bay Mud at different isotropic consolidation pressures and stress levels. For the creep tests with $p'_0 = 98kPa$ (or $1kg/cm^2$), the samples were subjected to the creep loads of 30%, 50%, and 70% of the ultimate deviatoric stress $q_{ult} = 77.5$ kPa (or $0.79kg/cm^2$).

5.6.1.1. Model Parameters

The material parameters used in the simulations were: $\kappa = 0.01$ and $\lambda = 0.29$ were obtained from the consolidation and swelling test results; $G = 14710$kPa, $M_{cs} = 1.44$, $\Gamma = 4.3516$ were determined from the triaxial compression test results. The bounding surface material constants obtained from back-calculation of the test results were $N = 1.02$, $R = 2.8043$, $A = 0.4$, and $k_m = 1.0$. The initial conditions of the samples were $p'_0 = 98.1$kPa and $e_0 = 2.3$. The viscoplastic parameter $c_\beta = 0.06$ was used in the simulations with the reference strain rate $\dot{\varepsilon}_{p,r}^{vp} = 10^{-3}/\text{min}$ and the threshold strain rate $\dot{\varepsilon}_{p,th}^{vp} = 0/\text{min}$.

5.6.1.2. Simulation Results

The variation of axial strain over time during the undrained creep test conducted on San Francisco Bay Mud is shown again in Figure 5.20 to demonstrate the capability of the model in capturing tertiary creep. As seen, the samples subjected to creep loads of 30% and 50% of q_{ult} show only a small increase in axial strain after the initial deformation, while samples subjected to creep loads of 70% show large axial strain leading to creep failure. Figure 5.21 depicts the reduction of the effective stress at constant deviatoric stress in the $(q - p')$ plane. It is observed that, at low levels of deviatoric stress, i.e. the creep loads of 30% and 50% of q_{ult}, the stress path ceases far away from the failure line, leading to a stable state. However, at high levels of deviatoric stress, i.e. creep load of 70% of q_{ult}, the stress path moves towards the critical state line, leading to creep rupture.

The development of excess pore water pressures is presented in Figure 5.22. As shown, the pore water pressure increases with time during the creep tests due to the change in deviatoric strain imposed by the constant deviatoric stress. This results in the decrease in mean effective stress and as the creep continues, the stress points in the $(q - p')$ plane progress towards the critical state line. It is also seen from the figure that the rate of pore water pressure build-up decreases until it reaches a steady state. If the stress state reaches the critical state line prior to the stabilisation of the mean effective stress, the deviatoric strain acceleration will become positive leading to undrained creep failure of the clay.

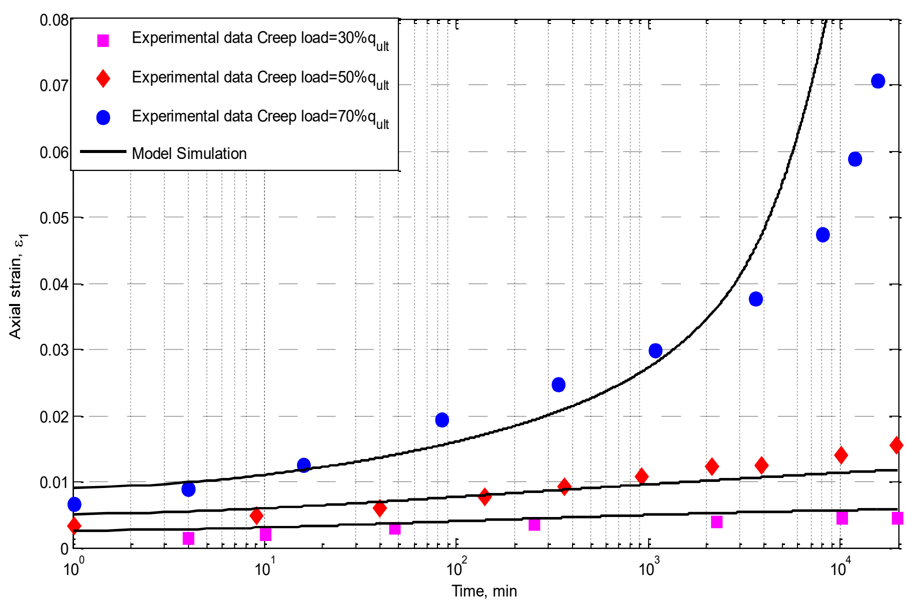

Figure 5.20 – Simulation results and experimental data of undrained creep tests on San Francisco Bay Mud with creep loading 30%, 50% and 70% of the ultimate deviator stress and initial cell pressure p'_0 = 98.1 kPa (1kg/cm^2): Axial strain versus Time

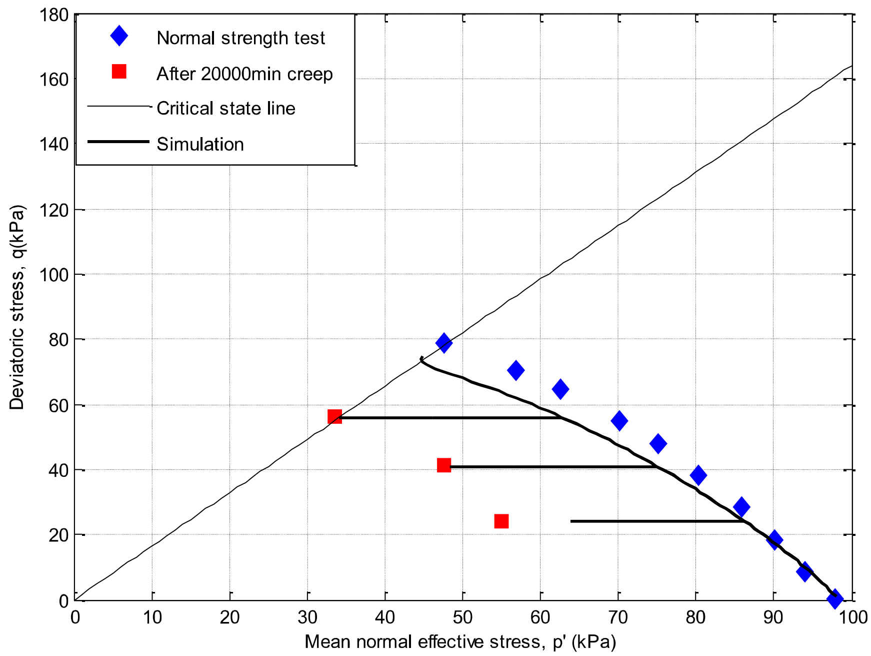

Figure 5.21 – Simulation results and experimental data of undrained creep tests on San Francisco Bay Mud with creep loading 30%, 50% and 70% of the ultimate deviator stress and initial cell pressure $p'_0 = 98.1$ kPa (1kg/cm^2): Deviatoric stress versus Mean normal effective stress

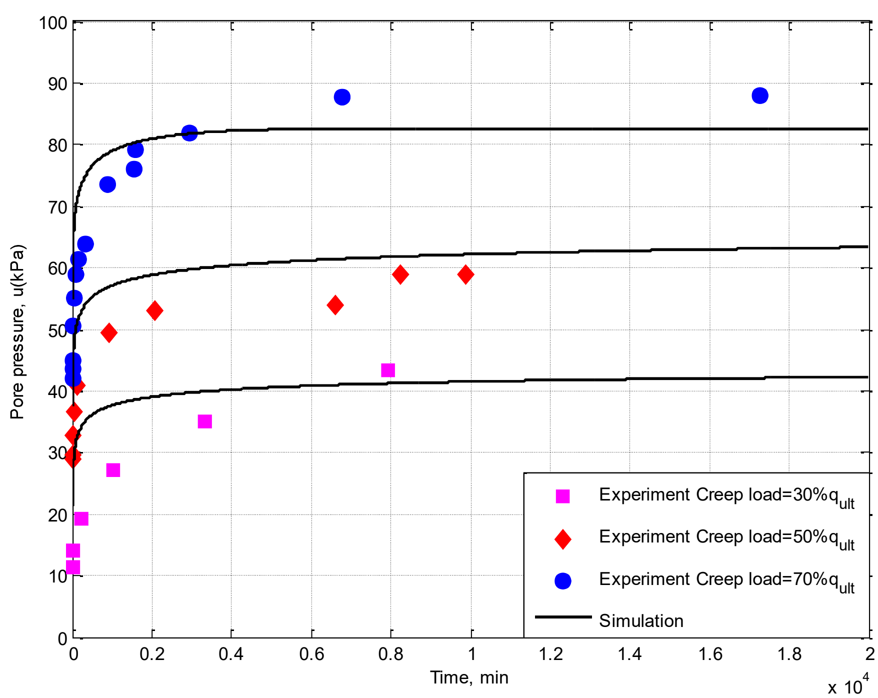

Figure 5.22 – Simulation results and experimental data of undrained creep tests on San Francisco Bay Mud with creep loading 30%, 50% and 70% of the ultimate deviator stress and initial cell pressure $p'_0 = 98.1$ kPa (1kg/cm^2): Pore water pressure versus Time

5.6.2. Haney Clay

The results of drained triaxial creep tests conducted by Snead (1970) on undisturbed Haney Clay are used to demonstrate the application of the proposed model to predict the creep rupture in heavily over-consolidated soils. The clay was defined as a sensitive marine silty clay, with 46% clay, 51% silt, and 3% fine sand.

The sample was initially consolidated isotopically to an effective stress of 517.1 kPa for 24 hours and then rebounded to an effective stress of 20.7 kPa for 44 hours. The initial conditions of the sample were $p'_0 = 20.7$ kPa and $e_0 = 0.667$. During the creep test, the sustained deviator stress was maintained at 90% of the ultimate deviator stress determined in a drained incremental loading test.

5.6.2.1. Model Parameters

The material parameters used in the simulations were calibrated using the experimental data. The parameters $\kappa = 0.018$ and $\lambda = 0.093$ were obtained from the consolidation and swelling test results; and $\nu = 0.3$, $M_{cs} = 1.39$, and $\Gamma_0 = 2.15$ were determined from the triaxial compression test results. The bounding surface material constants obtained from back-calculation of the test results were $N = 2.5$, $R = 1.714$, $A = 1.72$ and $k_m = 9.7$. The viscoplastic parameter $c_\beta = 0.06$ was used in the simulations with the reference strain rate $\dot{\varepsilon}_{p,r}^{vp} = 10^{-6}$/min and the threshold strain rate $\dot{\varepsilon}_{p,th}^{vp} = 0$/min.

5.6.2.2. Simulation Results

Figures 5.23 and 5.24 compare the experimental data and the simulation results for the test. As observed, there is good agreement between the experimental and simulation results demonstrating the capability of the model to capture drained creep rupture in over-consolidated soils. During the primary phase of creep, it is observed that the strain rate decreases over time. In this phase, the compressive strength of the soil reduces due to both increase in void ratio and decrease in viscoplastic volumetric strain rate. This leads the creep process into the secondary phase of creep with a transient minimum strain rate of 0.004%/min. The further reduction of the compressive strength due to increase in void ratio leads the process into tertiary creep with increasing strain rate, leading to creep failure of the soil.

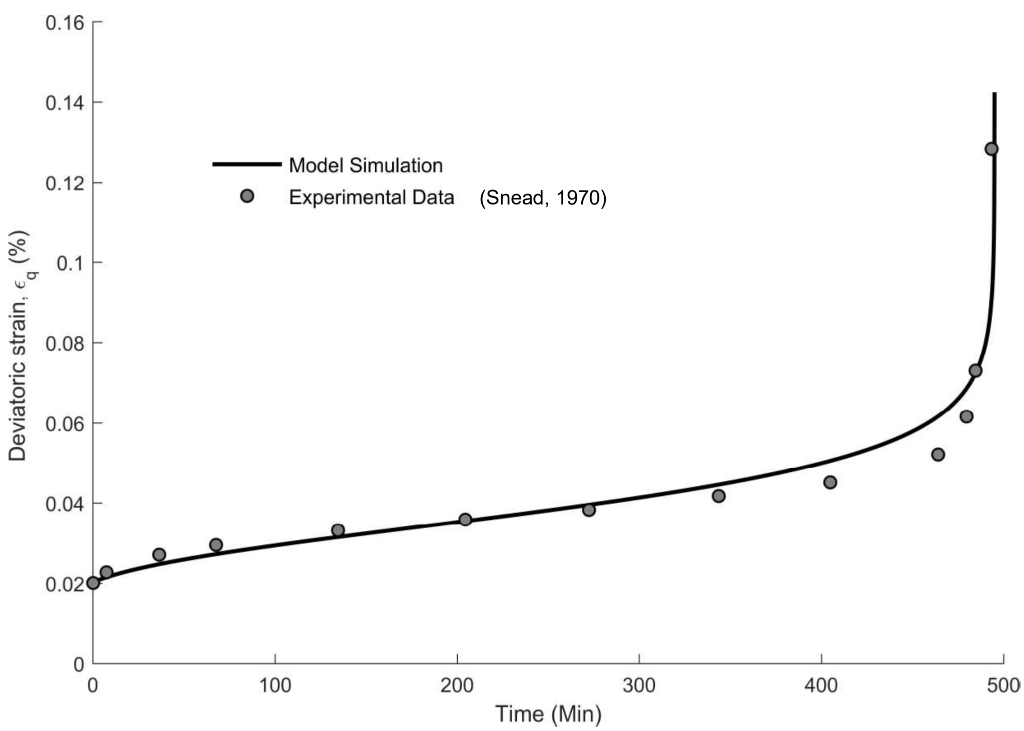

Figure 5.23 – Drained creep rupture test on over-consolidated Haney Clay: Deviatoric strain versus Time

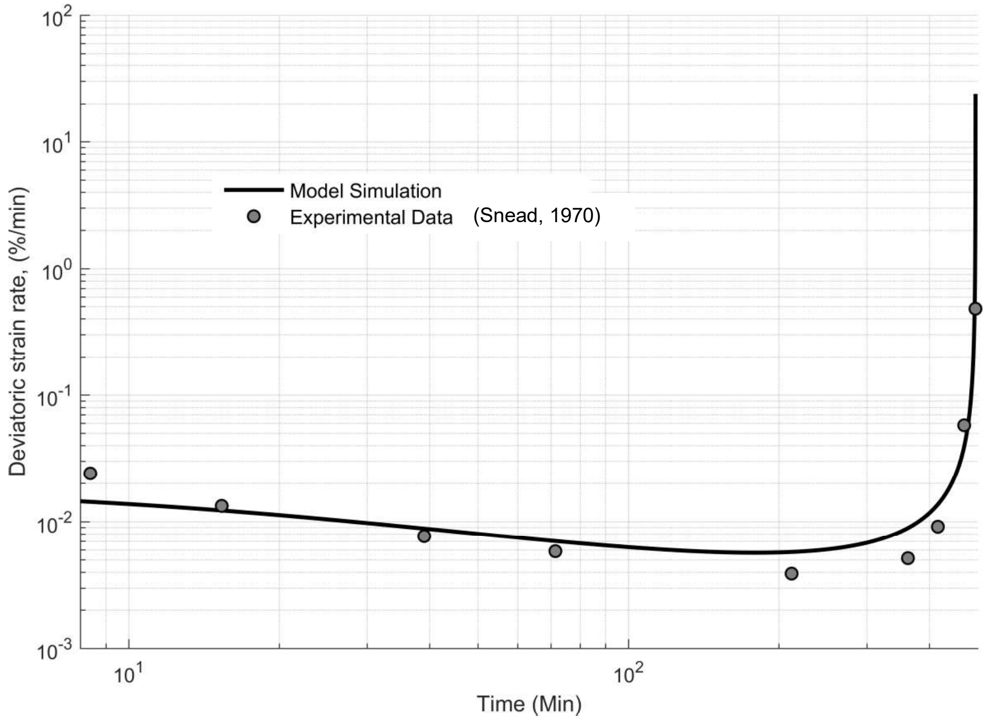

Figure 5.24 – Drained creep rupture test on over-consolidated Haney clay: Deviatoric strain rate versus Time

5.7. Application of Fully Coupled Flow-Deformation Model to the Analysis of Boundary Value Problems

A one-dimensional boundary value problem consisting of a multi-phase porous layer of 100m depth is considered. The material parameters of the heavily over-consolidated Weald Clay are considered for the analysis. The finite element mesh and the boundary conditions are shown in Figure 5.25. The upper boundary is drained and subjected to the step load with a uniform intensity $f(t)$ where t is time, while the remaining boundaries are impervious. As for the displacement boundary, all nodes are horizontally fixed and the nodes at the bottom are vertically constrained.

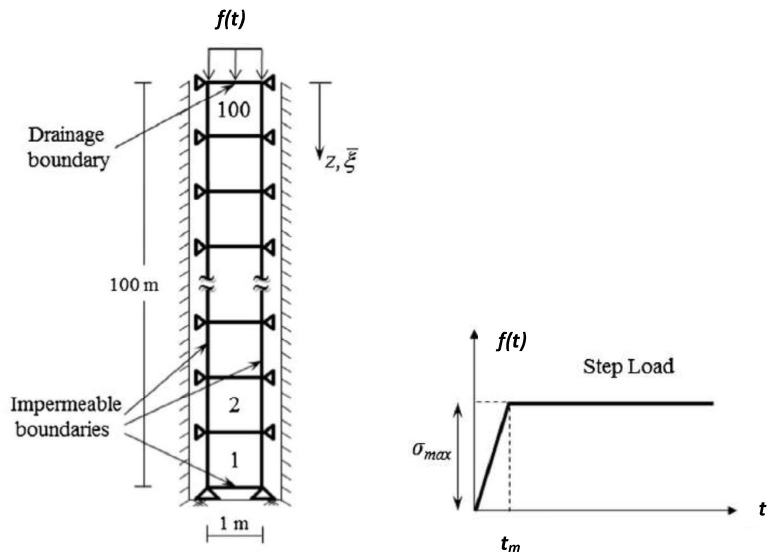

Figure 5.25 – Porous layer under uniform load: finite element mesh, boundary conditions and applied load

For the spatial interpolation of the solid displacement, an 8-node isoparametric quadrilateral element with a reduced Gaussian integration is adopted. For the coupled analysis, the 4-node quadrilateral element is utilised for pore water and air pressure fields. The mesh pattern of 1×100 (100 mixed elements) is considered as the default mesh configuration for the analyses.

5.7.1. Model Parameters

Henkel (1956) conducted a series of conventional drained triaxial tests on heavily over-consolidated Weald Clay. The material parameters used in the simulations were obtained from back-calculation of the test results. The swelling index $\kappa = 0.025$ and compression index $\lambda = 0.093$ were obtained from the consolidation and swelling test results; the Poisson's ratio $\nu = 0.3$, the slope of the critical state line $M_{cs} = 0.96$, and the specific volume on the critical state line at a unit confining pressure $\Gamma = 2.06$ were determined from the triaxial compression test results. The initial conditions were defined as $e_0 = 0.617$ and $p'_0 = 34.5$kPa. The bounding surface viscoplasticity model constants used in the simulations were $N = 4.5$, $R = 2.714$, $k = 2.0$ and $A = 0.72$, $k_m = 0.7$. The viscosity parameters were: $c_\beta = 0.07$, $\dot{\varepsilon}^{vp}_{p,ref} = 2.0 \times 10^{-5}/\mathrm{min}$ and $\dot{\varepsilon}^{vp}_{p,thr} = 1.0 \times 10^{-8}/\mathrm{min}$. The material parameters considered for the numerical analysis are presented in Table 5.3.

Table 5.3 – Material parameters for the one dimensional numerical analysis

Initial porosity	n_0	0.33	-
Lame's constant	λ	9355	kPa
Lame's constant	μ	6237	kPa
Initial permeability of liquid phase at S_r=1m/s	k_{ws0}	4.8 $\times 10^{-8}$	m/s
Initial permeability of gas phase at S_r=S_{res}	k_{Gs0}	0.05	m/s
Compressibility coefficient of liquid phase	c_w	2.2×10^{-6}	kPa^{-1}
Unit weight of liquid phase	γ_w	9.8	kN/m^3
Density of saturated mixture	γ_{sat}	1.8	t/m^3
Air entry suction value	s_{ae}	200.0	kPa
Air expulsion suction value	s_{ex}	200.0	kPa
Pore size distribution index	λ_p	0.15	-
Residual degree of saturation	S_{res}	0.2	-
Permeability constant	C_k	1.0	-

5.7.2. Comparison of Rate-Dependent and Rate-Independent Responses

In the first example, the response of the porous medium under the dry condition is examined by using different constitutive models. The external step load applied to the soil layer increases from zero to a maximum value of 500kPa within the time duration t_m =100s and remains constant afterward. Four models, i.e. linear elastic, non-linear elastic, bounding surface plastic and bounding surface viscoplastic constitutive models are used for the analyses. The simulation results are compared in Figure 5.26. The lowest levels of settlement are observed in the nonlinear elastic analysis, where the soil elastic shear modulus varies with changes in void ratio and the effective confining stress, whereas the highest levels of settlement are observed in the nonlinear elasto-plastic analysis. In the viscoplastic case, the effect of strain rate on the size of the bounding surface is taken into account. The CRS compression curve moves to the right in the $(e - lnp')$ plane, resulting in the enlargement of the bounding surface and the increase of the over-consolidation degree of the soil. In this case, the strength of the clay increases resulting in the lower levels of settlement in comparison with the Elasto-plastic response.

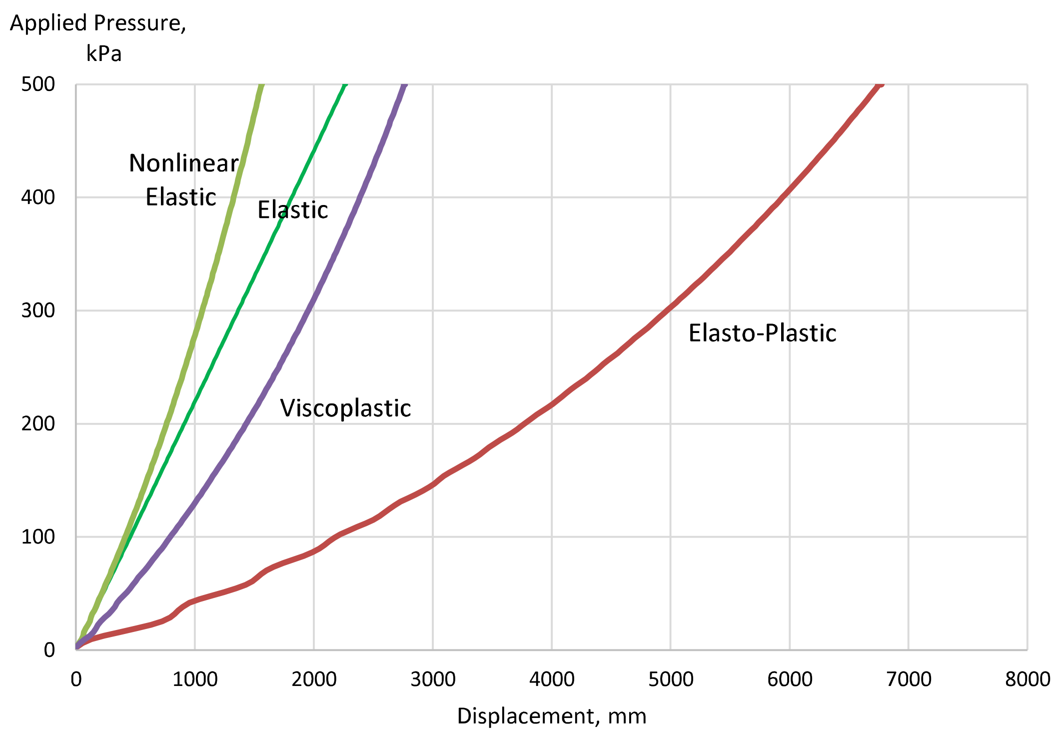

Figure 5.26 – The response of the dry porous medium under uniform step load: Applied pressure versus Vertical settlement

5.7.3. Effect of the Viscoplastic Parameter c_β

As defined in Chapter 3, the viscoplastic parameter c_β controls the evolution of the strain rate hardening

$$c_\beta = \frac{C_\alpha}{(\lambda - \kappa)\ln(10)} \tag{5.1}$$

The parameter c_β is nearly constant in a range of strain rates experienced by the soil during secondary compression in laboratory consolidation tests. In the proposed bounding surface viscoplasticity model, c_β plays an important role in modelling the time-dependent behaviour of soils.

Figure 5.27 shows the effect of c_β on the response of the soil layer subjected to the step load of 500kPa applied within the time duration t_m = 1000s. Different values $c_\beta = 0.02; 0.07; 0.2;$ and 0.5 are considered in the analysis. It is clear that, by using the smaller values of c_β, the viscoplastic soil response approaches the plastic response. In the case with $c_\beta = 0$, the proposed viscoplastic model changes back to the bounding surface plasticity. On the contrary, at large values of c_β the viscoplastic soil response approaches the nonlinear elastic response. If c_β approaches the infinity, the proposed model becomes the nonlinear elastic model. This demonstrates the capability of the bounding surface viscoplasticity model to allow a smooth transition from rate-independent plasticity to rate-dependent viscoplasticity.

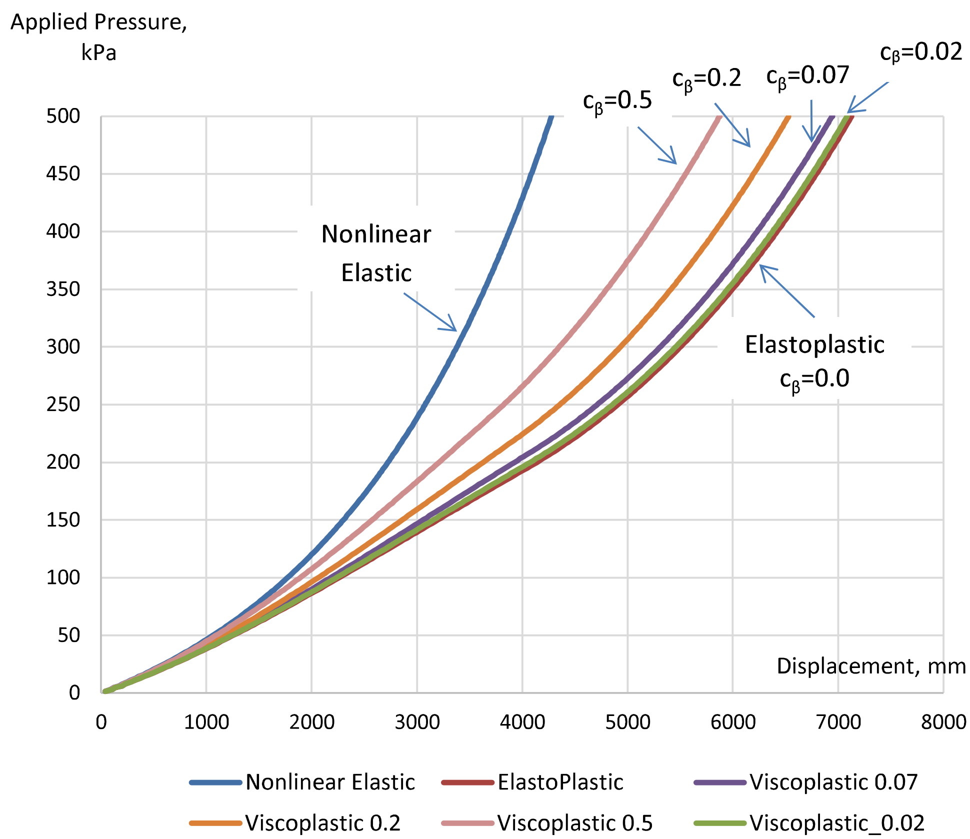

Figure 5.27 – Effect of the viscoplastic parameter c_β on the response of the soil layer: Applied pressure versus Vertical settlement

The effect of the loading rate on the response of the soil layer is demonstrated in Figures 5.28 – 5.31. The soil layer is subjected to the step load of 500kPa applied within different time durations t_m = 100s, 200s, 500s and 1000s. The figures also show the effect of the viscoplastic parameter c_β on the response of the soil. For the small value of $c_\beta = 0.02$ it is observed that the rate effects are quite small, while for larger values of $c_\beta = 0.1$ or 0.2, the effects of rate is more pronounced.

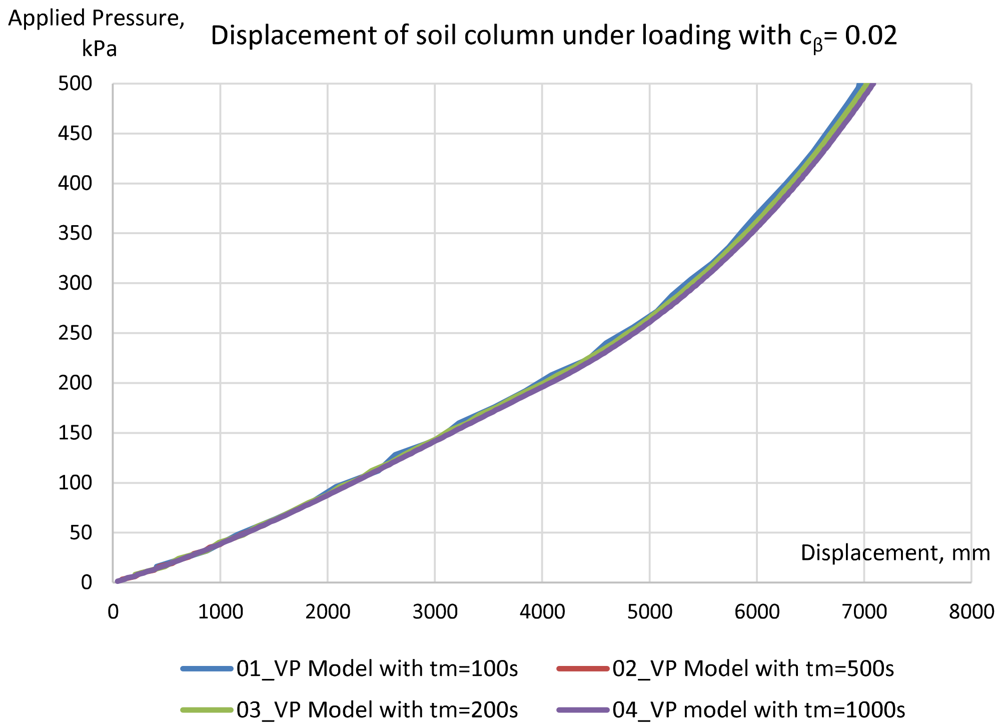

Figure 5.28 – Settlement of the soil column under the step load of 500kPa with $c_\beta = 0.02$

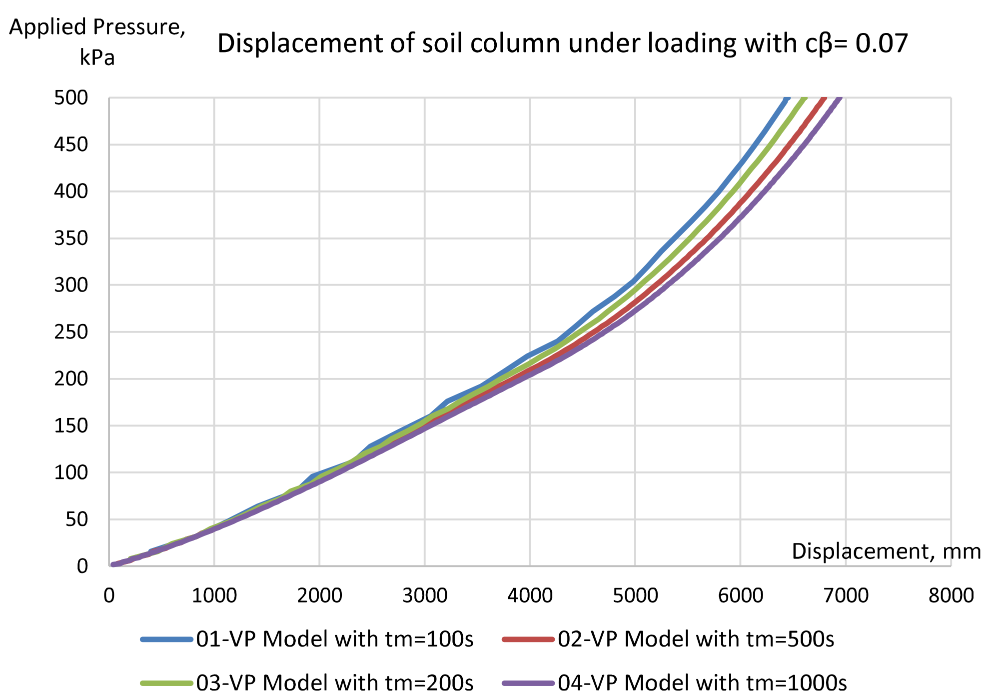

Figure 5.29 – Settlement of the soil column under the step load of 500kPa with $c_\beta = 0.07$

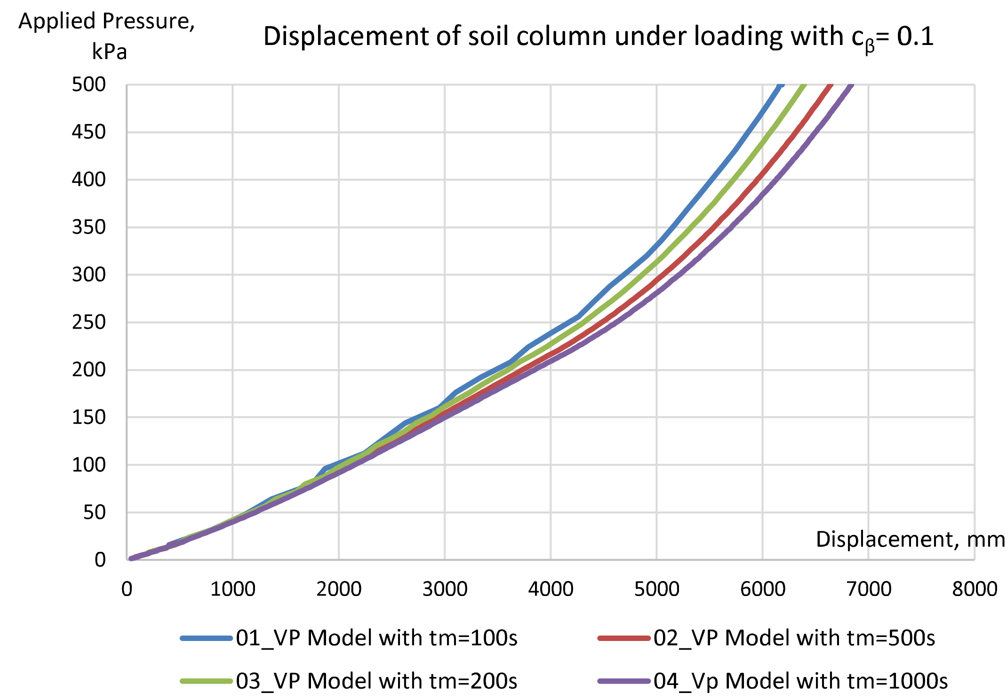

Figure 5.30 – Settlement of the soil column under the step load of 500kPa with $c_\beta = 0.1$

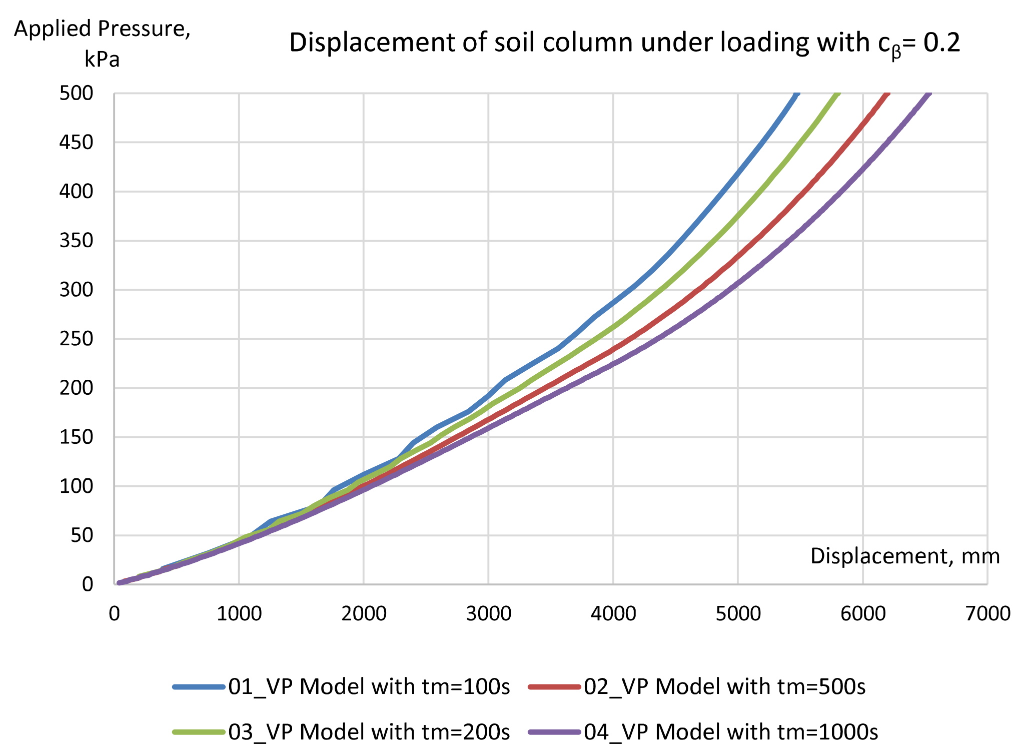

Figure 5.31 – Settlement of the soil column under the step load of 500kPa with $c_\beta = 0.2$

5.7.4. Analysis of Multiphase Porous Medium

The response of the multiphase porous medium subjected to the uniform step loading under different saturation conditions, i.e. dry, fully saturated and partially saturated, is shown in Figure 5.32. The applied pressure increases from zero to a maximum value of 500kPa within 100s and remains constant afterward. The figure demonstrates the continuity of response at transition between saturated and unsaturated states and between unsaturated and dry states.

The distributions of suction, pore water pressure and pore gas pressure at various time steps are shown in Figure 5.33 – 5.35. High levels of pore water and pore gas pressures are generated within the first 100 sec, and dissipated gradually afterward. As observed in Figure 5.35, even though the permeability of air at the dry condition is high, it is observed that the generation of excess pore air pressure cannot be neglected when the ratio of air permeability to rate of loading is low.

Figure 5.36 shows the settlement of the soil layer under the step load of 500kPa applied within different time durations t_m = 100s, 200s, 500s and 1000s. It demonstrates the effect of the loading rate on the response of the unsaturated soil layer. As observed, the longer the time duration to reach the maximum load, the larger settlement of the soil layer due to more dissipation of pore water and pore air pressures as well as the softer behaviour of the soil skeleton under lower strain rates. During the consolidation, the total strain rate is the function of both the rate of change in the effective stress and the rate of change in void ratio.

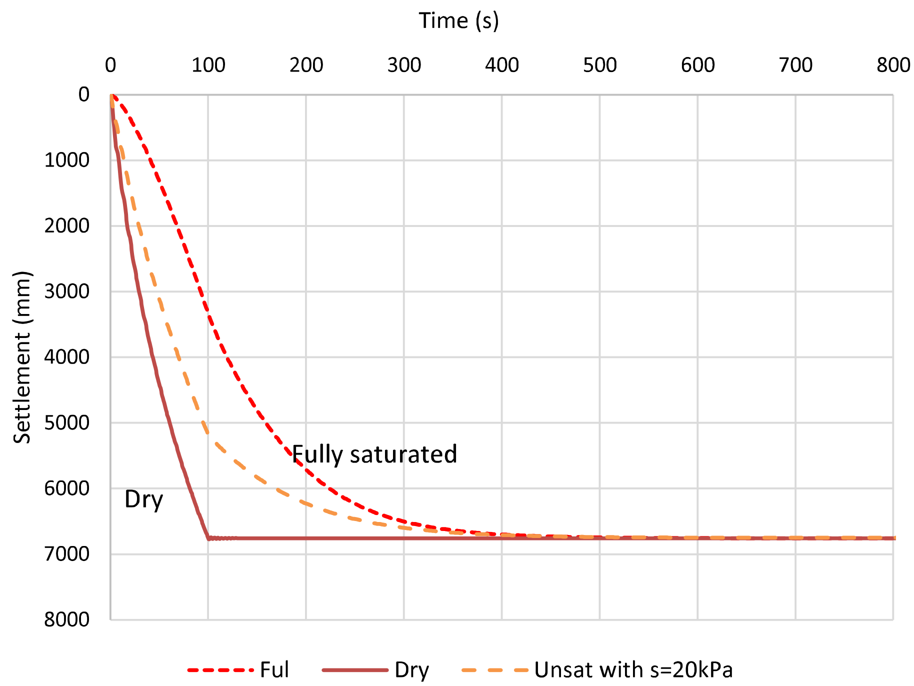

Figure 5.32 – The response of the multiphase porous medium under dry, fully saturated and partially saturated conditions

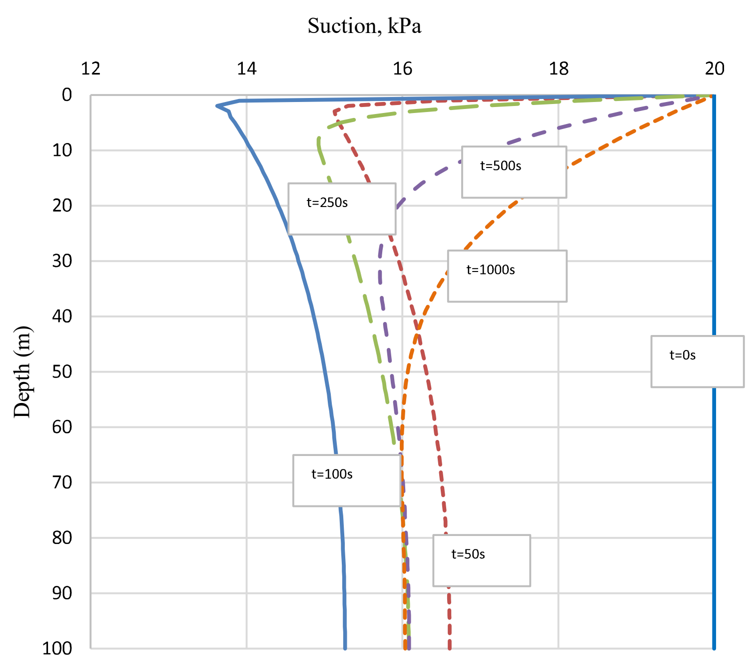

Figure 5.33 – The response of the unsaturated viscoplastic porous medium: Variation of suction with depth

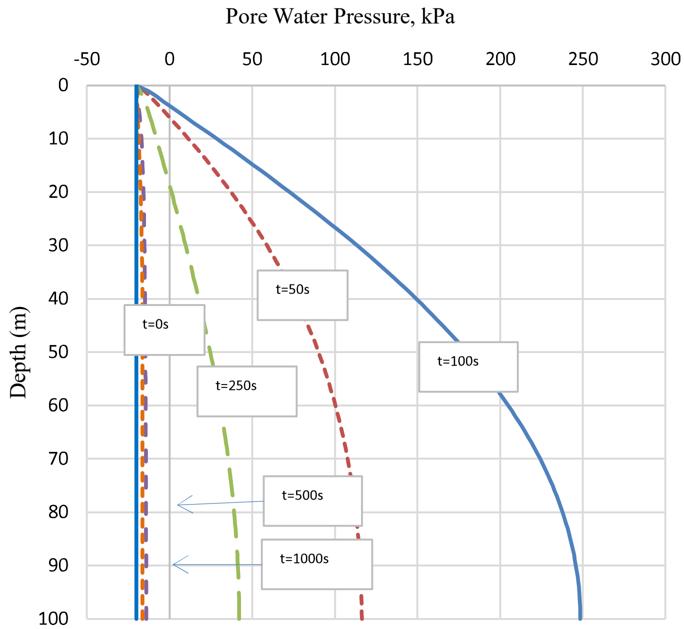

Figure 5.34 – The response of the unsaturated viscoplastic porous medium: Variation of pore water pressure with depth

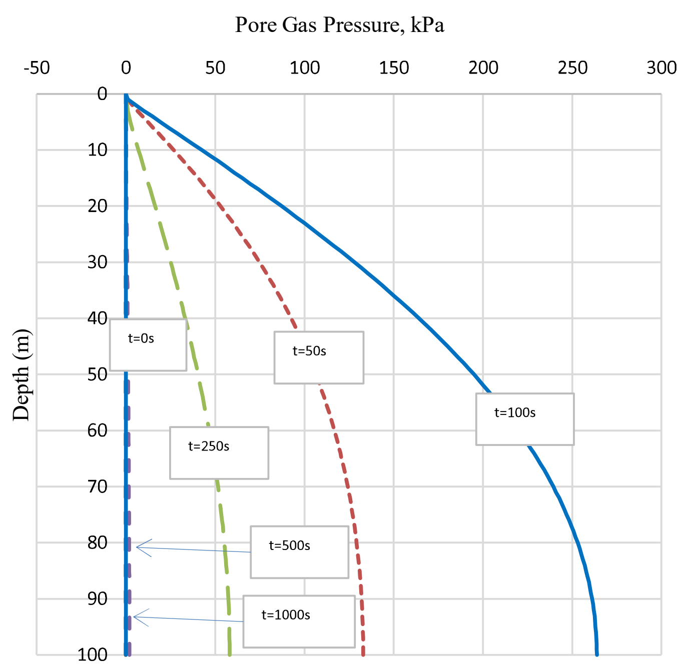

Figure 5.35 – The response of the unsaturated viscoplastic porous medium: Variation of pore gas pressure with depth

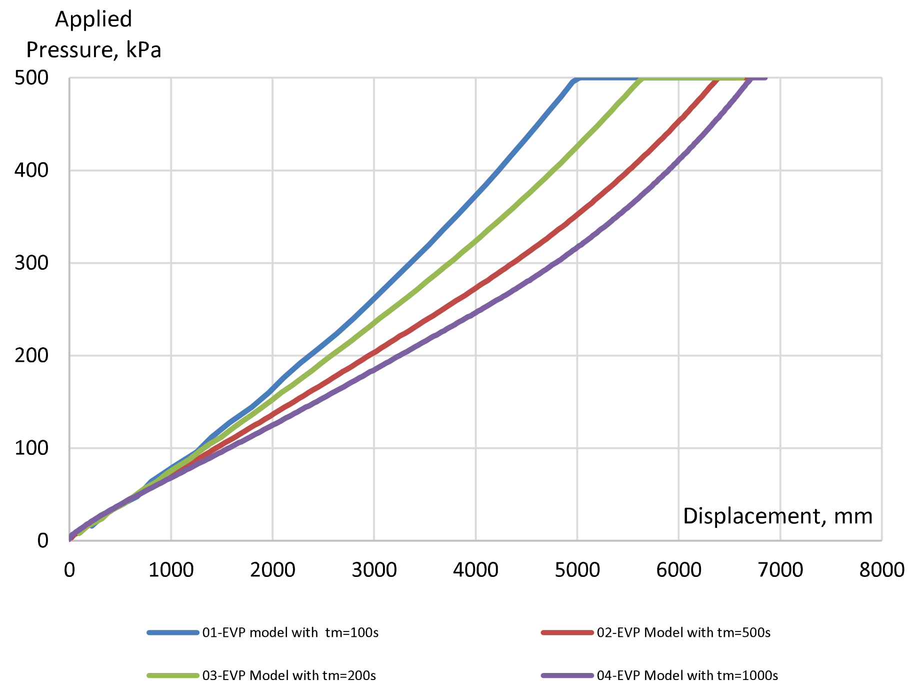

Figure 5.36 – Settlement of the unsaturated viscoplastic soil column under the step load of 500kPa applied within different time duration t_m = 100s, 200s, 500s and 1000s

5.7.4.1. *Effect of the Hydraulic Hysteresis*

The effect of hydraulic hysteresis on the response of the one-dimensional unsaturated soil layer with an initial suction of 300kPa is demonstrated in Figure 5.37. For the case with hysteresis effect, the unsaturated parameters $\mathrm{s_{ae}} = 220\ \mathrm{kPa}$, $\mathrm{s_{ex}} = 200\ \mathrm{kPa}$ are used in the simulations, whereas for the case without hysteresis effect $\mathrm{s_{ae}} = \mathrm{s_{ex}} = 200\ \mathrm{kPa}$ are adopted. The slope of the transition line between the main wetting and main drying paths in the ($\ln\chi \sim \ln s$) plane is $\zeta = 0.15$. The slope of the transition line between the main wetting and drying paths in the ($\ln S_{\mathrm{eff}} \sim \ln s$) plane is $\xi = 0.04$. The parameters adopted are representative of clay.

The initial suction is assumed to be placed on the main drying path. In the case with hydraulic hysteresis, wetting due to loading occurs along the scanning path whereas without hysteresis it remains along the main drying path. This affects the hydro mechanical coupling coefficients presented in Equation (4.52) in Chapter 4, leading to larger generations of pore pressures and reductions in suction when loading is applied at constant water content. The increased pore pressures reduce the rate of consolidation and thus settlement towards the equilibrium condition.

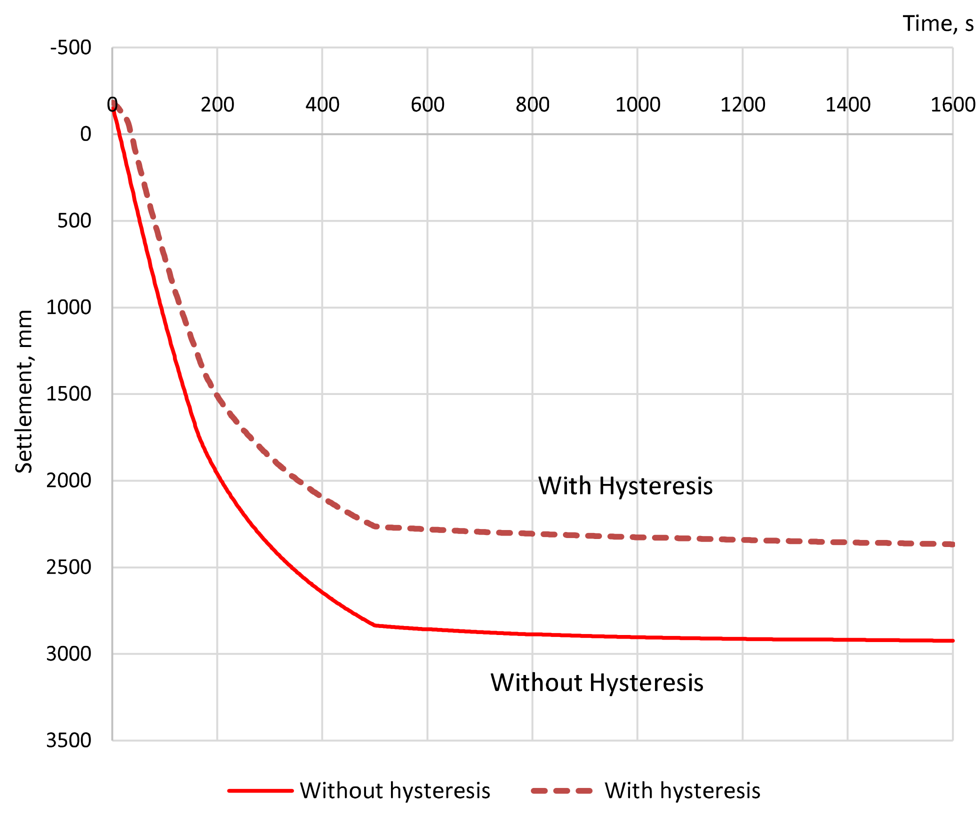

Figure 5.37 – Effect of hydraulic hysteresis on response of the unsaturated porous medium with initial suction of 300kPa under the uniform step load

5.8. Conclusions

The application of the bounding surface viscoplasticity model to predict the stress-strain behaviour of soils was demonstrated for both fully saturated and partially saturated geomaterials. A wide range of tests including undrained creep tests, undrained constant strain rate tests and undrained loading, unloading and relaxation tests were presented for fully saturated soils. Several numerical examples were presented to illustrate the time-dependent behaviour of cohesive soils under both drained and undrained conditions. It was demonstrated that the model is able to capture the tertiary creep and creep rupture in both drained and undrained creep rupture tests. Application of the fully coupled hydro-mechanical model in solving boundary value problems was also demonstrated.

CHAPTER 6

CONCLUSIONS AND RECOMMENDATIONS

6.1. General

The main objective of this study was to develop a unified viscoplastic constitutive model to capture the time-dependent behaviour of geomaterials with particular reference to drained and undrained tertiary creep. The main tasks accomplished are:

i) development of a new viscoplastic bounding surface constitutive model for the time-dependent behaviour of saturated and unsaturated geomaterials including tertiary creep and creep rupture;

ii) development of a numerical model for fully coupled flow-deformation analysis of three phase variably saturated viscoplastic soils;

iii) validation of the constitutive model and the resulting numerical code using the experimental data from the literature for creep tests, constant strain rate tests and unloading, reloading relaxation tests;

iv) solving several boundary value problems to demonstrate the application of the model.

6.2. Bounding Surface Viscoplasticity Model for Time-Dependent Behaviour of Soils

A unified bounding surface viscoplasticity model was developed to describe the time-dependent stress-strain behaviour of both saturated and unsaturated soils. The model was formulated incrementally within the critical state framework using the consistency theory. The total strain increment was decomposed into the elastic part and the viscoplastic part. Elastic behaviour was captured through the isotropic elasticity rule, while the viscoplastic behaviour was captured through the hardening/softening effects of viscoplastic strain and viscoplastic strain rate on the size of the bounding surface. A tear drop shape was selected for the bounding surface. The loading surface was assumed to have the same shape as the bounding surface and always passing through the current stress point. The radial mapping rule was adopted to capture the response under monotonic loading, while the mapping rule of Kan *et al.* (2014) which passes through stress reversal points was used to capture the stress-strain behaviour during unloading and reloading. A non-associated flow rule was used to generalise application of the model to all types of soils. The hardening rule was defined as a function of the viscoplastic strain as well as the viscoplastic strain rate tensors. A new hardening parameter, namely the strain rate hardening parameter, was introduced to take into account the rate dependency in the model. For unsaturated soils, suction was considered as another hardening parameter controlling the size of the bounding surface. The coupled effect of suction hardening was adopted with a multiplicative effect to the viscoplastic volumetric hardening.

The capability of the model to predict tertiary creep in drained and undrained conditions was proved. It is demonstrated that the bounding surface framework enables the model to capture all the three phases of drained creep in over-consolidated soils, which is particularly important in the stability analysis of clayey slopes.

6.3. A Numerical Model for Fully Coupled Flow-Deformation Analysis of Unsaturated Viscoplastic Soils

The governing equations for the fully coupled analysis of flow and deformation in variably saturated porous media were developed based on the concept of effective stress and the theory of multiphase mixtures. The effective stress was used as the basis stress variable through an experimentally based correlation between the effective stress parameter and the matric suction. The equations governing the flow of water and air were established from the conservation equations of mass and momentum. The deformation equations were derived by satisfying the equations of equilibrium and compatibility. The coupling between the flow and viscoplastic deformation models was obtained through the effective stress parameter. The coupled equations were written using a mixed formulation where the primary variables are pore air pressure, pore water pressure and soil matrix deformation vector.

Soil water characteristic curve was incorporated into the formulation to allow coupling between the water and air phases and to determine the compressibility coefficients of soil and water with respect to matric suction. The hydraulic hysteresis was accounted through the effective stress parameter and the soil water characteristic curve. The hydraulic hysteresis was captured by considering the difference between the air entry value and the air expulsion value on the drying and wetting sides of the soil water characteristic curve.

Numerical solution to the governing equations was obtained using the finite element method. The fully governing equations were discretised using Galerkin's approach, while time integration of the rate equations was accomplished using the finite difference method. Both global and local solution schemes were implemented with the intention of improving accuracy and efficiency. The global solution scheme used an incremental approach to solve the discretised system of equations. This approach incorporated a procedure to calculate any unbalanced residual forces at the end of each increment and to correct them accordingly to ensure the solutions satisfy the global equilibrium condition. The local solution scheme employed explicit integration approach to compute stresses and hardening parameters accurately.

6.4. Validation and Application of the Proposed Model

The essential elements of the model were validated by comparing numerical results with the experimental data from the literature. Application of the bounding surface viscoplasticity model to predict the stress-strain behaviour of fully saturated soils were demonstrated for undrained creep tests, undrained constant strain rate tests and undrained loading, unloading and relaxation tests. Several numerical examples were presented to illustrate the time-dependent behaviour of cohesive soils under both drained and undrained conditions. Particularly, it was demonstrated that the model was able to reproduce the tertiary creep and creep rupture in both drained and undrained creep rupture tests. Application of the fully coupled hydro-mechanical model in solving boundary value problems was also proved.

Application of the proposed bounding surface viscoplasticity model to capture the creep behaviour of several soft soils was verified. The simulations were carried out with different creep stress levels. In all cases, good agreement was obtained between the numerical and experimental results. The results showed that an increase in deviatoric stress level resulted in an increase in rate of creep. At low levels of deviator stress, the undrained creep rate decreased and then approached to zero before the stress point reached to the critical state, led to a stable state. However, at high levels of deviatoric stress, the stress point approached to the critical state line and then led to the undrained creep failure of the soil.

During the primary phase of drained creep, it was observed that the strain rate decreased over time. In this phase, the compressive strength of the soil reduced due to both increase in void ratio and decrease in viscoplastic volumetric strain rate. This led the creep process into the secondary phase of creep with a transient minimum strain rate. The further reduction of the compressive strength due to increase in void ratio led the process into tertiary creep with increasing strain rate, leading to creep failure in the over-consolidated clay.

In the constant strain rate tests, a number of cohesive soils were studied under drained and undrained testing conditions. The simulation results showed the capability of the proposed model in capturing the rate-dependent behaviour of normally consolidated as well as overconsolidated soils under both drained and undrained loading conditions. An increase in strain rate during soil compression was manifested by increase in soil stiffness, i.e. the larger the strain rate, the stiffer the soil. Moreover, it showed that the rate effect was more significant in normally consolidated or lightly consolidated clay in comparison with heavily consolidated clay.

A combination of undrained loading-unloading constant strain rate triaxial test and relaxation test on Hong Kong marine deposits was also modelled using the bounding surface viscoplastic model proposed. As expected, the model predicted the increase of the undrained shear strength of the soils at higher strain rate and thus the decrease in the excess pore water pressure. Model predictions of the deviatoric stress – axial strain, deviatoric stress – mean effective stress and pore water pressure – axial strain plots matched the experimental data reasonably well. The results confirmed the capability of the proposed model in capturing soil behaviour in undrained loading, unloading and relaxation tests.

For unsaturated soils, simulation results were also presented to demonstrate the application of the fully coupled viscoplastic model to capture unsaturated soil behaviour in constant strain rate tests. Simulations were conducted for a series of suction controlled tests in Bourke silt. The effects of suction on increasing the effective stress and hardening the soil response were included. In the tests considered, the stiffness and strength of the soils increased with the increase of strain rate. Performance of the model simulation in reproducing the rate dependency of unsaturated soil was satisfactory.

The capability of the proposed model in capturing the tertiary creep and creep rupture was particularly emphasised. Simulations were presented both for undrained creep tests on normally consolidated soil and for drained creep tests on heavily over-consolidated clay. There was the reduction of the mean effective stress at constant deviatoric stress. The pore water pressure increased with time during creep tests due to the change in deviatoric strain. However, the rate of pore water pressure build-up decreased until it reached a steady state. At low stress levels, the stress paths terminated far away from the critical state line and no creep-induced instability occurred. At higher stress levels, the stress paths moved towards the critical state line, led to undrained creep rupture. As predicted, the soils failed under creep stress levels less than the peak strength. Good agreement was observed between the simulation results and the experimental data demonstrating the capability of the proposed model in prediction of tertiary creep and creep rupture.

Several boundary value problems were also solved using the fully coupled hydro-mechanical model and the bounding surface viscoplastic constitutive model. A one-dimensional boundary value problem consisting of a multi-phase porous layer under step loading was considered. Firstly, the response of the porous medium under the dry condition was examined by using four constitutive models, linear elastic, non-linear elastic, bounding surface plasticity and the bounding surface viscoplasticity models. As expected, the lowest levels of settlement were observed in the nonlinear elastic analysis, while the highest levels of settlement were observed in the nonlinear elasto-plastic analysis. The effect of strain rate on the size of the bounding surface was included in the viscoplastic cases. The effect of the viscoplastic parameter was examined on the response of the soil layer subjected to the step load. The simulation results demonstrated the capability of the bounding surface viscoplasticity model to allow a smooth transition from rate-independent plasticity to rate-dependent viscoplasticity.

In addition, the continuity of response of the multiphase porous medium under different saturation conditions, dry, fully saturated and unsaturated, was demonstrated. Simulation results were also presented for the distributions of suction, pore water pressure and pore gas pressure at various time steps. The effect of the loading rate on the response of the unsaturated soil layer was also shown. As observed, the total strain rate was the function of both the rate of change in the effective stress and the rate of change in void ratio.

Finally, the effect of hydraulic hysteresis on the response of the one-dimensional unsaturated soil layer was demonstrated. In the case with hydraulic hysteresis, wetting due to loading occurred along the scanning path while in the case without hydraulic hysteresis, it remained along the main drying path. The use of separate air entry and air expulsion values had also enabled simulation of the hydraulic hysteresis between the drying and wetting paths. The hydro-mechanical coupling approach played an important role in these simulations with suction dependence of the effective stress parameter and incorporation of suction hardening. In the case with hydraulic hysteresis, the increased pore pressures reduced the rate of consolidation and settlement towards the equilibrium condition.

The results presented in this study demonstrated the capability of the proposed bounding surface viscoplasticity constitutive model to capture the time-dependent behaviour of geomaterials. The validation was successfully applied to saturated and unsaturated soils for a wide range of tests in both drained and undrained conditions. The numerical results also showed the capability of the proposed effective stress based fully coupled flow-deformation model to capture a number of boundary value problems.

6.5. Recommendations for Further Research

Based on the work presented, the following recommendations are proposed for further research:

1. Verifying the proposed model for creep occurring during primary consolidation. This would require further numerical and experimental investigations. A fully coupled analysis of consolidation process using the proposed time-dependent constitutive model and comparison with experimental data are necessary to reconcile the consolidation observed in the field and laboratory.

2. Experimental investigation into creep, constant strain rate and stress relaxation behaviour of unsaturated soils. This would require a set of triaxial tests under drained and undrained conditions at different confining pressures to determine the stress–strain–strain-rate relations. The experimental results will underpin the concepts developed in the constitutive modelling of this research work.

3. Numerical modelling of various geotechnical engineering problems. The proposed model can be applied to solve various geotechnical engineering problems wherein time-dependent behaviour is of interest. These include stability of natural and excavated slope, long-term settlement of structures on compressible ground, deformations of earth structures, and squeezing of soft ground around tunnels.

APPENDIX A – THE NUMERICAL PROGRAM

In order to simulate the time-dependent behaviour of geomaterials, the bounding surface viscoplasticity model developed is implemented into a numerical code. The integration of the constitutive equations was performed using the Euler's forward scheme. Distinction is made between the rate dependency problems solved under strain-controlled condition, and the creep tests solved under stress-controlled conditions. The main algorithms of the strain-controlled and stress-controlled codes are presented in Figures A1 and A2.

In the tables, $\lambda, \kappa, \varphi, M_{cs}, \Gamma_0, N, R, k, k_d, k_m, A, \tilde{t}$ are the bounding surface viscoplasticity model parameters, N^* is the number of time steps, T_{time} is the total time, and d_{time} is the time increment.

Figure A1 – Algorithm for strain-controlled tests

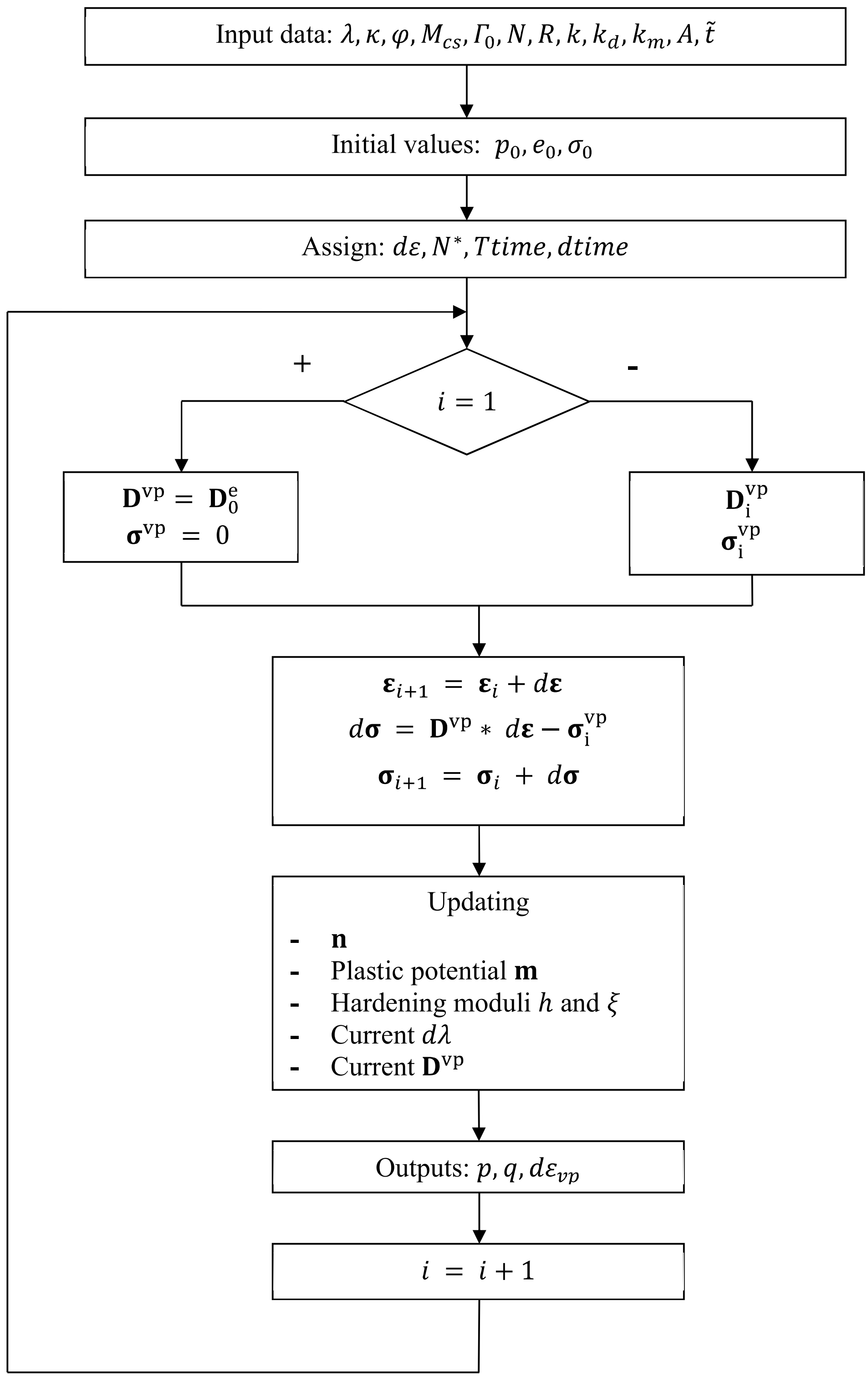

Figure A2 – Algorithm for stress-controlled tests

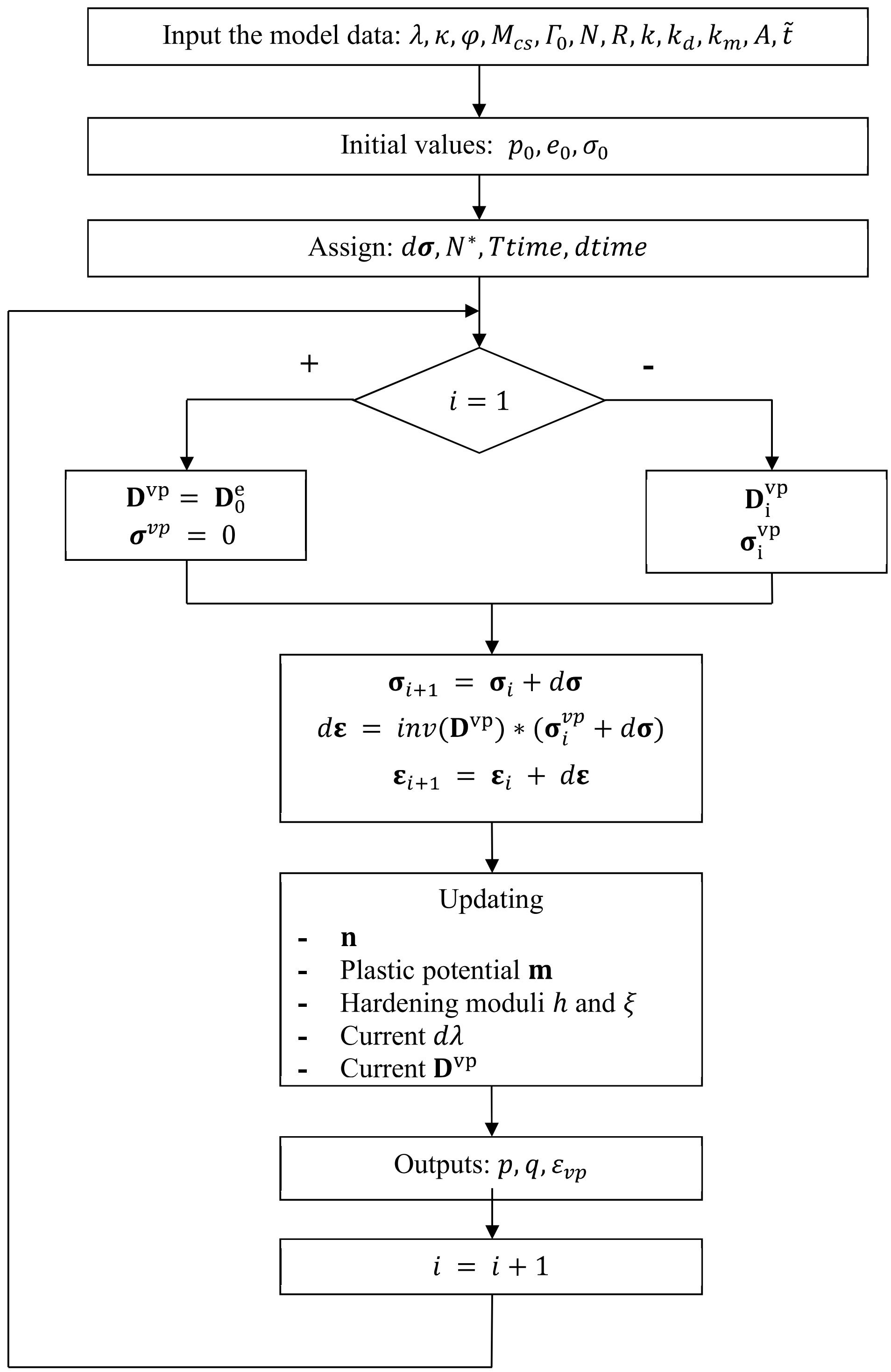

REFERENCES

ABOSHI, H. An experimental investigation on the similitude in the consolidation of a soft clay, including the secondary creep settlement. Proc. 8th Int. Conf. on Soil Mechanics and Foundation Engineering, 1973 Moscow. Speciality Session 2, 4.3, 88.

ADACHI, T. & OKA, F. 1982. Constitutive equations for normally consolidated clay based on elasto-viscoplasticity. *Soils and Foundations,* 22**,** 57-70.

ADACHI, T., OKA, F. & MIMURA, M. 1987. Mathematical structure of an overstress elasto-viscoplastic model for clay. *Soils and Foundations,* 27**,** 31-42.

ADACHI, T. & OKANO, M. 1974. A constitutive equation for normally consolidated clay. *Soils and Foundations,* 14**,** 55-73.

AKAI, K., ADACHI, T. & ANDO, N. 1975. EXISTENCE OF A UNIQUE STRESS-STRAIN-TIME RELATION OF CLAYS. *Soils and Foundations,* 15**,** 1-16.

AKAI, K., ADACHI, T. & NISHI, K. 1977. Mechanical properties of soft rocks. *Proc. 9th ICSMFE,,* 1**,** 7-10.

AL-SHAMRANI, M. A. & STURE, S. 1998. A time-dependent bounding surface model for anisotropic cohesive soils. *Soils and Foundations,* 38**,** 61-76.

ALONSO, E. E., GENS, A. & JOSA, A. 1990. A constitutive model for partially saturated soils. *Geotechnique,* 40**,** 405-430.

ARULANANDAN, K., SHEN, C. K. & YOUNG, R. B. 1971. Undrained creep behaviour of a coastal organic silty clay. *Geotechnique,* 21**,** 359-375.

AUGUSTESEN, A., LIINGAARD, M. & LADE, P. V. 2004. Evaluation of time-dependent behavior of soils. *International Journal of Geomechanics,* 4**,** 137-156.

BANERJEE, P. K. & STIPHO, A. S. 1978. ASSOCIATED AND NON-ASSOCIATED CONSTITUTIVE RELATIONS FOR UNDRAINED BEHAVIOUR OF ISOTROPIC SOFT CLAYS. *International Journal for Numerical and Analytical Methods in Geomechanics,* 2**,** 35-56.

BARDET, J. P. 1986. Bounding surface plasticity model for sands. *Journal of Engineering Mechanics,* 112**,** 1198-1217.

BISHOP, A. W. 1959. The principple of effective stress. *Teknisk Ukeblad,* 106(39)**,** 859-863.

BISHOP, A. W. & BLIGHT, G. E. 1963. Some aspects of effective stress in saturated and partly saturated soils. *Geotechnique,* 13**,** 177-197.

BISHOP, A. W. & LOVENBURY, H. T. 1969. Creep characteristics of two undisturbed clays. *Proceedings of the International Conference on Soil Mechanics and Foundation Engineering = Comptes Rendus du Congres International de Mecanique des Sols et des Travaux de Fondations,* 1**,** 29-37.

BJERRUM, L. 1967. Engineering geology of Norwegian normally-consolidated marine clays as related to settlements of buildings. *Geotechnique,* 17**,** 83-117.

BJERRUM, L. & AITCHISON, G. D. 1973. Problems of soil mechanics and construction on soft clays and structurally unstable soils (collapsible, expansive and others). *Proceedings of the International Conference on Soil Mechanics and Foundation Engineering = Comptes Rendus du Congres International de Mecanique des Sols et des Travaux de Fondations***,** 111-190.

BOLZON, G., SCHREFLER, B. A. & ZIENKIEWICZ, O. C. 1996. Elastoplastic soil constitutive laws generalized to partially saturated states. *Geotechnique,* 46**,** 279-289.

BORJA, R. I. 1992. Generalized creep and stress relaxation model for clays. *Journal of geotechnical engineering,* 118**,** 1765-1786.

BROOKS, R. H. & COREY, A. T. 1964. Hydraulic properties of porous media. *Colorado State University -- Hydrology Papers***,** 27.

BUISMAN, A. S. 1936. Results of long duration settlement tests. *Proc. 1st ICSMFE,* 1**,** 103-107.

CAMPANELLA, R. G. & VAID, Y. P. 1972. *Creep Rupture of a Saturated Natural Clay*.

CAMPANELLA, R. G. & VAID, Y. P. 1974. Triaxial and plane strain creep rupture of an undisturbed clay. *Canadian Geotechnical Journal,* 11**,** 1-10.

CAROSIO, A., WILLAM, K. & ETSE, G. 2000. On the consistency of viscoplastic formulations. *International Journal of Solids and Structures,* 37**,** 7349-7369.

CARTER, J. P., NAZEM, M., AIREY, D. W. & CHOW, S. H. Dynamic analysis of free-falling penetrometers in soil deposits. Geotechnical Special Publication, 2010. 53-68.

CASAGRANDE, A. & WILSON, S. D. 1951. Effect of rate of loading on the strength of clays and shales at constant water content. *Geotechnique,* 2**,** 251-263.

CHEN, W.-F. & WAI-FAH, C. 1985. *Soil plasticity : theory and implementation,* Amsterdam; New York, Amsterdam; New York : Elsevier.

CROUCH, R. S., WOLF, J. P. & DAFALIAS, Y. F. 1994. Unified critical-state bounding-surface plasticity model for soil. *Journal of Engineering Mechanics - ASCE,* 120**,** 2251-2270.

CUI, Y. J. & DELAGE, P. 1996. Yielding and plastic behaviour of an unsaturated compacted silt. *Geotechnique,* 46**,** 291-311.

DAFALIAS, Y. & HERMANN, L. R. 1986. Bounding surface plasticity. Ii: Application to isotropic cohesive soils. *Journal of Engineering Mechanics,* 112**,** 1263-1291.

DAFALIAS, Y. F. 1982. Bounding surface elastoplasticity- viscoplasticity for particulate cohesive media. *Deformation and failure of granular materials. IUTAM symposium, Delft, 1982***,** 97-107.

DAFALIAS, Y. F. 1986. Bounding surface plasticity. I: Mathematical foundation and hypoplasticity. *Journal of Engineering Mechanics,* 112**,** 966-987.

DAFALIAS, Y. F. & HERRMANN, L. R. 1980. BOUNDING SURFACE SOIL PLASTICITY MODEL. *Microstructural Science,* 1**,** 335-345.

DAFALIAS, Y. F. & MANZARI, M. T. 2004. Simple plasticity sand model accounting for fabric change effects. *Journal of Engineering Mechanics,* 130**,** 622-634.

DE GENNARO, V. & PEREIRA, J. M. 2013. A viscoplastic constitutive model for unsaturated geomaterials. *Computers and Geotechnics,* 54**,** 143-51.

DEBERNARDI, D. & BARLA, G. 2009. New viscoplastic model for design analysis of tunnels in squeezing conditions. *Rock Mechanics and Rock Engineering,* 42**,** 259-288.

DESAI, C. S. & ZHANG, D. 1987. Viscoplastic model for geologic materials with generalized flow rule. *International Journal for Numerical and Analytical Methods in Geomechanics,* 11**,** 603-20.

DI BENEDETTO, H., TATSUOKA, F. & ISHIHARA, M. 2002. Time-dependent shear deformation characteristics of sand and their constitutive modelling. *Soils and Foundations,* 42**,** 1-22.

DIXON, D. A., GRAY, M. N. & THOMAS, A. W. 1985. A study of the compaction properties of potential clay-sand buffer mixtures for use in nuclear fuel waste disposal. *Engineering Geology,* 21**,** 247-255.

DRAGON, A. & MROZ, Z. 1979. MODEL FOR PLASTIC CREEP OF ROCK-LIKE MATERIALS ACCOUNTING FOR THE KINETICS OF FRACTURE. *International Journal of Rock Mechanics and Mining Sciences,* 16**,** 253-259.

DRUCKER, D. C. & PRAGER, W. 1952. Soil mechanics and plastic analysis or limit design. *Quarterly of Applied Mathematics,* 10**,** 157-165.

EDIL, T., FOX, P. & LAN, L.-T. An assessment of one-dimensional peat compression. PROCEEDINGS OF THE INTERNATIONAL CONFERENCE ON SOIL MECHANICS AND FOUNDATION ENGINEERING-INTERNATIONAL SOCIETY FOR SOIL MECHANICS AND FOUNDATION ENGINEERING, 1994. AA BALKEMA, 229-229.

FABRE, G. & PELLET, F. 2006. Creep and time-dependent damage in argillaceous rocks. *International Journal of Rock Mechanics and Mining Sciences,* 43**,** 950-960.

FEDA, J. 1992. Creep of soils and related phenomena. *Creep of soils and related phenomena*.

FELL, R., HUNGR, O., LEROUEIL, S. & RIEMER, W. Keynote lecture - Geotechnical engineering of the stability of natural slopes, and cuts and fills in soil. ISRM International Symposium 2000, IS 2000, 2018.

FODIL, A., ALOULOU, W. & HICHER, P. Y. 1997. Viscoplastic behaviour of soft clay. *Geotechnique,* 47**,** 581-591.

FREDLUND, D. G. & MORGENSTERN, N. R. 1977. Stress state variables for unsaturated soils. *ASCE J Geotech Eng Div,* 103**,** 447-466.

GAJO, A. & MUIR WOOD, D. 1999. A kinematic hardening constitutive model for sands: The multiaxial formulation. *International Journal for Numerical and Analytical Methods in Geomechanics,* 23**,** 925-965.

GALLIPOLI, D., GENS, A., SHARMA, R. & VAUNAT, J. 2003. An elasto-plastic model for unsaturated soil incorporating the effects of suction and degree of saturation on mechanical behaviour. *Geotechnique,* 53**,** 123-135.

GARLANGER, J. E. 1972. The consolidation of soils exhibiting creep under constant effective stress. *Geotechnique,* 22**,** 71-78.

GHABOUSSI, J. & GIODA, G. 1977. On the time-dependent effects in advancing tunnels. *International Journal for Numerical and Analytical Methods in Geomechanics,* 1**,** 249-269.

GHAFFARIPOUR, O., ESGANDANI, G. A., KHOSHGHALB, A. & SHAHBODAGHKHAN, B. 2019. Fully coupled elastoplastic hydro-mechanical analysis of unsaturated porous media using a meshfree method. *International Journal for Numerical and Analytical Methods in Geomechanics*.

GOLDSTEIN, M. & TER-STEPANIAN, G. The long-term strength of clays and depth creep of slopes. Proc. 4th Int. Conf. Soil Mech. Found. Eng., London, 1957. 311-314.

GRAHAM, J., CROOKS, J. H. A. & BELL, A. L. 1983. TIME EFFECTS ON THE STRESS-STRAIN BEHAVIOUR OF NATURAL SOFT CLAYS. *Geotechnique,* 33**,** 327-340.

HABTE, M. A. C., ENVIRONMENTAL ENGINEERING, F. O. E. U., HABTE, M. A. C. & ENVIRONMENTAL ENGINEERING, F. O. E. U. 2006. Numerical and constitutive modelling of monotonic and cyclic loading in variably saturated soils. Thesis (Ph.D) - University of New South Wales.

HANSON, J. L., EDIL, T. B. & FOX, P. J. 2001. Stress-temperature effects on peat compression. *Geotechnical Special Publication,* 112**,** 331-345.

HASHIGUCHI, K. & OKAYASU, T. 2000. Time-dependent elastoplastic constitutive equation based on the subloading surface model and its application to soils. *Soils and Foundations,* 40**,** 19-36.

HAYANO, K., MATSUMOTO, M., TATSUOKA, F. & KOSEKI, J. 2001. Evaluation of time-dependent deformation properties of sedimentary soft rock and their constitutive modeling. *Soils and Foundations,* 41**,** 21-38.

HEERES, O. M., SUIKER, A. S. J. & DE BORST, R. 2002. A comparison between the Perzyna viscoplastic model and the consistency viscoplastic model. *European Journal of Mechanics, A/Solids,* 21**,** 1-12.

HENKEL, D. H. 1956. Effect of overconsolidation on behaviour of clays during shear. *Geotechnique,* 6**,** 139-150.

HINCHBERGER, S. D. & ROWE, R. K. 2005. Evaluation of the predictive ability of two elastic-viscoplastic constitutive models. *Canadian Geotechnical Journal,* 42**,** 1675-1694.

HOHENEMSER, K. & PRAGER, W. 1932. Ueber die Ansaetze der Mechanik isotroper Kontinua. *Zeitschrift fuer Angewandte Mathematik und Mechanik,* 12**,** 216-226.

HUANG, Y., ABOU-CHAKRA GUÉRY, A. & SHAO, J. F. 2015. Incremental variational approach for time dependent deformation in clayey rock. *International Journal of Plasticity,* 64**,** 88-103.

HUNTER, G. J. & KHALILI, N. A simple criterion for creep induced failure of over-consolidated clays. ISRM International Symposium 2000, IS 2000, November 19, 2000 - November 24, 2000, 2000 Melbourne, VIC, Australia. International Society for Rock Mechanics.

IMAI, G. & TANG, Y.-X. 1992. Constitutive equation of one-dimensional consolidation derived from inter-connected tests. *Soils and Foundations,* 32**,** 83-96.

JENNINGS, J. E. & BURLAND, J. B. 1962. Limitations to the use of Effective Stress in Partly Saturated Soils. *Geotechnique,* 12**,** 125-144.

JIANG, J., LING, H. I. & KALIAKIN, V. N. 2017. On a damage law for creep rupture of clays with accumulated inelastic deviatoric strain as a damage measure. *Mechanics Research Communications,* 83**,** 22-26.

JOMMI, C. 2000. *Remarks on the constitutive modelling of unsaturated soils,* Leiden, A a Balkema Publishers.

KABBAJ, M., TAVENAS, F. & LEROUEIL, S. 1988. In situ and laboratory stress-strain relationships. *Geotechnique,* 38**,** 83-100.

KALIAKIN, V. N. & DAFALIAS, Y. F. 1990a. Theoretical aspects of the elastoplastic-viscoplastic bounding surface model for cohesive soils. *Soils and Foundations,* 30**,** 11-24.

KALIAKIN, V. N. & DAFALIAS, Y. F. 1990b. Verification of the elastoplastic-viscoplastic bounding surface model for cohesive soils. *Soils and Foundations,* 30**,** 25-36.

KAN, M. E., TAIEBAT, H. A. & KHALILI, N. 2014. Simplified mapping rule for bounding surface simulation of complex loading paths in granular materials. *International Journal of Geomechanics,* 14**,** 239-253.

KATONA, M. G. 1984. Evaluation of a viscoplastic cap model. *Journal of Geotechnical Engineering,* 110**,** 1106-1125.

KAVAZANJIAN, E., JR. & MITCHELL, J. K. 1977. A general stress-strain-time formulation for soils. *Proceedings of the International Conference on Soil Mechanics and Foundation Engineering = Comptes Rendus du Congres International de Mecanique des Sols et des Travaux de Fondations***,** 113-119.

KAVVADAS, M. & KALOS, A. 2019. A time-dependent plasticity model for structured soils (TMS) simulating drained tertiary creep. *Computers and Geotechnics,* 109**,** 130-143.

KELLY, R. B., PINEDA, J. A., BATES, L., SUWAL, L. P. & FITZALLEN, A. 2017. Site characterisation for the ballina field testing facility. *Geotechnique,* 67**,** 279-300.

KHALILI, N., GEISER, F. & BLIGHT, G. E. 2004. Effective stress in unsaturated soils: Review with new evidence. *International Journal of Geomechanics,* 4**,** 115-126.

KHALILI, N., HABTE, M. A. & VALLIAPPAN, S. 2005. A bounding surface plasticity model for cyclic loading of granular soils. *International Journal for Numerical Methods in Engineering,* 63**,** 1939-1960.

KHALILI, N., HABTE, M. A. & ZARGARBASHI, S. 2008. A fully coupled flow deformation model for cyclic analysis of unsaturated soils including hydraulic and mechanical hystereses. *Computers and Geotechnics,* 35**,** 872-889.

KHALILI, N., KHABBAZ, M. & VALLIAPPAN, S. 2000. An effective stress based numerical model for hydro-mechanical analysis in unsaturated porous media. *Computational mechanics,* 26**,** 174-184.

KHALILI, N. & KHABBAZ, M. H. 1998. A unique relationship for X for the determination of the shear strength of unsaturated soils. *Geotechnique,* 48**,** 681-687.

KHALILI, N. & ZARGARBASHI, S. 2010. Influence of hydraulic hysteresis on effective stress in unsaturated soils. *Geotechnique,* 60**,** 729-734.

KIM, Y. T. & LEROUEIL 2001. Modeling the viscoplastic behaviour of clays during consolidation: Application to Berthierville clay in both laboratory and field conditions. *Canadian Geotechnical Journal,* 38**,** 484-497.

KIMOTO, S., SHAHBODAGH, B., MIRJALILI, M. & OKA, F. 2013. Cyclic elastoviscoplastic constitutive model for clay considering nonlinear kinematic hardening rules and structural degradation. *International Journal of Geomechanics,* 15**,** A4014005 (14 pp.).

KOGHO, Y., ASANO, I. & HAYASHIDA, Y. An elastoplastic model for unsaturated soils bases on cyclic plasticity. Proc, Int. Workshop on Deformation of Earth Materials, Oka, F. ed., TC34 of ISSMGE., Sendai, Japan, 2001. 129-140.

KUHN, M. R. & MITCHELL, J. K. 1993. New perspectives on soil creep. *Journal of Geotechnical Engineering,* 119**,** 507-524.

KUTTER, B. L. & SATHIALINGAM, N. 1992. Elastic - viscoplastic modelling of the rate-dependent behaviour of clays. *Geotechnique,* 42**,** 427-441.

LACERDA, W. A. Stress-relaxation and creep effects on soil deformation. 1976 University of California, Berkeley.

LACERDA, W. A. & HOUSTON, W. N. 1973. Stress relaxation in soils. *Proceedings of the International Conference on Soil Mechanics and Foundation Engineering = Comptes Rendus du Congres International de Mecanique des Sols et des Travaux de Fondations***,** 221-227.

LADD, C. C., FOOTR, R., ISHIHARA, K., SCHLOSSER, F. & POULOS, H. G. 1977. Stress-deformation and strength characteristics. *Proceedings of the International Conference on Soil Mechanics and Foundation Engineering = Comptes Rendus du Congres International de Mecanique des Sols et des Travaux de Fondations***,** 421-482.

LADE, P. V. Creep, stress relaxation, and rate effects in sand. Proceedings of the 17th International Conference on Soil Mechanics and Geotechnical Engineering: The Academia and Practice of Geotechnical Engineering, 2009. 264-267.

LADE, P. V., LIGGIO, C. D. & NAM, J. 2009. Strain rate, creep, and stress drop-creep experiments on crushed coral sand. *Journal of Geotechnical and Geoenvironmental Engineering,* 135**,** 941-953.

LADE, P. V. & LIU, C.-T. 1998. Experimental study of drained creep behavior of sand. *Journal of Engineering Mechanics,* 124**,** 912-920.

LALOUI, L., KLUBERTANZ, G. & VULLIET, L. 2003. Solid-liquid-air coupling in multiphase porous media. *International Journal for Numerical and Analytical Methods in Geomechanics,* 27**,** 183-206.

LALOUI, L., LEROUEIL, S. & CHALINDAR, S. 2008. Modelling the combined effect of strain rate and temperature on one-dimensional compression of soils. *Canadian Geotechnical Journal,* 45**,** 1765-1777.

LE, T. M., FATAHI, B. & KHABBAZ, H. 2015. Numerical optimisation to obtain elastic viscoplastic model parameters for soft clay. *International Journal of Plasticity,* 65**,** 1-21.

LEFEBVRE, G. 1981. Fourth Canadian geotechnical colloquium; Strength and slope stability in Canadian soft clay deposits. *Canadian Geotechnical Journal = Revue Canadienne de Geotechnique,* 18**,** 420-442.

LEROUEIL, S. The isotache approach. Where are we 50 years after its development by Professor Suklje? The 13th Danube-European Conference on Geotechnical Engineering, 2006 Ljubljana. pp.55-88.

LEROUEIL, S., KABBAJ, M. & TAVENAS, F. 1988. Study of the validity of a -$--$- model in in situ conditions. *Soils and Foundations,* 28**,** 13-25.

LEROUEIL, S., KABBAJ, M., TAVENAS, F. & BOUCHARD, R. 1985. Stress-strain-strain rate relation for the compressibility of sensitive natural clays. *Geotechnique,* 35**,** 159-180.

LEROUEIL, S. & MARQUES, M. E. S. Importance of strain rate and temperature effects in geotechnical engineering. Proceedings of the 1996 ASCE National Convention, November 10, 1996 - November 14, 1996, 1996 Washington, DC, USA. ASCE, 1-60.

LIINGAARD, M., AUGUSTESEN, A. & LADE, P. V. 2004. Characterization of models for time-dependent behavior of soils. *International Journal of Geomechanics,* 4**,** 157-177.

LO, K. & MORIN, J. 1972. Strength anisotropy and time effects of two sensitive clays. *Canadian Geotechnical Journal,* 9**,** 261-277.

LORET, B. & KHALILI, N. 2000. A three-phase model for unsaturated soils. *International Journal for Numerical and Analytical Methods in Geomechanics,* 24**,** 893-927.

LORET, B. & KHALILI, N. 2002. An effective stress elastic-plastic model for unsaturated porous media. *Mechanics of Materials,* 34**,** 97-116.

LUDWICK, P. J. P. Z. 1922. 'Uber den Einfluss der Deformationsgeschwindigkeit bei bleibenden Deformationen mit besonderer Berucksichtigung der Nachwirkungserscheinungen. 10**,** 411-417.

MAC, T. N., SHAHBODAGH, B. & KHALILI, N. A Bounding Surface Viscoplastic Constitutive Model for Unsaturated Soils. 6th Biot Conference on Poromechanics, Poromechanics 2017, July 9, 2017 - July 13, 2017, 2017 Paris, France. American Society of Civil Engineers (ASCE), 1045-1052.

MAC, T. N., SHAHBODAGH, B. & KHALILI, N. A fully coupled flow-deformation model for time-dependent analysis of unsaturated soils. 7th Asia-Pacific Conference on Unsaturated Soils, 2019 Nagoya, Japan. The Japanese Geotechnical Society.

MAC, T. N., SHAHBODAGHKHAN, B. & KHALILI, N. 2014. A Constitutive Model for Time-Dependent Behavior of Clay. *World Academy of Science, Engineering and Technology, International Journal of Civil, Environmental, Structural, Construction and Architectural Engineering,* 8**,** 596-601.

MALVERN, L. E. 1951. The propagation of longitudinal waves of plastic deformation in a bar of material exhibiting a strain-rate effect. *Journal of Applied Mechanics,* 18**,** 203-208.

MARQUES, M. E. S., LEROUEIL, S. & DE ALMEIDA, M. D. S. S. 2004. Viscous behaviour of St-Roch-de-l'Achigan clay, Quebec. *Canadian Geotechnical Journal,* 41**,** 25-38.

MATSUI, T. & ABE, N. Elasto/viscoplastic constitutive equation of normally consolidated clays based on flow surface theory. *In:* KAWAMOTO, T. & ICHIKAWA, Y., eds. Numerical methods in geomechanics, Nagoya; in three volumes, 1985. A. A. Balkema, Rotterdam, Netherlands, 407-413.

MATSUI, T. & ABE, N. Flow surface model of viscoplasticity for normally consolidated clay. Proc. 2nd Int. Symp. Num. Models Geotech, 1986. 157-164.

MATSUI, T. & ABE, N. 1988. Verification of elasto-viscoplastic model of normally consolidated clays in undrained creep. *Numerical Methods in Geomechanics,* 6**,** 453-459.

MATSUI, T., ABE, N. & HAYASHI, K. 1989. Viscoplastic modelling of time-dependent behaviour of clays. *Numerical models in geomechanics.***,** 100-107.

MATSUSHITA, M. 1999. Time effects on the pre-peak deformation properties of sands. *Proc. 2nd Int. Conf. on Pre-Failure Deformation Characteristics of Geomaterials, IS Torino '99,* 1**,** 681-689.

MESRI, G. & CHOI, Y. K. 1985a. Settlement analysis of embankments on soft clays. *Journal of Geotechnical Engineering,* 111**,** 441-464.

MESRI, G. & CHOI, Y. K. 1985b. The uniqueness of the end-of-primary (EOP): void ratio- effective stress relationship. *Proc. 11th international conference on soil mechanics and foundation engineering, San Francisco, August 1985. Vol. 2, (Balkema)***,** 587-590.

MESRI, G. & GODLEWSKI, P. M. 1977. Time and stress-compressibility interrelationship. *American Society of Civil Engineers, Journal of the Geotechnical Engineering Division,* 103**,** 417-430.

MITCHELL, J. K. 1993. *Fundamentals of soil behavior,* New York, New York : Wiley.

MITCHELL, J. K. & JAMES KENNETH, M. 2005. *Fundamentals of soil behavior,* Hoboken, NJ, Hoboken, NJ : John Wiley & Sons.

MIURA, K., OKUI, Y. & HORII, H. 2003. Micromechanics-based prediction of creep failure of hard rock for long-term safety of high-level radioactive waste disposal system. *Mechanics of Materials,* 35**,** 587-601.

MODARESSI, H. & LALOUI, L. 1997. A thermo-viscoplastic constitutive model for clays. *International Journal for Numerical and Analytical Methods in Geomechanics,* 21**,** 313-335.

MROZ, Z., NORRIS, V. A. & ZIENKIEWICZ, O. C. 1981. An anisotropic, critical state model for soils subject to cyclic loading. *Geotechnique,* 31**,** 451-469.

MURAYAMA, S. & SHIBATA, T. 1958. On the rheological character of clay. *Disaster Prevent. Inst.,* 26**,** 1-43.

MURAYAMA, S. & SHIBATA, T. Rheological properties of clays. Proc., 5th Int. Conf. on Soil Mechanics and Foundation Engineeing, 1961. 269-274.

NAGHDI, P. M. & MURCH, S. A. 1963. On the Mechanical Behavior of Viscoelastic/Plastic Solids. *Journal of Applied Mechanics,* 30**,** 321-328.

NASH, D. F. T., SILLS, G. C. & DAVISON, L. R. 1992. One-dimensional consolidation testing of soft clay from Bothkennar. *Geotechnique,* 42**,** 241-256.

NAZEM, M., CARTER, J. P., AIREY, D. W. & CHOW, S. H. 2012. Dynamic analysis of a smooth penetrometer free-falling into uniform clay. *Geotechnique,* 62**,** 893-905.

NOVA, R. VISCOPLASTIC CONSTITUTIVE MODEL FOR NORMALLY CONSOLIDATED CLAY. Deformation and Failure of Granular Materials, International Union of Theoretical and Applied Mechanics Symposium., 1982 Delft, Neth. A. A. Balkema, 287-295.

OKA, F., ADACHI, T. & MIMURA, M. Elasto-viscoplastic constitutive models for clays. *In:* KEEDWELL, M. J., ed. Proceedings of the international conference on rheology and soil mechanics, 1988. Elsevier Appl. Sci., London, United Kingdom, 12-28.

OKA, F., ADACHI, T. & YASHIMA, A. 1994. Instability of an elasto-viscoplastic constitutive model for clay and strain localization. *Mechanics of Materials,* 18**,** 119-129.

OKA, F., ADACHI, T. & YASHIMA, A. 1995. Strain localization analysis using a viscoplastic softening model for clay. *International journal of plasticity,* 11**,** 523-545.

OKA, F., KODAKA, T., KIMOTO, S., ISHIGAKI, S. & TSUJI, C. 2003. Step-changed strain rate effect on the stress-strain relations of clay and a constitutive modeling. *Soils and Foundations,* 43**,** 189-202.

OKA, F., KODAKA, T., KIMOTO, S., KIM, Y. S. & YAMASAKI, N. An elasto-viscoplastic model and multiphase coupled FE analysis for unsaturated soil. 4th International Conference on Unsaturated Soils, April 2, 2006 - April 5, 2006, 2006 Carefree, AZ, United states. American Society of Civil Engineers, 2039-2050.

OKA, F., SHAHBODAGH, B. & KIMOTO, S. 2019. A computational model for dynamic strain localization in unsaturated elasto-viscoplastic soils. *International Journal for Numerical and Analytical Methods in Geomechanics,* 43**,** 138-165.

OLDECOP, L. A. & ALONSO, E. E. 2007. Theoretical investigation of the time-dependent behaviour of rockfill. *Geotechnique,* 57**,** 289-301.

OLSZAK, W. 1970. Stationary and nonstationary viscoplasticity. *Inelastic Behavior of Solids*, 53-75.

OLSZAK, W. & PERZYNA, P. The constitutive equations of the flow theory for a non-stationary yield condition. *In:* GÖRTLER, H., ed. Applied Mechanics, 1966// 1966 Berlin, Heidelberg. Springer Berlin Heidelberg, 545-553.

OLSZAK, W. & PERZYNA, P. 1970. Stationary and nonstationary viscoplasticity. New York: MacGraw-Hill.

PARK, D. & HASHASH, Y. M. A. 2008. Rate-dependent soil behavior in seismic site response analysis. *Canadian Geotechnical Journal,* 45**,** 454-469.

PERZYNA, P. 1963. On the constitutive equations for work-hardening and rate sensitive plastic materials. *Bulletin de l'Academie Polonaise des Sciences, Serie des Sciences Techniques,* 12**,** 199-206.

PERZYNA, P. 1966. Fundamental problems in viscoplasticity. *Advances in Applied Mechanics.* Academic Press Inc.

PINEDA, J. A., SUWAL, L. P., KELLY, R. B., BATES, L. & SLOAN, S. W. 2016. Characterisation of Ballina clay. *Geotechnique,* 66**,** 556-577.

POTTS, D. M. & ZDRAVKOVIĆ, L. 1999. *Finite element analysis in geotechnical engineering. Theory,* London, London : Thomas Telford.

PRANDTL, L. 1928. Ein Gedankenmodell zur kinetischen Theorie der festen Körper. *J ZAMM-Journal of Applied Mathematics*

Mechanics/Zeitschrift für Angewandte Mathematik und Mechanik, 8**,** 85-106.

PREVOST, J.-H. 1976. UNDRAINED STRESS-STRAIN-TIME BEHAVIOR OF CLAYS. *American Society of Civil Engineers, Journal of the Geotechnical Engineering Division,* 102**,** 1245-1259.

QIAO, Y., FERRARI, A., LALOUI, L. & DING, W. 2016. Nonstationary flow surface theory for modeling the viscoplastic behaviors of soils. *Computers and Geotechnics,* 76**,** 105-119.

QU, G., HINCHBERGER, S. D. & LO, K. Y. 2010. Evaluation of the viscous behaviour of clay using generalised overstress viscoplastic theory. *Geotechnique,* 60**,** 777-789.

RAYMOND, G. P. & WAHLS, H. E. 1976. ESTIMATING 1-DIMENSIONAL CONSOLIDATION, INCLUDING SECONDARY COMPRESSION, OF CLAY LOADED FROM OVERCONSOLIDATED TO NORMALLY

CONSOLIDATED STATE. *Special Report - National Research Council, Transportation Research Board*, 17-25.

ROCCHI, G., FONTANA, M. & DA PRAT, M. 2003. Modelling of natural soft clay destruction processes using viscoplasticity theory. *Geotechnique,* 53, 729-745.

ROSCOE, K. H. & BURLAND, J. 1968. *On the Generalized Stress-Strain Behavior of Wet Clays*.

RUSSELL, A. R. & KHALILI, N. 2004. A bounding surface plasticity model for sands exhibiting particle crushing. *Canadian Geotechnical Journal,* 41, 1179-1192.

RUSSELL, A. R. & KHALILI, N. 2006. A unified bounding surface plasticity model for unsaturated soils. *International Journal for Numerical and Analytical Methods in Geomechanics,* 30, 181-212.

SABETAMAL, H., CARTER, J. P., NAZEM, M. & SLOAN, S. W. 2016. Coupled analysis of dynamically penetrating anchors. *Computers and Geotechnics,* 77, 26-44.

SADEGHI, H., KIMOTO, S., OKA, F. & SHAHBODAGH, B. Dynamic analysis of river embankments during earthquakes using a finite deformation FE analysis method. Computer Methods and Recent Advances in Geomechanics - Proceedings of the 14th Int. Conference of International Association for Computer Methods and Recent Advances in Geomechanics, IACMAG 2014, 2015. 637-642.

SAITO, M. & UEZAWA, H. Failure of soil due to creep. Proceeding 5th ICSMFE, 1961 Paris. 315-318.

SATAKE, M. 1989. Mechanics of Granular Materials. *Report of ISSMFE Technical Committee on Mechanics of Granular Materials*.

SEKIGUCHI, H. 1977. Rheological characteristics of clays. *Proceedings of the International Conference on Soil Mechanics and Foundation Engineering = Comptes Rendus du Congres International de Mecanique des Sols et des Travaux de Fondations*, 289-292.

SEKIGUCHI, H. 1984. Theory of undrained creep rupture of normally consolidated clay based on elasto-viscoplasticity. *Soils and Foundations,* 24, 129-147.

SHAHBODAGH, B. 2011. *Large deformation dynamic analysis method for partially saturated elasto-vicsoplastic soils.* PhD, Kyoto University, Kyoto, Japan.

SHAHBODAGH, B., HABTE, M. A., KHOSHGHALB, A. & KHALILI, N. 2017. A bounding surface elasto-viscoplastic constitutive model for non-isothermal cyclic analysis of asphaltic materials. *International Journal for Numerical and Analytical Methods in Geomechanics,* 41**,** 721-739.

SHAHBODAGH, B., KHALILI, N. & ALIPOUR ESGANDANI, G. 2015. A numerical model for nonlinear large deformation dynamic analysis of unsaturated porous media including hydraulic hysteresis. *Computers and Geotechnics,* 69**,** 411-423.

SHAHBODAGH, B., MAC, T. N., ESGANDANI, G. A. & KHALILI, N. 2020. A Bounding Surface Viscoplasticity Model for Time-Dependent Behavior of Soils Including Primary and Tertiary Creep. *International Journal of Geomechanics,* 20**,** 04020143.

SHAHBODAGH, B., MIRJALILI, M., KIMOTO, S. & OKA, F. 2014. Dynamic analysis of strain localization in water-saturated clay using a cyclic elasto-viscoplastic model. *International Journal for Numerical and Analytical Methods in Geomechanics,* 38**,** 771-793.

SHAHBODAGH, B., SADEGHI, H., KIMOTO, S. & OKA, F. 2019. Large deformation and failure analysis of river embankments subjected to seismic loading. *Acta Geotechnica*.

SHEAHAN, T. C., LADD, C. C. & GERMAINE, J. T. 1994. Time-dependent triaxial relaxation behavior of a resedimented clay. *Geotechnical Testing Journal,* 17**,** 444-452.

SHEAHAN, T. C., LADD, C. C. & GERMAINE, J. T. 1996. Rate-dependent undrained shear behavior of saturated clay. *Journal of Geotechnical Engineering,* 122**,** 99-108.

SHENG, D., SLOAN, S. W., GENS, A. & SMITH, D. W. 2003. Finite element formulation and algorithms for unsaturated soils. Part I: Theory. *International Journal for Numerical and Analytical Methods in Geomechanics,* 27**,** 745-765.

SHENG, D., SLOAN, S. W. & YU, H. S. 2000. Aspects of finite element implementation of critical state models. *Computational Mechanics,* 26**,** 185-196.

SHERARD, J. L. & COOKE, J. B. 1987. Concrete-face rockfill DAM: I. Assessment. *Journal of Geotechnical Engineering,* 113**,** 1096-1112.

SILVESTRI, V. Triaxial relaxation tests on a soft clay. Advanced Triaxial Testing of Soil and Rock, 1988 ASTM, Philadelphia. 321-337.

SILVESTRI, V., SOULIE, M., TOUCHAN, Z. & FAY, B. 1988. Triaxial relaxation tests on a soft clay. *Advanced triaxial testing of soil and rock, ASTM, Philadenphia.*

SIMO, J. C., KENNEDY, J. G. & GOVINDJEE, S. 1988. Non-smooth multisurface plasticity and viscoplasticity. Loading/unloading conditions and numerical algorithms. *International Journal for Numerical Methods in Engineering,* 26**,** 2161-85.

SINGH, A. & MITCHELL, J. K. 1968. General stress-strain-time function for soils. *American Society of Civil Engineers Proceedings, Journal of the Soil Mechanics and Foundations Division,* 94**,** 21-46.

SINGH, A. & MITCHELL, J. K. 1969. Creep potential and creep rupture of soils. *Proceedings of the International Conference on Soil Mechanics and Foundation Engineering = Comptes Rendus du Congres International de Mecanique des Sols et des Travaux de Fondations,* 1**,** 379-384.

SLOAN, S. W., ABBO, A. J. & SHENG, D. 2001. Refined explicit integration of elastoplastic models with automatic error control. *Engineering Computations,* 18**,** 121-54.

SNEAD, D. E. 1970. *Creep rupture of saturated undisturbed clays.*

SUKLJE, L. 1957. The analysis of the consolidation process by the isotaches method. *Proc. 4th ICSMFE,* 1**,** 200-206.

TAMAGNINI, R. 2004. An extended Cam-clay model for unsaturated soils with hydraulic hysteresis. *Geotechnique,* 54**,** 223-228.

TATSUOKA, F. 2000. Some new aspects of time effects on the stress-strain behaviour of stiff geomaterials, Keynote Lecture. *The Geotechnics of Hard Soils-Soft Rocks, Proc. of Second Int. Conf. on Hard Soils and Soft Rocks, Napoli, 1998,* 2**,** 1285-1371.

TAVENAS, F. & LEROUEIL, S. 1981. CREEP AND FAILURE OF SLOPES IN CLAY. *Canadian Geotechnical Journal,* 18**,** 106-120.

TAVENAS, F., LEROUEIL, S., LA ROCHELLE, P. & ROY, M. 1978. Creep behaviour of an undisturbed lightly overconsolidated clay. *Canadian Geotechnical Journal,* 15**,** 402-423.

TAYLOR, D. W. 1942. Research on consolidation of clays. *Mass Institute of Technology -- Department of Civil and Sanitary Engineering -- Serial***,** 147.

TER-STEPANIAN, G. 1975. Creep of a clay during shear and its rheological model. *Geotechnique,* 25**,** 299-320.

TERZAGHI, K. 1936. The shearing resistance of saturated soils and the angle between the planes of shear. *First international conference on soil Mechanics, 1936,* 1**,** 54-59.

TERZAGHI, K. & KARL, T. 1996. *Soil mechanics in engineering practice,* New York, New York : Wiley.

UCHAIPICHAT, A. 2005. *Experimental investigation and constitutive modelling of thermo-hydro-mechanical coupling in unsaturated soils.* Thesis (Ph. D.)--University of New South Wales, 2005.

VAID, Y. P., ROBERTSON, P. K. & CAMPANELLA, R. G. 1979. Strain rate behaviour of Saint-Jean-Vianney clay. *Canadian Geotechnical Journal = Revue Canadienne de Geotechnique,* 16**,** 34-42.

VARNES, D. J. Time-deformation relations in creep to failure of earth materials. Proceedings of the 7th Southeast Asian Geotechnical Conference., 1982 Hong Kong. 107-130.

VIALOV, S. & SKIBITSKY, A. Rheological processes in frozen soils and dense clays. Proc. 4th Int. Conf. Soil Mech. and Found. Engr, 1957. 120.

WAHLS, H. E. 1962. Analysis of primary and secondary consolidation. *Journal Soil Mechanics The Founnd. Div. ,* 88(SM6)**,** 207-231.

WALKER, L. K. & RAYMOND, G. P. 1968. The prediction of consolidation rates in a cemented clay. *Canadian Geotechnical Journal = Revue Canadienne de Geotechnique,* 5**,** 192-216.

WANG, W. M., SLUYS, L. J. & DE BORST, R. 1997. Viscoplasticity for instabilities due to strain softening and strain-rate softening. *International Journal for Numerical Methods in Engineering,* 40**,** 3839-3864.

WATABE, Y., UDAKA, K., NAKATANI, Y. & LEROUEIL, S. 2012. Long-term consolidation behavior interpreted with isotache concept for worldwide clays. *Soils and Foundations,* 52**,** 449-464.

WHEELER, S. J. & SIVAKUMAR, V. 1995. An elasto-plastic critical state framework for unsaturated soil. *Geotechnique,* 45**,** 35-53.

WOOD, D. M. 2004. *Geotechnical modelling,* London; New York, London; New York : Spon Press.

YAMAMURO, J. A., ABRANTES, A. E. & LADE, P. V. 2012. Effect of strain rate on the stress-strain behavior of sand. *Journal of Geotechnical and Geoenvironmental Engineering,* 137**,** 1169-1178.

YANG, C. & CARTER, J. P. 2017. Isotach Elastoplasticity: A Case Study on Osaka Bay Clay. *Indian Geotechnical Journal,* 47**,** 161-172.

YANG, C., CARTER, J. P., SHENG, D. & SLOAN, S. W. 2016. An isotach elastoplastic constitutive model for natural soft clays. *Computers and Geotechnics,* 77**,** 134-155.

YIN, J.-H. & GRAHAM, J. 1989. Viscous-elastic-plastic modelling of one-dimensional time-dependent behaviour of clays. *Canadian geotechnical journal,* 26**,** 199-209.

YIN, J.-H. & GRAHAM, J. 1994. Equivalent times and one-dimensional elastic viscoplastic modelling of time-dependent stress-strain behaviour of clays. *Canadian Geotechnical Journal,* 31**,** 42-52.

YIN, J.-H. & GRAHAM, J. 1999. Elastic viscoplastic modelling of the time-dependent stress-strain behaviour of soils. *Canadian Geotechnical Journal,* 36**,** 736-745.

YIN, J.-H., ZHU, J.-G. & GRAHAM, J. 2002. A new elastic viscoplastic model for time-dependent behaviour of normally and overconsolidated clays: Theory and verification. *Canadian Geotechnical Journal,* 39**,** 157-173.

YIN, J. H. 1999. Non-linear creep of soils in oedometer tests. *Geotechnique,* 49**,** 699-707.

YIN, Z.-Y., KARSTUNEN, M. & HICHER, P.-Y. 2010. Evaluation of the influence of elasto-viscoplastic scaling functions on modelling time-dependent behaviour of natural clays. *Soils and Foundations,* 50**,** 203-214.

YIN, Z. Y., KARSTUNEN, M., CHANG, C. S., KOSKINEN, M. & LOJANDER, M. 2011. Modeling time-dependent behavior of soft sensitive clay. *Journal of Geotechnical and Geoenvironmental Engineering,* 137**,** 1103-1113.

ZHEN-YU, Y., CHANG, C. S., KARSTUNEN, M. & HICHER, P. Y. 2010. An anisotropic elastic-viscoplastic model for soft clays. *International Journal of Solids and Structures,* 47**,** 665-77.

ZHU, J.-G. 2000. *Experimental study and elastic visco-plastic modelling of the time-dependent stress-strain behaviour of Hong Kong marine deposits.*

ZHU, J.-G., YIN, J.-H. & LUK, S.-T. 1999. Time-Dependent Stress-Strain Behavior of Soft Hong Kong Marine Deposits. *Geotechnical Testing Journal,* 22**,** 118-126.

ZIENKIEWICZ, O. C. & CORMEAU, I. C. 1974. Visco-plasticity - plasticity and creep in elastic solids - a unified numerical solution approach. *International Journal for Numerical Methods in Engineering,* 8**,** 821-845.